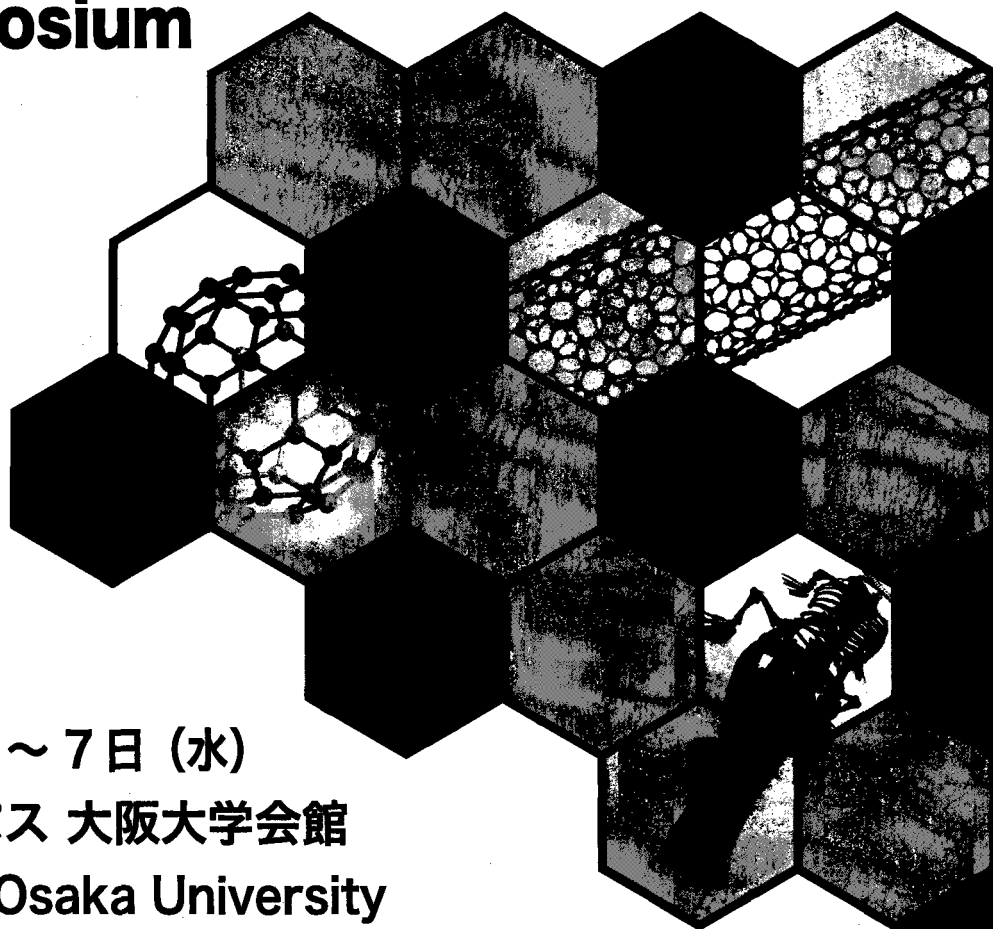


第45回 フラーレン・ナノチューブ・グラフェン 総合シンポジウム

The 45th Fullerenes-Nanotubes-Graphene General Symposium

講演要旨集 Abstracts



2013年8月5日(月)～7日(水)
大阪大学豊中キャンパス 大阪大学会館
Toyonaka Campus, Osaka University

主催 **フラーレン・ナノチューブ・グラフェン学会**
Fullerenes, Nanotubes and Graphene Research Society

共催 日本化学会 The Chemical Society of Japan
大阪大学工学研究科 Graduate School of Engineering, Osaka University

協賛 日本物理学会 The Physical Society of Japan
応用物理学会 The Japan Society of Applied Physics
高分子学会 The Society of Polymer Science, Japan
電気化学会 The Electrochemical Society of Japan



カーボンナノ材料新製品

グラフェン NEW!

- Monolayer graphene film, 1 cm x 1 cm on copper foil
773697-4EA ¥30,200
- Monolayer graphene film, 1 cm x 1 cm on quartz
773719-4EA ¥71,600
- Monolayer graphene film, 1 cm x 1 cm on SiO₂/Si substrate
773700-4EA ¥44,600

単層カーボンナノチューブ NEW!

- SWeNT® SG-65i SWCNTs, (6,5) chirality, ≥95% (carbon)
773735-250MG ¥35,800
773735-1G ¥103,700
- SWeNT CG 300 SWCNTs, 95% (carbon as SWCNT)
775533-250MG ¥35,800
775533-1G ¥105,600

SWeNT is a registered trademark of SouthWest NanoTechnologies, Inc.

www.aldrich.com/nano-jp

SIGMA-ALDRICH®

シグマ アルドリッチ ジャパン

〒140-0002 東京都品川区東品川2-2-24
天王洲セントラルタワー4階

■製品に関するお問い合わせは、弊社テクニカルサポートへ
TEL : 03-5796-7330 FAX : 03-5796-7335
E-mail : sialjpts@sial.com

■在庫照会・ご注文方法に関するお問い合わせは、弊社カスタマーサービスへ
TEL : 03-5796-7320 FAX : 03-5796-7325
E-mail : sialjpcs@sial.com

<http://www.sigma-aldrich.com/japan>

Abstracts

The 45th Fullerene-Nanotubes-Graphene General Symposium

第 45 回 フラーレン・ナノチューブ・グラフェン 総合シンポジウム 講演要旨集

Organizer: The Fullerene, Nanotubes and Graphene Research Society
Co-organizer: The Chemical Society of Japan
Graduate School of Engineering, Osaka University
Supporters: The Physical Society of Japan
Japan Society of Applied Physics
The Society of Polymer Science, Japan
The Electrochemical Society of Japan

主催 : フラーレン・ナノチューブ・グラフェン学会
共催 : 日本化学会・大阪大学大学院工学研究科
協賛 : 日本物理学会・応用物理学会・高分子学会・電気化学会

Date: August 5th(Mon) – 7th(Wed), 2013
Place: Osaka University, Osaka University Hall
Machikaneyamacho 1-13, Toyonaka, Osaka 560-0043, Japan
TEL: 06-6850-5977

Presentation: Plenary Lecture (40 min presentation, 5min discussion)
Special Lecture (25 min presentation, 5min discussion)
General Lecture (10 min presentation, 5min discussion)
Poster Preview (1 min presentation only)

日時 : 平成 25 年 8 月 5 日 (月) ~ 7 日 (水)
場所 : 大阪大学 大阪大学会館
〒560-0043 大阪府豊中市待兼山町 1-13
TEL: 06-6850-5977

発表時間 : 基調講演 (発表 40 分・質疑応答 5 分)
特別講演 (発表 25 分・質疑応答 5 分)
一般講演 (発表 10 分・質疑応答 5 分)
ポスタープレビュー (発表 1 分・質疑応答 なし)

展示団体御芳名

(五十音順、敬称略)

アイクストロン(株)

(株)ATR

コスモ・バイオ(株)

サーモフィッシャーサイエンティフィック株式会社

サイバネットシステム(株)

(株)島津製作所

(株)セントラル科学貿易

(株)テクノアイ

ナカライテスク(株)

ナノフォトン(株)

(株)名城ナノカーボン

(株)ニューメタルス エンド ケミカルス コーポレーション

(株)堀場製作所

広告掲載団体御芳名

(五十音順、敬称略)

アイクストロン(株)

イデアインターナショナル(株)

コスモ・バイオ(株)

シグマ アルドリッチ ジャパン(株)

(株)セントラル科学貿易

ナカライテスク(株)

日本分析工業(株)

日立工機(株)

フロンティアカーボン(株)

(株)フロンティア出版

(株)堀場製作所

目次

早見表	i
座長一覧	iii
プログラム	和文.....	iv
	英文.....	xvi
講演予稿	基調講演・特別講演.....	1
	一般講演	9
	ポスター発表	47
発表索引	155

Contents

Time Table	i
Chairpersons List	iii
Program	Japanese	iv
	English	xvi
Abstracts	Plenary Lecture, Special Lectures	1
	General Lectures	9
	Poster Previews	47
Author Index	155

プログラム早見表

8月5日 (月)	
	受付開始 8:45~ 講演開始 9:30~
9:30	一般講演 5件 (ナノチューブの物性) 9:30-10:45
10:45	休憩 10:45-11:00
11:00	特別講演 (大野雄高) 11:00-11:30
11:30	一般講演 3件 (ナノチューブの応用) 11:30-12:15
12:15	昼食 (幹事会) 12:15-13:30
13:30	一般講演 4件 (ナノチューブの応用・ 内包ナノチューブ) 13:30-14:30
14:30	休憩 14:30-14:45
14:45	特別講演 (塩澤秀次) 14:45-15:15
15:15	一般講演 4件 (ナノ炭素粒子・ナノホーン・ ナノ環境と安全評価) 15:15-16:15
16:15	ポスタープレビュー (1P-1 ~ 1P-37) 16:15-17:00
17:00	ポスターセッション (アセンブリホール) 17:00-18:30

18:30

8月6日 (火)	
	受付開始 8:45~ 講演開始 9:00~
9:00	一般講演 5件 大澤賞受賞対象者講演 飯島賞受賞対象者講演 9:00-10:40
10:40	休憩 10:40-11:00
11:00	特別講演 (C. Kocabas) 11:00-11:30
11:30	一般講演 3件 (グラフェンの生成と応用・その 他) 11:30-12:15
12:15	昼食 12:15-13:30
13:30	若手奨励賞表彰式
13:45	総会
14:15	基調講演 (片浦弘道) 14:15-15:00
15:00	一般講演 3件 (金属内包フラーレン) 15:00-15:45
15:45	休憩 15:45-16:00
16:00	ポスタープレビュー (2P-1 ~ 2P-37) 16:00-16:45
16:45	ポスターセッション (アセンブリホール) 16:45-18:15
18:15	
18:30	懇親会 (豊中福利会館・4F食堂) 18:30-20:30

20:30

8月7日 (水)	
	受付開始 8:45~ 講演開始 9:00~
9:00	特別講演 (日比野浩樹) 9:00-9:30
9:30	一般講演 3件 (グラフェンの物性) 9:30-10:15
10:15	特別講演 (加藤俊顕) 10:15-10:45
10:45	休憩 10:45-11:00
11:00	特別講演 (中谷真人) 11:00-11:30
11:30	一般講演 4件 (フラーレンの応用・ フラーレンの化学・フラーレン) 11:30-12:30
12:30	昼食 12:30-13:45
13:45	特別講演 (小松直樹) 13:45-14:15
14:15	一般講演 3件 (ナノチューブの生成と精製) 14:15-15:00
15:00	休憩 15:00-15:15
15:15	ポスタープレビュー (3P-1 ~ 3P-35) 15:15-16:00
16:00	ポスターセッション (アセンブリホール) 16:00-17:30

17:30

基調講演 発表40分・質疑5分
特別講演 発表25分・質疑5分
一般講演 発表10分・質疑5分
ポスタープレビュー 発表1分・質疑なし

Time Table

August 5 (Mon.)	
8:45	Registrasion begins at 8:45 Lectures begin at 9:30
9:30	General Lectures [5] (Properties of Nanotubes) 9:30-10:45
10:45	Coffee Break 10:45-11:00
11:00	Special Lecture (Y. Ohno) 11:00-11:30
11:30	General Lectures [3] (Applications of Nanotubes) 11:30-12:15
12:15	Lunch (Administrative meeting) 12:15-13:30
13:30	General Lectures [4] (Applications of Nanotubes • Endohedral Nanotubes) 13:30-14:30
14:30	Coffee Break 14:30-14:45
14:45	Special Lecture (N. Shiozawa) 14:45-15:15
15:15	General Lectures [4] (Carbon Nanoparticles, Nanohorn, Enviromental/Safety characteriz- ations, Others) 15:15-16:15
16:15	Poster Preview (1P-1 through 1P-37) 16:15-17:00
17:00	Poster Session (Assembly Hall) 17:00-18:30

18:30

August 6 (Tue.)	
8:30	Registrasion begins at 8:45 Lectures begin at 9:00
9:00	General Lectures [5] Lectures by Candidates for the Osawa Award and the Iijima Award 9:00-10:40
10:40	Coffee Break 10:40-11:00
11:00	Special Lecture (C. Kocabas) 11:00-11:30
11:30	General Lectures [3] (Synthesis and Applications of Graphene, Others) 11:30-12:15
12:15	Lunch 12:15-13:30
13:30	Award Ceremony
13:45	General Meeting
14:15	Plenary Lecture (H. Kataura) 14:15-15:00
15:00	General Lectures [3] (Endohedral Metallofullerenes) 15:00-15:45
15:45	Coffee Break 15:45-16:00
16:00	Poster Preview (2P-1 through 2P-37) 16:00-16:45
16:45	Poster Session (Assembly Hall) 16:45-18:15
18:15	
18:30	Banquet (COOP Building 4F-restaurant) 18:30-20:30

20:30

August 7 (Wed.)	
8:30	Registrasion begins at 8:45 Lectures begin at 9:00
9:00	Special Lecture (H. Hibino) 9:00-9:30
9:30	General Lectures [3] (Properties of Graphene) 9:30-10:15
10:15	Special Lecture (T. Kato) 10:15-10:45
10:45	Coffee Break 10:45-11:00
11:00	Special Lecture (M. Nakaya) 11:00-11:30
11:30	General Lectures [4] (Applications of Fullerenes • Chemistry of Fullerenes • Fullerenes) 11:30-12:30
12:30	Lunch 12:30-13:45
13:45	Special Lecture (N. Komatsu) 13:45-14:15
14:15	General Lectures [3] (Formation and Purification of Nanotubes) 14:15-15:00
15:00	Coffee Break 15:00-15:15
15:15	Poster Preview (3P-1 through 3P-35) 15:15-16:00
16:00	Poster Session (Assembly Hall) 16:00-17:30

17:30

Plenary Lecture: 40min (Presentation) + 5min (Discussion)
 Special Lecture: 25min (Presentation) + 5min (Discussion)
 General Lecture: 10min (Presentation) + 5min (Discussion)
 Poster Preview: 1min (Presentation)

座長一覧

8月5日(月)

(敬称略)

	時間	座長
一般講演	9:30 ~ 10:45	大野雄高
特別講演 (大野)	11:00 ~ 11:30	秋田成司
一般講演	11:30 ~ 12:15	
一般講演	13:30 ~ 14:30	松田一成
特別講演 (塩澤)	14:45 ~ 15:15	丸山茂夫
一般講演	15:15 ~ 16:15	阿知波洋次
ポスタープレビュー	16:15 ~ 17:00	平原佳織
ポスターセッション	17:00 ~ 18:30	

8月6日(火)

	時間	座長
大澤賞受賞対象者講演 飯島賞受賞対象者講演	9:00 ~ 10:40	岡崎俊也
特別講演 (Kocabas)	11:00 ~ 11:30	斎藤 晋
一般講演	11:30 ~ 12:15	白石誠司
基調講演 (片浦)	14:15 ~ 15:00	中山喜萬
一般講演	15:00 ~ 15:45	北浦 良
ポスタープレビュー	16:00 ~ 16:45	有江隆之
ポスターセッション	16:45 ~ 18:15	

8月7日(水)

	時間	座長
特別講演 (日比野)	9:00 ~ 9:30	前橋兼三
一般講演	9:30 ~ 10:15	
特別講演 (加藤)	10:15 ~ 10:45	
特別講演 (中谷)	11:00 ~ 11:30	岡田 晋
一般講演	11:30 ~ 12:30	菅井俊樹
特別講演 (小松)	13:45 ~ 14:15	小林慶裕
一般講演	14:15 ~ 15:00	千足昇平
ポスタープレビュー	15:15 ~ 16:00	三宅雅人
ポスターセッション	16:00 ~ 17:30	

8月5日(月)

特別講演 発表 25分・質疑応答 5分
一般講演 発表 10分・質疑応答 5分
ポスタープレビュー 発表 1分・質疑応答なし

一般講演 (9:30-10:45)

ナノチューブの物性

- 1-1 SWCNT/DWCNT の環境中における放射性元素の吸着能力とメカニズム 9
○荒木 拓海, 手島 正吾, 中村 壽, 古月 文志, 遠藤 守信
- 1-2 乾燥した二本鎖 DNA-単層カーボンナノチューブハイブリッドの光励起発光 10
○伊藤 雅浩, 伊藤 悠介, 小林 友樹, 林田 拓也, 二井 大輔, 梅村 和夫, 本間 芳和
- 1-3 カーボンナノチューブの X 線誘起欠陥とその構造におけるラマン散乱研究 11
○村上 俊也, 山本 勇樹, 松田 充晃, 木曾田 賢治, 伊東 千尋
- 1-4 ホールドープした単層カーボンナノチューブの光学非線形性 12
○秋月 直人,
- 1-5 高純度半導体型単層カーボンナノチューブバッキーペーパーの熱電能 13
○中井 祐介, 本田 和也, 宮田 耕充, 柳 和宏, 真庭 豊

☆☆☆☆☆☆ 休憩 (10:45-11:00) ☆☆☆☆☆☆

特別講演 (11:00-11:30)

- 1S-1 Flexible and stretchable carbon nanotube thin-film transistors and integrated circuits 1
大野 雄高

一般講演 (11:30-12:15)

ナノチューブの応用

- 1-6 カーボンナノチューブ薄膜トランジスタにおけるしきい電圧の直径依存性 14
○二瓶 史行, 菊地 悠太, 佐々木 扶紗子, 井原 和紀, 沼田 秀昭, 桑原 有紀, 大森 滋和, 斎藤 毅
- 1-7 カーボンナノチューブとカーボン蒸着複合膜の開発 15
○長谷部 裕雄, 久保木 浩功, 奥野 広樹, 山根 功, 今尾 浩士, 福西 暢尚, 加瀬 昌之, 上垣外 修一
- 1-8 Immunoassay with Single-Walled Carbon Nanotubes as Near-Infrared Fluorescent Labels 16
○飯泉 陽子, 岡崎 俊也, 池原 譲, 小倉 睦郎, 湯田坂 雅子

☆☆☆☆☆☆ 昼食 (12:15-13:30) ☆☆☆☆☆☆

一般講演 (13:30-14:30)

ナノチューブの応用, 内包ナノチューブ

- 1-9 熱力学的アプローチによる CNT/樹脂複合材料の導電率向上 17
○阿多 誠介, 尹 好苑, チャンドラモウリ スブラマニアン, 水野 貴瑛, 山田 健郎, 畠 賢治

8月5日(月)

- 1-10 Thermally conductive SG-CNT-Cu composite with low thermal expansion 18
○Yuzuri Yasuda, Chandramouli Subramaniam, Seisuke Ata, Motoo Yumura, Takeo Yamada,
Don N. Futaba, Kenji Hata
- 1-11 カーボンナノチューブ中における一次元硫黄結晶の金属化 19
○藤森 利彦, 村松 寛之, 二村 竜介, 瓜田 幸幾, 林 卓哉, 遠藤 守信, 金子 克美
- 1-12 カーボンナノチューブ内部で形成された π 共役系ポリマーの構造と電子物性 20
○宮浦 健志, 宮田 耕充, 北浦 良, 篠原 久典

☆☆☆☆☆☆ 休憩 (14:30-14:45) ☆☆☆☆☆☆

特別講演 (14:45-15:15)

- 1S-2 有機金属化合物からのカーボンナノ構造体の生成 2
塩澤 秀次

一般講演 (15:15-16:15)

ナノホーン, ナノ炭素粒子, ナノ環境と安全評価, その他

- 1-13 カーボンナノホーン内部への官能基化 C_{60} 分子の導入における官能基の効果 21
○小林 慶太, 上野 裕, 小久保 研, 保田 英洋
- 1-14 溶液中におけるポリイン誘導体とヨウ素分子の光誘起反応 22
○和田 資子, 若林 知成
- 1-15 Lysosomal membrane permeabilization induced by carbon nanohorns caused reactive oxygen species generation and apoptosis in RAW264.7 cell 23
○Mei Yang, Minfang Zhang, Yoshio Tahara, Sumio Iijima, Masako Yudasaka
- 1-16 気相移動度分析システムの開発 24
○菅井 俊樹, 廣芝 泰祐, 三上 仁奈子

ポスタープレビュー (16:15-17:00)

ポスターセッション (17:00-18:30)

★ … 若手奨励賞候補者

ナノチューブの生成と精製

- 1P-1 π 伸長した有限長単層カーボンナノチューブ分子のボトムアップ化学合成とその構造 47
★ ○松野 太輔, 鎌田 翔, 一杉 俊平, 磯部 寛之
- 1P-2 Initiation of carbon nanotube growth by well-defined carbon nanorings 48
★ ○Yasutomo Segawa, Haruka Omachi, Takuya Nakayama, Eri Takahashi, Kenichiro Itami
- 1P-3 PG-ACCVD 法で作製された単層カーボンナノチューブに対する Post-annealing 効果 49
伊藤 洋介, ○鈴木 信三, 長澤 浩, 小野 晶, 阿知波 洋次
- 1P-4 単一カイラリティ単層カーボンナノチューブにおける自己組織的配列集合体形成と電気伝導特性 50
河合 英輝, ○長谷川 凱, 中津 亨, 内藤 泰久, 高木 勇樹, 和田 義史, 竹延 大志, 柳 和宏
- 1P-5 単層カーボンナノチューブ成長中の自由電子レーザー照射によるカイラリティ制御の解明 51
○吉田 圭佑

8 月 5 日(月)

1P-6	単層カーボンナノチューブのゲルへの吸着における溶質と pH の影響 ○平野 篤, 卜部 泰子, 片浦 弘道, 田中 丈士	52
1P-7	ナノカーボンコンポジット膜合成における触媒種の影響 ○松岡 佑樹, 吉村 雅満	53
1P-8	面内配向した半導体単層カーボンナノチューブの直接成長 ○岩田 展幸, 相良 拓実, 津田 悠作, 吉田 圭佑, 石井 宏治, 矢島 博文, 山本 寛	54
1P-9 ★	高温ゲル濾過法による直径 1.1nm 単層カーボンナノチューブの濃縮 ○市村 遼太, 宮田 耕充, 中井 祐介, 柳 和宏, 真庭 豊	55
1P-10	高真空アルコールガスソース法による Pt 触媒からの単層カーボンナノチューブの低温成長と成長メカニズム ○近藤 弘基, ゴーシ ラナジツ, 成塚 重弥, 丸山 隆浩, 飯島 澄男	56
1P-11	光応答性有機電解質分子を用いた単層カーボンナノチューブの精製 ○松澤 洋子, 高田 裕子, 小平 哲也, 木原 秀元, 吉田 勝	57
1P-12	Ni 触媒による霜柱状 CNT 成長 ○楠本 雄司, 関家 一樹, 小路 紘史, 古田 寛, 八田 章光	58
1P-13	ナノダイヤモンド粒子を触媒として CVD 合成した単層カーボンナノチューブの直径分布 ○海野 貴徳, 井ノ上 泰輝, 千足 昇平, 本間 芳和, 丸山 茂夫	59
1P-14	Improved efficiency in metal-free carbon nanotube growth from nanodiamonds by switching growth driving force ○Hiraaki Kokame, Kazuki Fujimoto, Ryota Negishi, Tatsuji Arifuku, Noriko Kiyoyanagi, Yoshihiro Kobayashi	60
1P-15	単層 CNT 成長の分子動力学と密度汎関数法を用いたエタノール・コバルトクラスターの化学反応計算 ○久間 馨	61
1P-16 ★	ラマン分光法による水平配向単層カーボンナノチューブのカイラリティ分析 ○井ノ上 泰輝, 長谷川 大祐, 千足 昇平, 丸山 茂夫	62
1P-17	パルスプラズマ CVD における狭いカイラリティ分布を持つ単層カーボンナノチューブの成長機構 ○許 斌	63
ナノチューブの物性		
1P-18	垂直配向カーボンナノチューブフォレストの光学特性合成温度依存性 ○古田 寛, 関家 一樹, 高野 恵介, 萩行 正憲, 八田 章光	64
1P-19	削除.	
1P-20	半導体型単層カーボンナノチューブのコヒーレントフォノン分光 ○本田 裕貴, マレット エリザベス, 平野 篤, 田中 丈, 牧野 孝太郎, 長谷 宗明	65
1P-21	Interplay of wall number and diameter on the electrical conductivity of carbon nanotube thin films ○Guohai Chen, Don Futaba, Shunsuke Sakurai, Motoo Yumura, Kenji Hata	66

8月5日(月)

1P-22	カーボンナノチューブの詳細構造に対する格子振動の効果 ○是常 隆, 加藤 幸一郎, 斎藤 晋	67
1P-23	Temperature Dependence of Stokes and anti-Stokes photoluminescence from oxygen-doped carbon nanotubes ○Yuhei Miyachi, Naoto Akizuki, Munechiyo Iwamura, Shinichiro Mouri, Kazunari Matsuda	68
ナノチューブの応用		
1P-24 ★	ペロブスカイト型材料を被膜した単層カーボンナノチューブによる 極微量酸素ガスの検知 ○福田 洋志	69
1P-25	半導体単層カーボンナノチューブ薄膜を用いたガスセンシング ○鈴木 雄登	70
1P-26 ★	Interaction between Carbon Nanotubes and Neurons Studied With High-Density Microelectrode Arrays ○Florent Seichepine, Kosmas Deligkaris, Urs Frey	71
1P-27	単層カーボンナノチューブを担持体とする窒素ドープカーボンによる酸素還元 森田 潤一, ○藤ヶ谷 剛彦, 中嶋 直敏	72
1P-28 ★	Air-Stable High-Efficiency Nanotube-Si Heterojunction Solar Cells ○崔 可航	73
1P-29 ★	Influence of dispersion state of long SWCNTs on the electrical conductivity of composites ○尹 好苑, 阿多 誠介, 山田 健郎, 湯村 守雄, 畠 賢治	74
フラーレンの応用		
1P-30	フラーレン-ジアミン集合体膜を用いた逆型有機薄膜太陽電池の作製と評価 ○番家 翔人, 松本 泰輔, 奥 健夫, 秋山 毅	75
1P-31	有機薄膜太陽電池を指向したスピロ環を有するフラーレン誘導体の合成と評価 ○増田 寛之, 小久保 研, 伊熊 直彦, 三木江 翼, 佐伯 昭記, 関 修平, 大島 巧	76
1P-32	Preparation and microscopic analysis of fullerene-diamine adducts as organic electronic material ○小野 侑司, 秋山 毅, 奥 健夫	77
1P-33	C ₆₀ 薄膜への光渦照射による光重合体の伝導特性評価 ○龜山 航, 靱山 大輝, 鳥海 直人, 宮本 克彦, 尾松 孝茂, 落合 勇一, 青木 伸之	78
1P-34	LiF バッファ層の挿入による PTB7:PC71BM 有機薄膜太陽電池の効率向上 ○藤井 俊治郎, 柳館 樹, 大関 将矢, 柳 雄一郎, 新井 友樹, 奥川 孝紀, 吉田 哲, 田中 丈士, 西岡 泰城, 片浦 弘道	79
1P-35	C ₆₀ がドープされた固体シリコンのエネルギー論と電子状態 ○岡田 晋	80
1P-36	有機薄膜太陽電池におけるチオフェン含有フラーレン誘導体の合成および特性 ○林 達也, Oh Jaebuem, Lee Haeseong, Ann JongJun, Lee HeeJae, Jang Jin, Pac Chyongjin, 森山 広思	81
1P-37	有機薄膜太陽電池におけるシアノ基含有フラーレン誘導体の置換基効果 ○松本 華奈, Oh Jaebuem, Lee Haeseong, Ann JongJun, Lee HeeJee, Jang Jin, Pac Chyongjin, 森山 広思	82

8月6日(火)

基調講演発表	発表 40分・質疑応答 5分
特別講演	発表 25分・質疑応答 5分
大澤賞飯島賞対象者講演	発表 10分・質疑応答 10分
一般講演	発表 10分・質疑応答 5分
ポスターレビュー	発表 1分・質疑応答なし

大澤賞対象者講演 (9:00-9:40)

- 2-1 Enhanced photoelectrochemical performance of composite photovoltaic cells of $\text{Li}^+@C_{60}$ /sulfonated porphyrin supramolecular nanoclusters 25
○大久保 敬, 川島 雄樹, 酒井 隼人, 羽曾部 卓, 福住 俊一
- 2-2 Surface functionalization of nanodiamonds towards high solubility in physiological media and practical biomedical applications 26
○Zhao Li, Chen Xiao, Chano Tokuhiko, Komatsu Naoki

飯島賞対象者講演 (9:40-10:40)

- 2-3 ねじれたグラフェンナリボンからのカーボンナノチューブ成長 27
○林 宏恩, 宮田 耕充, 北浦 良, 西村 好史, 西本 佳央,, 片浦 弘道, 篠原 久典
- 2-4 カーボンナノチューブで作製した高耐久性固体高分子形燃料電池電極触媒 28
○藤ヶ谷 剛彦, 中嶋 直敏
- 2-5 Stabilities and Electronic Structures of Carbon Impurities in Hexagonal Boron-Nitride Monolayers and Bilayers 29
○Yoshitaka Fujimoto, Takashi Koretsune, Susumu Saito

☆☆☆☆☆☆ 休憩 (10:45-11:00) ☆☆☆☆☆☆

特別講演 (11:00-11:30)

- 2S-3 Graphene based optoelectronics in the visible spectra 3
Coskun Kocabas

一般講演 (11:30-12:15)

グラフェンの生成・応用

- 2-6 大気圧 CVD グラフェン合成における高圧アニールの影響 30
○鈴木 誠也, 永守 孝至, 松岡 佑樹, 吉村 雅満
- 2-7 Electronic structure of potassium doped MoS_2 31
○Nguyen Thanh Cuong, Minoru Otani, Susumu Okada
- 2-8 高熱・電気伝導性を持つナノグラフェンプレートレット/エポキシ樹脂複合材料 32
○アフシン エブラヒミ, 鈴木 慎悟, 澤谷 清一, 上野 真孝, 宮本 典彦, 飯田 勝康

☆☆☆☆☆☆ 昼食 (12:15-13:30) ☆☆☆☆☆☆

若手奨励賞表彰式 (13:30-13:45)

総会 (13:45-14:15)

8月6日(火)

基調講演 (14:15-15:00)

- 2S-4 Separation of Single-Wall Carbon Nanotubes using Gel Column Chromatography 4
片浦弘道

一般講演 (15:00-15:45)

金属内包フラーレン

- 2-9 $\text{Sc}_3\text{C}_2@\text{C}_{80}$ の紫外光電子スペクトル 33
○宮崎 隆文, 大北 壮祐, 財満 壮晋, 西 龍彦, 沖本 治哉, 泉 乃里子, 中西 勇介, 八木 創, 篠原 久典, 日野 照純
- 2-10 リチウム内包フラーレン溶液のイオン伝導度測定と電気化学的手法によるリチウム内包フラーレンラジカルアニオンの合成 34
○上野 裕, 小久保 研, 大久保 敬, 伊熊 直彦, 森山 広思, 福住 俊一, 大島 巧
- 2-11 Chemical Modifications of Lithium-Ion-Encapsulated [60]fullerene $[\text{Li}^+@\text{C}_{60}(\text{CpH})]\text{PF}_6^-$ and $[\text{Li}^+@\text{C}_{60}(\text{CPh}_2)]\text{PF}_6^-$ 35
○川上 裕貴, 岡田 洋史, 松尾 豊

☆☆☆☆☆☆ 休憩 (15:45-16:00) ☆☆☆☆☆☆

ポスタープレビュー (16:00-16:45)

ポスターセッション (16:45-18:15)

★ … 若手奨励賞候補者

グラフェンの生成

- 2P-1 二成分金属触媒によるグラフェンの層数制御 83
★ ○竹崎 悠一郎
- 2P-2 アモルファスカーボンの加熱による絶縁基板上へのグラフェンの直接成長 84
★ ○長谷部 洋平, 中原 仁, 安坂 幸師, 齋藤 弥八
- 2P-3 構造制御されたグラフェンと h-BN のヘテロ接合シートの合成 85
○前田 枝里子, 宮田 耕充, 北浦 良, 篠原 久典
- 2P-4 グラフェンナノリボン上のグラフェン成長における成長速度減少 86
○Haruki Kitakawa, Ryota Negishi, Hirofumi Tanaka, Minoru Fukumori, Takuji Ogawa, Yoshihiro Kobayashi
- 2P-5 急速加熱プラズマ CVD におけるグラフェン及びグラフェンナノリボンの成長機構 87
○鈴木 弘朗, 加藤 俊顕, 金子 俊郎
- 2P-6 eDIPS 法による SWCNTs 合成における窒素含有化合物添加の効果 88
○大森 滋和, 清宮 維春, 平井 孝佳, 栗原 有紀, 齋藤 毅

ナノホーン

- 2P-7 BNドープしたカーボンナノホーン集合体の作製と構造特性 89
○弓削 亮太, 眞子 隆志, 坂東 俊治, 湯田坂 雅子, 當山 清彦, 山口 貴司, 中原 謙太郎

8月6日(火)

2P-8	放射性同位元素ラベルしたカーボンナノホーンのマウス体内動態イメージング ○張 民芳, ジヤシム ヒファー, スネス アントニオ, メナードムヤン セシラ, ビアンコ アルベルト, 飯島 澄男, 湯田坂 雅子, コスタイラス コスタス	90
2P-9	Electrical resistance measurement of single carbon nanocoil ○國本 隆司, 米村 泰一郎, 須田 善行, 田上 英人, 滝川 浩史, 植 仁志, 清水 一樹, 梅田 良人	91
2P-10	多相交流アークプラズマによるフラーレンの効率的生成 ○佐野 弘, 中屋 亮二, 真木 教雄, 芦原 将彰, 真柄 宏之, 上野 幹広, 竹内 雅則, 佐治 栄治	92
ナノチューブの物性		
2P-11	架橋された孤立カーボンナノチューブの高効率合成と構造および光学特性 ★ ○Sihan Zhao, Tomoya Kitagawa, Yuhei Miyauchi, Kazunari Matsuda, Hisanori Shinohara, Ryo Kitaura	93
2P-12	超軽量カーボンナノチューブ繊維の信頼できる比強度の算出法 ★ ○西坂 光, 佐藤 義倫, 本宮 憲一, 田路 和幸	94
2P-13	ゲルに固定化した超微小径カーボンナノチューブのガス吸着特性 ★ ○犬飼 恵理, 宮田 耕充, 北浦 良, 篠原 久典	95
2P-14	走査ゲート顕微法による SWNT ネットワーク FET 内に形成された量子ドットでのクーロンブロックード ★ 現象の評価 ○松永 正広, 魏 小均, 前田 賢治, 矢萩 達朗, Jonathan P. Bird, 石橋 幸治, 落合 勇一, 青木 伸之	96
2P-15	酸素雰囲気下での単層カーボンナノチューブと有機硫黄化合物のカイラリティ選択的光反応における ★ 反応機構研究 ○天谷 優里, 前田 優, 大久保 敬, 福住 俊一, 山田 道夫, 長谷川 正, 赤阪 健	97
2P-16	カーボンナノチューブの X 線照射欠陥における熱アニール効果 ○松田 充晃, 山本 勇樹, 村上 俊也, 木曾田 賢治, 伊東 千尋	98
2P-17	SiC 表面分解法により作製した CNT/n型 4H-SiC 界面の電気的特性と電子構造 ○矢嶋 孝敏, 野本 豊和, 丸山 隆浩	99
2P-18	SWNT の表面増強ラマン散乱スペクトルを用いたレーザー照射された金属ナノ構造の局所温度上昇 測定 ○保田 諭	100
2P-19	単層カーボンナノチューブの赤外吸収スペクトルにおける紫外線、X 線、電子線照射効果 ○市田 正夫, 宮田 耕充, 伊東 千尋, 村上 俊也, 池本 夕佳, 川上 彰, 柳 和宏, 片浦 弘道, 安藤 弘明	101
2P-20	Charge transfer between polyoxometalates and SWNTs by means of photoluminescence spectroscopy ★ ○Liu Hong, Naotoshi Nakashima	102
フラーレンの化学		
2P-21	シクロパラフェニレンカチオンラジカルの超微細構造定数の決定 ★ ○香山 貴彦, 茅原 栄一, 山子 茂, 加藤 立久	103
2P-22	Photoinduced Charge Separation in Supramolecules between $\text{Li}^+@C_{60}$ and Chlorins ○川島 雄樹, 大久保 敬, 福住 俊一	104

8月6日(火)

- 2P-23 窒素内包フラーレン $N@C_n$ の超微細結合定数のサイズ依存性 105
○若林 知成, 金本 達也, 今村 隆希
- 2P-24 溶解性の高いフラーレン-ペンタセン付加体の合成、構造、および性質 106
○西濱 拓也
- 2P-25 $H_2O@C_{60}$ の固体反応ならびに[2+2]型二量体の X 線構造 107
★ ○張 銳, 村田 理尚, 若宮 淳志, 村田 靖次郎
- 2P-26 Photoinduced electron transfer in a porous organic salt composed of 9-(4-sulfophenyl)anthracene and triphenylmethylamine and fullerene. 108
○長谷川 哲也, 大久保 敬, 藤内 謙光, 久木 一朗, 宮田 幹二, 福住 俊一
- 2P-27 マルチアリアル化フラーレンのナノコンポジットポリマーの熱安定性評価 109
○高橋 遼, 小久保 研, 原田 昭夫, 伊熊 直彦, 大島 巧
- 2P-28 C_{60} regeneration by oxidative deamination of azafulleroids with peracids and substituent effects of azafulleroids 110
○藤岡 公一, 伊熊 直彦, 三澤 勇介, 小久保 研, 大島 巧
- 2P-29 C_{62} 異性体からの C_2 脱離における活性化エネルギー 111
○大 長島, 徹 佐藤, 一義 田中
- 2P-30 ペリ共役性フレロトリアゾリウム of one-pot 合成と自己集合性 112
○伊熊 直彦, 稲場 沙織, 小久保 研, 大島 巧
- 2P-31 1-アリル-4-(N-アルキルアミノ)フラーレンの合成と物性 113
○三木江 翼, 佐伯 昭紀, 伊熊 直彦, 小久保 研, 大島 巧, 関 修平
- 2P-32 Thermal Silylation Reactions of C_{60} Using Three-membered Ring Organosilicon Compounds 114
○稲葉 大樹, 飯田 亮介, 加固 昌寛, 長谷川 正, 前田 優, 山田 道夫, 赤阪 健
- 金属内包フラーレン**
- 2P-33 The density functional theory calculations of $Sc_2C_2@C_{82}$ 115
○清野 友真, 日石 孝宏, 八木 創, 宮崎 隆文, 日野 照純
- 2P-34 $Er_3N@C_{80}$ の光電子分光 116
○日石 孝宏
- 2P-35 Definite molecular structures of $M@C_{2v}(9)-C_{82}$ ($M = Sc, Y, \text{ and } Ce$) 117
★ ○鈴木 光明, Slanina, Zdenek, 溝呂木 直美, Lu, Xing, 山田 道夫, 前田 優, 長谷川 正, 永瀬 茂, Olmstead, Marilyn, Balch, Alan, 赤阪 健
- 2P-36 溶解度向上を志向した新規 $[Li^+@C_{60}]$ 塩の合成 118
○岡田 洋史, 松尾 豊
- 2P-37 リチウムと C_{60} フラーレンより形成されるクラスターの固体 LiNMR を用いた解析 119
○遠藤 智明

☆☆☆☆☆☆ 懇親会 (18:30-20:30) ☆☆☆☆☆☆
豊中福利会館・4 階食堂

8月7日(水)

特別講演 発表 25 分・質疑応答 5 分
一般講演 発表 10 分・質疑応答 5 分
ポスタープレビュー 発表 1 分・質疑応答なし

特別講演 (9:00-9:30)

3S-5 Low-energy electron microscopy study of graphene growth 5
日比野 浩樹

一般講演 (9:30-10:15)

グラフェンの物性

3-1 Tuning the Chemical Reactivity of Graphene by Mechanical Strain 36
○Mark A. Bissett, Satoru Konabe, Susumu Okada, Masaharu Tsuji, Hiroki Ago

3-2 グラフェンおよびシリセン複合膜の電子構造と安定性 37
○斎藤 晋, 是常 隆

3-3 単層遷移金属ダイカルコゲナイドにおけるバレーに依存した励起子多体効果 38
○小鍋 哲, 岡田 晋

特別講演 (10:15-10:45)

3S-6 高性能デバイス応用に向けたグラフェンナノリボンの超精密集積合成 6
加藤 俊頭

☆☆☆☆☆☆ 休憩 (10:45-11:00) ☆☆☆☆☆☆

特別講演 (11:00-11:30)

3S-7 Ultrahigh-density data storage using C_{60} molecules 7
中谷 真人

一般講演 (11:30-12:30)

フラーレンの化学, 応用

3-4 水酸化フラーレンナノシート・ナノ粒子の形態制御と物性 39
○佐野 喜章, 馬場 啓輔, 緒方 啓典

3-5 オクタブロモフラーレン $C_{60}Br_8$ の置換反応による新規オクタアルコキシフラーレン $C_{60}(OR)_8$ およびオクタアールフラーレン $C_{60}(4-MeOC_6H_4)_8$ の選択的合成 40
○内山 幸也, 森山 広思, 与座 健治

3-6 フラレノールとその誘導体の選択的合成; $C_{60}(OH)_5X$ と $C_{60}(OSiMe_3)_5X$ ($X = Cl, Br$) 41
○五十嵐 望紀, 山本 翔平, 上野 裕, 与座 健治, 森山 広思

3-7 $H_2O@C_{60}$ の結晶構造と誘電的性質 42
○青柳 忍, 星野 哲久, 芥川 智行, 北浦 良, 篠原 久典, 杉本 邦久, Zhang Rui, 村田 靖次郎

☆☆☆☆☆☆ 昼食 (12:30-13:45) ☆☆☆☆☆☆

8月7日(水)

特別講演 (13:45-14:15)

- 3S-8 ナノ炭素材料の水溶化、サイズ分離と生物医療応用 8
小松 直樹

一般講演 (14:15-15:00)

ナノチューブの生成と精製

- 3-8 実験・理論両面からみた(6,5)チューブ成長の考察 43
○阿知波 洋次, 兒玉 健, 橋本 健朗, 城丸 春夫, 岡崎 俊也
- 3-9 Bis(tert-butylpyrene) nanotweezers and nanocalipers: Enhanced extraction and recognition abilities for single-walled carbon nanotubes 44
○劉 剛, Rahman A. F. M. Mustafizur, 木村 隆英, 小松 直樹
- 3-10 単層カーボンナノチューブフォレスト成長を可能にするガス種の多様性 45
○木村 寛恵

☆☆☆☆☆☆ 休憩 (15:00-15:15) ☆☆☆☆☆☆

ポスタープレビュー (15:15-16:00)

ポスターセッション (16:00-17:30)

★ … 若手奨励賞候補者

グラフェンの応用

- 3P-1 ポリマーのグラフト化により修飾した酸化グラフェンの調製と特性 120
○住吉 徹雄, 永田 和寛, 八木 八木, 藤木 一浩, 山内 健
- 3P-2 Hybrid Graphene-Titanium Surface for Sensing Applications 121
○Kakimi Yousuke, Rius Gemma, Eryu Osamu
- 3P-3 トリス緩衝溶液中でのグラフェンの化学ドーピングにおける基板の影響 122
増田 祥也, ○佐野 正人
- 3P-4 Anomalous behavior of Raman signals from carbon nanotube-graphene hybrid structures 123
○楠本 太郎, 小亀 平章, 根岸 良太, 小林 慶裕
- 3P-5 Synthesis and characterization of Pt-Ru nanoparticles on carbon nanosheets by one-step electrodeposition 124
○Hayase Shohei
- 3P-6 Suppressed mobility degradation in large-area graphene oxide films by alcohol vapor treatments 125
○松崎 通弘, 根岸 良太, 大野 恭秀, 前橋 兼三, 松本 和彦, 小林 慶裕
- 3P-7 ポリグリセロール修飾によるグラフェンの水溶化 126
★ ○保田 徳, 趙 利, 劉 剛, 青沼 秀児, 木村 隆英, 小松 直樹

グラフェンの物性

- 3P-8 フラーレン-グラフェンおよびフラーレン-ナノチューブ-グラフェン複合体の形成 127
○梅山 有和, 白 鎮碩, 手塚 記庸, 森田 和樹, 今堀 博
- 3P-9 SiC 基板上に成長したグラフェン薄膜層数のラマン分光法による評価 128
○中原 仁, 前田 大輔, 齋藤 弥八

8月7日(水)

3P-10	5員環からなる2次元 sp^2 炭素結晶の電子構造	129
★	○丸山 実那, 岡田 晋	
3P-11	グラフェンとナノチューブの G'バンドのフェルミエネルギー依存性	130
	○佐藤 健太郎, 齋藤 理一郎	
3P-12	電界下におけるグラフェンの電子物性	131
★	○山中 綾香, 岡田 晋	
3P-13	超伝導グラフェンにおける集団励起	132
	○猪谷 太輔, 大橋 洋士, 岡田 晋	
その他		
3P-14	熱処理による酸化鉄ナノチューブの構造変化	133
	○坂東 俊治, 白木 勇喜	
3P-15	カーボンナノコイルの高収率化に向けた合成条件の改善	134
	○丸山 皓司, 須田 善行, 田上 英人, 滝川 浩史, 植 仁志, 清水 一樹, 梅田 良人	
3P-16	カーボンナノコイルの電磁波吸収特性	135
	○加藤 諒, 安富 進悟, 須田 善行, 田上 英人, 滝川 浩史, 植 仁志, 清水 一樹, 梅田 良人, 江口 宇三郎	
3P-17	カーボンナノコイルのばね定数測定	136
★	○米村 泰一郎, 須田 善行, 田上 英人, 滝川 浩史, 植 仁志, 清水 一樹, 梅田 良人	
3P-18	In-situ observation of carbon nanocoil growth by optical microscope	137
	○郷原 丈弘, 有江 隆之, 秋田 成司	
3P-19	単層 WSe ₂ 膜における電界誘起 p-n 接合	138
★	○清水 諒, 蒲 江, 張 奕勁, 岩佐 義宏, 竹延 大志	
3P-20	MoS ₂ の光学特性の層数依存性	139
★	○小川 泰徳	
ナノチューブの応用		
3P-21	炭素繊維で修飾したダイヤモンド微粒子の合成	140
	○木村 和, 藤木 一浩, 山内 健, 坪川 紀夫	
3P-22	Synthesis of ordered carbon nanotube network using pillar molecules	141
	○Tashiro Kosuke, Song Hayong, Ishii Yosuke, Kawasaki Shinji	
3P-23	Carbon nanotubes functionalized with carboxylic acid dispersed in 3D polymeric microstructures	142
	○A. J. G. Otuka, V. Tribuzi, D. S. Correa, A. R. Zanatta, C. R. Mendonca	
3P-24	極少量の高配向 CNT を含有させた高機能フッ素樹脂	143
	○三好 健太郎, 矢嶋 尊, 坂井 徹, 豊田 真沙美, 中山 喜萬	
3P-25	カーボンナノチューブヒータ表面に担持したシリコンナノ粒子の炭素との反応その場 TEM 観察	144
	○安坂 幸師, 寺田 朋広, 齋藤 弥八	
3P-26	大電流制御可能なカーボンナノチューブフォレストを用いた液体ゲート FET	145
	○明道 三穂	

8月7日(水)

- 3P-27** 半導体単層カーボンナノチューブ/Si ヘテロ接合太陽電池における太陽電池特性の制限要因について 146
○中野 陸, 緒方 啓典
- 3P-28** 単層カーボンナノチューブ対極の構造が色素増感太陽電池に与える影響 147
○千葉 孝昭, 木下 英典, 崔 可航, エイナルソン エリック, 千足 昇平, 丸山 茂夫
- 3P-29** Fabrication of flexible and transparent capacitance-type touch panel with single-walled carbon nanotubes based on simple transfer process 148
○深谷 徳宏, 岸本 茂, 野田 優, 大野 雄高
- 内包ナノチューブ**
- 3P-30** Charge state of capsule prepared by coalescence of $\text{Sc}_3\text{N}@C_{80}$ molecules in a carbon nanotube 149
★ ○米谷 祐輝, Ahmadreza Fallah Gilvaei, 千賀 亮典, 平原 佳織, 北浦 良, 篠原 久典, 中山 喜萬
- 3P-31** C_{60} を内包した[n]シクラセンの生成過程のエネルギー論 150
★ ○木暮 聖太, 岡田 晋
- ナノ炭素粒子**
- 3P-32** 異なる種類の炭素担体による触媒ナノ微粒子の触媒活性効果 151
○尾崎 公洋, 須田 善行, 滝川 浩史, 田上 英人, 植 仁志, 清水 一樹
- 3P-33** 窒素ガス中衝突反応による炭素ナノカプセルと袋状ナノ炭素の合成 152
○三重野 哲, 近藤 和彦, 長谷川 直, 黒澤 耕介
- 3P-34** LaC_2 内包カーボンナノカプセル酸化過程での LaCO_3OH の生成 153
○山本 和典, 山口 憲司, 社本 真一, 赤阪 健
- 3P-35** カーボンナノバルーンの酸化による電気二重層キャパシタの比容量向上 154
★ ○岡部 雄太, 須田 善行, 滝川 浩史, 田上 英人, 植 仁志, 清水 一樹

August 5, Mon.

Special Lecture	25 min (Presentation) + 5 min (Discussion)
General Lecture	10 min (Presentation) + 5 min (Discussion)
Poster Preview	1 min (Presentation)

General Lectures (9:30-10:45)

Properties of Nanotubes

1-1	The mechanism and ability of SW/DWCNT adsorbing radioactive elements in the environment ○Takumi Araki, Syogo Tejima, Hisashi Nakamura, Bunshi Fugetsu, Morinobu Endo	9
1-2	Photoluminescence from dried hybrids of double-stranded DNA and single-walled carbon nanotubes ○Masahiro Ito, Yusuke Ito, Tomoki Kobayashi, Takuya Hayashida, Daisuke Nii, Kazuo Umemura, Yoshikazu Homma	10
1-3	Raman study on X-ray induced defect and its structure in carbon nanotube ○Toshiya Murakami, Yuki Yamamoto, Mitsuki Matsuda, Kenji Kisoda, Chihiro Itoh	11
1-4	Photoluminescence Nonlinearity of Hole-doped Single-walled Carbon Nanotubes ○Naoto Akizuki, Shinichiro Mouri, Yuhei Miyouchi, Kazunari Matsuda	12
1-5	Thermopower in Highly Purified Semiconducting Single-Wall Carbon Nanotube Buckypaper ○Yusuke NAKAI, Kazuya HONDA, Yasumitsu MIYATA, Kazuhiro YANAGI, Yutaka MANIWA	13

☆☆☆☆☆☆ Coffee Break (10:45-11:00) ☆☆☆☆☆☆

Special Lecture (11:00-11:30)

1S-1	Flexible and stretchable carbon nanotube thin-film transistors and integrated circuits Yutaka Ohno	1
------	---	---

General Lectures (11:30-12:15)

Application of Nanotubes

1-6	Diameter-Dependent Threshold Voltages of Carbon Nanotube Thin-Film Transistors ○Fumiyuki Nihey, Yuta Kikuchi, Fusako Sasaki, Kazuki Ihara, Hideaki Numata, Yuki Kuwahara, Shigekazu Ohmori, Takeshi Saito	14
1-7	Development of compounded foil of carbon nanotube and sputter-deposition carbon ○Hiroo Hasebe, Hironori Kuboki, Hiroki Okuno, Isao Yamane, Hiroshi Imao, Nobuhisa Fukunishi, Masayuki Kase, Osamu Kamigaito	15
1-8	Immunoassay with Single-Walled Carbon Nanotubes as Near-Infrared Fluorescent Labels ○Yoko Iizumi, Toshiya Okazaki, Yuzuru Ikehara, Mutsuo Ogura, Masako Yudasaka	16

☆☆☆☆☆☆ Lunch (12:15-13:30) ☆☆☆☆☆☆

General Lectures (13:30-14:30)

Applications of Nanotubes, Endohedral Nanotubes

1-9	Highly Conductive CNT/Polymer Composite on Arbitrary Rubber Matrices Based on Thermodynamics ○Seisuke Ata, Howon Yoon, Chandramouli Subramaniam, Takaaki Mizuno, Takeo Yamada, Kenji Hata	17
-----	--	----

August 5, Mon.

- 1-10 Thermally conductive SG-CNT-Cu composite with low thermal expansion 18
○Yuzuri Yasuda, Chandramouli Subramaniam, Seisuke Ata, Motoo Yumura, Takeo Yamada, Don N. Futaba, Kenji Hata
- 1-11 Metallization of 1D sulfur crystals inside carbon nanotubes 19
○Toshihiko Fujimori, Aaron Morelos-Gomez, Zhen Zhu, Hiroyuki Muramatsu, Ryusuke Futamura, Koki Urita, Mauricio Terrones, Takuya Hayashi, Morinobu Endo, David Tomanek, Katsumi Kaneko
- 1-12 Structure and electronic properties of π -conjugated polymers formed in carbon nanotubes 20
○Kenshi Miyaura, Yasumitsu Miyata, Ryo Kitaura, Hisanori Shinohara

☆☆☆☆☆☆ Coffee Break (14:30-14:45) ☆☆☆☆☆☆

Special Lecture (14:45-15:15)

- 1S-2 Symmetric carbon nanostructures produced from organometallic compounds 2
Hidetsugu Shiozawa

General Lectures (15:15-16:15)

Nanohorn, Carbon Nanoparticles, Environmental/Safety Characterization of Nanomaterials and the Others

- 1-13 Effect of functional groups on encapsulation of functionalized C_{60} molecules inside carbon nanohorns 21
○Keita Kobayashi, Hiroshi Ueno, Ken Kokubo, Hidehiro Yasuda
- 1-14 Photoinduced Reaction of Polyyne Derivatives and Iodine Molecules in Solution 22
○Yoriko Wada, Tomonari Wakabayashi
- 1-15 Lysosomal membrane permeabilization induced by carbon nanohorns caused reactive oxygen species generation and apoptosis in RAW264.7 cell 23
○Mei Yang, Minfang Zhang, Yoshio Tahara, Sumio Iijima, Masako Yudasaka
- 1-16 Development of Ion Mobility Measurement System 24
○Toshiki Sugai, Yasuhiro Hiroshiba, Ninako Mikami

Poster Preview (16:15-17:00)

Poster Session (17:00-18:30)

★: Candidates for the Young Scientist Poster Award

Formation and Purification of Nanotubes

- 1P-1 Bottom-up synthesis and structures of π -lengthened finite single-wall carbon nanotube molecules 47
★ ○Matsuno Taisuke, Kamata Sho, Hitosugi Shunpei, Isobe Hiroyuki
- 1P-2 Initiation of carbon nanotube growth by well-defined carbon nanorings 48
★ ○Yasutomo Segawa, Haruka Omachi, Takuya Nakayama, Eri Takahashi, Kenichiro Itami
- 1P-3 Post-annealing effect on single-wall carbon nanotubes prepared by PG-ACCVD technique 49
Ito Yosuke, ○Suzuki Shinzo, Nagasawa Hiroshi, Ono Akira, Achiba Yohji
- 1P-4 String-like Assembly of Aligned Single-Wall Carbon Nanotubes in a Single-Chiral State 50
Hideki Kawai, ○Kai Hasegawa, Toru Nakatsu, Yasuhisa Naitou, Yuki Takagi, Yoshihumi Wada, Taishi Takenobu, Kazuhiro Yanagi

August 5, Mon.

1P-5	Elucidation of the Chirality Control of Single-Walled Carbon Nanotube by Irradiating Free Electron Laser during Growth ○Keisuke Yoshida	51
1P-6	SWCNT adsorption onto hydrogels is affected by solute and pH value ○Atsushi Hirano, Yasuko Urabe, Hiromichi Kataura, Takeshi Tanaka	52
1P-7	Effect of Catalytic Elements to the Growth of Nano-Carbon Composite Films ○Yuki Matsuoka, Masamichi Yoshimura	53
1P-8	Fabrication of in-plane Aligned and Semiconducting as-grown Single-Walled Carbon Nanotubes ○Nobuyuki Iwata, Takumi Sagara, Yusaku Tsuda, Keisuke Yoshida, Koji Ishii, Hirofumi Yajima, Hiroshi Yamamoto	54
1P-9 ★	Enrichment of 1.1 nm-diameter single-wall carbon nanotubes by high-temperature gel filtration ○Ryota Ichimura, Yasumitsu Miyata, Yusuke Nakai, Kazuhiro Yanagi, Yutaka Maniwa	55
1P-10	Low-temperature single-walled carbon nanotubes synthesis from Pt catalysts in the alcohol gas source method and its growth mechanism ○Hiroki Kondo, Ranajit Ghosh, Shigeo Naritsuka, Takahiro Maruyama, Sumio Iijima	56
1P-11	Purification of Single-Walled Carbon Nanotubes by Applying Photochemical Reaction of an Ionic Organic Molecule ○Yoko Matsuzawa, Yuko Takada, Tetsuya Kodaira, Hideyuki Kihara, Masaru Yoshida	57
1P-12	“Frost column like CNTs” growth by thin Ni catalyst films ○Yuji Kusumoto, Kazuki Sekiya, Hirofumi Koji, Hiroshi Furuta, Akimitsu Hatta	58
1P-13	Diameter Distribution of Single-Walled Carbon Nanotubes from Nanodiamond Particles as the Catalysts for CVD Growth ○Takanori Umino, Taiki Inoue, Shohei Chiashi, Yoshikazu Homma, Shigeo Maruyama	59
1P-14	Improved efficiency in metal-free carbon nanotube growth from nanodiamonds by switching growth driving force ○Hiraaki Kokame, Kazuki Fujimoto, Ryota Negishi, Tatsuji Arifuku, Noriko Kiyoyanagi, Yoshihiro Kobayashi	60
1P-15	Molecular Dynamics Simulation of SWNT Growth and DFT Calculation of the Chemical Reaction of Ethanol and Cobalt Clusters ○Kaoru Hisama	61
1P-16 ★	Chirality Analysis of Horizontally Aligned Single-Walled Carbon Nanotubes by Raman Spectroscopy ○Taiki Inoue, Daisuke Hasegawa, Shohei Chiashi, Shigeo Maruyama	62
1P-17	Growth kinetics of narrow-chirality distributed single-walled carbon nanotube under pulse plasma CVD ○Bin Xu	63

Properties of Nanotubes

1P-18	Optical properties of vertically aligned CNT forests formed at various growth temperature ○Hiroshi Furuta, Kazuki Sekiya, Keisuke Takano, Masanori Hangyo, Akimitsu Hatta	64
1P-19	Deleted.	

August 5, Mon.

1P-20	Coherent phonon spectroscopy of semiconducting single-wall carbon nanotubes ○Yuki Honda, Elizabeth Maret, Atsushi Hirano, Takeshi Tanaka, Kotaro Makino, Muneaki Hase	65
1P-21	Interplay of wall number and diameter on the electrical conductivity of carbon nanotube thin films ○Guohai Chen, Don Futaba, Shunsuke Sakurai, Motoo Yumura, Kenji Hata	66
1P-22	Effect of lattice vibration on the geometry of carbon nanotubes ○Takashi Koretsune, Koichiro Kato, Susumu Saito	67
1P-23	Temperature Dependence of Stokes and anti-Stokes photoluminescence from oxygen-doped carbon nanotubes ○Yuhei Miyaochi, Naoto Akizuki, Munechiyo Iwamura, Shinichiro Mouri, Kazunari Matsuda	68

Applications of Nanotubes

1P-24 ★	Highly Sensitive Detection of Oxygen Gas by Perovskite Materials Decorated Single-Walled Carbon Nanotubes ○Fukuda Hiroshi	69
1P-25	Gas Sensing using Semiconducting Single-Walled Carbon Nanotubes Thin Film ○Suzuki Yuto	70
1P-26 ★	Interaction between Carbon Nanotubes and Neurons Studied With High-Density Microelectrode Arrays ○Florent Seichepine, Kosmas Deligkaris, Urs Frey	71
1P-27	Oxygen Reduction Reaction of Nitrogen-doped Graphitic Structure Using Single-walled Carbon Nanotubes as a Catalyst Support Junich Morita,○Tsuyohiko Fujigaya, Naotoshi Nakashima	72
1P-28 ★	Air-Stable High-Efficiency Nanotube-Si Heterojunction Solar Cells ○Kehang Cui	73
1P-29 ★	Influence of dispersion state of long SWCNTs on the electrical conductivity of composites ○Howon Yoon, Seisuke Ata, Takeo Yamada, Motoo Yumura, Kenji Hata	74

Applications of Fullerenes

1P-30	Fabrication and characterization of inverted-type organic thin-film solar cells using [60] fullerene-diamine assembly films ○Banya Shoto, Matsumoto Taisuke, Oku Takeo, Akiyama Tsuyoshi	75
1P-31	Synthesis and evaluation of spiro-acetalized [60]fullerene toward organic photovoltaic devices ○Masuda Hiroyuki, Kokubo Ken, Ikuma Naohiko, Tsubasa Mikie, Saeki Akinori, Seki Shu, Oshima Takumi	76
1P-32	Preparation and microscopic analysis of fullerene-diamine adducts as organic electronic material ○Yuji Ono, Tsuyoshi Akiyama, Takeo Oku	77
1P-33	The electrical transport properties of photo-polymerization of C ₆₀ thin film using focused optical vortex ○Wataru Akiyama, Daiki Momiyama, Naoto Toriumi, Katsuhiko Miyamoto, Takashige Omatsu, Jonathan Bird, Yuichi Ochiai, Nobuyuki Aoki	78
1P-34	Efficiency improvement of PTB7:PC71BM organic solar cells by inserting LiF cathode buffer layer ○Shunjiro Fujii, Tatsuki Yanagidate, Masaya Ohzeki, Yuichiro Yanagi, Yuki Arai, Takanori Okukawa, Akira Yoshida, Takeshi Tanaka, Yasuhiro Nishioka, Hiromichi Kataura	79

August 5, Mon.

- 1P-35** Energetics and Electronic Structure of C₆₀ doped Bulk Si 80
○Okada Susumu
- 1P-36** Synthesis and Characterization of Fullerene Derivatives with a Thiophene Moiety in Organic Photovoltaic Devices 81
○Tatsuya Hayashi, Jaebuem Oh, Haeseong Lee, JongJun Ann, HeeJae Lee, Jin Jang, Chyongjin Pac, Hiroshi Moriyama
- 1P-37** Structural Effect of Fullerene Derivatives with a Cyano Group in Organic Photovoltaic Devices 82
○Kana Matsumoto, Jaebuem Oh, Haeseong Lee, JongJun Ann, HeeJee Lee, Jin Jang, Chyongjin Pac, Hiroshi Moriyama

August 6, Tue.

Plenary Lecture	40 min (Presentation) + 5 min (Discussion)
Special Lecture	25 min (Presentation) + 5 min (Discussion)
General Lecture by Candidate for Osawa Award and Iijima Award	10 min (Presentation) + 10 min (Discussion)
General Lecture	10 min (Presentation) + 5 min (Discussion)
Poster Preview	1 min (Presentation)

General Lectures by Candidates for Osawa Award (9:00-9:40)

- 2-1 Enhanced photoelectrochemical performance of composite photovoltaic cells of Li⁺@C₆₀/sulfonated porphyrin supramolecular nanoclusters 25
OKei Ohkubo, Yuki Kawashima, Hayato Sakai, Taku Hasobe, Shunichi Fukuzumi
- 2-2 Surface functionalization of nanodiamonds towards high solubility in physiological media and practical biomedical applications 26
OZhao Li, Chen Xiao, Chano Tokuhiko, Komatsu Naoki

General Lectures by Candidates for Iijima Award (9:40-10:40)

- 2-3 Carbon Nanotubes Growth via Twisted Graphene Nanoribbons 27
OHong En Lim, Yasumitsu Miyata, Ryo Kitaura, Yoshifumi Nishimura, Yoshio Nishimoto, Stephan Irle, Jamie H. Warner, Hiromichi Kataura, Hisanori Shinohara
- 2-4 Highly Durable Polymer Electrolyte Fuel Cell Electrocatalyst Based on Carbon Nanotube 28
OTsuyohiko Fujigaya, Naotoshi Nakashima
- 2-5 Stabilities and Electronic Structures of Carbon Impurities in Hexagonal Boron-Nitride Monolayers and Bilayers 29
OYoshitaka Fujimoto, Takashi Koretsune, Susumu Saito

☆☆☆☆☆☆ Coffee Break (10:45-11:00) ☆☆☆☆☆☆

Special Lecture (11:00-11:30)

- 2S-3 Graphene based optoelectronics in the visible spectra 3
Coskun Kocabas

General Lectures (11:30-12:15)

Formation and Applications of Graphene

- 2-6 Effect of High Pressure Pre-Annealing on Graphene Growth on Copper by Chemical Vapor Deposition 30
OSeiya Suzuki, Takashi Nagamori, Yuki Matsuoka, Masamichi Yoshimura
- 2-7 Electronic structure of potassium doped MoS₂ 31
ONguyen Thanh Cuong, Minoru Otani, Susumu Okada
- 2-8 Highly Conductive NGP/Epoxy Composites 32
OAfshin J. Ebrahimi, Suzuki Shingo, Sawatani Seiichi, Ueno Masataka, Miyamoto Norihiko, Iida Masayasu

☆☆☆☆☆☆ Lunch (12:15-13:30) ☆☆☆☆☆☆

August 6, Tue.

Young Scientist Poster Award Ceremony (13:30-13:45)

General Meeting (13:45-14:15)

Plenary Lecture (14:15-15:00)

2S-4 Separation of Single-Wall Carbon Nanotubes using Gel Column Chromatography 4
Hiromichi Kataura

General Lectures (15:00-15:45)

Endohedral Metallofullerenes

2-9 Ultraviolet Photoelectron spectra of $\text{Sc}_3\text{C}_2@\text{C}_{80}$ 33
○Takafumi Miyazaki, Sousuke Ookita, Takeyuki Zaima, Tatsuhiko Nishi, Haruya Okimoto, Noriko Izumi, Yuusuke Nakanishi, Hajime Yagi, Hisanori Shinohara, Shojun Hino

2-10 Electrochemical synthesis of $\text{Li}^+@\text{C}_{60}^-$ based on the high ionic conductivity of $[\text{Li}^+@\text{C}_{60}](\text{PF}_6^-)$ in aromatic solvent 34
○Hiroshi Ueno, Ken Kokubo, Kei Ohkubo, Naohiko Ikuma, Hiroshi Moriyama, Shunichi Fukuzumi, Takumi Oshima

2-11 Chemical Modifications of Lithium-Ion-Encapsulated [60]fullerene $[\text{Li}^+@\text{C}_{60}(\text{CpH})]\text{PF}_6^-$ and $[\text{Li}^+@\text{C}_{60}(\text{CPh}_2)]\text{PF}_6^-$ 35
○Hiroki Kawakami, Hiroshi Okada, Yutaka Matsuo

☆☆☆☆☆☆ Coffee Break (15:45-16:00) ☆☆☆☆☆☆

Poster Preview (16:00-16:45)

Poster Session (16:45-18:15)

★: Candidates for the Young Scientist Poster Award

Formation of Graphene

2P-1 Controlling the number of layers of graphene by binary metal catalyst 83
★ ○Takesaki Yuichiro

2P-2 Direct Growth of Graphene on Insulating Substrates by Annealing of Amorphous Carbon 84
★ ○Yohei Hasebe, Hitoshi Nakahara, Koji Asaka, Yahachi Saito

2P-3 Shape-controlled synthesis of graphene and h-BN heterostructures 85
○Eriko Maeda, Yasumitsu Miyata, Ryo Kitaura, Hisanori Shinohara

2P-4 Decreasing growth rate of graphene layers on graphene nanoribbons 86
○Haruki Kitakawa, Ryota Negishi, Hirofumi Tanaka, Minoru Fukumori, Takuji Ogawa, Yoshihiro Kobayashi

2P-5 Growth mechanism for graphene and graphene nanoribbon under rapid-heating plasma CVD 87
○Hiroo Suzuki, Toshiaki Kato, Toshiro Kaneko

2P-6 The effect of adding N-containing compounds on the eDIPS-CVD synthesis of SWCNTs 88
○Shigekazu Ohmori, Masaharu Kiyomiya, Takayoshi Hirai, Yuki Kuwahara, Takeshi Saito

August 6, Tue.

Nanohorn

- 2P-7** Preparation and structural properties BN-doped carbon nanohorn aggregates 89
○Ryota Yuge, Takashi Manako, Shunji Bandow, Masako Yudasaka, Kiyohiko Toyama, Takashi Yamaguchi, Kentaro Nakahara
- 2P-8** Dynamic whole-body imaging of radiolabelled carbon nanohorns in mice 90
○Minfang Zhang, Dhifaf Jasim, Antonio Nunes, Cécilia Ménard-Moyon, Alberto Bianco, Sumio Iijima, Masako Yudasaka, Kostas Kostarelos
- 2P-9** Electrical resistance measurement of single carbon nanocoil 91
○Ryuji Kunimoto, Taiichiro Yonemura, Yoshiyuki Suda, Hideto Tanoue, Hirofumi Takikawa, Hitoshi Ue, Kazuki Shimizu, Yoshito Umeda
- 2P-10** Efficient synthesis of fullerenes in multi-phase ac arc plasma 92
○Hiroshi Sano, Ryoji Nakaya, Norio Maki, Masaaki Ashihara, Hiroyuki Magara, Mikihiro Ueno, Masanori Takeuchi, Eiji Saji

Properties of Nanotubes

- 2P-11** Direct CVD Synthesis of Suspended Double-walled Carbon Nanotubes and Their Characterization by 93
★ TEM and Optical Spectroscopy
○Sihan Zhao, Tomoya Kitagawa, Yuhei Miyauchi, Kazunari Matsuda, Hisanori Shinohara, Ryo Kitaura
- 2P-12** Evaluation method of reliable specific strength of ultra-light MWCNT fiber based on uncertainty 94
★ ○Hikaru Nishizaka, Yoshinori Sato, Kenichi Motomiya, Kazuyuki Tohji
- 2P-13** Gas adsorption properties of gel-immobilized ultrathin carbon nanotubes 95
★ ○Eri Inukai, Yasumitsu Miyata, Ryo Kitaura, Hisanori Shinohara
- 2P-14** Coulomb Blockade Effect at Quantum Dots Formed in SWNTs Network FET Studied via Scanning 96
★ Gate Microscopy
○Masahiro Matsunaga, Xiaojun Wei, Kenji Maeda, Taturou Yahagi, Jonathan P. Bird, Koji Ishibashi, Yuichi Ochiai, Nobuyuki Aoki
- 2P-15** Mechanistic Studies on the Helicity-Selective Photoreaction of Single-Walled Carbon Nanotubes with 97
★ Organosulfur Compounds in the Presence of Oxygen
○Yuri Amagai, Yutaka Maeda, Kei Ohkubo, Shunichi Fukuzumi, Michio Yamada, Tadashi Hasegawa, Takeshi Akasaka
- 2P-16** Thermal annealing effect of X-ray irradiation defect in carbon nanotube 98
○Mitsuaki Matsuda, Yuki Yamamoto, Toshiya Murakami, Kenji Kisoda, Chihiro Itoh
- 2P-17** Electric and electronic properties of CNT/n-type 4H-SiC interface formed by surface decomposition 99
of SiC
○Takatoshi Yajima, Toyokazu Nomoto, Takahiro Maruyama
- 2P-18** Precise Probing of Local Thermal Elevation of Metal Nanostructure during Laser Illumination 100
Utilizing Surface-enhanced Raman Scattering from a Single-Walled Carbon Nanotube
○Satoshi Yasuda, Hideki Nabika, Mai Takase, Shinji Hoshina, Masanobu Nara, Ryukou Shito
- 2P-19** UV, X-ray and e-beam irradiation effects of IR absorption bands in single-walled carbon nanotubes 101
○Masao Ichida, Yasumitsu Miyata, Chihiro Ito, Toshiya Murakami, Yuka Ikemoto, Akira Kawakami, Kazuhiro Yanagi, Hiromichi Kataura, Hiroaki Ando

August 6, Tue.

- 2P-20 Charge transfer between polyoxometalates and SWNTs by means of photoluminescence spectroscopy 102
★ ○Liu Hong, Naotoshi Nakashima

Chemistry of Fullerenes

- 2P-21 Determination of Hyperfine Coupling Constants of Cycloparaphenylene Cation Radical 103
★ ○Takahiko Koyama, Eiichi Kayahara, Shigeru Yamago, Tatsuhisa Kato
- 2P-22 Photoinduced Charge Separation in Supramolecules between $\text{Li}^+@C_{60}$ and Chlorins 104
○Yuki Kawashima, Kei Ohkubo, Shunichi Fukuzumi
- 2P-23 A trend in the hyperfine constant for the series of $N@C_n$ endofullerenes 105
○Tomonari Wakabayashi, Tatsuya Kanemoto, Ryuki Imamura
- 2P-24 Synthesis, structure, and properties of a highly soluble fullerene-pentacene adduct 106
○Takuya Nishihama
- 2P-25 Solid-State Reaction of $H_2O@C_{60}$ and X-Ray Structure of the [2+2] Dimer 107
★ ○Rui Zhang, Michihisa Murata, Atsushi Wakamiya, Yasujiro Murata
- 2P-26 Photoinduced electron transfer in a porous organic salt composed of 9-(4-sulfophenyl)anthracene and triphenylmethylamine and fullerene. 108
○Tetsuya Hasegawa, Kei Ohkubo, Norimitsu Tohnai, Ichiro Hisaki, Mikiji Miyata, Shunichi Fukuzumi
- 2P-27 Evaluation of Thermal Stability of Nanocomposite Polymers with Multiarylated Fullerenes 109
○Ryo Takahashi, Ken Kokubo, Akio Harada, Naohiko Ikuma, Takumi Oshima
- 2P-28 C_{60} regeneration by oxidative deamination of azafulleroids with peracids and substituent effects of azafulleroids 110
○Koichi Fujioka, Naohiko Ikuma, Yusuke Misawa, Ken Kokubo, Takumi Oshima
- 2P-29 Activation Energies of C_2 Elimination from C_{62} Isomers 111
○Dai Nagashima, Tohru Sato, Kazuyoshi Tanaka
- 2P-30 One-pot Synthesis of Periconjugated Fullerotriazolium and its Aggregation Behavior 112
○Naohiko Ikuma, Saori Inaba, Ken Kokubo, Takumi Oshima
- 2P-31 Synthesis and Properties of 1-Aryl-4-(N-alkylamino)fullerenes 113
○Tsubasa Mikie, Akinori Saeki, Naohiko Ikuma, Ken Kokubo, Takumi Oshima, Shu Seki
- 2P-32 Thermal Silylation Reactions of C_{60} Using Three-membered Ring Organosilicon Compounds 114
○Daiki Inaba, Ryosuke Iida, Masahiro Kako, Tadashi Hasegawa, Yutaka Maeda, Michio Yamada, Takeshi Akasaka

Endohedral Metallofullerene

- 2P-33 The density functional theory calculations of $Sc_2C_2@C_{82}$ 115
○Yuma Seino, Takahiro Hinoishi, Hajime Yagi, Takafumi Miyazaki, Shojun Hino
- 2P-34 Photoelectron spectroscopy of $Er_3N@C_{80}$ 116
○Takahiro Hinoishi
- 2P-35 Definite molecular structures of $M@C_{2v}(9)-C_{82}$ ($M = Sc, Y, \text{ and } Ce$) 117
★ ○Mitsuaki Suzuki, Zdenek Slanina, Naomi Mizorogi, Xing Lu, Michio Yamada, Yutaka Maeda, Tadashi Hasegawa, Shigeru Nagase, Marilyn Olmstead, Alan Balch, Takeshi Akasaka

August 6, Tue.

- 2P-36** Synthesis of new [Li⁺@C₆₀] salts for improved solubility 118
○Hiroshi Okada, Yutaka Matsuo
- 2P-37** Solid State Lithium NMR Studies on Complexes Composed of Lithium and C₆₀ Fullerene 119
○Tomoaki Endo

☆☆☆☆☆ Banquet (18:30-20:30) ☆☆☆☆☆
Toyonaka Fukuri Kaikan (Coop building)・4F Restaurant

August 7, Wed.

Special Lecture	25 min (Presentation) + 5 min (Discussion)
General Lecture	10 min (Presentation) + 5 min (Discussion)
Poster Preview	1 min (Presentation)

Special Lecture (9:00-9:30)

- 3S-5 Low-energy electron microscopy study of graphene growth 5
Hiroki Hibino

General Lectures (9:30-10:15)

Properties of Graphene

- 3-1 Tuning the Chemical Reactivity of Graphene by Mechanical Strain 36
○Mark Bissett, Satoru Konabe, Susumu Okada, Masaharu Tsuji, Hiroki Ago
- 3-2 Stabilities and Electronic Properties of Silicene- and Graphene-based Composite Materials 37
○Susumu Saito, Takashi Koretsune
- 3-3 Valley Dependence of Exciton Many-Body Effects in Monolayer Transition-Metal Dichalcogenides 38
○Satoru Konabe, Susumu Okada

Special Lecture (10:15-10:45)

- 3S-6 Growth of highly-integrated graphene nanoribbon toward high performance device applications 6
Toshiaki Kato

☆☆☆☆☆☆ Coffee Break (10:45-11:00) ☆☆☆☆☆☆

Special Lecture (11:00-11:30)

- 3S-7 Ultrahigh-density data storage using C_{60} molecules 7
Masato Nakaya

General Lectures (11:30-12:30)

Chemistry and Applications of Fullerenes

- 3-4 Morphology control and solid state properties of fullerene nanosheets and nano crystals 39
○Yoshiaki Sano, Keisuke Baba, Hironori Ogata
- 3-5 Selective Synthesis of Novel Octaalkoxyfullerenes $C_{60}(OR)_8$ and Octaarylfullerene $C_{60}(4-MeOC_6H_4)_8$ 40
by a Substitution Reaction of Octabromofullerene $C_{60}Br_8$
○Kouya Uchiyama, Hiroshi Moriyama, Kenji Yoza
- 3-6 Selective Synthesis of Fullerenols and their Derivatives; $C_{60}(OH)_5X$ and $C_{60}(OSiMe_3)_5X$ ($X = Cl, Br$) 41
○Miki Igarashi, Shouhei Yamamoto, Hiroshi Ueno, Kenji Yoza, Hiroshi Moriyama
- 3-7 Crystal Structure and Dielectric Property of $H_2O@C_{60}$ 42
○Shinobu Aoyagi, Norihisa Hoshino, Tomoyuki Akutagawa, Ryo Kitaura, Hisanori Shinohara, Kunihisa Sugimoto, Rui Zhang, Yasujiro Murata

☆☆☆☆☆☆ Lunch (12:30-13:45) ☆☆☆☆☆☆

August 7, Wed.

Special Lecture (13:45-14:15)

- 3S-8 Preparation, size-separation and biomedical application of water-soluble nanocarbons 8
Naoki Komatsu

General Lectures (14:15-15:00)

Formation and Purification of Nanotubes

- 3-8 Why is (6,5) nanotube so special in the tube growth processes? - Experimental and theoretical considerations- 43
○Yohji Achiba, Takeshi Kodama, Kenro Hashimoto, Haruo Shiromaru, Toshiya Okazaki
- 3-9 Bis(tert-butylpyrene) nanotweezers and nanocalipers: Enhanced extraction and recognition abilities for single-walled carbon nanotubes 44
○Gang Liu, A. F. M. Mustafizur Rahman, Takahide Kimura, Naoki Komatsu
- 3-10 The Infinite Possible Growth Ambients that Support Single-Wall Carbon Nanotube Forest Growth 45
○Hiroe Kimura

☆☆☆☆☆☆ Coffee Break (15:00-15:15) ☆☆☆☆☆☆

Poster Preview (15:15-16:00)

Poster Session (16:00-17:30)

Applications of Graphene

- 3P-1 Preparation and Properties of Surface Modified Graphene Oxide by Grafting of Polymers 120
○Tetsuo Sumiyoshi, Kazuhiro Nagata, Yusuke Yagi, Kazuhiro Fujiki, Norio Tsubokawa
- 3P-2 Hybrid Graphene –Titanium Surface for Sensing Applications 121
○Kakimi Yousuke, Rius Gemma, Eryu Osamu
- 3P-3 Substrate effects on chemical doping of graphene in tris buffer 122
Katsuya Masuda, ○Masahito Sano
- 3P-4 Anomalous behavior of Raman signals from carbon nanotube-graphene hybrid structures 123
○Taro Kusumoto, Hiraaki Kokame, Ryota Negishi, Yoshihiro Kobayashi
- 3P-5 Synthesis and characterization of Pt-Ru nanoparticles on carbon nanosheets by one-step electrodeposition 124
○Hayase Shohei
- 3P-6 Suppressed mobility degradation in large-area graphene oxide films by alcohol vapor treatments 125
○Michihiro Matsuzaki, Ryota Negishi, Yasuhide Ohno, Kenzo Maehashi, Kazuhiko Matsumoto, Yoshihiro Kobayashi
- 3P-7 Water-Soluble Graphene through Polyglycerol Grafting 126
★ ○Toku Yasuda, Li Zhao, Gang Liu, Syuji Aonuma, Takahide Kimura, Naoki Komatsu

Properties of Graphene

- 3P-8 Fabrications of Fullerene-Graphene and Fullerene-Nanotube-Graphene Composites 127
○Tomokazu Umeyama, Jinseok Baek, Noriyasu Tezuka, Kazuki Morita, Hiroshi Imahori
- 3P-9 Layer Number Determination using Raman Spectroscopy for Graphene Films Grown on SiC Substrate 128
○Hitoshi Nakahara, Daisuke Maeta, Yahachi Saito

August 7, Wed.

3P-10 ★	A Two-dimensional Carbon Network of Fused Pentagons: All Carbon Magnetic Sheet ○Mina Maruyama, Susumu Okada	129
3P-11	Fermi energy dependence of G' band of graphene and single wall carbon nanotubes ○Kentaro Sato, Riichiro Saito	130
3P-12 ★	Electronic Properties of Graphene under an Electric Field ○Ayaka Yamanaka, Susumu Okada	131
3P-13	Collective excitations in superconducting graphene ○Inotani Daisuke, Ohashi Yoji, Okada Susumu	132

The Others

3P-14	Structural transformation of iron oxide nanotubes by heat treatment ○Shunji Bandow, Yuki Shiraki	133
3P-15	Improvement of synthesis conditions for high yield of carbon nanocoils ○Maruyama Koji, Suda Yosiyuki, Tanoue Hideto, Takikawa Hirohumi, Ue Hitoshi, Shimizu Kazuki, Umeda Yoshito	134
3P-16	Electromagnetic wave absorption properties of carbon nanocoils ○Ryo Kato, Shingo Yasudomi, Yoshiyuki Suda, Hideto Tanoue, Hirofumi Takikawa, Hitoshi Ue, Kazuki Shimizu, Yoshito Umeda, Usaburo Eguchi	135
3P-17 ★	Spring Constant Measurement of Carbon Nanocoils ○Taiichiro Yonemura, Yoshiyuki Suda, Hideto Tanoue, Hirofumi Takikawa, Hitoshi Ue, Kazuki Shimizu, Yoshito Umeda	136
3P-18	In-situ observation of carbon nanocoil growth by optical microscope ○Takehiro Gohara, Takayuki Arie, Seiji Akita	137
3P-19 ★	Electrically Induced P-N Junction in WSe ₂ Monolayer Film ○Ryo Shimizu, Jiang Pu, Lain-Jong Li, Yoshihiro Iwasa, Taishi Takenobu	138
3P-20 ★	Layer Number Dependence of Optical Properties of MoS ₂ ○Yasunori Ogawa	139

Applications of Nanotubes

3P-21	Preparation of Diamond Particle Decorated with Carbon Nanotube ○Wataru Kimura, Kazuhiro Fujiki, Takeshi Yamauchi, Norio Tsubokawa	140
3P-22	Synthesis of ordered carbon nanotube network using pillar molecules ○Tashiro Kosuke, Song Hayong, Ishii Yosuke, Kawasaki Shinji	141
3P-23	Carbon nanotubes functionalized with carboxylic acid dispersed in 3D polymeric microstructures ○A. J. G. Otuka, V. Tribuzi, D. S. Correa, A. R. Zanatta, C. R. Mendonca	142
3P-24	High-Performance fluorinated resin with Low-content Aligned carbon nanotube ○Kentaro Miyoshi, Takeru Yajima, Toru Sakai, Masami Toyoda, Yoshikazu Nakayama	143
3P-25	In-situ TEM study on reaction of silicon nanoparticles with carbon supported on a carbon nanotube heater ○Koji Asaka, Tomohiro Terada, Yahachi Saito	144

August 7, Wed.

- 3P-26** Large current controllable solution-gate FET by carbon nanotube forest 145
○Miho Myodo
- 3P-27** Limiting factors of photovoltaic efficiency in semiconducting Single-walled Carbon Nanotubes/Si heterojunction cells: Correlation between cell structure, morphology, interface states and photovoltaic properties 146
○Nakano Atsushi, Ogata Hironori
- 3P-28** Effect of the Structure of Single-Walled Carbon Nanotube Counter Electrode on Dye-Sensitized Solar Cells 147
○Takaaki Chiba, Hidenori Kinoshita, Kehang Cui, Eric Einarsson, Shohei Chiashi, Shigeo Maruyama
- 3P-29** Fabrication of flexible and transparent capacitance-type touch panel with single-walled carbon nanotubes based on simple transfer process 148
○Norihiko Fukaya, Shigeru Kishimoto, Suguru Noda, Yutaka Ohno

Endohedral Nanotubes

- 3P-30** Charge state of capsule prepared by coalescence of $\text{Sc}_3\text{N}@C_{80}$ molecules in a carbon nanotube 149
★ ○Yuki Yonetani, Ahmadreza Fallah Gilvaei, Ryosuke Senga, Kaori Hirahara, Ryo Kitaura, Hisanori Shinohara, Yoshikazu Nakayama
- 3P-31** Energetics of Formation Process of C_{60} included [n]Cyclacene 150
★ ○Kigure Shota, Okada Susumu

Carbon nanoparticles

- 3P-32** Effect of the catalytic activity of catalyst nanoparticles on different types of carbon supports 151
○Masahiro Ozaki, Yoshiyuki Suda, Hirofumi Takikawa, Hideto Tanoue, Hitoshi Ue, Kazuki Shimizu
- 3P-33** Production of carbon nano-capsules and sacklike nano-carbons by impact reaction in nitrogen gas 152
○Mieno Tetsu, Kondo Kazuhiko, Sunao Hasegawa, Kosuke Kurosawa
- 3P-34** Formation of LaCO_3OH in the oxidation process of carbon nanocapsules encaging LaC_2 153
○Kazunori Yamamoto, Kenji Yamaguchi, Shin-ichi Shamoto, Takeshi Akasaka
- 3P-35** Improvement in specific capacitance of electric double-layer capacitors by oxidization of carbon nanoballoon 154
★ ○Yuta Okabe, Yoshiyuki Suda, Hirofumi Takikawa, Hideto Tanoue, Hitoshi Ue, Kazuki Shimizu

基調講演
Plenary Lecture

特別講演
Special Lecture

1S - 1 ~ 1S - 2

2S - 3 ~ 2S - 4

3S - 5 ~ 3S - 8

Flexible and stretchable carbon nanotube thin-film transistors
and integrated circuits

○Yutaka Ohno

¹ *Department of Quantum Engineering, Nagoya University, Nagoya 464-8603, Japan*

Flexible and stretchable electronics are attracting much attention because of the variety of possible new applications from flexible e-papers through sensors and medical devices having an affinity with human body. Among various kinds of semiconductor materials, carbon nanotube thin films have advantages in flexibility, stretchability, performance, and cost because of the excellent electronic and mechanical properties and processability.

In the presentation, recent works on carbon nanotube-based flexible and stretchable electronics will be introduced, including high-mobility carbon nanotube thin-film transistors (TFTs) and integrated circuits (ICs) realized on a transparent plastic film [1] and all-carbon ICs demonstrating excellent stretchability and mouldability [2]. TFTs fabricated with high-speed flexographic printing technique [3] will also be presented.

Acknowledgements: This work was partially supported by '08 NEDO Grant, R&D promotion scheme funding international joint research promoted by NICT, ALCA-JST, Grant-in-Aid of MEXT, the Aalto University MIDE program via the CNB-E project, and the Academy of Finland (Pr. No. 128445).

[1] D.-M. Sun et al., *Nature Nanotech.* 6 156 (2011).

[2] D.-M. Sun et al. (submitted)

[3] Higuchi et al. (submitted)

Corresponding Author: Y. Ohno

Tel: +81-52-789-5387, Fax: +81-52-789-5387,

E-mail: yohno@nuee.nagoya-u.ac.jp

Symmetric carbon nanostructures produced from organometallic compounds

○Hidetsugu Shiozawa¹

¹Faculty of Physics, University of Vienna, Vienna 1090, Austria

Our research focuses on understanding and control of nanoscale shape formation and physical properties via studies of novel synthesis routes to carbon nanostructures. We use organometallic compounds, such as metallocenes and metal acetylacetonates, as a single precursor to perform synthesis being confined in various dimensions ranging from nanometres to centimetres across.

Inside a single-wall carbon nanotube (SWCNT), or nano test tube, organometallic compounds can be densely packed at an elevated temperature where they react with each other to form nano metal catalysts out of which small diameter nanotubes grow [1,2]. Using nano test tubes of selected diameters we study formation mechanism for SWCNTs as function of tube chirality and metal type, Fig 1. Unique physical properties of metal-carbon nanotube hybrids we study using various experimental techniques include low dimensional electronic and magnetic properties [3,4].

In a macroscale test tube molecules react to form self-assembled carbon nanostructures. Vacuum sealed in a glass ampoule ferrocene can get pressured at elevated temperatures and then react to form novel symmetric carbon nanostructures [5]. The growth symmetry is determined for a given temperature and effective vapour pressure. In particular, at pressures that exceed 5 MPa bilateral carbon spirals are produced, Fig 2. A parametric plot of their surface geometry displays the fractal growth of the conical helix made with the logarithmic spiral. Microscopy studies in a cross section along the spirals show graphitic flakes arranged in a herringbone structure, normal to which are nano line defects. Local-wave-pattern analysis reveals that nano defect patterns of two-fold symmetry around the metal core shape emerging hexagonal carbon into a fractal structure [6].

- [1] H. Shiozawa *et al.* Adv. Mater. **20**, 1443 (2008).
- [2] H. Shiozawa *et al.* Adv. Mater. **22**, 3685 (2010).
- [3] H. Shiozawa *et al.* Phys.Rev.Lett. **102**, 046804 (2009).
- [4] A. Briones-Leon *et al.* Phys. Rev. B **87**, 195435 (2013).
- [5] H. Shiozawa *et al.* Nano Lett. **11**, 160 (2011).
- [6] H. Shiozawa *et al.* Sci. Rep. **3**, 1840 (2013).

Corresponding Author: H. Shiozawa
Tel: +43-1-4277-72628, Fax: +43-1-4277-9726,
E-mail: hidetsugu.shiozawa@univie.ac.at

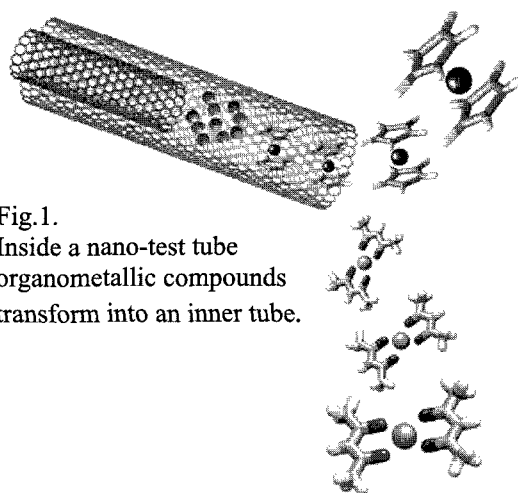


Fig.1.
Inside a nano-test tube organometallic compounds transform into an inner tube.

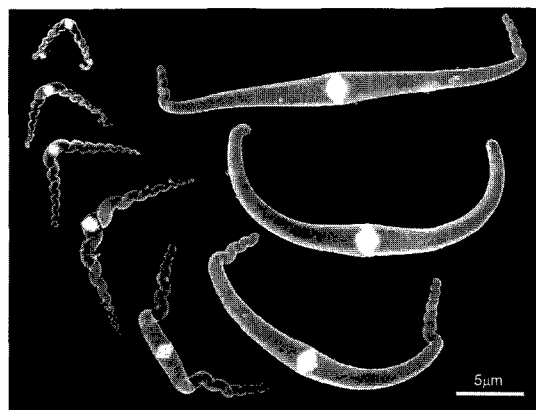


Fig.2.
SEM micrographs of bicone spirals of different sizes.

2S-3

Graphene based optoelectronics in the visible spectra

Coskun Kocabas¹

¹ *Department of Physics, Bilkent University, Ankara 06800, Turkey*

Controlling and manipulating light on the nanometer length scale using the properties of the collective electronic excitations is the central goal of nanophotonics. Weak light-matter interactions, the inability to control the electronic excitations and the lack of electric-field effect in metals have been the challenges hindering the active control of plasmonic and optoelectronic devices.

In this talk, I will present new class of optoelectronic devices using graphene incorporated with photon emitters. Placing photon emitters in close proximity of graphene in transistor geometry, gives us an extraordinary ability to modify the spontaneous emission of the emitters. These tools yield electrical control of the spontaneous emission of single photon emitters which can be widely applicable in physics.

Corresponding Author: C. Kocabas
Tel: +90-312-290-1965,
E-mail: ckocabas@fen.bilkent.edu.tr

Separation of Single-Wall Carbon Nanotubes using Gel Column Chromatography

○Hiromichi Kataura, Huaping Liu, Maki Shimizu, Yasuhiro Ito, Shunjiro Fujii, Astushi Hirano, and Takeshi Tanaka

Nanosystem Research Institute (NRI), AIST, Tsukuba 305-8562, Japan

Because single-wall carbon nanotube (SWCNT) is always produced as a mixture of variety of structures, such as diameter, chirality, and length, structure sorting is one of the most important issues not only in the fundamental researches but also in applications. To solve this problem, so many separation techniques were developed and reported to date.

In AIST, as one of them, we have developed a gel column chromatography method for the metal/semiconductor separation of SWCNTs [1]. This method is based on a specific interaction between semiconducting (s-) SWCNTs and the agarose gel when the SWCNTs are wrapped with sodium dodecyl sulfate (SDS). This simple separation technique realized a large scale (2 g/day) metal/semiconductor separation. After farther improvements, we have developed a multicolumn chromatography method for the chirality sorting of s-SWCNTs and obtained 13 kinds of single chirality s-SWCNTs using Sephacryl gel (GE Healthcare) for a column medium [2]. However, this method required two-step separation processes and was not suitable for a large scale single chirality separation. To solve this problem, we analyzed separation mechanism and found that the interaction between the gel and s-SWCNTs is highly depending on the system temperature. Finally, we have realized one-step chirality sorting using temperature controlled gel column chromatography [3]. Seven kinds of single chirality s-SWCNTs could be separated by one step separation procedure. Furthermore, we found that the multicolumn method works for enantiomer separation [4]. Clear circular dichroism (CD) signals were observed from nine kinds of single chirality s-SWCNTs. The enantiomer separation is the final goal of structure sorting of s-SWCNTs.

The remaining structure parameter of SWCNT is the length. The precise length sorting was already possible using a size exclusion column using the Sephacryl gel, but the sorting range was limited to be shorter than five micrometer. Recently, however, we found a specific interaction between deoxyribonucleic acid (DNA) and a silica gel can be used for length separation of very long SWCNTs. When the SWCNT was dispersed in water using DNA, SWCNTs longer than 10 micron were selectively adsorbed in a silica gel column while the shorter SWCNTs could flow out the column. By this process, we have obtained very long SWCNT solution in which 60 % of SWCNTs are longer than 10 μm .

Now all the structural parameters of SWCNTs can be sorted out using the simple gel column system. Anybody can try the precise structure separation of s-SWCNTs with very low cost.

This work was supported by JST-CREST.

[1] Takeshi Tanaka et al., Appl. Phys. Express 2 (2009) 125002.

[2] Huaping Liu et al., Nat. Commun. 2 (2011) 309.

[3] Huaping Liu et al. Nano Lett. 13 (2013) 1996.

[4] Huaping Liu et al. *unpublished*.

Corresponding Author: Hiromichi Kataura, Tel: +81-29-861-2551, Fax: +81-29-861-2786,

E-mail: h-kataura@aist.go.jp

Low-energy electron microscopy study of graphene growth

○Hiroki Hibino

NTT Basic Research Laboratories, NTT Corporation, Atsugi, Kanagawa 243-0198, Japan

Low-energy electron microscopy (LEEM), a type of electron microscopy, uses electron beams with typical energies of 1-100 eV and is therefore sensitive to differences in the surface structure of a material. Recently, we have been investigating growth processes of graphene and h-BN using LEEM. In this paper, I will explain how useful LEEM is for such studies from the following four aspects.

Dynamics of graphene growth: LEEM is suitable for dynamical observations of surface structural changes. We observed graphene growth on polycrystalline metal foil by carbon segregation. When the metal surfaces are sufficiently smooth, graphene grows continuously like a carpet across the boundaries of the metal grains [1]. Therefore, by reducing the number of the graphene nucleation sites, macroscopic single-domain graphene may be obtainable even on polycrystalline metal foil.

Number of graphene layers: To understand the growth mechanism of graphene, a method of evaluating the number of graphene layers is essential. The quantum size contrast, which appears in LEEM images due to the interference of electron waves reflected from the surface and interface of a thin film, can be used to count the number of graphene layers digitally [2]. We investigated the graphene growth process on SiC by thermal decomposition using LEEM, and, from the insights gained, we succeeded in growing highly uniform monolayer and bilayer graphene. These substrates allow us to analyze electronic transport properties at each thickness.

Crystallographic orientation: The interchange of B and N atoms in monolayer h-BN corresponds to the rotation of the crystallographic orientation by 180°. Dark-field (DF) LEEM images produced using diffracted beams can discriminate h-BN domains with opposite B-N bond directions. We used DF-LEEM imaging to map the crystallographic orientation of monolayer h-BN grown on heteroepitaxial Co thin films using chemical vapor deposition, and clarified that nucleation and coalescence of triangular h-BN islands with opposite B-N bond directions lead to domain structures [3]. To produce single-crystal h-BN, we need to control the initial orientation of the h-BN islands.

Stacking sequence: Graphene sheets epitaxially grown on SiC(0001) have the same orientation but have a degree of freedom of the stacking sequence. DF LEEM images of bilayer graphene on SiC indicate that bilayer graphene consists of two types of domains. Graphene has two carbon atoms at A and B sites in a unit cell, and graphite has ABAB (Bernal) stacking. We therefore infer that the two types of domains correspond to the AB and BA stackings, and the analysis of the energy dependence of the DF LEEM image intensity verifies this [4]. Bilayer graphene on SiC is polycrystalline and its crystal quality needs to be improved for better transport properties.

[1] G. Odahara *et al.*, Appl. Phys. Exp. 5, 035501 (2012).

[2] H. Hibino *et al.*, Phys. Rev. B 77, 075413 (2008).

[3] C. M. Orofeo *et al.*, Nano Res. 6, 335 (2013).

[4] H. Hibino *et al.*, Phys. Rev. B 80, 085406 (2009).

Corresponding Author: H. Hibino

Tel: +81-46-240-3467, Fax: +81-46-240-4718,

E-mail: hibino.hiroki@lab.ntt.co.jp

Growth of highly-integrated graphene nanoribbon toward high performance device applications

○Toshiaki Kato, Rikizo Hatakeyama, and Toshiro Kaneko

Department of Electronic Engineering, Tohoku University, Sendai 980-8579, Japan

Graphene nanoribbons combine the unique electronic and spin properties of graphene with a transport gap that arises from quantum confinement and edge effects. This makes them an attractive candidate material for the channels of next generation transistors. Although nanoribbons can be made in a variety of ways, the reliable site and alignment control of nanoribbons with high on/off current ratios remains a challenge. Plasma chemical vapor deposition (CVD) is known as a fruitful method for the structural-controlled growth and damage-free functionalization of nano carbon materials such as carbon nanotubes (CNTs) [1-3] and graphene [4,5]. We have developed a new, simple, and scalable method for integrating graphene nanoribbon devices based on a bottom-up approach. The Ni nanobar structures (Fig. 1a,b) were converted into graphene nanoribbon (Fig. 1c) after rapid heating plasma CVD (RH-PCVD). A clear transport gap with high on and off current ratio ($\sim 1.5 \times 10^4$) was obtained from a narrower graphene nanoribbon device (Fig. 1d). This result is the first indication of a high on/off ratio for the bottom-up-grown graphene nanoribbons [6].

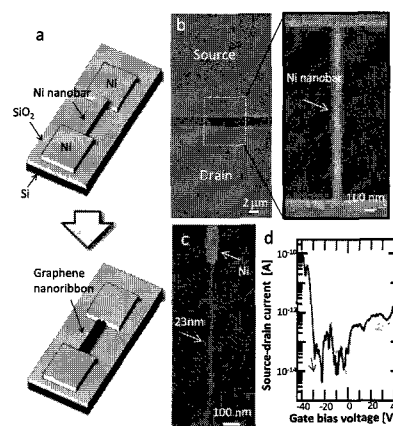


Fig. 1 (a) Schematic illustration of the graphene nanoribbon growth method. (b, c) SEM images of Ni nanobars before (b) and after (c) the RH-PCVD. (d) Typical electrical feature of graphene nanoribbon transistor.

- [1] T. Kato and R. Hatakeyama, *J. Am. Chem. Soc.* **130**, 8101 (2008).
- [2] T. Kato and R. Hatakeyama, *ACS Nano* **4**, 7395 (2010).
- [3] Z. Ghorannevis, T. Kato, T. Kaneko, and R. Hatakeyama, *J. Am. Chem. Soc.* **132**, 9570 (2010).
- [4] T. Kato, L. Jiao, X. Wang, H. Wang, X. Li, L. Zhang, R. Hatakeyama, and H. Dai, *Small* **7**, 574 (2011).
- [5] T. Kato and R. Hatakeyama, *ACS Nano* **6**, 8508 (2012).
- [6] T. Kato and R. Hatakeyama, *Nature Nanotechnology* **7**, 651 (2012).

Corresponding Author: T. Kato

Tel: +81-22-795-7046, Fax: +81-22-263-9225,

E-mail: kato12@ecei.tohoku.ac.jp

Ultrahigh-density data storage using C₆₀ molecules

○Masato Nakaya¹, Masakazu Aono¹, Tomonobu Nakayama^{1,2}

¹MANA, NIMS, Tsukuba, 305-0044, Japan

²Graduate School of Pure and Appl. Sci., Univ. of Tsukuba, Tsukuba, 305-0044, Japan

Owing to the rapid advance of information technology, novel data storage devices with greater data density than Tbit/inch² are required. Since the functionalities of C₆₀ molecules are altered by forming intermolecular covalent bonds, controlling the bound and unbound states of C₆₀ molecules at the molecular scale is essential for realizing molecular-based ultradense data storage.

In this presentation, first, we show that the unbound and bound states of C₆₀ molecules in the C₆₀ thin films can be controlled at room temperature with molecular scale using a scanning tunneling microscope (STM). Formation and annihilation of the intermolecular covalent bonds are selectively induced between C₆₀ molecules by applying appropriate negative and positive voltages (V_s) to the C₆₀ films, respectively [1]. The STM-induced intermolecular reactions occur via the electrostatic ionization of C₆₀ molecules. This methodology is useful for the ultradense data storage [2]. The bit data “0” and “1” correspond to the unbound and bonded states of C₆₀ molecules in multilayer films, respectively (Fig. 1a). Figure 1b shows an STM image before and after writing bit data “1” by applying V_s of -2.0 V at each position. In Fig. 2b, dark molecules correspond to bound C₆₀ molecules. The dark contrast of the bound molecules comes from the geometrical depression of surface C₆₀ molecules that chemically bond with the adjacent molecule in the beneath molecular layer. Applying V_s of +3.5 V at each bound molecule (crosses in Fig. 1c) enables us to dissociate only selected bound molecules into individual C₆₀ molecules, which corresponds to data erasing. The rewriting of data is also achieved (Fig. 1c). We have also shown that the data density is further improved by multi-bit operation [3].

[1] M. Nakaya et al., *small* 4, 538 (2008).

[2] M. Nakaya et al., *Adv. Mater.* 22, 1622 (2010).

[3] M. Nakaya et al., *ACS Nano* 5, 7830 (2011).

Corresponding Author: M. Nakaya

Tel: +81-044-299-9061, Fax: +81-044-299-9062,

E-mail: mnakaya@ncassembly.jst.go.jp

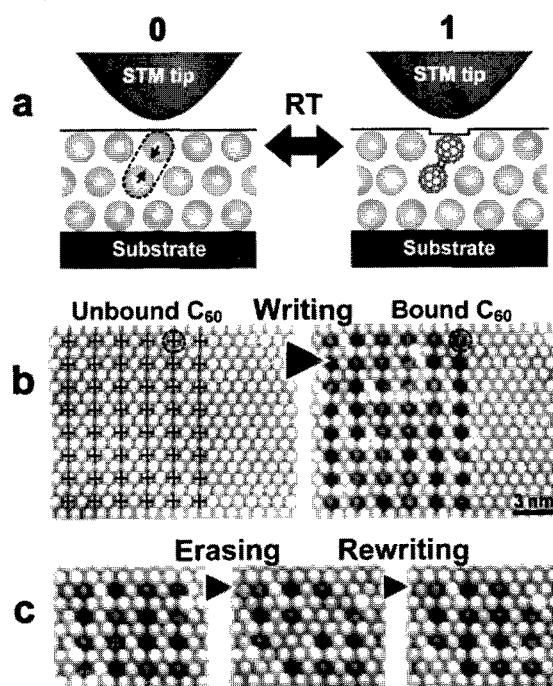


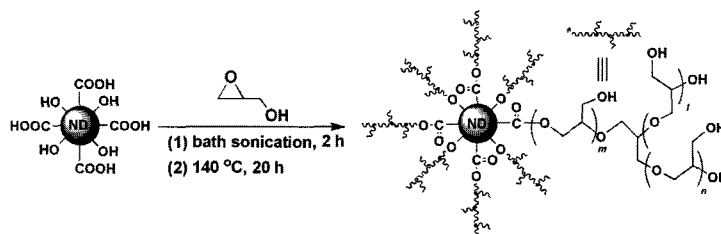
Fig.1. Ultrahigh-density data storage into multilayer film of C₆₀ molecules

Preparation, size-separation and biomedical application of water-soluble nanocarbons

○Naoki Komatsu

Department of Chemistry, Shiga University of Medical Science (SUMS), Seta, Otsu, 520-2192, Japan

Biomedical application of nanocarbon has been investigated extensively due to their low toxicity, good availability with high quality, and characteristic physical properties such as fluorescence. For in vivo application as drug carrier and



Scheme 1. Synthesis of ND functionalized by hyperbranched polyglycerol through ring-opening polymerization of glycidol.

imaging probe, nanocarbon should form a stable hydrosol under a physiological environment. In this context, we have recently developed useful methodology to impart high hydrophilicity to nanocarbons through hyperbranched polyglycerol (PG) grafting as shown in Scheme 1 [1]. The PG grafted nanodiamond (ND-PG) exhibited high dispersibility (16 mg/mL) in phosphate buffer saline (PBS), which is much higher than PEG functionalized ND [2]. The high dispersibility enabled the ND-PG to pass through silica-based columns in size exclusion chromatography (SEC), resulting in size separation of ND-PG [1]. This PG-functionalization is found to be applied to various nanocarbons such as ND [1], graphene [3], and SWNTs [4] as well as metal oxide nanoparticles such as iron oxide [5] and zinc oxide [6]. In addition to the good dispersibility, the PG layer was amenable to further chemical functionalizations, such as targeting peptide immobilization and drug loading, through covalent bonding at the hydroxyl group [7]. At the lecture, our recent progress on the biomedical applications of the functionalized nanocarbons in collaboration with medical doctors of Shiga University of Medical Science (SUMS) will be also presented from the viewpoints of diagnosis (fluorescence and MR imaging) and therapy (gene and drug delivery).

Reference: [1] L. Zhao, N. Komatsu, *Angew. Chem. Int. Ed.* **2011**, *50*, 1388. [2] T. Takimoto, N. Komatsu, *Chem. Mater.*, **22**, 3462 (2010). [3] T. Yasuda, L. Zhao, N. Komatsu, 43rd FNTG symposium, 1-14. [4] K. Nakamura, L. Zhao, N. Komatsu, 44th FNTG symposium, 3P-21. [5] L. Zhao, N. Komatsu, *Adv. Funct. Mater.*, **2012**, *22*, 5107. [6] L. Zhao, N. Komatsu, *J. Indian Chem. Soc.*, **2011**, *88*, 1787. [7] L. Zhao, X. Chen, N. Komatsu, submitted.

Corresponding Author: Naoki Komatsu, **E-mail:** nkomatsu@belle.shiga-med.ac.jp

Tel: +81-77-548-2102, **Fax:** +81-77-548-2405

一般講演
General Lecture

1-1 ~ 1-16

2-1 ~ 2-11

3-1 ~ 3-10

The mechanism and ability of SW/DWCNT adsorbing radioactive elements in the environment

○Takumi Araki¹, Syogo Tejima¹, Hisashi Nakamura¹, Bunshi Fugetsu², Morinobu Endo³

¹Research Organization for Information Science & Technology, Tokyo 2-32-3, Japan

²Graduate School of Environmental Science, Hokkaido University, Sapporo 060-0810, Japan

³Factory of Engineering, Shinsyu University, Nagano 4-17-1, Japan

Nanocarbons, such as carbon nanotubes or, single, double and multi-walled CNTs, graphenes, their novel properties have attracted scientists and engineers to new findings and innovations. By applying their novel properties, it is strongly expected that CNTs can clean up the radioactive elements from lands, rivers, lakes and coastal sea, effectively and safely^[1], for the environmental remediation after severe events as Fukushima nuclear power plant in Japan, or Goiania accident in Brazil.

For investigating the applicability of nanocarbons to the environmental remediation, CNT has been studied on the adsorption for Cesium (Cs) and Strontium (Sr) by the first principle theory. The mechanism of adsorption is that Cs and Sr become ion due to the electron transfer through the π orbitals of CNT and the remaining valence electrons of Cs and Sr form orbitals that easily bind the π orbitals. This mechanism contributes to CNT that adsorbs Cs stably. As for the effect of CNT characteristics on the adsorption, it is pointed out that there are no clear differences in the adsorption ability between structures such as single, double or multi-walled CNT for Cs adsorption especially. But the adsorption becomes strong as the CNT radius decreases, or curvature increases.

As for the effect of environment on the adsorption, the state of Cs is a judging factor for evaluating the ability of adsorption. If Cs is metals or atoms as in vacuum space, CNT can well adsorb Cs. If Cs is Cs^+ as in water or seawater environments, CNT also well adsorbs Cs^+ (Fig.1.). However, the ability of adsorption is influenced by the number of water molecules existing in the space of the first shell. If Cs is Cs^+ in the mixture of AM⁺'s as Na^+ and K^+ , the effect of Na^+ or K^+ on CNT adsorbing Cs^+ is small. As for the Cs compound such as CsOH as the solid state after reaction with water vapor in air, CNT cannot adsorb. It should be noted that Cs compounds are easily dissolved and ionized in water. Through adsorbing Cs^+ or the ionized state, CNTs such as SWCNT, DWCNT and MWCNT can be basically applicable for the environmental remediation of the radioactive products as in river, lakes and coasts.

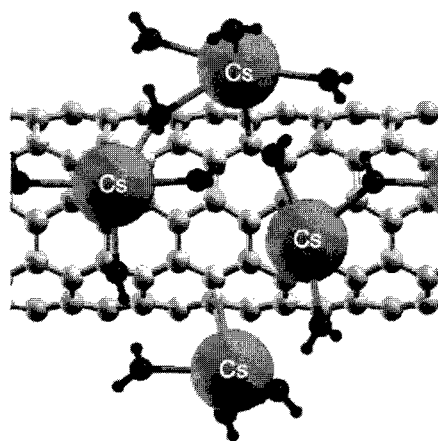


Fig.1. Cesium cluster with three or four water molecules adsorption on CNT (5,5).

[1] S. Tsuruoka *et al.* Material Express. 3, 21 (2013).

Corresponding Author: T. Araki

Tel: +81-03-6433-0670, Fax: +81-03-6433-0673,

E-mail: araki@rist.or.jp

Photoluminescence from dried hybrids of double-stranded DNA and single walled carbon nanotubes

○Masahiro Ito, Yusuke Ito, Tomoki Kobayashi, Takuya Hayashida,
Daisuke Nii, Kazuo Umemura, Yoshikazu Homma.

Department of Physics, Tokyo University of Science, Tokyo 162-8601, Japan

To obtain photoluminescence (PL) from single-walled carbon nanotubes (SWNTs), it is necessary to disperse SWNTs in aqueous solutions with surfactants such as sodium dodecyl sulfate (SDS) and DNA [1, 2]. The PL spectra appear in solution with each dispersant. However, the PL spectra of SWNTs wrapped with SDS almost disappear under dry condition. In this study, we report the PL spectra of SWNTs wrapped with double-stranded DNA (dsDNA: derived salmon testes) in dry condition.

Figure 1 shows the PL spectra of DNA-SWNTs (A) in TE buffer solution and (B) under dry condition. Various spectra corresponding to different chiralities appeared strongly in dry condition compared with in solution. This is because DNA-SWNTs were condensed during evaporation of the solution and the density of DNA-SWNTs in the laser spot (2 μm) increased.

In addition, while carrying out PL measurement with excitation laser (785 nm), we put a droplet of DNA-SWNT aqueous solution on the SiO_2 substrate and observed drying process (Figure 2). At first, DNA-SWNTs were in aqueous solution (5 μl). After 400 s, the PL peaks red-shifted by 10 nm due to evaporation of the solution. We restored DNA-SWNTs in aqueous solution again by dropping water of 5 μl at 500 s. Then, the PL peaks blue-shifted by 10 nm. The reproducible changes in intensity and shift were obtained. From these results, PL from DNA-SWNTs under dry condition was found to be stable.

[1] N. Nakashima *et al.* Chem. Lett. **32**, 456 (2003). [2] M. Zheng *et al.* Nat. Mater. **2**, 338 (2002).

Tel: +81-3-3260-4271 (ext. 2298), Fax: +81-3-5261-1023,

E-mail: m-ito@rs.tus.ac.jp

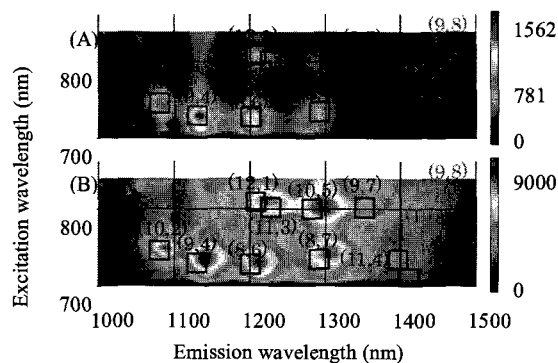


Figure 1. The PL maps of DNA-SWNTs (A) in solution and (B) under dry condition.

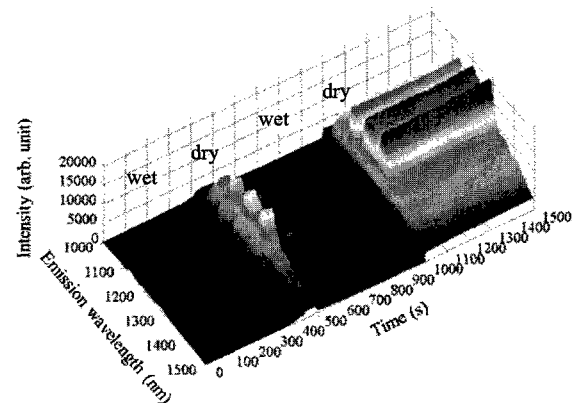


Figure 2. Time evolution of PL intensity during evaporation of the solution.

Raman study on X-ray induced defect and its structure in carbon nanotube

○Toshiya Murakami¹, Yuki Yamamoto¹, Mitsuaki Matsuda¹, Kenji Kisoda², Chihiro Itoh¹

¹Department of Material Science and chemistry, Wakayama University, Wakayama, 640-8510, Japan

²Department of Physics, Wakayama University, Wakayama, 640-8510, Japan

Carbon materials, like graphite, are generally believed to be tolerant to X-ray irradiation. However, X-ray irradiation of carbon nanotube (CNT) gives rise to the formation of Frenkel defects (vacancy and interstitial pairs), which eventually leads to structural change.[1, 2] Elucidation of the characteristics of the irradiation-induced defect in CNT is essential to utilize this effect as a tool for the structural modification of CNT. In particular, understanding the stability of interstitial atoms in CNT is pivotal for controlling the structural change. Moreover, reveal of the stability of Frenkel defect gives a clue to the understanding why CNT is sensitive to the X-ray irradiation. In this report, we show the results of the thermal treatment of the X-ray irradiated single-walled CNTs (SWNTs) probed by resonant Raman scattering spectroscopy and discuss the thermal stability of the defect.

SWNTs grown by chemical vapor deposition were irradiated by X-ray ($K\alpha$ line of Mg) in an evacuated chamber. Irradiated SWNTs were subsequently annealed in argon atmosphere. Resonant Raman spectra were measured with the excitation wavelength of 532 nm (2.33 eV).

After X-ray irradiation, D band intensity in Raman spectrum was enhanced (not shown here), indicating the formation of X-ray induced defects in SWNT. Figure 1(a) shows the radial breathing modes (RBMs) of the SWNTs before and after X-ray irradiation. The peak intensity was normalized with respect to that of G band. After X-ray irradiation, RBM peaks of (15, 2), (7, 7) and (8, 5) (dented by ○) were enhanced, but the others (▲) were reduced. The irradiation-induced intensity changes of RBMs can be explained if we consider that the optical transition energy, which is responsible to the resonance of the Raman probe, was reduced by 50-100 meV by the X-ray irradiation. The optical transition energies of the tubes observed in the present study are shown in Fig. 2(b). From above assumption, the optical transition energy of (15, 2), (7, 7) and (8, 5) tubes approach the excitation energy (2.33 eV) after X-ray irradiation. On the other hand, the other peaks get away from it. Therefore, the intensity enhancement of (15, 2), (7, 7) and (8, 5) tubes and the intensity reduction of the other tubes can be explained by the change of resonant energy. For clarifying the structure of X-ray induced defect, isochronal-annealing experiments were performed on X-ray irradiated SWNT. The estimated activation energy (~500 meV) was good agreement with the migration energy of the bridge interstitial proposed by the theoretical study of graphite with one layer [3].

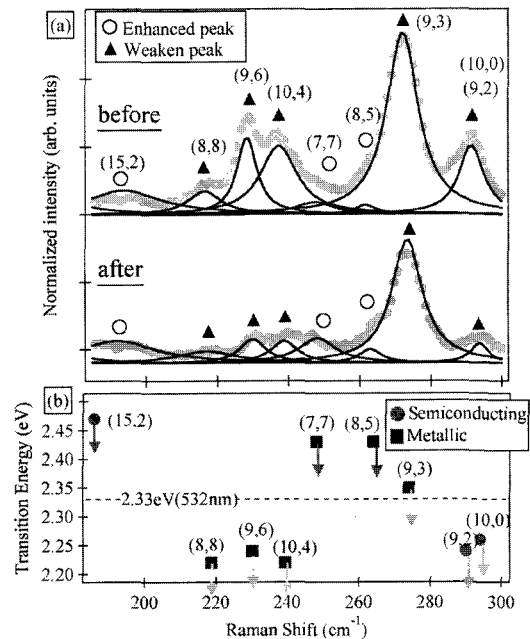


Fig. 1 (a) RBM of SWNT before and after irradiation and (b) Kataura plot

[1] T. Murakami, *et al.*, Eur. Phys. J. B, **86** (2013) 187, [2] C. Itoh, *et al.*, Nucl. Inst. Meth B, **266** (2008) 2772

[3] H. Zhang, *et al.*, Diamond and Related Materials **19** (2010) 1240

Corresponding Author: T. Murakami, Tel: +81-73-457-8532, E-mail: murakami@sys.wakayama-u.ac.jp

Photoluminescence Nonlinearity of Hole-doped Single-walled Carbon Nanotubes

○Naoto Akizuki¹, Shinichiro Mouri¹, Yuhei Miyauchi^{1,2}, and Kazunari Matsuda¹

¹ Institute of Advanced Energy, Kyoto University, Uji, Kyoto 611-0011, Japan

² Japan Science and Technology Agency, PRESTO, 4-1-8 Honcho, Kawaguchi, Saitama 332-0012, Japan

Carrier-doped single-walled carbon nanotubes (SWNTs) are attracted much attention as quasi-one dimensional (1D) materials not only for the fundamental 1D physics researches but also various optoelectronics applications. In hole-doped SWNTs, the charged exciton (trion) which is the bound state of an exciton and a hole, is formed. Because of the strong quantum confinement effect in the SWNTs, the trion has a large binding energy and is stable even at room temperature. Moreover, the application of trion using spin degree of freedom has been expected. However, the detailed optical properties of trion including the optical nonlinearity have not been clarified yet.

In this study, we measured the excitation intensity dependence of photoluminescence (PL) spectra of hole-doped (7,5) SWNTs to discuss the optical nonlinearity and mechanism of trion formation. The SWNTs (CoMoCAT) were dispersed with PFO in toluene. Hole-doped SWNTs were prepared using F₄TCNQ as a *p*-type dopant. The inset in Fig. 1 shows PL spectra of hole-doped SWNTs excited by femtosecond pulsed laser (1.55eV) with varying the excitation intensity. The peaks around 1.00eV, 1.18eV have been attributed to trion [1] and exciton (E_{11}) PL peaks. Each spectrum is normalized by the corresponding excitation intensity. Figure 1 shows excitation density dependence of integrated PL intensity. We found that the PL intensities of both trion and exciton peaks show a saturation behavior, when the trion PL exhibits the stronger saturation than that of the exciton exhibits. These optical nonlinearities reflect the dynamics of the trion formation. The mechanism of trion formation will be discussed in detail.

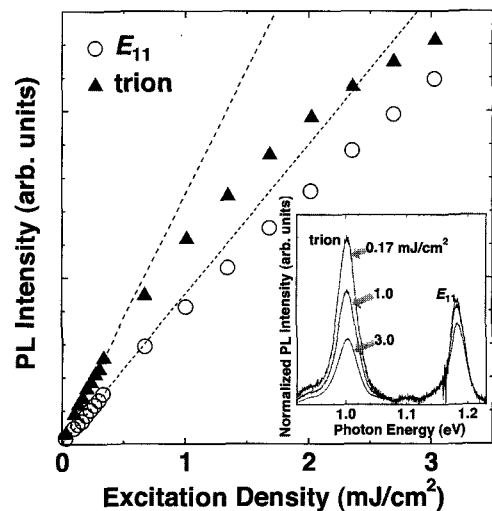


Fig. 1. E_{11} exciton (white circles) and trion (solid triangles) PL nonlinearities of hole-doped SWNTs. The dotted lines indicate the linear dependence. The inset shows normalized PL spectra.

[1] R. Matsunaga *et al.*, Phys. Rev. Lett. 106, 037404 (2011).

Corresponding Author: N. Akizuki

Tel: +81-774-38-3465,

E-mail: akizuki.naoto.88x@st.kyoto-u.ac.jp

Thermopower in Highly Purified Semiconducting Single-Wall Carbon Nanotube Buckypaper

○Yusuke Nakai¹, Kazuya Honda¹, Yasumitsu Miyata¹, Kazuhiro Yanagi¹, Yutaka Maniwa^{1,2}

¹*Department of Physics, Graduate School of Science and Engineering, Tokyo Metropolitan University, Hachioji 192-0397, Japan,*

²*JST-CREST, Kawaguchi, 332-0012, Japan*

Due to growing energy demands, thermoelectric devices to generate electrical power from waste heat have attracted much attention. Although single-wall carbon nanotubes (SWCNTs) have not been considered as a thermoelectric material, there seems to be a plenty room for optimization of the thermoelectric parameters, electrical resistivity, thermal conductivity and thermopower or Seebeck coefficient. SWCNT mats or buckypaper, consisting of the mixture of semiconducting and metallic tubes, have a low Seebeck coefficient of 60 $\mu\text{V}/\text{K}$ at room temperature as a thermoelectric material [1]. In general, semiconducting tubes are expected to have a larger Seebeck coefficient, which is preferable for thermoelectric application. Indeed, an individual semiconducting SWCNT exhibits a largely enhanced Seebeck coefficient of 260 $\mu\text{V}/\text{K}$ at room temperature [2], which is comparable to that of the commercial thermoelectric material Bi_2Te_3 and its alloys. However, the Seebeck coefficient of semiconducting SWCNT buckypaper has not been investigated due to the lack of separation technique

We prepared SWCNT buckypaper with different semiconducting SWCNTs fractions through a density gradient ultra-centrifugation (DGU) method [3], and measured the electrical resistivity and Seebeck coefficient of these samples. The Optical absorption spectra and electrical resistivity revealed good separation of metallic and semiconducting SWCNTs (See Fig. 1). We found that the Seebeck coefficient of semiconducting SWCNT buckypaper is an order of magnitude larger than that of metallic one. In addition, we investigated the effects of acid treatments and high-temperature annealing on the samples in order to tune a carrier number of SWCNT buckypaper. We will show the detail of our experiment and discuss a possible origin of the large Seebeck coefficient observed in semiconducting SWCNT buckypaper.

[1] See for example, J. Hone *et al.* Phys. Rev. Lett. **80**, 1042 (1998).

[2] J. P. Small *et al.* Phys. Rev. Lett. **91**, 256801 (2003).

[3] K. Yanagi *et al.* Appl. Phys. Expr. **1**, 034003 (2008).

Corresponding Author: Yusuke Nakai

Tel: +81-42-677-2498, Fax: +81-42-677-1413,

E-mail: nakai@tmu.ac.jp

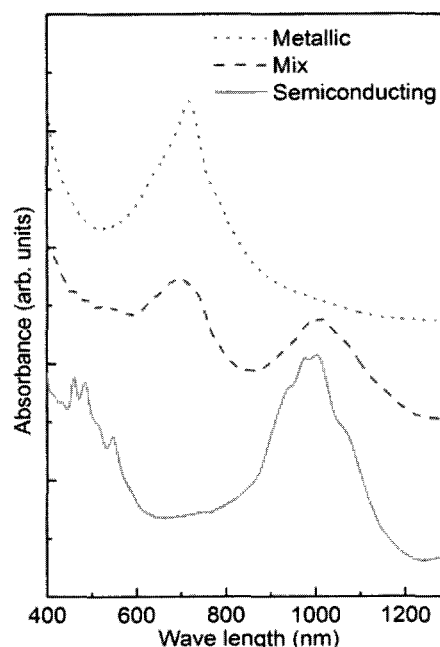


Fig.1. Optical absorption spectra of SWCNT buckypaper with different semiconducting SWCNT fractions.

Diameter-Dependent Threshold Voltages of Carbon Nanotube Thin-Film Transistors

○Fumiyuki Nihey,^{1,2} Yuta Kikuchi,¹ Fusako Sasaki,¹ Kazuki Ihara,^{1,2} Hideaki Numata,^{1,2}
Yuki Kuwahara,^{1,3} Shigekazu Ohmori,^{1,3} Takeshi Saito^{1,3}

¹Technology Research Association for Single Wall Carbon Nanotubes (TASC),
Tsukuba 305-8565, Japan

²Smart Energy Research Laboratories, NEC Corporation, Tsukuba 305-8501, Japan

³National Institute of Advanced Industrial Science and Technology (AIST),
Tsukuba 305-8565, Japan

Carbon nanotubes (CNTs) have attracted much attention for various applications such as flexible, printable thin-film transistors (TFTs). In the previous work, we reported that the diameter of CNTs greatly influences the performance of CNT-TFTs such as mobility and on/off current ratio [1]. In this work, we focus on the diameter dependence of threshold voltage, V_{th} , which is also an important parameter for digital and analog applications.

Three kinds of CNTs with different average diameters, $d = 1.0, 1.3,$ and 1.8 nm, were synthesized by using the enhanced direct-injection pyrolytic synthesis (eDIPS) method [2]. Semiconductive CNTs with purities $> 95\%$ were obtained by using an electric-field-induced layer formation (ELF) method [3]. Separated CNTs were deposited on heavily Sb-doped Si substrates with a 100-nm-thick SiO_2 layer as a gate dielectric. Source and drain electrodes were defined by Au evaporation through a metal mask. Each channel region with $600 \mu\text{m}$ in width and $100 \mu\text{m}$ in length was masked by PMMA and isolated by oxygen plasma. Electrical measurements were carried out at room temperature in dry air by changing the voltage of a substrate as a back-gate.

Figure 1 (a), (b), and (c) show the square-root of drain current, $I_D^{1/2}$, as a function of back-gate voltage, V_{GS} , in the saturation regime (drain voltage, $V_{DS} = -10$ V) for samples with $d = 1.0, 1.3,$ and 1.8 nm, respectively. It is apparent that the hysteresis in the curves was well suppressed [4]. For each, V_{th} was extracted by linear fit to the curve. As shown in Fig. 1 (d), the distribution of V_{th} shifts toward the positive direction as the diameter increases. This result clearly shows that the control of CNT diameters is important to optimize the device performance.

This work was supported by New Energy and Industrial Technology Development Organization (NEDO).

[1] Y. Asada *et al.*, *Adv. Mater.* **23**, 4631 (2011).

[2] T. Saito *et al.*, *J. Nanosci. Nanotechnol.* **8**, 6153 (2008).

[3] K. Ihara *et al.*, *J. Phys. Chem. C* **115**, 22827 (2011).

[4] S. Ohmori *et al.*, *RSC Adv.* **2**, 12408 (2012).

Corresponding Author: F. Nihey

Tel: +81-29-861-3772, Fax: +81-29-858-6330, E-mail: nihey@tasc-nt.or.jp

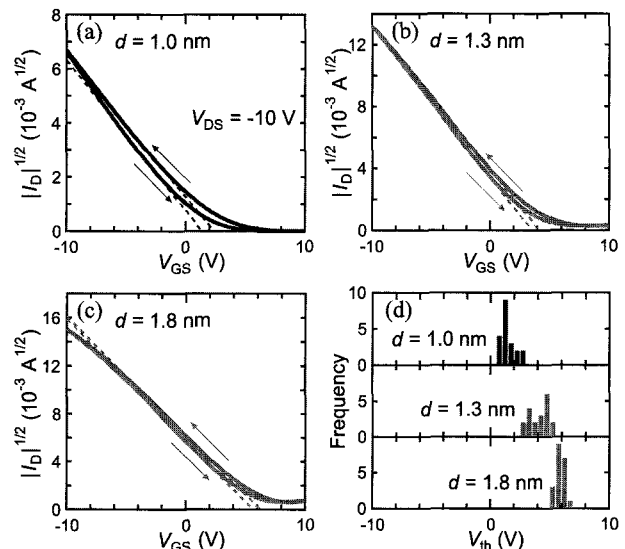


Fig. 1 $I_D^{1/2} - V_{GS}$ characteristics ($V_{DS} = -10$ V) of devices with (a) $d = 1.0$, (b) 1.3 , and (c) 1.8 nm. Dashed lines serve as guide to extract V_{th} . (d) Histograms of V_{th} for each diameter.

Development of compounded foil of carbon nanotube and sputter-deposition carbon

○Hiroo Hasebe, Hironori Kuboki, Hiroki Okuno, Isao Yamane, Hiroshi Imao, Nobuhisa Fukunishi, Masayuki Kase, and Osamu Kamigaito

Nishina Center for Accelerator-Based Science, RIKEN, Saitama 351-0198, Japan

In a heavy ion accelerator facility, Carbon foils (C-foils) were usually used to strip electrons from ions for an efficient acceleration by enhancing charge states of ions. At RIKEN RI Beam Factory (RIBF), a C-foil with a thickness of $0.3 \text{ mg}\cdot\text{cm}^{-2}$ ($1.5 \text{ }\mu\text{m}$) was used to strip uranium (U) beams to U^{71+} . Because of increasing U beam intensity, lifetimes of conventional static-type Sputter-Deposition C-foil (SDC-foil) strippers decreased as less than half a day. We tried to extend lifetimes by enlarging an irradiated area with rotating larger SDC-foils. However, we had no success due to mechanical fragility of large SDC-foils [1-3]. In contrast, Carbon-Nanotube (CNT) foil had sufficient mechanical strength, however, considerably lower charge states of U^{66+} were obtained with a pure CNT foil because of its low density.

Development of CNT-SDC-foils was proposed to overcome this incompatible problem [4]. The CNT-SDC-foils were fabricated by depositing carbon on both sides of surfaces of a large CNT sheet by a magnetron sputtering method. Since SDC layers compensated low density of CNT, the CNT-SDC foil had both advantages of mechanical strength and high density. The CNT-SDC foils were practically used for the 2-month-long U beam time at RIBF in 2011 (Fig.1). The lifetimes of the CNT-SDC-foils were drastically extended as 2-5 C (3-5 days), which was 100 times longer than those of static C-foils ever used. The structures of CNT-SDC foil were observed by a scanning electron microscope. It was found that CNT bundles in a CNT-SDC-foil were grown after carbon deposition and CNT structure and bundles were broken by beam irradiation.

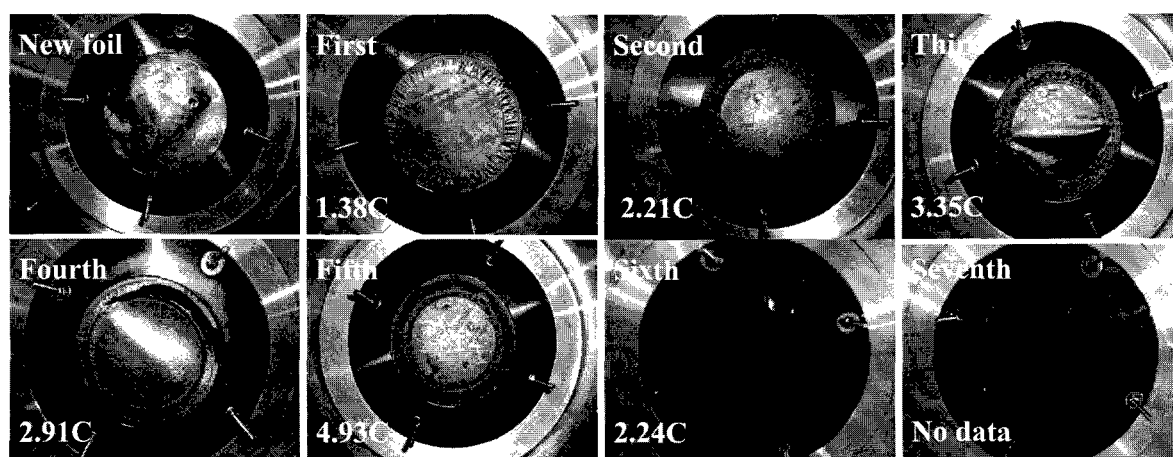


Fig.1. Photographs of CNT-SDC foil. Upper left: before irradiation, others: used foils. 7 foils were used in total. Total irradiated charges are also shown in the figure.

- [1] H. Hasebe *et al.* Nucl. Instr. and Meth. A **590**, 13 (2008).
 - [2] H. Hasebe *et al.* Nucl. Instr. and Meth. A **613**, 453-456 (2010).
 - [3] H. Hasebe *et al.* Nucl. Instr. and Meth. A **655** (2011) 57.
 - [4] H. Hasebe *et al.* Proc. of the 9th annual meeting of Particle Accelerator Society of Japan, p.84-88, (2012).
- Corresponding Author: H. Hasebe, Tel: +81-48-467-4938, Fax: +81-48-462-4943, E-mail: hasebe@riken.jp

Immunoassay with Single-Walled Carbon Nanotubes as Near-Infrared Fluorescent Labels

○Yoko Iizumi¹, Toshiya Okazaki¹, Yuzuru Ikehara², Mutsuo Ogura³, Masako Yudasaka¹

¹ *Nanotube Research Center*, ² *Research Center for Medical Glycoscience*
³ *Nanotube Research Institute, National Institute of Advanced Industrial Science and Technology, Tsukuba, Ibaraki, Japan*

One of the most critical issues in clinical tests is the low sensitivity for detecting antigens in blood. An immunoassay is often employed for antigen detection, where a fluorescent label molecule linked to an antibody is the key. The excitation and fluorescence wavelengths of the label molecule are in the visible region in most cases, which limits improvements in immunoassay sensitivity due to the strong absorption of the red blood cells. The detection level could be improved if near-infrared (NIR) light becomes available because of the low interference by bioorganic molecules and the deep tissue penetration. Single-walled carbon nanotubes (CNTs) are promising candidates for such fluorescent labels as it absorbs and emits light in NIR region. In the present work, to show the potential ability of the CNT labels in the immunological tests, we conjugated CNTs with immunoglobulin G (IgG) antibodies by using a linker molecule of phospholipid polyethylene glycol (PEG), and their immunoprecipitation using protein G magnetic beads was examined.

The CNTs (CoMoCAT) were dispersed with DSPE-PEG-NHS in buffer solution. Rabbit IgG was attached to DSPE-PEG-NHS by the reaction of IgG with NHS. The obtained complex showed the fluorescence and Raman scattering spectra characteristic of CNTs. Following a typical immunoassay process, the CNT-PEG-IgG was mixed with protein G magnetic beads (Pr.G-beads), IgG and Pr.G specifically combine each other, and the CNT-IgG/Pr.G-beads were taken out and washed. The CNT-IgG/Pr.G-beads showed fluorescence and Raman spectra of CNTs,

indicating that IgG retained binding ability against Pr.G (Fig. 1). At the last stage, CNT-PEG-IgG was eluted from the beads. The eluted solution showed the CNT fluorescence spectra and residual beads did not. These results showed that most of the CNT-PEG-IgG was immunoprecipitated on and eluted from the beads, which was confirmed from the fluorescence intensities of CNTs at 1000–1200 nm and the fluorescence intensity of CNT from the CNT-PEG antibody was strong enough to detect antigens at 4 nM by our simple procedures. The present results, using CNTs as the NIR fluorescent labels for the immunoassay, will pave a new way for medical applications of CNTs.

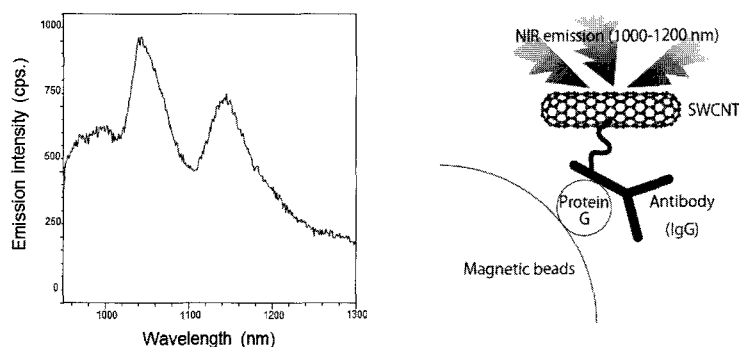


Fig. 1 NIR emission spectrum obtained from CNT-IgG/Pr.G-beads.

Corresponding Authors:

T. Okazaki, E-mail: toshi.okazaki@aist.go.jp,

M. Yudasaka, E-mail: m-yudasaka@aist.go.jp

Highly Conductive CNT/Polymer Composite on Arbitrary Rubber Matrices Based on Thermodynamics

○Seisuke Ata¹, Howon Yoon², Chandramouli Subramaniam², Takaaki Mizuno² Takeo Yamada¹ and Kenji Hata¹

¹ *Nanotube Research Center, National Institute of Advanced Industrial Science and Technology (AIST), Tsukuba 305-8565, Japan*

² *Technology Research Association for Single Wall Carbon Nanotubes (TASC), Tsukuba, 305-8565, Japan*

In this presentation, we propose the solubility parameter [1] as an important parameter that determines the degree of long super growth carbon nanotube (SG-SWNT [2]) dispersion in the rubber matrix, and thus the conductivity or other properties of the SG-SWNT-polymer composite. This finding explains why fluorinated rubber/SG-SWNT composite, with a solubility parameter matching with that of SG-SWNT, shows the highest volume conductivity compare with other rubber at a same CNT loading. Based on this finding, we speculate that the addition of a small amount of fluorinated rubber into the rubber matrix as a unified and practical technology to improve the conductivity of the SG-SWNT/rubber composite for a various kinds of rubber matrices.

Such SG-SWNT/rubber composites reported here, possesses additional advantages such as excellent mechanical durability, oil-resistance, chemical-resistance and electromagnetic shielding property etc. originating from the ability of long, high-aspect and traversing SWNTs to deform in concert with the elastomer or resin with minimum stress concentration at their interfaces. Moreover, the SG-SWNT synthetic methodology has been scaled-up to a pilot plant where large growth substrates are continuously conveyed through the reactor enabling annual ton-scale SWNT production for the first time. When these features are combined with the results of this work, we envision they would open up versatile applications for CNT rubber or resin with various polymer matrix such as, stretchable electronics, flexible displays, and automobile parts.

[1] JN Coleman et al, ACS Nano 3(8), 2340 (2009).

[2] K. Hata et al, Science. 306, 1362 (2004)

Corresponding Author: K. Hata

Tel: +81-29-861-4654, Fax: +81-29-861-4851,

E-mail: kenji-hata@aist.go.jp

Thermally conductive SG-CNT-Cu composite with low thermal expansion

○Yuzuri Yasuda¹, Chandramouli Subramaniam¹, Seisuke Ata^{1,2}, Motoo Yumura^{1,2}, Takeo Yamada^{1,2}, Don N. Futaba^{1,2} and Kenji Hata^{1,2}

¹ *Technology Research Association for Single Wall Carbon Nanotubes (TASC), Ibaraki 305-8565, Japan*

² *National Institute of Advanced Industrial Science and Technology (AIST), Ibaraki 305-8565, Japan*

Composite of carbon nanotube (CNT) with metals have received significant attention for applications ranging from microelectronics packaging to macroscopic automobile components. Varied approaches for obtaining high thermal conductivity using carbon nanotubes as fillers in metal have been explored. However, all such investigations result in lowering of thermal conductivity of the metal component due to the addition of carbon nanotube fillers. For example, electronic packaging materials required high thermal conductivity and low thermal expansion to minimize the overall thermal strain at the silicon interface. High strain reduce device lifetime of performance.

To address this demand, we report a carbon nanotube-copper (CNT-Cu) composite with thermal conductivity (395 W/mK) similar to pure Cu (400 W/mK) at room temperature. However, the material exhibits 1/3 the thermal expansion of Cu. The aligned CNT present in the composite assists in faster heat propagation, resulting in higher thermal diffusivity compared to Cu. CNT present in large volume fraction (~50 vol %) in the composite is able to compensate for the high thermal expansion of Cu, thereby providing the material with an overall low thermal expansion coefficient. The thermal expansion coefficient (CTE) values measured using (a) temperature X-ray diffraction and (b) thermo-mechanical analysis showed good agreement.

The ratio of thermal expansion to thermal conductivity “Thermal distortion parameter (TDP)” is a measure of the thermal strain generated at interface. This is of particular significance in electronics packaging and interfacing, with a lower TDP indicating higher cohesiveness among two different materials. As a result of its high thermal conductivity and low thermal expansion, CNT-Cu composite displayed the lowest TDP among materials currently used for packaging and thermal management in electronics (Fig 1).

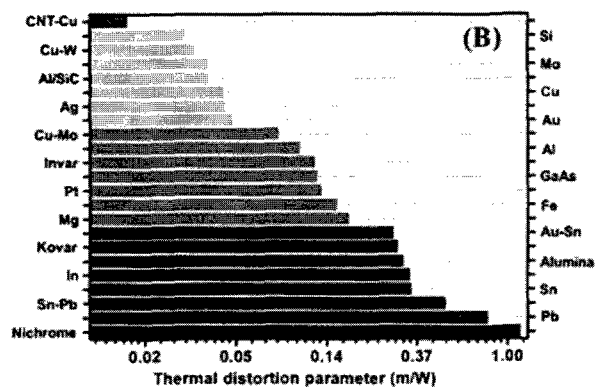


Fig. 1 Map of thermal distortion parameter for various materials, with CNT-Cu having the lowest value.

[1] C. Subramaniam *et al.* Nature Communication. (Accepted).

Corresponding Author: K. Hata

Tel: +81-29-861-4654, Fax: +81-29-861-4851,

E-mail: kenji-hata@aist.go.jp

Metallization of 1D sulfur crystals inside carbon nanotubes

○Toshihiko Fujimori¹, Aaron Morelos-Gómez², Zhen Zhu³, Hiroyuki Muramatsu⁴, Ryusuke Futamura¹, Koki Urita⁵, Mauricio Terrones^{1,6}, Takuya Hayashi⁷, Morinobu Endo¹, David Tomanek³, Katsumi Kaneko¹

¹ *Research Center for Exotic Nanocarbons (JST), Shinshu University, Nagano 380-8553, Japan*

² *Institute of Carbon Science and Technology, Shinshu University, Nagano 380-8553, Japan*

³ *Physics and Astronomy Department, Michigan State University, Michigan 48824, USA*

⁴ *Department of Materials Science and Technology, Nagaoka University of Technology, Niigata 940-2188, Japan*

⁵ *Faculty of Engineering, Nagasaki University, Nagasaki 852-8521, Japan*

⁶ *Department of Physics, Department of Material Science and Engineering and Materials Research Institute, The Pennsylvania State University, Pennsylvania 16802, USA*

⁷ *Faculty of Engineering, Shinshu University, Nagano 380-8553, Japan*

Despite extensive research, experimental isolation of one-dimensional (1D) sulfur crystals, which is predicted to exhibit a metallic property [1], has been eluded.

Here we demonstrate the synthesis of a previously not observed crystalline phase of elemental sulfur, consisting of monatomic 1D crystals stabilized inside carbon nanotubes (S@CNTs) [2]. This 1D phase is confirmed by high-resolution transmission electron microscopy and synchrotron X-ray diffraction (Fig.1). These 1D sulfur crystals exhibit long domain sizes up to 160 nm. Due to the covalent bonding character of sulfur, we found high thermal stability of the 1D sulfur crystals inside CNTs (~800 K). Our X-ray diffraction analysis shows a sharp structural transition of the 1D sulfur occurring at *ca* 450-650 K, indicating unique thermodynamic behavior differing from the bulk sulfur phase which undergoes complicated crystallographic and structural transitions.

Our observations by Raman spectroscopy and direct-current electric resistance measurements indicate a metallic character of the 1D sulfur crystals under ambient pressure, which is also supported by corresponding electronic structure and quantum transport calculations. The 1D sulfur crystals are in stark contrast to bulk sulfur that requires ultra-high pressures exceeding ~90 GPa to become metallic.

[1] M. Springborg and R. O. Jones *Phys. Rev. Lett.* **57**, 1145 (1986).

[2] T. Fujimori *et al.* *Nat. Commun.* (2013). *in Press*

Acknowledgements

T.F., M.T., M.E. and K.K. were supported by Exotic Nanocarbons, Japan Regional Innovation Strategy Program by the Excellence, JST.

Corresponding Author: T. Fujimori

Tel: +81-(0)26-269-5742, Fax: +81-(0)26-269-5736,

E-mail: t_fujimori@shinshu-u.ac.jp

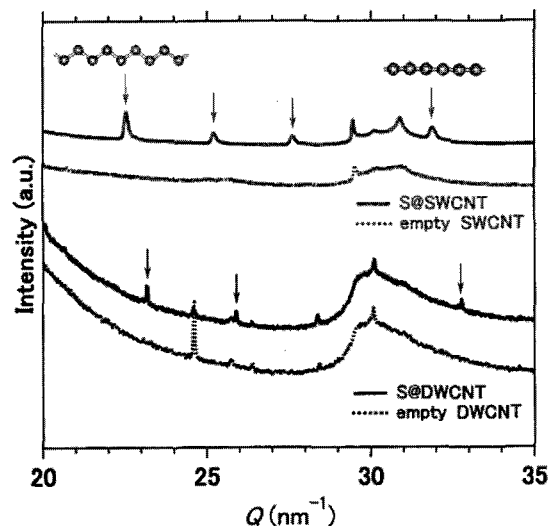


Fig.1. X-ray diffraction profiles of empty CNTs and S@CNTs obtained at 300 K.

Structure and electronic properties of π -conjugated polymers formed in carbon nanotubes

○Kenshi Miyaura, Yasumitsu Miyata, Ryo Kitaura, Hisanori Shinohara

*Department of Chemistry & Institute for Advanced Research, Nagoya University,
Nagoya 464-8602, Japan*

Carbon nanotubes (CNTs) have attracted much attention as an ideal nano-test tube to fabricate various one-dimensional materials. So far, we have reported the polymerization reaction of encapsulated molecules to produce π -conjugate polymers such as polythiophene (PT, Fig.1a), graphene nanoribbons, and polyynes [1-3]. In particular, the PT can be obtained in very high yield and exhibits remarkable optical response in visible region, which enables us to use it as a Raman imaging marker [1]. These advantages also provide a suitable system to study the structure and electronic properties of encapsulated π -conjugated polymers.

Here, we report the HRTEM observations and optical response to electrochemical doping of PT@CNTs (Fig.1b). HRTEM observations reveal that the presence of a single or double long-chain inside CNTs (Fig.1c). The absorption peak derived from PT is observed around 500 nm and shows bleaching by applying a positive gate voltage (Fig.1d,e). These spectral changes strongly suggests the hole doping to PT, which leads to a promising one-dimensional conductive wire inside CNTs.

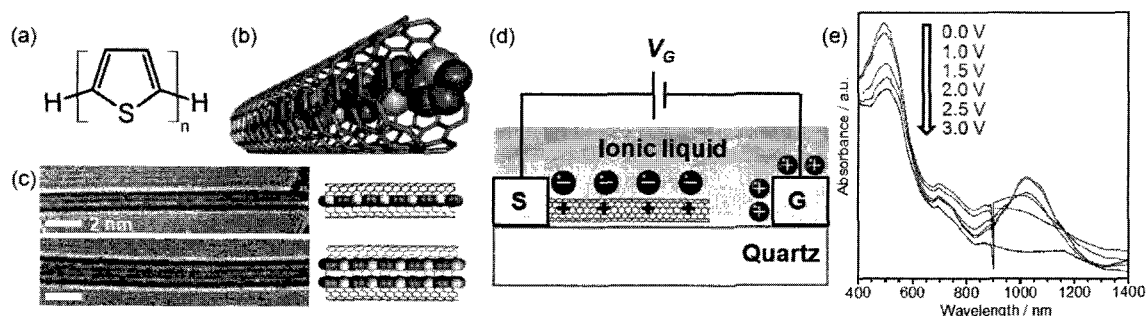


Figure 1. (a)The structure of polythiophene and (b)Image of PT@CNT. (c) HRTEM images and model structures of single(above) and double(bottom) chains of PT in CNTs. (d)The schematic of electrochemical doping and (e)the voltage dependence of optical absorption spectra of PT@CNT.

[1] K. Miyaura *et al.* The 43, 44th FNTG General Symposium. [2] M. Fujihara *et al.*, *J.Phys. Chem. C*.116, 15141 (2012). [3] C. Zhen *et al.*, *J. Phys. Chem. C*. 115, 13166 (2011)

Corresponding authors : Yasumitsu Miyata, Hisanori Shinohara

Tel:052-789-3660 Fax: 052-747-6442 E-mail: miyata-yasumitsu@tmu.ac.jp, noris@cc.nagoya-u.ac.jp

Effect of functional groups on encapsulation of functionalized C₆₀ molecules inside carbon nanohorns

○Keita Kobayashi¹, Hiroshi Ueno², Ken Kokubo², Hidehiro Yasuda¹

¹ *Research Center for Ultra-High Voltage Electron Microscopy, Osaka University, Ibaraki, Osaka 567-0047, Japan*

² *Division of Applied Chemistry, Osaka University, Suita, Osaka 565-0871, Japan*

Recently, transmission electron microscopy (TEM) has achieved atomic resolution. However, direct TEM observation of isolated organic molecules is still problematic because the molecules cannot be distinguished from contaminations. A single C₆₀ molecule encapsulated within a carbon nanotube (CNT) or a carbon nanohorn (CNH) can be distinguished easily by TEM because of its unique molecular shape [1, 2]. Since many organic molecules bind covalently to C₆₀, C₆₀ is useful for tagging organic molecules in order to elucidate their structure by TEM, and many unique molecular structures and behaviors have been observed in this way [3, 4].

The covalent bonding of C₆₀ tag to organic molecules changes the electronic state and molecule size of C₆₀. Although C₆₀ can be easily encapsulated in tubular carbon nanomaterials owing to the π - π interactions with the inner tube walls, the electronic and structural changes of C₆₀ caused by functionalization may prevent encapsulation. Therefore, it is important to clarify the effect of functionalization on the encapsulation of C₆₀ in tubular carbon nanomaterials.

In this study, we encapsulated C₆₀, its hydroxides (C₆₀(OH)_n, n = 10, 36, 44) and hydride (C₆₀H₃₆) in the inner space of CNHs in liquid phases, and evaluated the effect of the functional groups on the encapsulation with TEM. The C₆₀(OH)₃₆ and C₆₀(OH)₄₄ did not undergo encapsulation readily, whereas C₆₀, C₆₀(OH)₁₀, and C₆₀H₃₆ were easily encapsulated. Since molecular size of C₆₀(OH)₁₀ is almost same as C₆₀(OH)₃₆ and C₆₀(OH)₄₄, we consider that the molecular size is not a dominant factor for the encapsulation. Moreover, easy encapsulation of C₆₀H₃₆ in CNHs suggests that the molecules can be encapsulated into the carbon nanomaterials even when they have weak π - π interaction with the *sp*² carbon walls. Based on these results, we consider that the polarity of the C₆₀ derivatives dominantly influences the encapsulation tendency of them inside the carbon nanospace. Namely, since C₆₀(OH)₃₆ and C₆₀(OH)₄₄ have strong polarity, they are more stabilized by the solvation than by adsorbing to the walls of carbon nanomaterials, resulting in the poor accumulation inside the nanocarbon tubules. Having lower polarity, C₆₀, C₆₀(OH)₁₀, and C₆₀H₃₆ show the opposite tendencies, leading to their easy encapsulation inside the nanocarbon tubules.

This work was supported by KAKENHI (#25790003) from JSPS.

[1] B. W. Smith *et al.* *Nature* **396**, 323 (1998).

[2] K. Ajima *et al.* *Adv. Mater.* **16**, 397 (2004).

[3] Z. Liu *et al.* *Phys. Rev. Lett.* **96**, 088304 (2006).

[4] Z. Liu *et al.* *Nature Nanotechnol.* **2**, 422 (2007).

Corresponding Author: K. Kobayashi

Tel: +81-6-6879-7941, Fax: +81-6-6879-7942,

E-mail: kobayashi-z@uhvem.osaka-u.ac.jp

Photoinduced Reaction of Polyynes Derivatives and Iodine Molecules in Solution

○Yoriko Wada and Tomonari Wakabayashi

*Department of Chemistry, School of Science and Engineering, Kinki University,
Higashi-Osaka 577-8502, Japan*

Polyynes, $H(C\equiv C)_nH$ ($n \geq 2$), are sp -hybridized linear carbon chain molecules with two hydrogen atoms at both ends. These molecules have cylindrically symmetric π -electron systems and exhibit absorption bands for the allowed transition in the UV and those for a forbidden transition in the near UV region [1,2]. We have reported that absorption bands for the allowed transition disappeared and those for the forbidden transition are intensified upon addition of iodine molecules into the solution of polyyne molecules $C_{2n}H_2$ ($n=5-9$) under illumination with visible light [3,4]. The observation clearly indicates the formation of a molecular complex of polyyne and iodine molecules by photoinduced reaction [3].

In this work, we report new observations in which some polyyne derivatives form molecular complexes with iodine molecules. The absorption spectrum of methyldecacahexayne, $C_{13}H_4$, which is a derivative of the hydrogen-end-capped polyyne, $C_{12}H_2$, changed similarly to that of $C_{12}H_2$ when iodine molecules were added into the solution of $C_{13}H_4$ [5]. Figure 1 shows the absorption spectrum of a mixture of $C_{13}H_4$ and iodine molecules in hexane after irradiation with visible light. Unreacted iodine molecules were removed by reductant. The spectrum of $C_{13}H_4$ in hexane is superposed for comparison. The separation of peaks in 330-440 nm for the mixture was roughly 2000 cm^{-1} . The frequency is characteristic for the stretching vibration of the sp -hybridized carbon chain. Therefore, $C_{13}H_4$ retained its polyynic carbon chain after the reaction with iodine. These observations suggest that $C_{13}H_4$ formed molecular complex with iodine molecules.

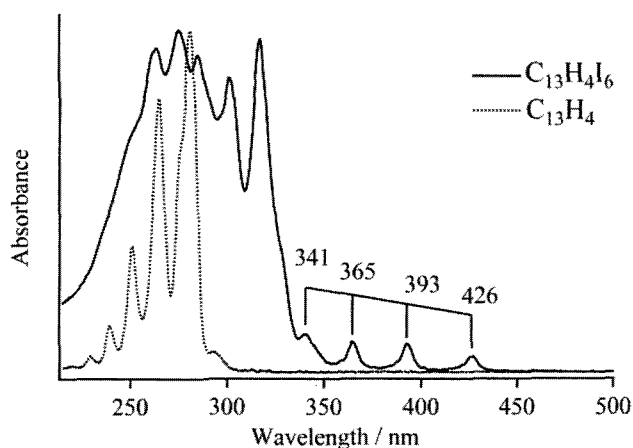


Figure 1. Absorption spectra of $C_{13}H_4I_6$ (solid line) and $C_{13}H_4$ (dotted line) in hexane.

- [1] E. Kloster-Jensen et al. *Helv. Chem. Acta.* 57, 1731 (1974).
 [2] T. Wakabayashi et al. *Chem. Phys. Lett.* 446, 65 (2007).
 [3] Y. Wada et al. *J. Phys. Chem. B.* 115, 8439 (2011).
 [4] Y. Wada et al. *Chem. Phys. Lett.* 541, 54 (2012).
 [5] Y. Wada et al. *Eur. Phys. J. D* 66, 322 (2012).

Corresponding Author: T. Wakabayashi
 Tel: +81-6-6730-5880 (ex. 4101),
 Fax: +81-6-6723-2721,
 E-mail: wakaba@chem.kindai.ac.jp

Lysosomal membrane permeabilization induced by carbon nanohorns caused reactive oxygen species generation and apoptosis in RAW264.7 cell.

○Mei Yang¹, Minfang Zhang¹, Yoshio Tahara¹, Sumio Iijima^{1,2}, Masako Yudasaka¹

¹ *Nanotube Research Center, National Institute of Advanced Industrial Science and technology 5-2, Tsukuba, Japan*

² *Department of Material Science and Engineering, Meijo University, Nagoya, Japan*

Carbon nanomaterials have offered a wide range of potential applications including biomedicine and nanotechnology [1]. In the meantime, public concern on their environmental and health effects is growing rapidly. Many adverse effects such as inflammatory response, oxidative stress, and thrombus induction have been reported *in vitro* and *in vivo* studies [2-4]. Recent studies showed that carbon nanomaterials induced cell apoptosis, and reactive oxygen species (ROS) generation was considered as the main adverse effects [5], but the details are still unclear. Therefore, the extensive toxicological studies of carbon nanomaterials at molecular level are necessary.

In this study, we investigated the cell death mechanism of macrophage (RAW264.7) induced by excess uptake of oxidized carbon nanohorns (CNH_{Laox}). We found that neither the mitochondria nor oxidase systems were directly involved in the CNH_{Laox}-related ROS production and provided another ROS generation process induced by carbon nanohorns. The results showed (Fig.1.) that the overload of CNH_{Laox} in lysosomes induced lysosomal membrane permeabilization (LMP), leading to the cathepsins (lysosomal enzyme) release, and the cathepsin caused ROS generation. Both cathepsin and ROS induced mitochondrial dysfunction, subsequently, the caspases activation and the cell apoptosis. Our studies clarified the macrophage apoptotic pathway induced by nanocarbons, provided some clues about how nanocarbons induce the ROS production and indicated LMP are the initial effectors for nanocarbon-related cell death. This work may complement the understanding of toxicology mechanism of nanocarbons and be quite helpful for establishing the safe manufacturing guidelines for carbon nanomaterials.

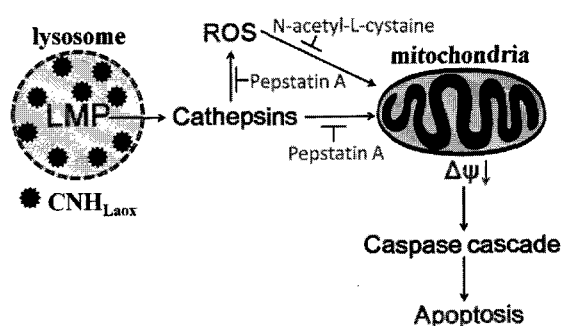


Fig.1. Proposed CNH_{Laox}-induced cell death pathway.

[1] M. F. De Volder *et al.* Science. 339, 535(2013).

[2] A. A. Shvedova *et al.* Am. J. Physiol. Lung Cell. Mol. Physiol. 289, L698 (2005).

[3] M. Horie *et al.* Carbon. 54, 155(2013).

[4] S. K. Singh *et al.* ACS Nano. 5, 4987(2011).

[5] R. K. Srivastava *et al.* Nanotoxicology. 5, 195(2011)

Corresponding Author: M. Yang and M. Yudasaka.

Tel:029-861-4818, TEL/Fax: +81-29-861- 6290

E-mail: m-yan@aist.go.jp (M. Yang), m-yudasaka@aist.go.jp (M. Yudasaka).

Development of Ion Mobility Measurement System

○Toshiki Sugai, Yasuhiro Hiroshiba, Ninako Mikami

Department of Chemistry, Toho University, Miyama 2-2-1 Funabashi, 274-8510, Japan

Ion mobility measurements have been a powerful tool for analysis on structures of nanocarbon materials. Structures of Metal-fullerenes show significant dependence on the number of metal atoms and the cage size and their novel structures have been also clarified[1]. To study further, we have been developing an ion trap mobility system and structural changes of polystyrene particles were monitored for more than 2 hours[2]. The measurements have revealed the stability and the sensitivity of the system. Despite of these advantages, the trap system has low mobility resolution because of the small size of the trap and has difficulty on measuring nano materials because of the light scattering detection system. To improve the resolution and to research nano materials, we have been developing new mobility system.

The system consists of ion funnel for efficient particle injection and linear ion trap for long movement and high resolution measurement. The system also is equipped with connection between ion mobility and mass spectrometer. Those functions are realized by newly developed power supply for the system. Controlled RF and DC voltage manipulate the particle to realize efficient measurement for long time. The details of the system will be presented.

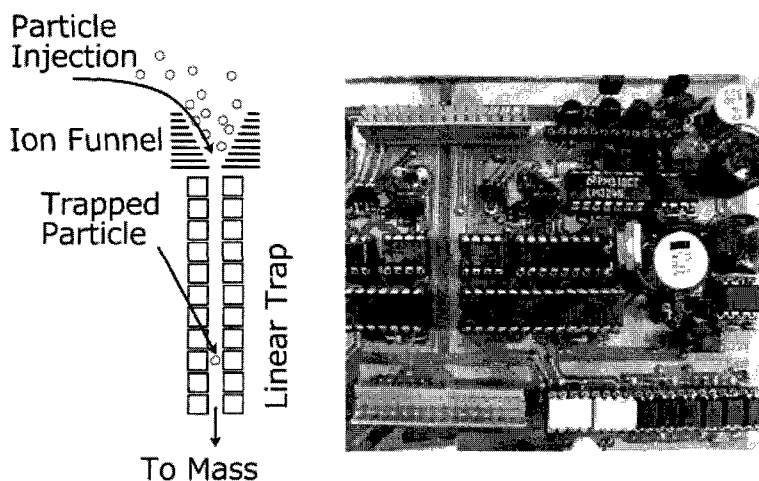


Fig. 1 Schematic view of mobility system and power supply

- [1] T. Sugai *et al.*, *J. Am. Chem. Soc.* **123**, 6427 (2001).
 [2] T. Sugai *et al.*, The 38th and 44th symposium.
 TEL: +81-47-472-4406, E-mail: sugai@chem.sci.toho-u.ac.jp

Enhanced photoelectrochemical performance of composite photovoltaic cells of $\text{Li}^+@C_{60}$ /sulfonated porphyrin supramolecular nanoclusters

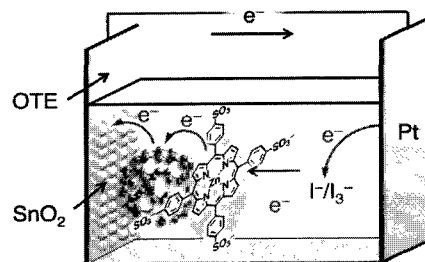
○Kei Ohkubo¹, Yuki Kawashima¹, Hayato Sakai², Taku Hasobe², Shunichi Fukuzumi¹

¹ Department of Material and Life Science, Graduate School of Engineering, Osaka University, ALCA, Japan Science and Technology Agency, Osaka 565-0871, Japan

² Department of Chemistry, Faculty of Science and Technology, Keio University, Yokohama, 223-8522, Japan

Photoelectrochemical cells (PECs) have been widely investigated as a next-generation solar cell because of their simple structure. The photoinduced charge separation between the excited state of dye and the electrode plays an important role in improvement of PEC performance. Extensive efforts have so far been devoted to design and synthesize electron donor-acceptor linked molecules to achieve efficient photoinduced charge separation for applications to PECs. We have recently designed and synthesized simple electron donor-acceptor supramolecular complexes composed of lithium ion encapsulated fullerene ($\text{Li}^+@C_{60}$) and sulfonated zinc *meso*-tetraphenylporphyrin (ZnTPPS^{4-}). Photoexcitation of the supramolecule exhibited extremely slow charge-recombination of the CS state ($\tau = 0.3$ ms) in benzonitrile (PhCN).[1] The driving force of photoinduced electron transfer from ZnTPPS^{4-} to the triplet excited state of $\text{Li}^+@C_{60}$ is highly positive ($-\Delta G_{\text{ET}} = 0.98$ eV) in polar PhCN,[1] which is large enough to afford the CS states even under the non-polar environment in nanoclusters. We report herein photovoltaic cells using $\text{Li}^+@C_{60}/\text{ZnTPPS}^{4-}$ nanoclusters, which are assembled on optically transparent electrode (OTE) of nanostructured SnO_2 (OTE/ SnO_2) as shown in Scheme 1.

Photoelectrochemical measurements were performed using a standard two-electrode system consisting of a working electrode and a Pt wire gauze electrode in air-saturated MeCN containing 0.5 M LiI and 0.01 M I_2 . The maximum IPCE values of OTE/ $\text{SnO}_2/(\text{Li}^+@C_{60})_n$ and OTE/ $\text{SnO}_2/(\text{ZnTPPS}^{4-})_n$ are only 5% (425 nm) and 22% (445 nm), respectively. In contrast with the reference experiments, the IPCE value of OTE/ $\text{SnO}_2/(\text{ZnTPPS}^{4-}/\text{Li}^+@C_{60})_n$ is much higher than the sum of the two individual IPCE values of the individual systems OTE/ $\text{SnO}_2/(\text{ZnTPPS}^{4-})_n$ and OTE/ $\text{SnO}_2/(\text{Li}^+@C_{60})_n$ in the visible region. The maximum IPCE value attained in these experiments was 77% at 450 nm [2]. The photocurrent generation occurred via photoinduced electron transfer from ZnTPPS^{4-} to $\text{Li}^+@C_{60}$ in the supramolecular nanoclusters (Scheme 1), which was confirmed by nanosecond time-resolved transient absorption spectral measurements and EPR spectroscopy [2].



Scheme 1 Schematic image of photoelectrochemical cell of OTE/ $\text{SnO}_2/\text{ZnTPPS}^{4-}/\text{Li}^+@C_{60}$

[1] Ohkubo, K.; Fukuzumi, S. et al., *Chem. Commun.* **2012**, 48, 4314; [2] *Chem. Commun.* **2013**, 49, 4474.

Corresponding Author: K. Ohkubo

Tel: +81-6-6879-7369, Fax: +81-6-6879-7370,

E-mail: ookubo@chem.eng.osaka-u.ac.jp

Surface functionalization of nanodiamonds towards high solubility in physiological media and practical biomedical applications

Li Zhao¹, Xiao Chen², Tokuhiro Chano³, Naoki Komatsu¹

¹*Department of Chemistry, Shiga University of Medical Science, Otsu, 520-2192, Japan*

²*Department of Biomedical, Dental Materials and Engineering, Graduate School of Dental Medicine, Hokkaido University, Sapporo, 060-8586, Japan*

³*Department of Clinical Laboratory Medicine, Shiga University of Medical Science, Otsu, 520-2192, Japan*

Biomedical applications of nanodiamond (ND) have been investigated extensively due to its low toxicity, excellent biocompatibility and non-bleaching fluorescence. However, to date, practical biomedical applications are elusive because of poor solubility and inadequate colloidal stability of ND in physiological media. To address this problem, we have covalently grafted hydrophilic polyglycerol (PG) on the surface of ND using hydroxyl and carboxyl groups on ND surface as initiating sites.^[1] PG grafting not only endowed ND with good solubility under physiological environments, but also provided possibility for further surface functionalization to incorporate multiple functionalities by taking advantage of the extensibility of the PG layer.

The further functionalization on the PG grafted ND (ND-PG) was performed through stepwise organic transformations. As a result, some of the hydroxyl groups on ND-PG were converted to azide and amino groups, which can be conjugated with various functional moieties through click chemistry or amidation. Versatility of this strategy provided various kinds of ND-PG derivatives with aqueous solubility and many other functionalities such as near-infrared (NIR) fluorescence, targeting specificity and drug loading, which have applied successfully to fluorescence cell labeling, *in vivo* NIR imaging and targeted drug delivery (Fig. 1).^[2]

It is worth mentioning that the strategy of PG grafting and further functionalization is applied not only to ND, but also other nanocarbon materials (CNT and graphene) as well as metal oxide nanoparticles (iron oxide and zinc oxide),^[3-4] indicating that this is a general and practical method for surface functionalization of nanomaterials especially in view of biomedical applications.

Reference [1] L. Zhao, *et al. Angew. Chem. Int. Ed.*, 50, 1388 (2011); [2] L. Zhao, *et al.* submitted; [3] L. Zhao, *et al. Adv. Funct. Mater.*, 22, 5107 (2012); [4] L. Zhao, *et al. J. Ind. Chem. Soc.*, 88, 1787 (2011).

Corresponding Author: Li Zhao

Tel: +81-77-548-2102, Fax: +81-77-548-2405, E-mail: lzhao@belle.shiga-med.ac.jp

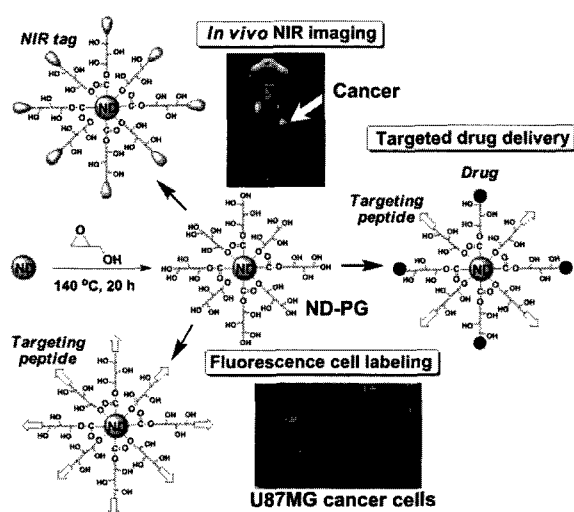


Fig. 1 Biomedical applications of functionalized ND.

Carbon Nanotubes Growth via Twisted Graphene Nanoribbons

○ Hong En Lim¹, Yasumitsu Miyata², Ryo Kitaura¹, Yoshifumi Nishimura¹, Yoshio Nishimoto¹, Stephan Irle¹, Jamie H. Warner³, Hiromichi Kataura⁴ and Hisanori Shinohara¹

¹Department of Chemistry, Nagoya University, Nagoya, Japan

²Department of Physics, Tokyo Metropolitan University, Hachioji, Japan

³Department of Materials, University of Oxford, Oxford, United Kingdom

⁴Nanosystem Research Institute, AIST, Tsukuba, Japan

Advances in nano-carbon studies have introduced the different means [1, 2] by which a carbon nanotube (CNT) can be unfolded into a narrow strip of graphene, the so-called graphene nanoribbon (GNR). However, how can these flimsy ribbons of carbon be actually rolled to achieve a tubular geometry still remains elusive. Despite of the recently prevailing rolling-up model, no one has successfully identified any phenomenon alike experimentally during the past decade. Recently, the theoretical studies of Kit *et al.* [3] and Jiang *et al.* [4] have demonstrated that CNTs can be formed through the twisting of GNR and the GNR resides within a CNT would retain a helical conformation. These predictions may provide a possible route for a novel synthesis of CNTs through the twisting of GNR.

Here, we report the first experimental fabrication and characterization of a thermally-induced, self-intertwining of GNRs for the preferential synthesis of CNTs with chiral indices of (7, 2) and (8, 1). The GNR is constructed inside an outer tube template by using a perylene derivative (PTCDA, C₂₄H₈O₆). Optical measurements performed on the newly grown CNTs reveal a significant enhancement in these two chiralities (Fig. 1, left), consistent with those of the predicted CNTs formed via the twisting of armchair-edge GNRs with a width of N=5 [5] (Fig.1, right). We believe that the current findings contribute greatly to complement the present understanding towards CNT synthesis, which provides future chirality tuning and novel nanomaterials engineering.

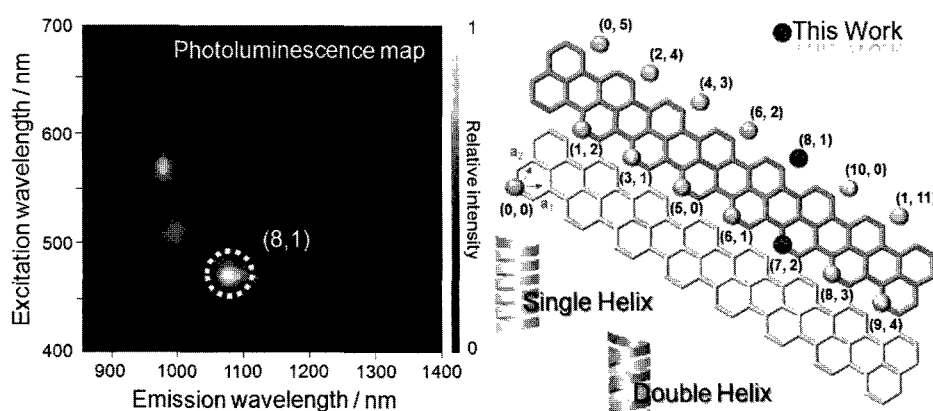


Fig. 1. (Left) PL map of the newly synthesized CNTs.

(Right) Possible chiral vectors obtained when the single/double chains of the PTCDA-derived armchair-edge GNR with a width, N=5 intertwined.

[1] X. Li *et al.* Science 319, 1229 (2008).

[3] O. O. Kit *et al.* Phys. Rev. B 85, 085428 (2011).

[5] M. Fujita *et al.* J. Phys. Soc. Jpn. 65, 1920 (1996).

[2] D. V. Kosynkin *et al.* Nature 458, 872 (2009).

[4] Y. Jiang *et al.* ACS Nano 3, 2126 (2011).

Corresponding Author: H. Shinohara

Tel: +81-52-789-2482, Fax: +81-52-747-6442, E-mail: noris@nagoya-u.jp

Highly Durable Polymer Electrolyte Fuel Cell Electrocatalyst Based on Carbon Nanotube

○Tsuyohiko Fujigaya^{1,2} and Naotoshi Nakashima^{1,2,3}

1 Department of Applied Chemistry, Graduate School of Engineering.

Kyushu University, 744, Motooka Nishi-ku Fukuoka, 819-0395, Japan

2 WPI I2CNER, Kyushu University, 744 Motooka, Nishi-ku, Fukuoka, 819-0395, Japan

3 JST-CREST, 5 Sanbancho, Chiyoda-ku, Tokyo 102-0075, Japan

Fuel cell is key technology to convert hydrogen energy into electric power quite efficiently. Especially, polymer electrolyte fuel cell (PEFC) is promising candidate for the energy source of car, portable electronic device, and house. Carbon nanotubes (CNTs) have been emerged as a better conductive supporting material for catalyst nanoparticle than conventional material such as carbon black due to their excellent electron conductivity, better electrochemical durability and fibrous structure. The key issue to utilize the CNTs as a supporting material is to develop a proper method to immobilize the metal nanoparticle onto CNT surface. We have reported polybenzimidazole (PBI) adsorbed onto the surface of CNTs and acts as the good dispersant of CNTs [1-4]. By taking the advantage of uniform wrapping of PBI on CNTs surface, we utilized this composite (CNT/PBI) as a novel carbon supporting materials for the loading of platinum (Pt) nanoparticles to fabricate an electrocatalyst for PEFC. The obtained electrocatalyst (CNT/PBI/Pt) shows excellent Pt utilization efficiency mainly due to the formation of ideal interfacial structure around Pt [2,3,4].

We fabricated the PEFC membrane electrode assembly (MEA) using CNT/PBI/Pt doped with acid (Fig. 1) as an electrolyte electrocatalyst, respectively, and measured the fuel cell performance using hydrogen and air as fuels at 120 °C without humidification [5,6]. As a comparison, electrocatalyst fabricated based on carbon black (CB) in place of CNT was also prepared and employed for MEA. Quite interestingly, CNT-based MEA showed 100 times higher durability compared to that of CB-based MEA. Our unique technique to immobilize Pt onto a non-oxidized CNT largely contributed to such a high lifetime of the electrocatalyst.

References

- [1] M. Okamoto, T. Fujigaya, and N. Nakashima *Adv. Funct. Mater.* 18, 1776-1782 (2008).
- [2] M. Okamoto, T. Fujigaya, and N. Nakashima *Small* 5, 735-740 (2009).
- [3] T. Fujigaya, M. Okamoto, and N. Nakashima *Carbon* 47, 3227-3232 (2009).
- [4] T. Fujigaya, N. Nakashima *Adv. Mater.*, 25, 1666-1681 (2013).
- [5] K. Matsumoto, T. Fujigaya, K. Sasaki and N. Nakashima *J. Mater. Chem.* 21, 1187-1190 (2011).
- [6] M. R. Berber, T. Fujigaya, K. Sasaki, and N. Nakashima *Sci. Rep.*, 3, Art. No. 1764 (2013).

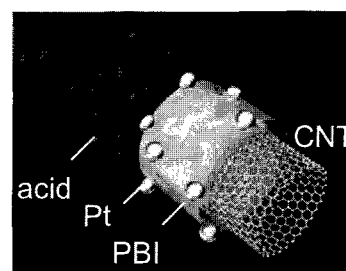


Fig. 1 Structure of CNT-based electrocatalyst

Stabilities and Electronic Structures of Carbon Impurities in Hexagonal Boron-Nitride Monolayers and Bilayers

○Yoshitaka Fujimoto, Takashi Koretsune, and Susumu Saito

Department of Physics, Tokyo Institute of Technology, Tokyo 152-8551, Japan

Due to the similarity to a graphene, a two-dimensional monolayer sheet of hexagonal boron nitride (h-BN) has attracted much attention from the viewpoint of basic nanoscience and relevant nanotechnology in nanoelectronics. Although graphene and h-BN sheet have similar geometrical properties, they exhibit different electronic properties; graphene is a semimetal, whereas h-BN monolayer is a semiconductor with a substantially wide energy gap. Hence, the h-BN monolayers with the semiconducting properties are the promising candidates for next-generation nanoelectronics materials. Substitutional doping with foreign atoms often offers a firm route to modify the electronic properties such as band gap and electrical conductivity. Actually, the carbon doping into h-BN monolayer has been carried out [1], and it has been reported that the electronic properties of h-BN monolayers change from insulating property into metallic one [2]. However, our knowledge as to the electronic properties and the stabilities of carbon defects in h-BN sheets is still limited at present.

In the present work, we perform thorough first-principles investigations that clarify the effects of the carbon doping on the electronic structures and the energetics of not only the monolayer but also the bilayer of the h-BN sheets. We show that the donor and acceptor-type states can be induced by the C atoms placed at B and N sites, respectively (Fig. 1). These impurity states are found to be relatively deep, and we therefore show the possible methods to manipulate the ionization energies of the C-impurity induced states. It is also revealed that the manipulation of the ionization energies could open the new conduction channels. We further study the stabilities on the stacking patterns of the bilayer h-BN sheets and the C-doping effects into them. It is found that the most energetically favorable stacking patterns of heavily C-doped h-BN bilayers are different from those of undoped bilayers. In addition, we also find that the most preferable stacking patterns of the C-doped bilayers placed at B and N sites are different from each other. Finally, we show the electronic structures of C-doped and undoped h-BN bilayer sheets, and the ionization energies of C-doped h-BN bilayers placed at B and N sites are found to be relatively small compared with those of monoalyers, respectively.

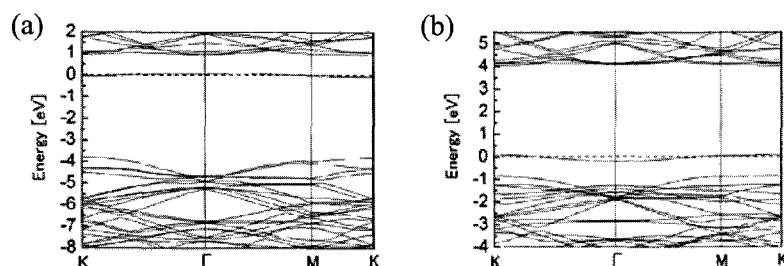


Figure 1 Energy bands of C-doped h-BN monolayers placed at (a) B and (b) N sites. The Fermi energy is set to 0 eV.

[1] O. L. Krivnek, M. F. Chisholm, V. Nicolosi, T. J. Penycook *et al.*, *Nature* **464**, 571 (2010).

[2] X. Wei, M. S. Wang, Y. Bando, and D. Golberg, *ACS Nano* **5**, 2916 (2011).

Corresponding Author: Yoshitaka Fujimoto

TEL: +81-3-5734-2368, FAX: +81-3-5734-2368, E-mail: fujimoto@stat.phys.titech.ac.jp

Effect of High Pressure Pre-Annealing on Graphene Growth on Copper by Chemical Vapor Deposition

○Seiya Suzuki, Takashi Nagamori, Yuki Matsuoka, and Masamichi Yoshimura

Graduate School of Engineering, Toyota Technological Institute, 2-12-1 Hisakata, Tempaku, Nagoya 468-8511, Japan

Recently developed chemical vapor deposition methods have produced large-size single-crystal graphene on catalytic metal surfaces, especially on copper (Cu) [1], and further increase in the crystal size is desirable for electro/optic applications. In this report, we performed high pressure annealing (~ 0.34 MPa) of Cu substrate prior to the atmospheric chemical vapor deposition (APCVD) growth of graphene, and studied the effect of the annealing on the nucleation and growth.

Single-layer graphenes were grown on Cu foils (100 μm thick) by APCVD at 1050 $^{\circ}\text{C}$ under the flows of Ar, H_2 , and CH_4 after high or ambient pressure annealing for 5 h. Figures 1(a) and (b) show SEM images of the graphene on Cu grown by APCVD for 20 min with high or ambient pressure pre-annealing, respectively. It was observed that the high pressure annealing suppressed the nucleation of graphene and resulted in large-size single-crystal. Atomic force microscope observations revealed the existence of impurity particles on both surfaces; the particles on Cu after high pressure annealing had smaller density but larger size than those of ambient pressure annealing.

Carbon KLL Auger imaging of the graphene with ambient pressure pre-annealing clearly showed the hexagonal shape of graphene (Fig.1 (c)). Silicon (Si) KLL Auger imaging (Fig.1 (d)), which was taken on the same area as Fig.1 (c), revealed that relatively small (S) and large (L) particles containing Si existed in Cu and graphene, respectively. Since oxygen KLL also had relatively high signal on the particles, the particles would be silicon oxide from quartz tube of our APCVD furnace.

Since the number of particles and nucleation had good correlation, we suggest that the nucleation of the graphene on Cu in APCVD is initiated on the particles. It is also noted that a sub-millimeter-size (~ 0.5 mm) single-crystal graphene has been grown by combining high pressure annealing and electropolishing of Cu.

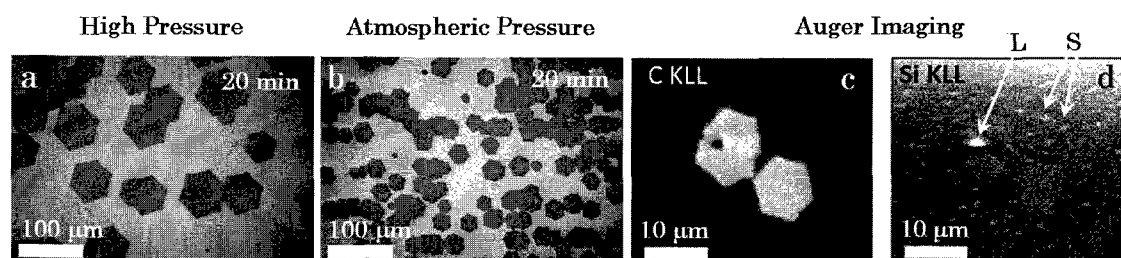


Fig.1 SEM images of graphene on Cu grown by APCVD with (a) high or (b) ambient pressure pre-annealing. (c) Carbon KLL and (d) Si KLL Auger imaging of graphene on Cu grown by APCVD.

[1] Z. Yan *et al.* ACS Nano **6**, 9110 (2012).

Corresponding Author: Seiya Suzuki (Tel: +81-52-809-1852, E-mail: sd11502@toyota-ti.ac.jp)

Electronic structure of potassium doped MoS₂

○Nguyen Thanh Cuong^{1,3}, Minoru Otani^{1,3}, Susumu Okada^{2,3}

¹*Nanosystem Research Institute, National Institute of Advanced Industrial Science and Technology (AIST), Tsukuba 305-8568, Japan*

²*Graduate school of Pure and Applied Sciences, University of Tsukuba, Tsukuba 305-8571, Japan*

³*Japan Science and Technology Agency, CREST, 7 Gobancho, Chiyoda-ku, Tokyo 102-0076, Japan*

Molybdenum disulfide (MoS₂) has been attracted a lot of research interests because of its peculiar electronic and geometric structures: it has two-dimensional planar structure with massive Dirac electrons leading to unusual optical properties [1]. For practical applications, it is essential to modify and control the electronic structure of MoS₂. One of plausible pathway is the chemical doping alkali/alkaline earth metals to MoS₂ by analogy with graphite-intercalated compounds [2]. In this work, we explore the possibility of tailoring the electronic structure of MoS₂ monolayer by doping potassium atoms on the surface using first-principles total-energy calculations. We find that potassium atoms strongly bound to the surface of MoS₂ with a binding energy of 1.5 eV per potassium atom. The potassium-doped MoS₂ is a metal due to the charge transfer from potassium atom to the conduction band of MoS₂. On the other hand, we also find that the nearly-free electron (NFE) state of MoS₂ shifts downward with increasing the concentration of doped potassium, and finally crosses the Fermi level at the concentration of 0.22 potassium atom per unitcell. The NFE state is known to have the floating character with the maximum amplitude distribution in vacuum region where the atoms are absent. Under the situation, the NFE state of MoS₂ acts as the conducting channel for the injected carrier. These results indicate the possibility to induce the superconductivity in MoS₂ by doping alkali/alkaline earth metals.

[1] Q. H. Wang *et al.*, *Nature Nanotech.* 7, 699 (2012).

[2] M. S. Dresselhaus *et al.*, *Adv. Phys.* 30, 139 (1981).

Corresponding Author: Nguyen Thanh Cuong

E-mail: cuong-nguyen@aist.go.jp

Tel: +81-29-861-6067, Fax:+81-29-861-3171

Highly Conductive NGP/Epoxy Composites

○Afshin J. Ebrahimi, Shingo Suzuki, Seiichi Sawatani, Masataka Ueno,
Miyamoto Norihiko, Masayasu Iida

ITEC Co.Ltd, 4-132-1, Kannabe chō, Sakai ku, Sakai, Osaka 590-0984, Japan

The increasing demand for smart, small and faster equipment and electronic devices has created a need for novel materials. In addition, industry has a growing need to tailor the properties of materials, including thermal and electrical conductance, for designated applications. Polymers are commonly known due to their thermal and electrical isolating properties. Conductive polymer composites can substitute metals in many vast applications. Carbon based nano materials had an important role to increase or modify polymer properties such as thermal and electrical conductivities.

Some of the advantages of conductive polymers comparing to metals are their chemical resistance, lower density; corrosion or erosion resistance, oxidation resistance, increased processibility, low cost production and possibility of properties adjustment to fit the special purposes.

The main application for thermally conductive polymers is heat sinks and spreaders. The use of nano-scale fillers such as metals, semiconductors, organic and inorganic particles, and fibers, especially carbon structures are of particular interest and the subject of intense investigation. On the other hand the unique properties of carbon allotropes such as CNT and Graphene offer crucial advantages over other nano-fillers.

Our current efforts to exploit the attractive properties of carbon based material have focused on composites containing engineered produced Multi and Few Layer Graphene Sheets (MLGS and FLGS), which have outstanding thermal, electrical and mechanical properties with significant promise in a vast range of applications.

The potential of using MLGS and FLGS as filler in polymer composite compare to other allotropes has not been fully investigated yet. Our research shows that compare to other carbon containing material, MLGS have magnificent results for enhancing both electrical and thermal conductivity.

Thermal conductivity of the composites increases as the filler content increases, as instance for just 20 percent MLGS containing epoxy composite, In-plane and out-plane thermal conductivity can reach 35 and 15W/mK respectively, with the same composition electrical resistivity decreased to $5.00 \cdot 10^{-2} \Omega \cdot \text{cm}$.

Corresponding Author: A. Ebrahimi

Tel: +81-72-226-8853, Fax: +81-072-226-6653

E-mail: afshin@itec-es.co.jp

Ultraviolet Photoelectron Spectra of $\text{Sc}_3\text{C}_2@C_{80}$

○Takafumi Miyazaki¹, Sousuke Ookita¹, Takeyuki Saima¹, Tatsuhiko Nishi², Okimoto Haruya³,
Norino Izumi³, Yuusuke Nakanishi³, Hajime Yagi¹, Hisanori Shinohara³ and Shojun Hino¹

¹Graduate School of Science and Engineering, Ehime University, Matsuyama 790-8577, Japan

²Institute for Molecular Science, Okazaki, 444-8585, Japan

³Graduate School of Science, Nagoya University, Nagoya 464-8602, Japan

We have been measuring ultraviolet photoelectron spectra (UPS) of endohedral fullerenes to elucidate their electronic structure. Here, we present UPS and the DFT simulated spectra of $\text{Sc}_3\text{C}_2@C_{80}$ and discuss the structure of the entrapped Sc_3C_2 cluster.

The UPS of $\text{Sc}_3\text{C}_2@C_{80}$ were measured at UVSOR BL8B of the Institute for Molecular Science. The UPS onset energy of $\text{Sc}_3\text{C}_2@C_{80}$ is 0.9 eV, which is slightly smaller than empty C_{80} . While, the deeper valence band UPS ($\text{BE} > 5$ eV) of $\text{Sc}_3\text{C}_2@C_{80}$ are analogous to those of other endohedral fullerenes, the upper valence band UPS ($\text{BE} < 5$ eV) are significantly different from those of other endohedral fullerenes.

As for the structure of the entrapped Sc_3C_2 , trifoliate [1] and planar [2] structures were proposed (Fig. 1). The

UPS is well reproduced by a simulated spectrum obtained from DFT geometry optimized structure having the trifoliate cluster. NPA revealed the oxidation state of the cluster to be $\text{Sc}^{2+} \sim 3+$ and C_2^{2-} . A comparison of the molecular orbitals of $\text{Sc}_3\text{C}_2@C_{80}$ and empty $C_{80}-I_h$ suggests six electrons transfer, namely $(\text{Sc}_3\text{C}_2)^{+6}@C_{80}^{6-}$ electronic configuration.

[1] K. Tan *et al.*, *J. Phys. Chem. A* 2006,

110, 1171-1176, [2] Nishibori *et al.*, *J. Phys. Chem. B* 2006, 110, 19215-19219.

Corresponding Authors: T. Miyazaki, E-mail: miyazaki@eng.ehime-u.ac.jp, phone: 089-927-9930; S. Hino, E-mail: hino@eng.ehime-u.ac.jp, phone: 089-927-9924.

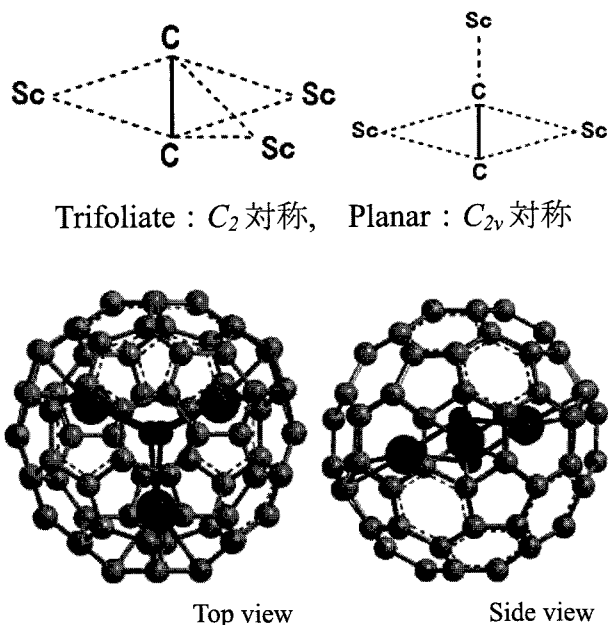


Figure 1. DFT geometry optimized structure of the entrapped Sc_3C_2 cluster of $\text{Sc}_3\text{C}_2@C_{80}$.

Electrochemical synthesis of $\text{Li}^+\text{@C}_{60}^{\cdot-}$ based on the high ionic conductivity of $[\text{Li}^+\text{@C}_{60}](\text{PF}_6^-)$ in aromatic solvent

○Hiroshi Ueno¹, Ken Kokubo¹, Kei Ohkubo², Naohiko Ikuma¹, Hiroshi Moriyama³,
Shunichi Fukuzumi^{2,4}, Takumi Oshima¹

¹ *Division of Applied Chemistry, Graduate School of Engineering, Osaka University, 2-1 Yamadaoka, Suita, Osaka 565-0871, Japan.*

² *Department of Material and Life Science, Graduate School of Engineering, Osaka University, and ALCA, Japan Science and Technology (JST), Suita, Osaka 565-0871, Japan*

³ *Department of Chemistry, Faculty of Science, Toho University, 2-2-1 Miyama, Funabashi, Chiba 274-8510, Japan*

⁴ *Department of Bioinspired Science, Ewha Womans University, Seoul, 120-750, Korea*

One of the most remarkable properties of $\text{Li}^+\text{@C}_{60}$ is its high ionicity resulting from the encapsulation of a lithium cation. The cationic $\text{Li}^+\text{@C}_{60}$ forms ion-pair with a suitable anion as reported [1], which brings about its unique behavior in comparison with other endohedral fullerenes. However, such ionic nature of $\text{Li}^+\text{@C}_{60}$ is stated to be responsible for its rock-salt-type crystal with PF_6^- counter anion [2], no other detail about the ionic property has been reported [3,4]. In this study, we measured the ionic conductivity of $[\text{Li}^+\text{@C}_{60}](\text{PF}_6^-)$ salt in organic solvents, and thus, based on the results, we succeeded in the electrochemical synthesis of Li^+ -encapsulated C_{60} radical anion without any supporting electrolytes.

The ionic conductivity measurement was performed in *o*-dichlorobenzene (*o*-DCB) and benzonitrile (PhCN) on account of the sufficient solubility and the electrochemical stability of $[\text{Li}^+\text{@C}_{60}](\text{PF}_6^-)$ in these aromatic solvents. Figure 1 shows the molar conductivity (Λ) for various concentrations (c) of $[\text{Li}^+\text{@C}_{60}](\text{PF}_6^-)$ and $\text{TBA}^+\text{PF}_6^-$, the latter is a common supporting electrolyte for organic solvents. The exponential change in Λ with $c^{1/2}$ suggested that $[\text{Li}^+\text{@C}_{60}](\text{PF}_6^-)$ acts as a weak electrolyte. The observed higher ionic conductivity of $[\text{Li}^+\text{@C}_{60}](\text{PF}_6^-)$ than that of $\text{TBA}^+\text{PF}_6^-$ can be ascribed to the weak interaction between the outer PF_6^- and the encapsulated Li^+ due to the shielding by the fullerenyl cage. The electrochemical reduction of $[\text{Li}^+\text{@C}_{60}](\text{PF}_6^-)$ in *o*-DCB without any supporting electrolyte gave Li^+ -encapsulated C_{60} monovalent radical anion $\text{Li}^+\text{@C}_{60}^{\cdot-}$ selectively, which was characterized by NIR and EPR spectroscopy. In this $\text{Li}^+\text{@C}_{60}^{\cdot-}$ species, the *cation* is encapsulated *by anion*, and thus the ionic property is expected to be far more different from the starting *ion-pair* type $[\text{Li}^+\text{@C}_{60}](\text{PF}_6^-)$.

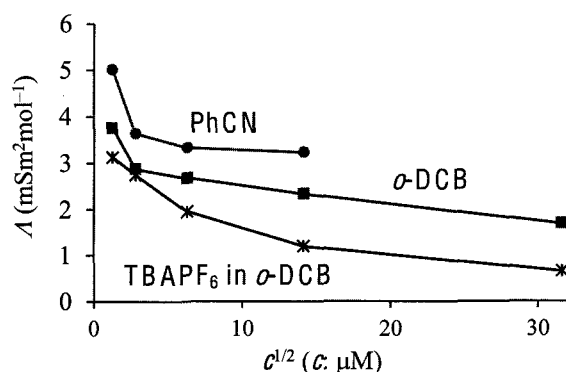


Fig. 1 Molar conductivity Λ of $[\text{Li}^+\text{@C}_{60}](\text{PF}_6^-)$ measured in PhCN and *o*-DCB for various concentrations at 298 K. The conductivity of $\text{TBA}^+\text{PF}_6^-$ was also measured as a reference.

[1] Sawa, H. and Tobita, H. *et al. Nat. Chem.* 2010, 2, 678. [2] Aoyagi, S. *et al. Angew. Chem. Int. Ed.* 2012, 51, 3377. [3] Fukuzumi, S. *et al. Chem. Commun.* 2012, 48, 4314. [4] Kokubo, K. *et al. Nanoscale* 2013, 5, 2317.

Corresponding Author: K. Kokubo

Tel: +81-6-6879-4592, Fax: +81-6-6879-4593, E-mail: kokubo@chem.eng.osaka-u.ac.jp

Chemical Modifications of Lithium-Ion-Encapsulated [60]Fullerene [Li⁺@C₆₀(CpH)]PF₆⁻ and [Li⁺@C₆₀(CPh₂)]PF₆⁻

○Hiroki Kawakami, Hiroshi Okada, Yutaka Matsuo

*Department of Chemistry, School of Science, The University of Tokyo, 7-3-1 Hongo,
Bunkyo-ku, Tokyo 113-0033, Japan*

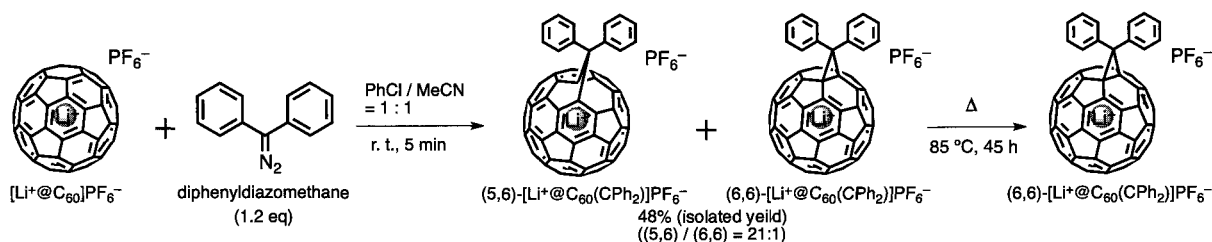
Lithium-ion-encapsulated [60]fullerene (Li⁺@C₆₀) is the first example of metallo[60]fullerene that was isolated and structurally characterized [1]. The Li⁺@C₆₀ derivatives are expected to be applicable to organic electronic devices such as organic solar cells. Although chemical modifications of Li⁺@C₆₀ should be needed toward the device applications, there are a few reports on covalently chemical modifications of Li⁺@C₆₀, [Li⁺@PCBM]PF₆⁻ [2] and Li⁺@C₆₀(OH)₇O⁻ [3].

Here, we have demonstrated Diels-Alder reaction with cyclopentadiene (CpH) as a diene and [3+2] cycloaddition reaction with a diphenyldiazomethane resulting in Li⁺@C₆₀ derivatives, which have 58π conjugated systems. These reactions immediately proceeded to give [Li⁺@C₆₀(CpH)]PF₆⁻ and [Li⁺@C₆₀(CPh₂)]PF₆⁻. The products could be isolated by electrolyte-associated HPLC technique.

In the case of [Li⁺@C₆₀(CPh₂)]PF₆⁻, a product containing [5,6]-[Li⁺@C₆₀(CPh₂)]PF₆⁻ with a small amount of [6,6]-[Li⁺@C₆₀(CPh₂)]PF₆⁻ could be purified HPLC technique and recrystallization to obtain pure [5,6]-[Li⁺@C₆₀(CPh₂)]PF₆⁻. Thermal conversion reaction from [5,6]-[Li⁺@C₆₀(CPh₂)]PF₆⁻ to [6,6]-[Li⁺@C₆₀(CPh₂)]PF₆⁻ was very slow at room temperature, but the conversion reaction was completed after heating at 85 °C for 45 h (Scheme 1). It was monitored by ⁷Li-NMR ([5,6]-[Li⁺@C₆₀(CPh₂)]PF₆⁻: δ -10.6 ppm, [6,6]-[Li⁺@C₆₀(CPh₂)]PF₆⁻: δ -12.4 ppm in 1,2-dichlorobenzene).

In the presentation, we will discuss about differences of the properties for the Li⁺@C₆₀ derivatives having 58π-conjugated system with different substituents.

Scheme 1. Synthesis of [Li⁺@C₆₀(CPh₂)]PF₆⁻



[1] Sawa, H.; Tobita H. *et al. Nat. Chem.* **2010**, *2*, 678–683. [2] Matsuo, Y. *et al. Org. Lett.* **2012**, *14*, 3784–3787.
[3] Kokubo, K. *et al. Nanoscale* **2013**, *5*, 2317–2321.

Corresponding Author: Y. Matsuo

Tel: 03-5841-1476, Fax: 03-5841-1476, E-mail: matsuo@chem.s.u-tokyo.ac.jp

Tuning the Chemical Reactivity of Graphene by Mechanical Strain

○Mark A. Bissett¹, Satoru Konabe², Susumu Okada², Masaharu Tsuji¹, and Hiroki Ago¹

¹ *Institute for Materials Chemistry and Engineering, Kyushu University, Fukuoka, 816 8580, Japan.*

² *Graduate School of Pure and Applied Sciences, University of Tsukuba, Tsukuba, 305-8577, Japan.*

Control over chemical reactivity is a central topic in the fields of chemistry and materials science. Graphene is a two-dimensional atomic sheet of sp^2 hybridized carbon with exceptional properties that can be altered by chemical functionalization. When mechanical strain is applied to the graphene lattice distortion leads to the electronic structure being altered. The effect of strain has been previously investigated, specifically for polycrystalline graphene, as domain boundaries can strongly affect the properties [1, 2]. Chemical functionalization can also be used to dope graphene as well as introduce a band-gap. Recently, it has been theoretically suggested that the distortion of the graphene lattice can lead to increased chemical reactivity for simple molecules such as hydrogen, or metal nanoparticles [3, 4].

In this work we transferred single-layer graphene onto a flexible substrate and investigated the chemical functionalization using different molecules while applying mechanical strain. We found that mechanical strain can be used to increase the reaction rate by up to a factor of 10. Both the rate and final degree of reactivity were significantly increased upon the addition of mechanical strain, demonstrating a simple method for tuning the electronic properties of graphene. Theoretical calculations were also performed to support the experimental findings, and explain this impressive reactivity behavior. Our findings offer a new and simple approach to control the chemical reactivity of graphene through the application of mechanical strain, allowing for a tuning of the properties of graphene.

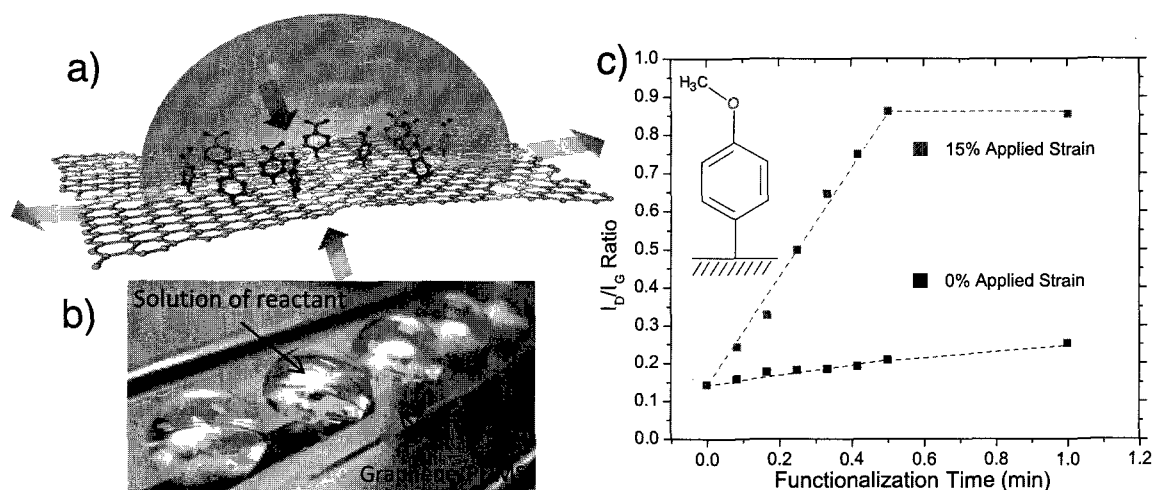


Fig. 1: (a) Schematic depicting the chemical functionalization of mechanically strained graphene by an aqueous solution of aryl diazonium molecules. (b) Photo showing graphene on a flexible PDMS substrate being functionalized by droplets of diazonium solution. (c) Plot of I_D/I_G ratio, indicating degree of functionalization, showing increased reactivity of strained graphene compared to relaxed graphene.

[1] Bissett, M. A. *et al.*, *ACS Nano*, 6, 10229 (2012). [2] Bissett, M. A. *et al.*, *J. Phys. Chem. C*, 117, 3152 (2013). [3] P. L. D. Andres, J. A. Verges, *Appl. Phys. Lett.*, 93, 171915 (2008). [4] G. Kim, *et al.*, *J. Phys. Chem. Lett.*, 3 1989 (2012).

Corresponding Author: H. Ago, Tel & Fax : +81-92-583-7817, E-mail: Ago@cm.kyushu-u.ac.jp

3-2

Stabilities and Electronic Properties of Silicene- and Graphene-based Composite Materials

○Susumu Saito and Takashi Koretsune

*Department of Physics, Tokyo Institute of Technology
2-12-1 Oh-okayama, Meguro-ku, Tokyo 152-8551, Japan*

Graphene now attracts much attention due to its scientifically interesting and technologically important electronic properties. Similar atomic-layer materials are therefore also studied extensively and “silicene”, the two-dimensional hexagonal-network material of Si, is now rather intensively studied both experimentally and theoretically. Although the free-standing silicene (Fig. 1) should be less stable than graphene, silicene layers are expected to be stable either with other layered materials or on the surface of other materials. Therefore, the composite atomic-layer materials consisting of silicene and/or graphene are now of high importance.

We study the composite atomic-layer materials consisting of silicene, graphene, and the hexagonal BN sheet in the framework of the density functional theory. The energetic stabilities and the electronic properties of Graphene/Silicene and h-BN/Silicene/h-BN are discussed in detail. In the case of Silicene/Graphene, the interlayer interaction is found to modify slightly the massless Dirac fermion behavior and small but finite gap is found to appear. On the other hand, the interlayer interaction in h-BN/Silicene/h-BN is found to be considerably smaller. The electronic properties of free-standing silicene should be well maintained in this system.

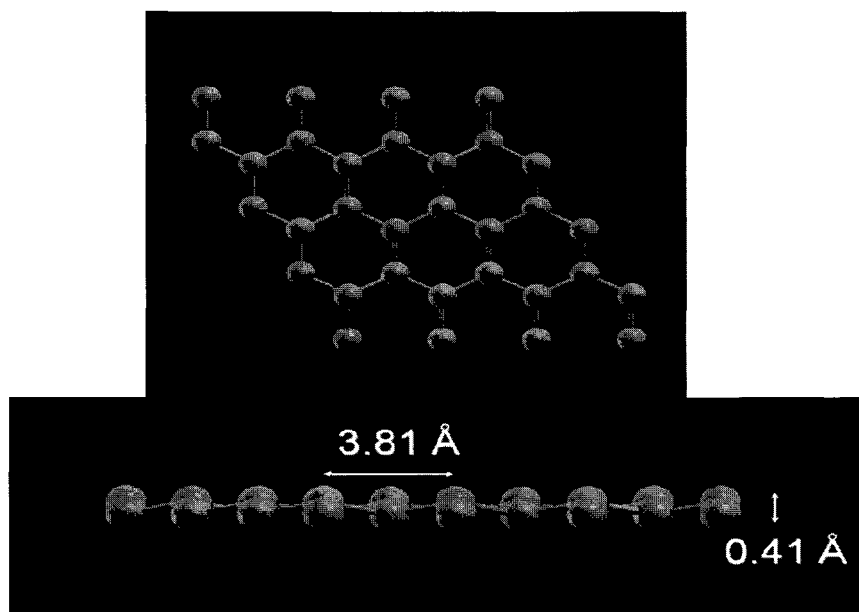


Figure 1 Geometry of free-standing silicene obtained in the framework of the density-functional theory.

Corresponding Author: S. Saito

Fax: +81-3-5734-2739

E-mail: saito@stat.phys.titech.ac.jp

Valley Dependence of Exciton Many-Body Effects in Monolayer Transition-Metal Dichalcogenides

○Satoru Konabe^{1,2} and Susumu Okada^{1,2}

¹*Graduate School of Pure and Applied Sciences, University of Tsukuba, Tsukuba, Ibaraki 305-8571, Japan*

²*Japan Science and Technology Agency, CREST, 5 Sanbancho, Chiyoda, Tokyo 102-0075, Japan*

Monolayer transition-metal dichalcogenides (MTD) have recently attracted a lot of attentions since they are two-dimensional semiconducting alternatives to metallic graphene [1]. Among fascinating aspects of MTDs, the interesting physics of coupled spin and valley degrees of freedom emerges as a result of interplay between the strong spin-orbit interaction and the inversion symmetry breaking [2]. This leads to peculiar optical properties of MTDs. Through excitation by the right- and left-hand polarized light, excess populations of a selected valley can be generated, which makes MTDs a possible candidate for valleytronics devices [2,3]. In addition, optical responses of MTDs show remarkable excitonic effects attributing to strong Coulomb interaction in the less-screened monolayer structure. So far, many experiments and calculations have been performed to clarify the excitonic properties of MTDs [2,3,4]. However, many-body effects of excitons are yet inadequately understood; the effects could deeply affect the optical properties due to the strong Coulomb interaction between excitons.

In this work, we theoretically investigate optical excited states of MTDs, focusing on exciton many-body effects. Using an effective low-energy theory, we study optical responses and discuss the novel valley dependence of exciton-exciton scattering processes.

References:

- [1] Q. H. Wang *et al.* Nature Nanotechnology. **7**, 699 (2012).
- [2] D. Xiao *et al.* Phys. Rev. Lett. **108**, 196802 (2012).
- [3] H. Zeng *et al.* Nat. Nanotechnol. **7**, 490 (2012). K. F. Mak *et al.* Nat Nanotechnol. **7**, 494 (2012). T. Cao *et al.* Nat. Commun. **3**, 887 (2012).
- [4] A. Ramasubramaniam, Phys. Rev. B **86**, 115409 (2012).

Corresponding Author: Satoru Konabe

E-mail: konabe@comas.frsc.tsukuba.ac.jp

Tel: +81-2-9853-5600 ext.8233

Morphology control and solid state properties of fullerene nanosheets and nanocrystals

○Yoshiaki Sano¹, Keisuke Baba², Hironori Ogata^{1,2}

¹Graduate School of Engineering, Hosei University, Tokyo 184-8584, Japan

²Department of Faculty of Biosci. and Applied Chem., Hosei University, Tokyo 184-8584, Japan

Fullerenol (Polyhydroxylated Fullerene: $C_{60}(OH)_x$) have been thought to have potential application in a variety of areas, including optoelectronics, medical therapeutics, biotechnology, chemical mechanical polishing, and fuel cells, owing to their high solubility in a large variety of solvents (depending on the number of hydroxyl groups, x). We previously reported the fabrication of both fullerene nanosheets and nearly monodispersed single crystalline fullerene nanocrystals by reprecipitation or liquid-liquid interfacial precipitation method using both good and poor solvents. In this study, we investigated the possibility of morphology control in fullerene nanosheets and nanocrystals. We also investigated the properties of proton conduction in fullerene nanosheets.

Figure 1 shows the typical TEM images of $C_{60}(OH)_{13.5}$ (average) nanosheets (a) and nanocrystals (b) by using tetrahydropyran (good solvent) and deionized water (poor solvent). $C_{60}(OH)_{38.7}(O)_{1.6}$ (average) nanocrystals by deionized water (good solvent) and tetrahydropyran (poor solvent) (c). The average diameter and CV value of both crystals were 7.87 nm, 11.6% ($C_{60}(OH)_{13.5}$) and 8.06 nm, 12.3% ($C_{60}(OH)_{38.7}(O)_{1.6}$), respectively. The detailed results on the chemical composition and solvent dependences on the thickness and crystal size of fullerene nanosheets /nanocrystals will be presented.

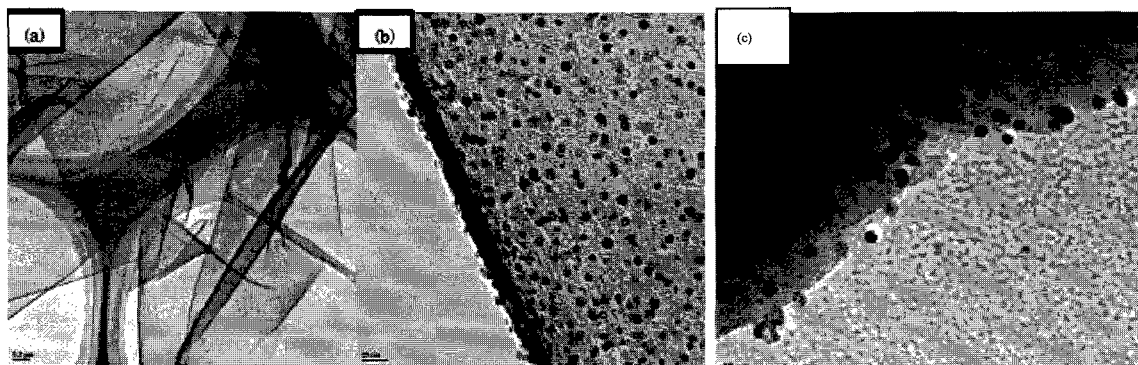


Figure 1. TEM image of $C_{60}(OH)_{13.5}$ nanosheets (a), $C_{60}(OH)_{13.5}$ nanocrystals (b) and $C_{60}(OH)_{38.7}(O)_{1.6}$ nanocrystals.

References:

- [1] Chiang *et al.* Org. Cem. **59**, 3960 (1994).
- [2] Kokubo *et al.*, Nano Res., **4**, 204 (2011)
- [3] K. Baba *et al.*, Proc. of the 42th Fullerene-Nanotubes-Graphene General Symposium (2-5).

Corresponding Author: H. Ogata

Tel: +81-42-387-6229, Fax: +81-42-387-6229,

E-mail: hogata@hosei.ac.jp

Selective Synthesis of Novel Octaalkoxyfullerenes $C_{60}(OR)_8$ and Octaarylfullerene $C_{60}(4-MeOC_6H_4)_8$ by a Substitution Reaction of Octabromofullerene $C_{60}Br_8$

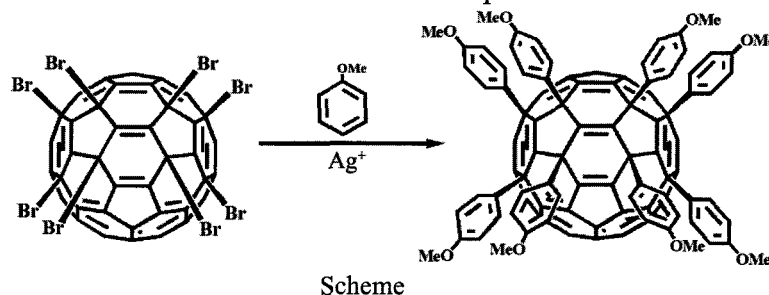
○Kouya Uchiyama¹, Hiroshi Moriyama¹, Kenji Yoza²

¹ Department of Chemistry, Toho University, Funabashi, 274-8510, Japan

² Bruker AXS, Yokohama, 221-0022, Japan

Synthesis of various halofullerenes, such as fluorofullerenes, chlorofullerenes and bromofullerenes, gave a unique structure that has rarely been observed for other fullerene derivatives and cannot be produced without halogenation of fullerene. It is well known that the addition of organic groups to the π systems of fullerene derivatives greatly affects their electronic and optical properties; therefore, fullerene derivatives having a unique structure can be key materials in the field of organic electronic devices and life sciences. Unfortunately, although octabromofullerene $C_{60}Br_8$ has a unique structure, it is thermally unstable and scarcely dissolves in organic solvents. For the application of its unique π system, it is therefore necessary to convert $C_{60}Br_8$ to more stable and soluble fullerene derivatives.

We have reported in this symposium that octaalkoxyfullerenes, $C_{60}(OR)_8$ ($R = CH_3, C_2H_5$), can be obtained by a substitution reaction of $C_{60}Br_8$ with corresponding alcohols in the presence of a silver salt that facilitates elimination of bromine atoms, and the result of the single-crystal X-ray diffraction analysis of $C_{60}(OMe)_8$ shows that it retains the addition pattern of $C_{60}Br_8$. $C_{60}(OR)_8$ are more stable because of the conversion of unstable C–Br bonds to C–OR bonds; furthermore, its solubility can be increased easily by changing the alkyl groups. Here, we report the synthesis of novel octaalkoxyfullerenes with longer alkyl chains, $C_{60}(OR)_8$ ($R = n-C_3H_7, n-C_4H_9, n-C_5H_{11}, n-C_6H_{13}, n-C_7H_{15}, n-C_8H_{17}, i-C_3H_7$), and the crystal structure of $C_{60}(OEt)_8$. On the basis of the single-crystal X-ray diffraction analysis of $C_{60}(OEt)_8$, it was found that the 6:6 bond surrounded by four ethoxy groups was significantly shorter (1.32Å) than other 6:6 bonds (1.35–1.40Å) because of the isolation of the 6:6 bond from the π -conjugated system of fullerene. In addition to the substitution reaction with alcohols, we succeeded with the new anisole derivatives of fullerene to prepare octaarylfullerene, $C_{60}(4-MeOC_6H_4)_8$. In view of further application of the substitution reaction of $C_{60}Br_8$, it is important to establish the reactions with various nucleophiles. We believe that the substitution reaction of $C_{60}Br_8$ can be a new synthetic method for forming multifunctionalized fullerene derivatives. Further work is in progress to investigate the reactivity with other nucleophiles.



[1] P. R. Birkett, P. B. Hitchcock, H.W. Kroto, R. Taylor, D. R. M. Walton, *Nature* 1992, 357, 479–481.

[2] K. Uchiyama, H. Moriyama, K. Yoza, The 43rd FNTG Symposium Abstract 1P-14 (2012); JP2012-194209.

Corresponding Author: Hiroshi. Moriyama

TEL: +81-47-472-1211, FAX: +81-47-476-9449 E-mail: moriyama@chem.sci.toho-u.ac.jp

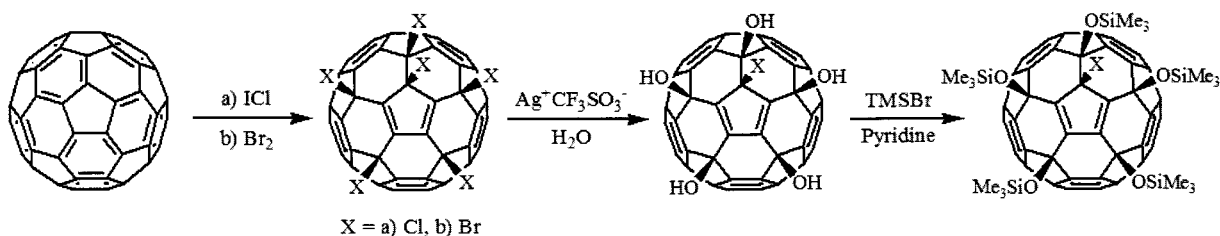
Selective Synthesis of Fullerenols and their Derivatives; C₆₀(OH)₅X and C₆₀(OSiMe₃)₅X (X = Cl, Br)

○Miki Igarashi¹, Shouhei Yamamoto¹, Hiroshi Ueno^{1†}, Kenji Yoza², Hiroshi Moriyama¹

¹ Department of Chemistry, Toho University, Funabashi, 274-8510, Japan

² Bruker AXS, Yokohama, 221-0022, Japan

Polyhydroxylated fullerenes (fullerenols) have attracted much attention because they have useful properties and various potential applications, especially in the biological and medicinal fields. Several synthetic methods for fullerenols have been reported. However, usually only the average structures of fullerenols are determined by elemental analysis and thermogravimetric analysis because it is difficult to isolate fullerenols with many isomers or fullerenols with slightly different numbers of hydroxyl groups. In addition, lack of control of the hydroxylation reaction hampers the selective synthesis of a given fullereneol. As a well-characterized fullereneol, only the structure of a fullereneol that has eight hydroxyl groups, C₆₀(OH)₈ [1], has been reported by Zhang *et al.* as the result of a multistep reaction in low yield.



Scheme 1

In this study, we will report a facile selective synthesis of five-fold fullerenols, as shown in the scheme. Our key step in the synthesis is a nucleophilic attack by water in the presence of a silver salt, which facilitates the substitution reaction of halogen atoms to give novel hydroxylated fullerenes. We believe that the present reaction by water is a novel use as a precursor material. ¹H and ¹³C NMR spectra show that the products, C₆₀(OH)₅X and C₆₀(OSiMe₃)₅X (X = Cl, Br), have C_s symmetry, the same as C₆₀Cl₆ [2] and C₆₀Br₆ [3] in which the ¹³C NMR spectra exhibited the signals for the corresponding fullerene skeleton. The single-crystal X-ray crystal structures of C₆₀(OSiMe₃)₅Cl and C₆₀(OSiMe₃)₅Br (Fig. 1) were completely consistent with the ¹H and ¹³C NMR spectra and the addition pattern for C₆₀(OSiMe₃)₅Cl and C₆₀(OSiMe₃)₅Br was found to remain, as shown in the scheme.

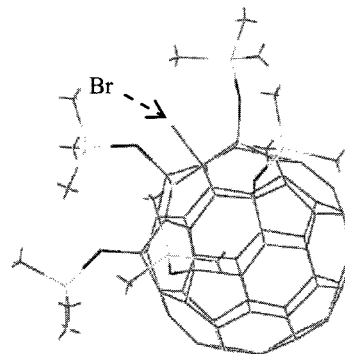


Fig. 1 X-ray crystal structure of C₆₀(OSiMe₃)₅Br

[1] Ghang, Z.; Yun, Li.; Dehai, L.; Liangbing, G.; Yuliang, L. *Angew. Chem. Int. Ed.* **2010**, *49*, 5293-5295. [2] Kuvychko, I. V.; Streleskii, A. V.; Shustova, N. B.; Seppelt, K.; Drewello, T.; Popov, A. A.; Strauss, S. H.; Boltalina, O.V. *J. Am. Chem. Soc.* **2010**, *132*, 6443-6462. [3] Semenov, K. N.; Charykov, N. A.; Keskinov, V. A.; Pyartman, A. K.; Yakovlev, V. V. *Russ. J. Phys. Chem. A.* **2009**, *11*, 1935-1939.

[†]present address: Division of Applied Chemistry, Graduate School of Engineering, Osaka University, 565-0871, Japan

Corresponding Author: Hiroshi Moriyama

TEL: +81-47-472-1211, FAX: +81-47-476-9449, E-mail: moriyama@chem.sci.toho-u.ac.jp

Crystal Structure and Dielectric Property of $\text{H}_2\text{O}@\text{C}_{60}$

○Shinobu Aoyagi¹, Norihisa Hoshino^{2,3}, Tomoyuki Akutagawa^{2,3}, Ryo Kitaura⁴,
Hisanori Shinohara⁴, Kunihisa Sugimoto⁵, Rui Zhang⁶, Yasujiro Murata⁶

¹ *Department of Information and Biological Sciences, Nagoya City University, Nagoya
467-8501, Japan*

² *Institute of Multidisciplinary Research for Advanced Materials, Tohoku University, Sendai
980-8577, Japan*

³ *Graduate School of Engineering, Tohoku University, Sendai 980-8579, Japan*

⁴ *Department of Chemistry and Institute for Advanced Research, Nagoya University, Nagoya
464-8602, Japan*

⁵ *SPring-8/JASRI, Kouto, Sayo, Hyogo 679-5198, Japan*

⁶ *Institute for Chemical Research, Kyoto University, Uji, Kyoto 611-0011, Japan*

Buckminsterfullerene C_{60} can possess electric dipole moments by encapsulating a polar molecule such as a water molecule in its inner nanospace. The $\text{H}_2\text{O}@\text{C}_{60}$ molecule was recently synthesized by the molecular surgical approach [1]. The easy separation of $\text{H}_2\text{O}@\text{C}_{60}$ from the empty C_{60} by high-performance liquid chromatography implies that $\text{H}_2\text{O}@\text{C}_{60}$ has polarity. The dipole moment of $\text{H}_2\text{O}@\text{C}_{60}$ has been calculated theoretically [1-3]. Molecular dynamics simulations also showed that the encapsulated water molecule rotates freely and has various orientations at finite temperature [2,3].

Here we report the crystal structure and dielectric property of pure $\text{H}_2\text{O}@\text{C}_{60}$ crystal at low temperature. The dielectric response, thermal motion, and conformation of the water molecule trapped inside the carbon cage is revealed by the X-ray structure analysis and dielectric measurement. The crystal has a cubic structure similar to that of the empty C_{60} crystal except that water molecules are trapped inside the carbon cages. The water molecule rotates around its oxygen atom at the cage center even at 20 K. The dominant positions of the disordered two hydrogen atoms suggest that the $\text{H}_2\text{O}@\text{C}_{60}$ molecule has C_{2v} symmetry. The rotating water molecules respond to an external electric field due to its permanent dipole moment. A slowdown of the rotational motion of the water molecule at low temperature increases the dielectric permittivity according to the Curie-Weiss law.

[1] K. Kurotobi and Y. Murata, *Science* 333, 613 (2011).

[2] D. Bucher, *Chem. Phys. Lett.* 534, 38 (2012).

[3] B. Ensing, F. Costanzo, and P. L. Silvestrelli, *J. Phys. Chem. A* 116, 12184 (2012).

Corresponding Author: S. Aoyagi

Tel: +81-52-872-5061,

E-mail: aoyagi@nsc.nagoya-cu.ac.jp

Why is (6,5) nanotube so special in the tube growth processes?

- Experimental and theoretical considerations-

- Yohji Achiba¹⁾, Takshi Kodama¹⁾, Kenro Hashimoto¹⁾, Haruo Shiromaru¹⁾ and Toshiya Okazaki²⁾

1) *Department of Chemistry, Tokyo Metropolitan University, Minami Osawa 1-1, Hachioji, Tokyo 192-0367, Japan*

2) *Advanced Industrial Science and Technology, Tsukuba, 305-8565, Ibaragi, Japan*

Controlling size and chirality distributions in the production of single wall carbon nanotubes (SWNTs) is undoubtedly one of the most important issues in the potential applications of the SWNTs to nano-material technology. So far, many experimental attempts have been carried out on the selective production of specific (n,m) tubes by various kinds of production methods. The laser vaporization method combined with a metal catalyst under a specific condition gives a good example for the highly selective SWNT growth of a single chirality, in which over 90% selective growth of (6,5) species has clearly been shown, suggesting the presence of some special reasons for the favorable growth of (6,5) tube. It should be interesting to note here that there have been no evidence for the formation of the (5,5) nanotubes under the specific condition optimized for the growth of the (6,5) carbon nanotube, although both (5,5) and (6,5) tubes possess similar chiral angle and diameter.

In order to understand the reason why the (6,5) tube is so special, theoretical study has also been carried out employing B3LYP/6-31G method. In the present work, the stepwise additions of C₂ molecules to C₃₀ and C₃₁ initial cap structures (shown in Fig.1) have been focused, C₃₀ + nC₂ → C_{30+2n}, and C₃₁ + nC₂ → C_{31+2n}. In this scheme, the C₃₀ and C₃₁ structures were reasonably assumed to be the seeds of the (5,5) and (6,5) tubes, respectively. The addition of a single C₂ is exothermic by 8-10 eV, and each C₂ addition to the bays A-E possibly forms two different networks, pentagon or hexagon. For (6,5) tube, it has been found that the structure with the near armchair moiety is more stable for each n up to C₉₇ than other isomers whose bays are bound by the C₂ in the different manners.

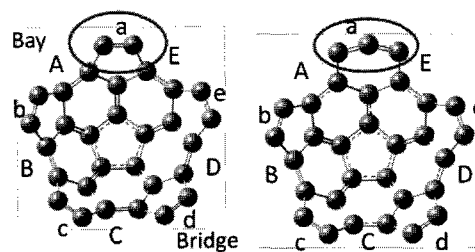


Fig.1. Structures of (5,5) C₃₀ and (6,5) C₃₁. Bays are labeled by A-E,

Corresponding Author Yohji Achiba

E-mail achiba-yohji@tmu.ac.jp Tel&Fax: +81-52-789-2482, +81-52-789-1169

Bis(*tert*-butylpyrene) nanotweezers and nanocalipers: Enhanced extraction and recognition abilities for single-walled carbon nanotubes

○Gang Liu, A. F. M. Mustafizur Rahman, Takahide Kimura, Naoki Komatsu

Department of Chemistry, Shiga University of Medical Science, Otsu 520-2192, Japan.

We have been developing host-guest methodology for separation of single-walled carbon nanotubes (SWNTs) according to the handedness, diameter, and even metallicity by use of diporphyrin nanotweezers and nanocalipers [1-3]. Although pyrene has been frequently used in the replacement of porphyrin due to a similar affinity to the surface of SWNTs and better availability, the extraction and recognition abilities of dipyrene nanotweezers were not so good as those of diporphyrin ones [4-5]. Recently, a newly employed pyrene derivative, *tert*-butylpyrene, was found to enhance the extraction and recognition abilities of the pyrene-based nanotweezers and nanocalipers to SWNTs.

While the nanotweezers **1** (Fig. 1) extracts no SWNTs, the *tert*-butyl substituted counterpart **2** selectively extract (6,5)-SWNTs from 65-CoMoCAT, which was confirmed by the absorption spectra (Fig. 2a). In case of nanocalipers, the *tert*-butyl substituted ones, **4** in Fig. 1, also show much better extraction and recognition abilities than the unsubstituted ones (**3**). After the extraction with **4**, metallic SWNTs were highly enriched as shown in the absorption spectra (Fig. 2b) [5].

[1] G. Liu, F. Wang, N. Komatsu, in *Handbook of Carbon Nano Materials*, World Scientific, **2012**; Vol. 3, p 203.

[2] G. Liu, N. Komatsu, *Org. Biomol. Chem.* **2012**, 10, 5830.

[3] G. Liu, N. Komatsu, *J. Am. Chem. Soc.* **2013**, 135, 4805.

[4] A. F. M. M. Rahman, N. Komatsu, *Chem. Sci.* **2011**, 2, 862.

[5] G. Liu, N. Komatsu, to be submitted.

Corresponding Author: Gang Liu

Tel: +81-77-548-2102, Fax: +81-77-548-2405, E-mail:

gliu@belle.shiga-med.ac.jp

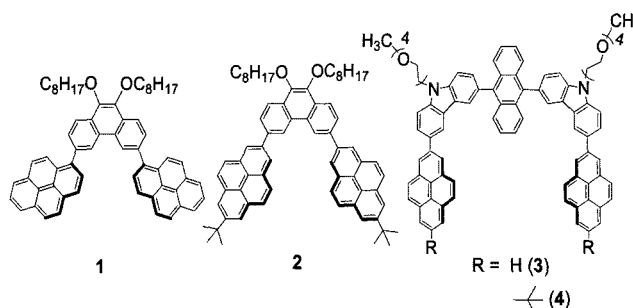


Fig. 1 Structures of dipyrene nanotweezers **1** and **2**, and nanocalipers **3** and **4**.

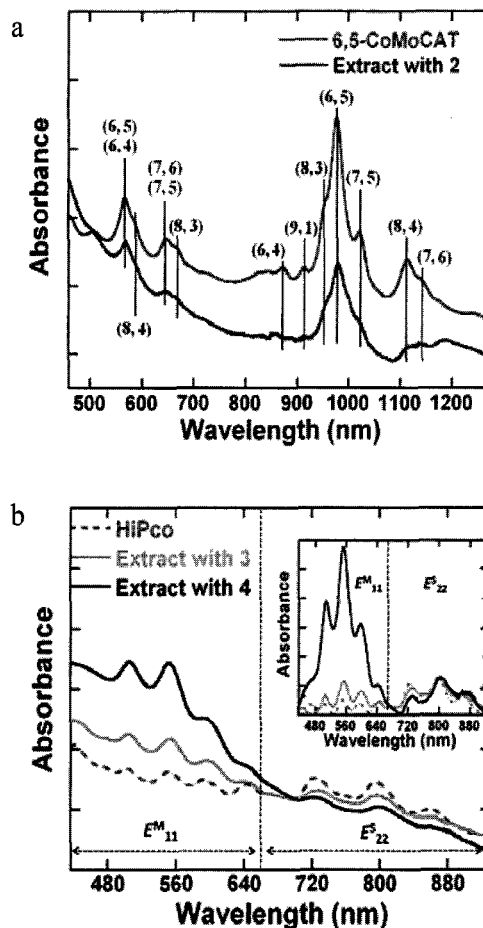


Fig. 2 Absorption spectra of SWNTs before and after extraction with **2** (a), **3**, and **4** (b). The inset in b is the absorption spectra after subtracting the baseline.

The Infinite Possible Growth Ambients that Support Single-Wall Carbon Nanotube Forest Growth

○Hiroe Kimura^{1,3}, Jundai Goto¹, Satoshi Yasuda¹, Shunsuke Sakurai¹, Motoo Yumura¹,
Don N. Futaba*¹ and Kenji Hata*^{1,2,3}

¹ *Nanotube Research Center, National Institute of Advanced Industrial Science and Technology (AIST), Tsukuba, 305-8565, Japan*

² *Japan Science and Technology Agency (JST), Kawaguchi, 332-0012, Japan*

³ *Tsukuba University, Department of Pure and Applied Sciences, Tsukuba University, Tsukuba, 305-8573, Japan*

The development of scientific research and industrial applications for carbon nanotubes (CNTs) has been primarily limited by its synthesis, and as a result, immense research encompassing the control of the structure and underlying growth mechanism has been invested over the past two decades to improve growth efficiency, e.g. yield, crystallinity, and chirality. Apt examples include the water-assisted chemical vapor deposition (CVD) method^[1] to increase yield, floating catalyst CVD method to improve crystallinity, and catalyst gas pretreatments for metal conductor selective growth.

In the synthesis of CNTs by CVD, numerous carbon feedstocks have been applied, often in the form of hydrocarbons, such as methane, acetylene, and ethylene, and even anthracene. However, each synthesis method, i.e. thermal CVD, plasma-enhanced CVD, floating catalyst CVD, laser ablation, seems to prefer a certain carbon feedstock. For example, in plasma-enhanced CVD, methane or other low molecular-weight carbon feedstocks are preferred, while for floating catalyst CVD carried out at high temperatures, cyclic aromatic hydrocarbons, eg. toluene, xylene, benzene are most commonly used due to their high decomposition temperatures. For typical thermal CVD, acetylene and ethylene have become the commonly-used carbon feedstock due to their high reactivities. However, carbon feedstocks are not limited to the previously listed examples, and some research has even shown that natural derivatives of carbon, such as camphor, or eventire rubber can be used as a carbon feedstock in the synthesis of CNTs.

Here, we report the virtually infinite possible carbon feedstocks which support the highly efficient growth of single-wall carbon nanotubes (SWCNTs) based on the water-assisted chemical vapor deposition method^[1]. Our results demonstrate that diverse varieties of carbon feedstocks, in the form of hydrocarbons, spanning saturated rings (e.g. trans-deca-hydronaphthalene), saturated chains (e.g. propane), unsaturated rings (e.g. dicyclopentadiene), and unsaturated chains (e.g. ethylene) could be used as a carbon feedstocks with SWCNT forests with heights exceeding 100 ums. Further, we found that all the resultant SWCNTs possessed similar average diameter indicating that the diameter was mainly determined by the catalyst rather than the carbon feedstock within this synthetic system. A demonstration of the generality was the synthesis of a carbon nanotube forest from a highly unorthodox combination of gases where trans-decahydronaphthalene acted as the carbon feedstock and benzaldehyde acted as the growth enhancer.

[1] K. Hata *et al*, Science, 306, 1241 (2004)

Corresponding Author: Kenji Hata, Don N. Futaba

Tel: (029) 861-4654, FAX: (029) 861-4851, E-mail: kenji-hata@aist.go.jp, d-futaba@aist.go.jp

ポスター発表
Poster Preview

1P - 1 ~ 1P - 37

2P - 1 ~ 2P - 37

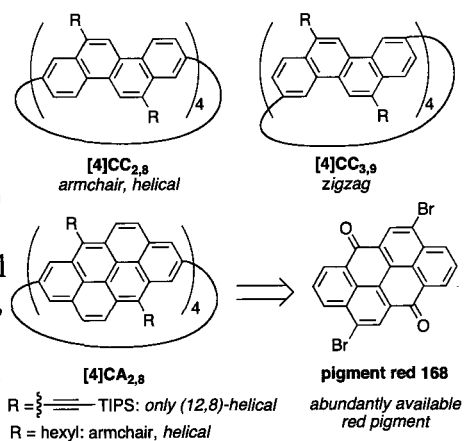
3P - 1 ~ 3P - 35

Bottom-up synthesis and structures of π -lengthened finite single-wall carbon nanotube molecules

○Taisuke Matsuno, Sho Kamata, Shunpei Hitosugi, Hiroyuki Isobe

Department of Chemistry and Advanced Institute for Materials Research,
Tohoku University, Sendai 980-8577, Japan

Structural chemistry of singlewall carbon nanotubes (SWNT) started flourishing after the advent of bottom-up synthesis of finite congeners, such as cycloparaphenylene (CPP) as frameworks of armchair SWNT and our belt-persistent cybarylene, [4]cyclochrysenylenes ([4]CC) as armchair-, helical- and zigzag-SWNT^{2,3} molecules. These studies brought molecular precision to the structural chemistry of SWNT as “molecular entities”. However, there are remaining challenges such as π -lengthening of finite SWNTs. In this work, we report the synthesis and structural analysis of π -lengthened finite SWNT, [4]cyclo-2,8-anthanthrenylene ([4]CA_{2,8}, Figure 1).



[4]CA_{2,8} was effectively synthesized from abundantly available red pigment (Figure 1). The introduction of bulky TIPS ethynyl (TIPS) groups allowed for the diastereoselective production of a singlehelical SWNT. Hexyl-substituted [4]CA_{2,8} was obtained as mixture of armchair and helical SWNTs (Figure 2). The crystallographic analysis of TIPS-substituted (12,8)-[4]CA_{2,8} revealed that, molecules of an identical handedness form a column, and the columns are further assembled in a layer through intermolecular π -contacts. The layers of opposite handedness alternately stack to form hexagonal bundles (Figure 3). Because π -contact motifs predominate in the intercolumnar contacts to form the layers of identical handedness, we may expect a similar homohelical layers in infinite helical SWNT assembly.

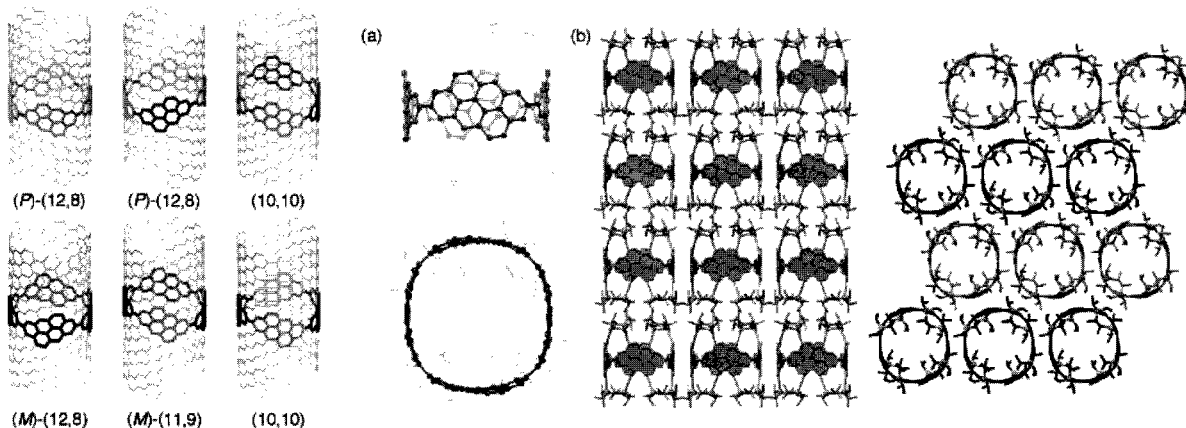


Figure 2. Atropisomers of [4]CA_{2,8} **Figure 3.** (a) Molecular structure and (b) packing structure of [4]CA_{2,8}

- [1] Jasti, R.; Bhattacharjee, J.; Neaton, J. B.; Bertozzi, C. R. *J. Am. Chem. Soc.* **2008**, *130*, 17646-17647.
 [2] Hitosugi, S. *et al. Nat. Commun.* **2011**, *2*, doi: 10.1038/ncomms1505 (5 pages).
 [3] S. Hitosugi, W. Nakanishi, T. Yamasaki, H. Isobe *Nat. Commun.* **2011**, *2*, doi: 10.1038/ncomms1505 (5 pages).
 [4] Matsuno, T.; Kamata, S.; Hitosugi, S.; Isobe, H. *Chem. Sci.* **2013**, published online. (doi: 10.1039/C3SC50645B)

Corresponding Author: H. Isobe

Tel: +81-22-795-6585, Fax: +81-22-795-6589,

E-mail: isobe@m.tohoku.ac.jp

Initiation of carbon nanotube growth by well-defined carbon nanorings

○Yasutomo Segawa¹, Haruka Omachi¹, Takuya Nakayama¹, Eri Takahashi²,
Kenichiro Itami^{1,3}

¹ Department of Chemistry, Graduate School of Science, Nagoya University,
Aichi 464-8602, Japan

² Synthetic Organic Chemistry Laboratories, Research and Development Management
Headquarters, FUJIFILM Corporation, Kanagawa 258-8577, Japan

³ Institute of Transformative Bio-Molecules (WPI-ITbM), Nagoya University,
Aichi 464-8602, Japan

Carbon nanotubes (CNTs), tubular molecular entities that consist of sp^2 -hybridized carbon atoms, are currently produced as mixtures that contain tubes of various diameters and different sidewall structures. The electronic and optical properties of CNTs are determined by their diameters and sidewall structures and so a controlled synthesis of uniform-diameter, single-chirality CNTs would provide access to pure samples with predictable properties. Here we report a rational bottom-up approach to synthesize structurally uniform CNTs using carbon nanorings (cycloparaphenylenes)[1] as templates and ethanol as the carbon source[2]. The average diameter of the CNTs formed is close to that of the carbon nanorings used, which supports the operation of a “growth-from-template” mechanism in CNT formation. This bottom-up organic chemistry approach is intrinsically different from other conventional approaches to making CNTs and, if it can be optimized sufficiently, offers a route to the programmable synthesis of structurally uniform CNTs.

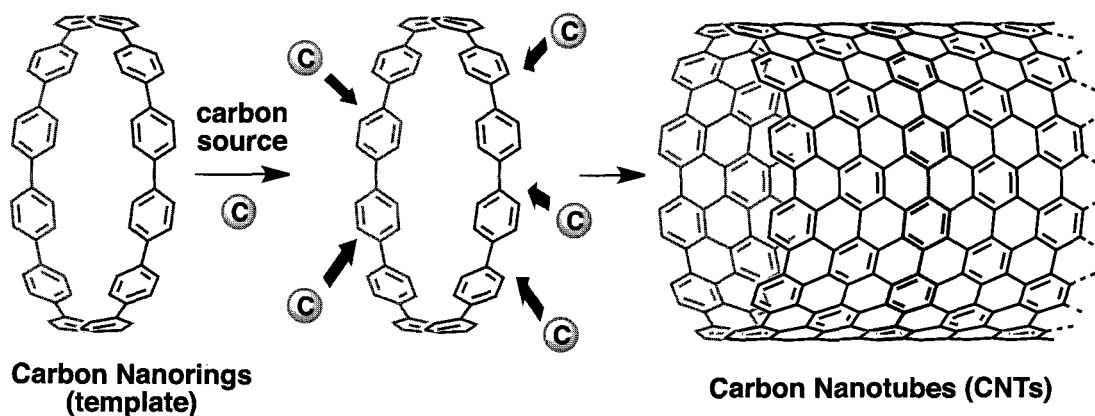


Fig.1. CNT Growth from Carbon Nanorings

[1] H. Omachi, Y. Segawa, K. Itami, *Acc. Chem. Res.*, **45**, 1378 (2012) and references therein.

[2] H. Omachi, T. Nakayama, E. Takahashi, Y. Segawa, K. Itami, *Nat. Chem.*, DOI:10.1038/NCHEM.1655 (2013).

Corresponding Author: K. Itami

Tel/Fax: +81-52-789-6098

E-mail: itami.kenichiro@a.mbox.nagoya-u.ac.jp

Post-annealing effect on single-wall carbon nanotubes prepared by PG-ACCVD technique

Yosuke Ito¹, Shinzo Suzuki¹, Hiroshi Nagasawa², Akira Ono³, Yohji Achiba⁴

¹*Department of Physics, Kyoto Sangyo University, Kyoto 603-8555, Japan*

²*Nano-support Co., Ltd., Kanagawa 251-0024, Japan*

³*Department of Engineering, Kanagawa University, Yokohama 221-8686, Japan*

⁴*Department of Chemistry, Tokyo Metropolitan University, Tokyo 192-0397, Japan*

Abstract:

In 2012, J. Liu et al. reported about chirality-controlled synthesis of single-wall carbon nanotubes (SWNTs) using vapor-phase epitaxy technique [1], where either methanol or methane as carbon feed was used for subsequent metal catalyst free growth of SWNTs with predefined chiralities. On the other hand, in 2001, Sen et al. reported about the growth of SWNTs from the condensed phase using laser-oven technique, where the existence of precursors was considered to be necessary for the subsequent growth of SWNTs with post-annealing process [2]. It is interesting to check whether post-annealing effect could also influence on the subsequent growth of SWNTs prepared by PG-ACCVD technique [3].

Briefly, 3.0 wt% of Co (as cobalt acetate) was introduced in PG (30 nm pore size) in ethanol solution. This solution was then sonicated for 30 min, centrifuged at 2000G for 30 seconds. After removing ethanol, the resultant PG was placed in quartz tube (i.d. 20 mm), heated at 80°C for 12 hours in air, and was further used for ACCVD treatment using ethanol as carbon supply. The ambient temperature was first set to 700 °C, and after SWNTs were prepared in PG, the material was heated up to 800 °C furthermore for the subsequent growth of SWNTs. Raman spectroscopy was used for the SWNTs before and after post-annealing effect.

Comparison of Raman spectra (532 nm and 633 nm excitation) obtained for the material containing SWNTs prepared by using PG-ACCVD technique at 700 °C at first, and those obtained for the material after subsequent heating process (up to 800 °C), demonstrated that new Raman peak appeared in the wavenumber region below 200 cm⁻¹, corresponding to SWNTs having diameters larger than 1.2 nm. More experimental findings are shown in the presentation.

References:

- [1] J. Liu, C. Wang, X. Tu, B. Liu, L. Chen, M. Zheng, and C. Zhou, *Nature Commu*, **3**, 1199(2012).
- [2] R. Sen, S. Suzuki, H. Kataura, and Y. Achiba, *Chem. Phys. Lett.*, **349**, 383(2001).
- [3] Y. Aoki, S. Suzuki, S. Okubo, H. Kataura, H. Nagasawa, and Y. Achiba, *Chem. Lett.*, **34**, 562(2005).

Corresponding Author: Shinzo Suzuki

Tel: +81-75-705-1631, Fax: +81-75-705-1631,

E-mail: suzukish@cc.kyoto-su.ac.jp

String-like Assembly of Aligned Single-Wall Carbon Nanotubes in a Single-Chiral State

H. Kawai¹, K. Hasegawa¹, T. Nakatsu², Y. Naitou³, Y. Takagi⁴, Y. Wada⁴, T. Takenobu⁴, K. Yanagi¹

¹ Tokyo Metropolitan Univ., ² Kyoto Univ., ³ AIST, ⁴ Waseda Univ.

Single Wall Carbon Nanotubes (SWCNTs) have various electronic structures depending on their chirality. Recent progress of separation technique, such as density gradient ultracentrifugation or gel chromatography, enable us to extract metallic, semiconducting and single chiral state of SWCNTs from the mixed state sample. It is expected that fabrication of SWCNTs device exploiting their intrinsic high mobility and unique electronic structure. However, typical device are fabricated as random network of SWCNTs, which produces reduction of conducting carriers originated from scattering and localization of electron in the connection of SWCNTs. Therefore, control of SWCNTs network is necessary to take advantage of characteristics of SWCNTs and improve device performance in microscale.

In our study, we investigated aggregation process of (6,5) SWCNTs, dispersed in solutions with surfactant. It is possible to aggregate mono-dispersed SWCNTs by adding salts and alcohol. In that case, we observed aggregates (alga-like aggregations) such as Fig. 1(a), which no alignment was observed. However we found that temperature of the solutions and reaction time significantly influenced their aggregation processes and morphologies of the aggregates. When we adjusted the solution temperature and incubation time, string-like assemblies with diameters of approximately 10 μm and lengths of greater than 1 mm self-formed, as observed in Fig. 1 (b)^[1]. Micro-Raman measurement and scanning electron microscopy measurements clearly shows that the (6,5) SWCNTs were aligned to string axis in the assembly. Moreover, these assemblies exhibited good field effect performances, exhibiting an on/off ratio of 6.8×10^3 and a maximum mobility of $106.5 \text{ cm}^2 \text{ V}^{-1} \text{ s}^{-1}$.

[1]Kawai et al., Appl. Phys. Express 6 (2013) 065103.

Corresponding Author: K. Yanagi
Tel: +81-42-677-2494, Fax: +81-42-677-2483,
E-mail: yanagi-kazuhiro@tmu.ac.jp

process of (6,5) SWCNTs, dispersed in

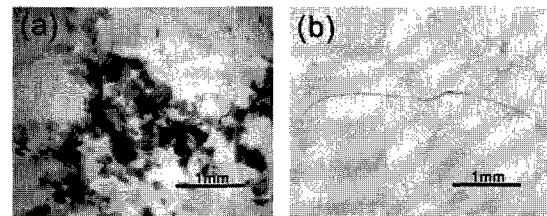


Fig1. (a)Alga-like aggregation (b)String-like assembly

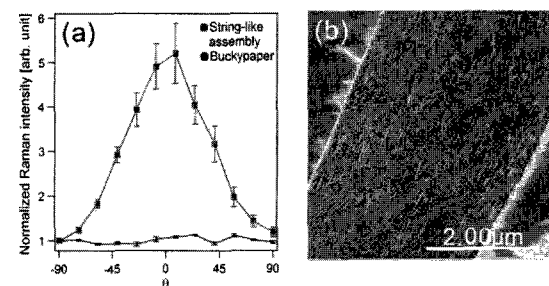


Fig2. (a)Micro-Raman measurement
(b)Scanning electron microscopy measurement

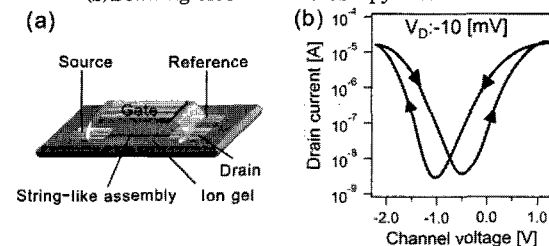


Fig.3 (a)Field effect transistor
(b)Transport characteristics.

Elucidation of the Chirality Control of Single-Walled Carbon Nanotube by Irradiating Free Electron Laser during Growth

○Keisuke Yoshida¹, Takumi Sagara¹, Yusaku Tsuda¹, Koji Ishii², Kenichi Yamakawa¹, Hirofumi Yajima², Nobuyuki Iwata¹ and Hiroshi Yamamoto¹

¹ Department of Electronics & Computer Science, College of Science & Technology, Nihon University, 7-24-1 Narashinodai, Funabashi, Chiba 274-8501 Japan

² Department of Applied Chemistry, Faculty of Science, Tokyo University of Science, 1-3 Kagurazaka, Shinjyuku-ku, Tokyo 162-0826, Japan

Single-Walled carbon nanotubes (SWNTs) have been regarded as one of the best candidates for future applications in nanoelectronic devices due to its high mobility, high current-carrying capacities, and so on. The drawback for nanoelectronics using SWNTs is that almost all of the current available technologies for the SWNTs growth can only produce a mixture of metallic and semiconducting one. We demonstrate the novel technique to synthesis as-grow SWNTs with only semiconducting properties at a limited area using free electron laser (FEL) irradiation during growth and surface treatment^[1]. However, the mechanism to control the chirality by the FEL has not been clear yet. The aim of this study is to elucidate the role of the FEL irradiation for the selective SWNTs growth.

Figure 1 shows the Raman spectra of the SWNTs grown with the 800 nm FEL irradiation. The RBM peaks were observed only in the spectrum with 785 nm excitation laser. Figure 2 shows the graphene sheet with the arc of a circle of the diameter calculated from the RBM peak position as shown in Fig.1. The result insisted the growth of only semiconducting SWNTs with possible four chiral indices at most; (14,0), (13,2), (10,6), (9,7). It was demonstrated that the FEL irradiation was able to control the chirality of the SWNTs. In addition, this chiral control was achieved after covering approximately nm-thick amorphous carbon on catalysts.

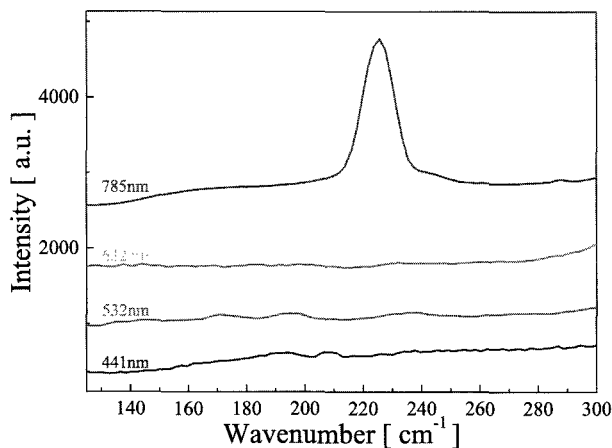


Fig.1 Raman spectra of the SWNTs grown with the 800nm FEL. Used excitation laser was 441nm, 532nm, 632nm and 785nm.

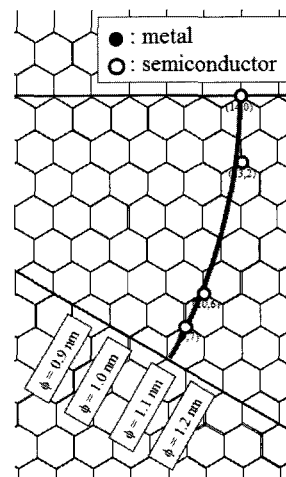


Fig.2 Chiral indices of the SWNTs grown with the 800nm FEL.

[1] K.Sakai, *et al.*, IEICE TRANS. Electron, E94-C (2011) 1861.

SWCNT adsorption onto hydrogels is affected by solute and pH value

○Atsushi Hirano¹, Yasuko Urabe¹, Hiromichi Kataura¹, Takeshi Tanaka¹

¹Nanosystem Research Institute, National Institute of Advanced Industrial Science and Technology, Tsukuba, Ibaraki 305-8562, Japan

Separation of single-wall carbon nanotubes (SWCNTs) using hydrogels is one of the most successful methods enabling the high-purity and large-scale separations.^[1] Understanding the mechanism of the gel separation is necessary to improve the quality and quantity of the separation.^[2,3] In this study, pH and solute-dependent adsorption of SWCNTs onto hydrogels (agarose gel and Sephacryl) was investigated.

The adsorption is reduced at acidic pH values because of the protonation of SWCNTs (Fig.1). The pH dependence is different between metallic and semiconducting species; thus, the adsorption is ascribed to band-structure-dependent protonation of SWCNTs. Because the protonation confers positive charges on SWCNTs through oxidation reaction,^[4] electrostatic interaction of SWCNTs with anionic sodium dodecyl sulfate (SDS) is enhanced by the protonation. The electrostatic interaction likely condenses SDS on SWCNTs, which results in the reduction of the adsorbability of SWCNTs onto the hydrogels. At highly basic conditions, i.e. pH ~13, or in the presence of salts, the adsorption is completely dissociative (Fig.2), which is attributed to the condensation of SDS on SWCNTs through electrostatic screening by the counterions. These results suggest that the metal/semiconductor separation using hydrogels is accounted for by the conformational differences of SDS on the SWCNTs.

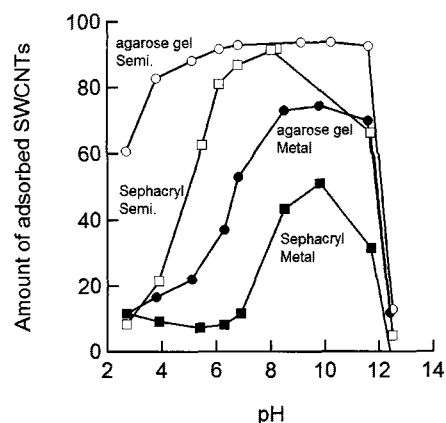


Fig.1 Amount of the adsorbed SWCNTs at various pH values.

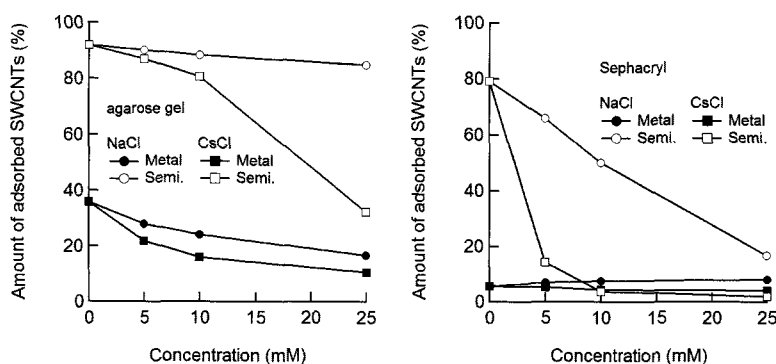


Fig.2 Amount of the adsorbed SWCNTs in the presence of NaCl and CsCl.

[1] T. Tanaka *et al.* Appl. Phys. Express **2**, 125002 (2009).

[2] A. Hirano *et al.* J. Phys. Chem. C **115**, 21723 (2011).

[3] A. Hirano *et al.* ACS Nano **6**, 10195 (2012)

[4] G. Dukovic *et al.*, J. Am. Chem. Soc. **126**, 15269 (2004)

Corresponding Author: T. Tanaka

Tel: +81-29-861-2903, Fax: +81-29-861-2786,

E-mail: tanaka-t@aist.go.jp

Effect of Catalytic Elements to the Growth of Nano-Carbon Composite Films

○Yuki Matsuoka, Masamichi Yoshimura

Graduate School of Engineering, Toyota Technological Institute, Nagoya, 468-8511, Japan

Perpendicularly aligned multiwalled carbon nanotubes (CNTs) terminated with multi-graphene layers [1] have attracted attention as a thermal bump, a sliding surface and so on. However, the growth mechanism is unclear at this moment. In this study, an effect of catalytic elements to grow the composite film has been studied.

Cobalt and iron were deposited as catalysts by arc-plasma evaporation on Al₂O₃ (20 nm)/SiO₂ (50 nm)/Si substrates. The catalytic film thicknesses were measured by dynamic force microscopy (Co: 1.9 ~ 4.6 nm, Fe: 2.1~ 15.8 nm). The composite films were synthesized by cold wall chemical vapor deposition using ethanol gas source (150 torr) at the constant growth temperature of 670 °C. As-grown carbon films were characterized by scanning electron microscopy (Fig.1 (a) and b).

As shown in Fig.1 (a) and (b), same tendency was confirmed on both catalytic elements; a thin, intermediate and thick catalytic film results in vertically aligned CNTs film, the composite film and thick graphite film including not-aligned CNTs, respectively. The thickness to synthesize composite film on cobalt was thinner than that on iron. It is caused by the difference of graphitization behavior of each catalytic metal. Shibuta et al. have reported cobalt cluster has stronger graphitization action than iron clusters [2]. Thus, cobalt film seems to start to precipitate graphite film at thinner catalytic thickness than Iron. In case of iron, composite film was synthesized in wider region of catalytic thickness than cobalt. It is explained by the difference of additional carbon dissolution during graphite precipitation. Shibuta et al. have also reported an iron cluster precipitates imperfect graphite network with solving additional carbon atoms [2]. Therefore, iron could precipitate CNTs under top graphite film at thick catalytic film because thicker iron film is expected to dissolve more carbon atoms.

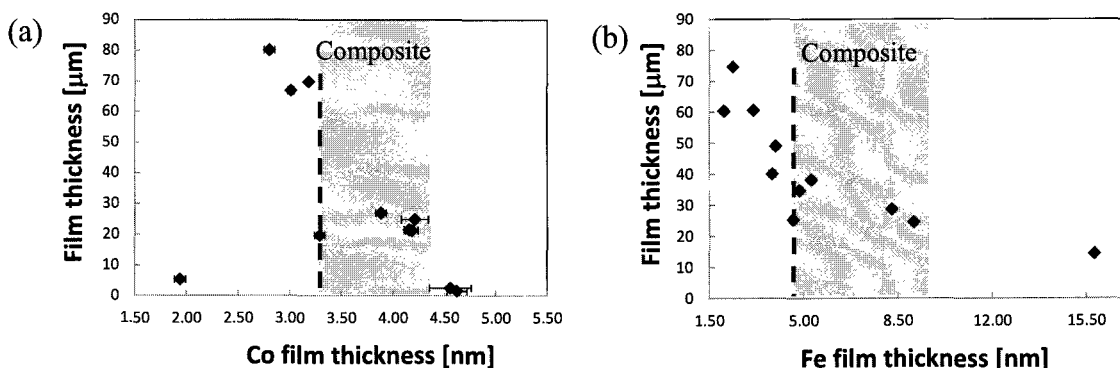


Fig.1 Carbon film thickness grown at different (a) cobalt and (b) iron catalyst thickness

[1] D. Kondo *et al.*, Appl. Phys. Express, 1 (2008) 074003.

[2] Y. Shibuta et al., Comp. Mater. Sci., 39 (2007), 842.

Corresponding Author: Y. Matsuoka

Tel: +81-52-809-1852, Fax: +81-52-809-1851

E-mail: sd11503@toyota-ti.ac.jp

Fabrication of in-plane Aligned and Semiconducting as-grown Single-Walled Carbon Nanotubes

○Nobuyuki Iwata¹, Takumi Sagara¹, Yusaku Tsuda¹, Keisuke Yoshida¹,
Koji Ishii², Hirofumi Yajima², and Hiroshi Yamamoto¹

¹ *Department of Electronics & Computer Science, College of Science & Technology, Nihon University, 7-24-1 Narashinodai, Funabashi, Chiba 274-8501 Japan*

TEL/FAX: +81-47-469-5457 E-mail: iwata.nobuyuki@nihon-u.ac.jp

² *Department of Applied Chemistry, Faculty of Science, Tokyo University of Science, 1-3 Kagurazaka, Shinjyuku-ku, Tokyo 162-0826, Japan*

We have been investigating the novel method to grow single-walled carbon nanotubes (SWNTs) with controlled chirality, growth position, and in-plane alignment during a chemical vapor deposition (CVD) process for nanoscale electronic devices. Specific method to control the chirality is free electron laser (FEL) irradiation and the growth position is surface treatment before CVD process in advance. In this research, we demonstrate the notable effect of FEL irradiation to control the chirality, and then apply it to the in-plane aligned SWNTs.

Triangle Au/Cr electrodes were prepared on SiO₂/Si substrate. The surface of the electrodes and the area between the electrodes were treated to be hydrophilic by exposure to the ozone atmosphere. The Co/Mo catalysts were formed by dipping technique on the surface treated substrate. The SWNTs growth was carried out by alcohol chemical vapor deposition (ACCVD) method. After reduction process, the SWNTs were grown at 700°C for 15 min using ethanol at 2kPa atmosphere. The 800 nm FEL was irradiated during the growth.

Fig. 1 shows Raman spectra of the grown SWNTs without FEL. From the RBM peaks position, the possible chirality is expected to be 25 with the mixture of semiconducting and metallic properties. The inset figure shows the G/D ratio vs. diameter of the SWNTs, which was calculated using the highest RBM peaks detected by 532 nm. High quality SWNTs with 1.69 nm in diameter grew. In the meantime, with 800-nm FEL irradiation, the RBM peak, 1.12 nm in diameter, indicated by the closed star symbol in the inset figure exhibited the highest G/D ratio. It is noteworthy that the diameter with a high quality SWNTs drastically changed from 1.69 to 1.12 nm by the FEL. In addition, the RBM appeared only in the spectra with 785 nm excitation laser, indicating that the four possible semiconducting chirality. The FEL irradiation to the aligned SWNTs will be discussed.

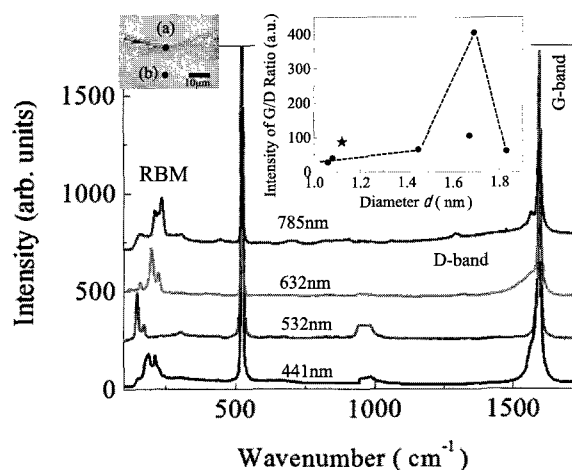


Fig. 1 Raman spectra of the grown SWNTs without FEL analyzed using five excitation lasers. The inset graph (right-up) shows the G/D ratio vs. diameter of the grown SWNTs. The connecting line is guide to the eye. The data indicated by closed star were of the SWNTs grown with FEL and calculated from the results of Raman spectra detected using 785 nm excitation laser. Raman spectrum indicated by closed star was detected at the area (a) in the left-up inset figure. At (b) nothing peaks related CNT was detected.

Enrichment of 1.1 nm-diameter single-wall carbon nanotubes by high-temperature gel filtration

Ryota Ichimura¹, Yasumitsu Miyata¹, Yusuke Nakai¹, Kazuhiro Yanagi¹, Yutaka Maniwa^{1,2}

¹*Department of Physics, Tokyo Metropolitan University, Hachioji, 192-0397*

²*JST, CREST, Kawaguchi, 332-0012*

Development of chirality separation techniques is a current central topic in single-wall carbon nanotube (SWCNT) research. Even though many separation studies have been reported, most of them are applied only to narrow nanotubes less than 1 nm in diameter. In contrast, only a few studies have successfully separate SWCNTs with relatively large diameter [1]. Recently, the rapid chirality separation has been achieved through gel filtration at a low temperature of 10–26 °C [2]. This result strongly suggests that the use of higher temperature leads the separation of larger-diameter nanotubes.

In this study, we have investigated the gel-based chirality separation at higher temperatures up to 70 °C. It is noteworthy that two-step filtration with heated columns enables us to separate nanotubes with 1.1 nm in diameter (Fig.1a). In this process, narrow SWCNTs less than 1.0 nm in diameter are first adsorbed to the gel column at 40 °C (Col.1). Then, non-adsorbed nanotubes are filtered again through the other column at 50 °C (Col.2). Optical absorption spectra reveal that the diameter of nanotubes adsorbed to Col.2 ranges from 1.0 to 1.1 nm (Fig. 1b). This result shows that high-temperature gel filtration provides an effective chirality separation of large-diameter SWCNTs.

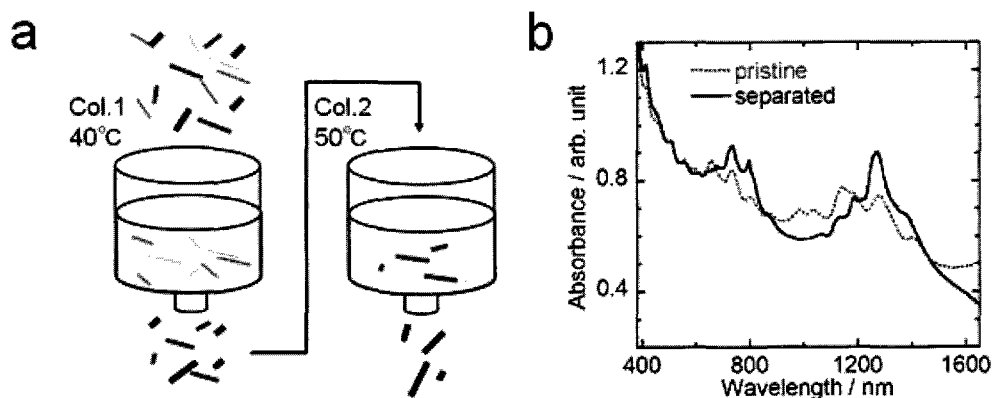


Fig.1 (a) Schematic illustration of the present high-temperature gel filtration.
(b) Optical absorption spectra of pristine and separated CoMoCAT SWCNTs.

[1] M. Kawai *et al.* *J. Am. Chem. Soc.*, 134 (2012) 9545.

[2] H. Liu *et al.* *Nano Lett.*, 13 (2013) 1996.

Corresponding Author: Yutaka Maniwa

Tel: 042-677-2490,

E-mail: maniwa@phys.se.tmu.ac.jp

Low-temperature single-walled carbon nanotubes synthesis from Pt catalysts in the alcohol gas source method and its growth mechanism

○Hiroki Kondo¹, Ranajit Ghosh², Shigeya Naritsuka¹,
Takahiro Maruyama^{1,2}, Sumio Iijima^{1,3}

¹Department of Materials Science and Engineering, Meijo University, Nagoya 468-8502, Japan

²Department of Applied Chemistry, Meijo University, Nagoya 468-8502

³AIST, Tsukuba, Ibaraki 305-8565, Japan

Single-walled carbon nanotubes (SWNTs) have been anticipated for applications in a lot of future nanodevices. To fabricate SWNT devices in a conventional LSI process, it is important to grow SWNTs at low temperature under high vacuum. So far, we have grown SWNTs with small diameters by using Pt catalysts in the alcohol gas source method [1]. In this study, we attempted to grow SWNTs at low temperature from Pt catalysts by optimizing the growth conditions. In addition, we investigated the effects of the growth temperature on the SWNT structural properties (chirality, diameter).

After deposition of Pt catalyst on the SiO₂/Si substrates using an EB gun, the SWNT growth was carried out using alcohol gas source method in a high vacuum [1, 2]. The growth temperature was set between 350°C and 700°C, and the ethanol pressure was varied between 1×10⁻⁵ Pa and 1×10⁻¹ Pa. The grown SWNTs were characterized by FE-SEM, TEM and Raman spectroscopy.

When the growth temperature was decreased to 350°C, the G band intensity was reduced, but the RBM peaks were still observed. As the growth temperature decreased, the SWNT yield decreased, but their diameter distribution became narrower, which should be due to the reduction of catalyst particle size. Our results indicates that Pt catalyst is suitable for low temperature growth of SWNTs with the smaller-diameter and the narrower diameter distributions.

This work was partially supported by the JSPS, Grant-in-aid for Scientific Research (c) 21510119 and Challenging Exploratory Research 25600031) and conducted at the Institute for Molecular Science (IMS), supported by “Nanotechnology Platform” of the MEXT.

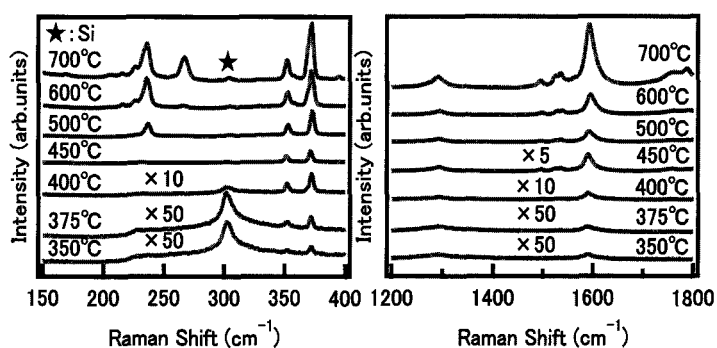


Fig. 1 The growth temperature dependence of grown SWNTs using EB gun. (Excitation wavelength: 785 nm)

References

- [1] T. Maruyama et al., J. Nanosci. Nanotechnol. 10 (2010) 1.
[2] T. Maruyama et al. Mater. Express 1 (2011) 267.

Corresponding author: Takahiro Maruyama

Phone: +81-52-838-2386, Fax: +81-52-832-1179

E-mail: takamaru@meijo-u.ac.jp

Purification of Single-Walled Carbon Nanotubes by Applying Photochemical Reaction of an Ionic Organic Molecule

○Yoko Matsuzawa, Yuko Takada, Tetsuya Kodaira, Hideyuki Kihara, Masaru Yoshida

*Nanosystem Research Institute,
National Institute of Advanced Industrial Science and Technology, Tsukuba 305-8656, Japan*

The as-prepared SWCNTs contain substantial amount of impurities such as amorphous carbons, graphite nanoparticles, and catalytic metal particles. In order for SWCNTs to be used in various scientific investigations and industrial applications, SWCNTs with low impurities and defectiveness are needed to be synthesized. Since most of procedures of purification of SWCNTs are based on exposing them to oxidatives at high temperature in an acidic atmosphere, formation of damages of the SWCNTs cannot be avoided in these processes. Improvement of solubility of SWCNTs is one of key approaches to separate and purify as-grown SWCNTs. Bundled aggregates due to strong intertubular van der Waals interactions causes the poor solubility of SWCNTs. Recently, various studies on the solution chemistry of SWCNTs have been reported. In particular, non-covalent methods using solubilizing agents are of particular interest because well-dispersed SWCNTs can easily be prepared without a significant deterioration in the intrinsic electronic properties. However, removal of dispersants is an issue, because they are tightly adsorbed on the surface of SWCNTs via π - π interactions, van der Waals interactions, and dispersion forces. To solve this issue, tuning dispersibility of SWCNTs using stimuli responsive dispersants is a powerful tool to obtain "pure" SWCNTs in solution phase. Recently, we have reported dispersibility tuning of SWCNTs by applying photochemical reaction of a water-soluble stilbene as a dispersant.^[1] The rigid and nearly planar structure of **1** enables the molecule to interact with the SWCNTs via π - π interactions, resulting in a stable dispersion of the SWCNTs without bundling. In contrast, the photocyclized product **2** having a highly twisted and bent structure is unfavorable for the π - π interactions with the SWCNTs. Because such drastic change in the molecular structure of the dispersant affects the affinity between the dispersant and the surface of SWCNTs, the on-off switching of the dispersibility control of the SWCNTs has successfully been demonstrated by in-situ photoreaction of the **1**/SWCNTs dispersion. In this study, physical characteristics of the photoinduced precipitation of SWCNTs are described on the basis of the analytical results of electron microscopy, TGA, and Raman spectroscopy. As a result, it was found that the photofunctional dispersant **1** acts as a "smart" dispersant for purifying SWCNTs in solution phase.

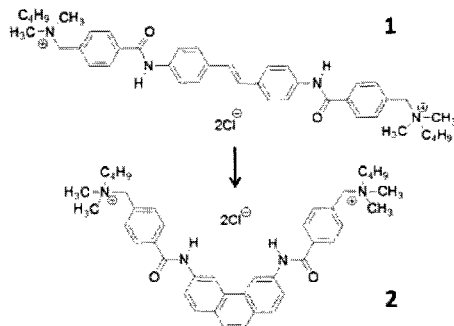


Fig.1 Structures of the photoresponsive dispersant

[1] Y. Matsuzawa *et al.* Adv. Mater., **23**, 3922 (2011).

Corresponding Author: Y. Matsuzawa

Tel: +81-29-861-2958, Fax: +81-29-861-4673,

E-mail:yoko-matsuzawa@aist.go.jp

“Frost column like CNTs” growth by thin Ni catalyst films

○Yuji Kusumoto¹, Kazuki Sekiya¹, Hirofumi Koji¹, Hiroshi Furuta^{1,2}, Akimitsu Hatta^{1,2}

¹ *Electronic and Photonic Systems Engineering, Kochi University of Technology,
Kochi 782-8502, Japan*

² *Institute for Nanotechnology, Kochi University of Technology*

Carbon nanotubes (CNTs) have been of great interest to researchers because of their superior electrical, thermal and photonic properties. Ni thin films are widely examined as a CVD catalyst for control of CNTs growth structures such as chirality[1] and density[2]. Nano-structures of Ni catalysts, such as diameter and density, are quite important to control the growth of CNTs. However, detailed behaviors of Ni catalyst have not been clarified yet even by high-resolution microscopy studies using SEM, TEM and AFM. The aim of this research is to investigate the Ni thin film structures via in-situ conductance (G) measurements during deposition and to achieve highly controlled CNT growth from the Ni catalyst.

Sputtering deposition of Ni was carried out at discharge current of 20 mA with Ar gas of 10 sccm flow rate and 0.8 Pa pressure in the base pressure around 3 mPa. The electrical conductivity of thin Ni deposited on glass substrates was monitored in the vacuum chamber without breaking the vacuum. A pair of Au electrodes was prepared on the glass substrate and they were electrically connected to a digital multi meter through a feed through installed on the vacuum chamber. Sputtering for 5 sec was repeatedly carried out with 10 sec interval. The electrical conductivity of the deposited Ni films was measured during the intervals. CNTs were grown by thermal CVD using C₂H₂ source gas of 10 sccm, 54 Pa at 730°C for 10 min on SiO₂/Si substrate.

Figure 1 shows plots of conductance of Ni films as a function of deposition time. Initial rise of conductance was observed at 45 sec. In our previous work, by using the Ni film at 45 sec, it was succeeded to grow fine CNTs[3]. In this work, we examined CNTs growth using Ni films around 45sec (35sec, 40sec, 50sec, 55sec) deposition times. Figure 2 shows CNTs grown on Ni catalyst deposited for 55sec on SiO₂/Si. Characteristic nano-structures, frost column like CNTs, were found. In the presentation, we will discuss about the relationship between the grown CNT structures and the electrical conductivity of Ni thin films.

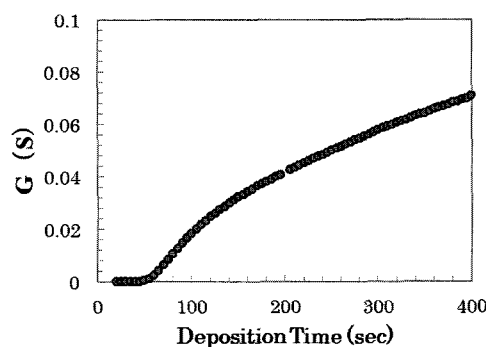


Fig. 1 A plot of conductance of Ni film as functions of total deposition time duration.

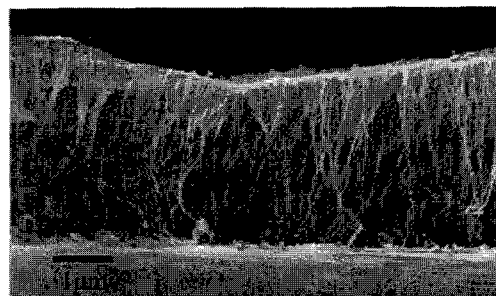


Fig. 2 SEM image of frost column like CNTs grown with Ni (55sec) catalyst on SiO₂/Si.

[1] M. He *et al.*, Nano Res. 4(4), (2011)334.

[2] H. Koji, H. Furuta, K. Sekiya, N. Nitta and T. Harigai, A. Hatta, Dia. Rel. Mat. 36(2013)1.

[3] Y. Kusumoto *et al.*, ISSP2013, (Kyoto, Jul. 2013).

Corresponding Author: H. Furuta

Tel: +81-3-123-4567, Fax: +81-887-57-2211,

E-mail: furuta.hiroshi@kochi-tech.ac.jp

Diameter Distribution of Single-Walled Carbon Nanotubes from Nanodiamond Particles as the Catalysts for CVD Growth

○Takanori Umino¹, Taiki Inoue¹, Shohei Chiashi¹,
Yoshikazu Homma² and Shigeo Maruyama¹

¹ Department of Mechanical Engineering, The University of Tokyo, Tokyo 113-8656, Japan

² Department of Physics, Tokyo University of Science, Tokyo 162-8601, Japan

The chirality controlled synthesis is a challenging topic in the studies of single-walled carbon nanotubes (SWNTs). The catalysts have important roles in controlling SWNT structure, and thus the catalysts with controllable size are needed. Here, we performed the chemical vapor deposition (CVD) growth of SWNTs using nanodiamond particles as the catalysts [1] and investigated the SWNT structure. The diameter of nanodiamond particles was decreased to about 1 nm by oxidation in air at 600 °C before the CVD growth. Co/Mo catalysts prepared by dip-coating process [2] were used for comparison. The CVD growth was performed at 800, 700 and 650 °C.

SWNTs were characterized by scanning electron microscope (SEM) and Raman scattering spectroscopy with 5 different excitation lasers. Figure 1 shows RBM peaks of SWNTs grown at 800 and 700 °C from (A) nanodiamond particles and (B) Co/Mo catalysts. In the case of nanodiamond particles, RBM peaks appear in a narrow range and do not show great change by the growth temperature. In contrast, RBM peaks of SWNTs from Co/Mo catalysts appear in a wide range and show different distribution between 800 and 700 °C. This indicates that the diameter distribution of nanodiamond particles does not change during the CVD growth and the diameter of SWNTs strongly depends on the controlled size of nanodiamond particles. On the other hand, the size of Co/Mo catalysts is easily changed owing to aggregation at the growth temperature. It is suggested that by controlling the diameter distribution of nanodiamond particles before the CVD growth, the structure of SWNTs could be strictly determined.

[1] D. Takagi, et al., *J. Am. Chem. Soc.*, **131** (2009) 6922.
[2] Y. Murakami, et al., *Chem. Phys. Lett.*, **377** (2003) 49.

Corresponding Author:
Shigeo Maruyama
E-mail:
maruyama@photon.t.u-tokyo.ac.jp
TEL: +81-3-5841-6421
FAX: +81-3-5800-6983

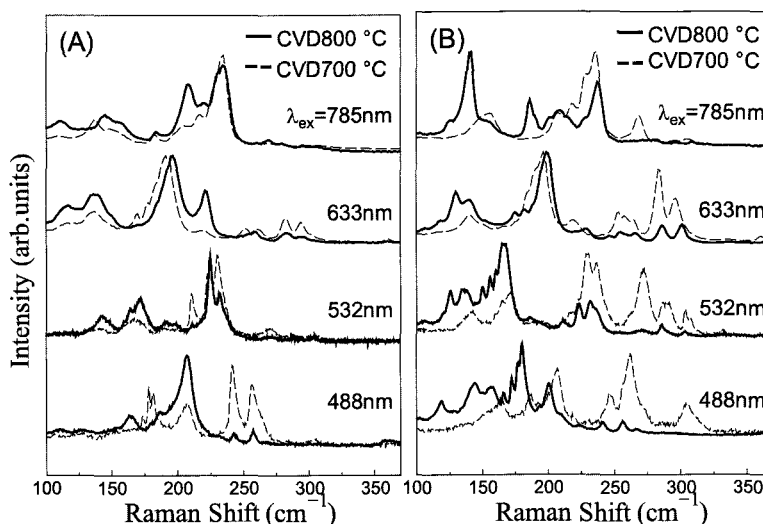


Fig. 1 Raman scattering spectra (RBM peaks) of SWNTs grown from (A) nanodiamond particles and (B) Co/Mo catalysts.

Improved efficiency in metal-free carbon nanotube growth from nanodiamonds by switching growth driving force

○Hiraaki Kokame¹, Kazuki Fujimoto¹, Ryota Negishi¹, Tatsuji Arifuku²,
Noriko Kiyoyanagi², Yoshihiro Kobayashi¹

¹ Graduate School of Engineering, Osaka University, Osaka 565-0871, Japan

² Nippon Kayaku Co., Ltd, Tokyo 115-8588, Japan

Single-walled carbon nanotubes (SWCNTs) almost free of metal impurities have been synthesized by the chemical vapor deposition (CVD) process using nanodiamond particles as the growth nuclei [1]. For applications of SWCNT such as conductive thin films, SWCNT production efficiency strongly affects their performance. Under conventional conditions, the growth efficiency is notably low, because of serious conflict between optimum conditions for efficient SWCNT growth at initial and stationary growth stages. At the initial stage, where SWCNT precursors (cap structures) are formed, the nucleated cap density increases for higher pressure of carbon feedstock gases with carbon rich composition. At the stationary stage after the initial nucleation stage, on the other hand, lower carbon composition and partial pressure of the carbon source gases is preferable to longer life time of the growth nuclei, resulting in growth of longer SWCNTs. Consequently, it is very difficult to achieve highly efficient SWCNT growth under specific fixed growth condition. In this study, we explore a new process to improve the growth efficiency by switching gas phase conditions during CVD.

SWCNTs were synthesized by thermal CVD process from nanodiamond particles dispersed on thermally-oxidized Si substrates. Ethanol, acetylene (3% diluted by Ar) and their mixture were used as carbon feedstock gases. The gas phase condition (the growth driving force) was controlled by switching partial pressure of acetylene from 250 Pa to 50 Pa, and gas composition of acetylene and ethanol from 9:1 to 0:10.

Figure 2 shows typical Raman spectra from the samples grown by various conditions. Fig.2 (a) and (b) indicates that composition switching from acetylene/ethanol mixture to pure ethanol increases the SWCNT yield estimated from intensity ratio of Raman signals of G-bands and Si substrates ($I(G)/I(Si)$). Oxygen-containing species generated by pyrolysis of ethanol may significantly reduce the driving force by their etching effect and elongate the lifetime of nanodiamond particles as the growth nuclei. Similarly, switching the driving force by changing acetylene partial pressure from 250 Pa to 50 Pa also causes the higher yield (Fig.2 (c), (d)). It should be noted that the quality of grown SWCNT estimated by Raman intensity ratio of G- and D-bands ($I(G)/I(D)$) is also enriched by the driving force switching. The growth process optimizing the growth conditions separately at initial and stationary growth stages will open up a novel production route for metal-free SWCNTs in a massive scale.

[1] D. Takagi et al., J. Am. Chem. Soc. 131(2009)6922.

Corresponding Author: Hiraaki Kokame

E-mail: kokame@ap.eng.osaka-u.ac.jp

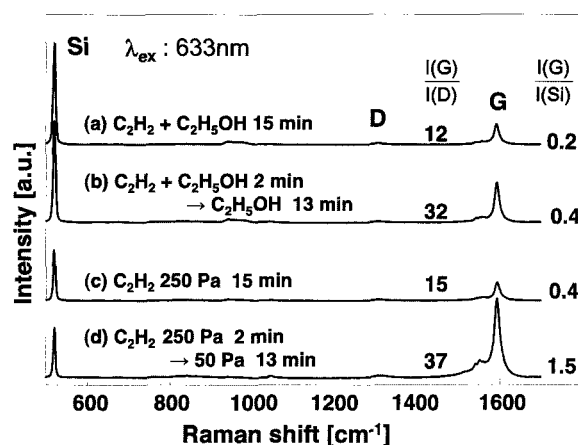


Fig.1 Raman spectra observed from samples grown under various conditions

Molecular Dynamics Simulation of SWNT Growth and DFT Calculation of the Chemical Reaction of Ethanol and Cobalt Clusters

○Kaoru Hisama¹, Tomoya Kawasuzuki¹, Shohei Chiashi¹, Tomofumi Tada² and Shigeo Maruyama¹

¹ *Department of Mechanical Engineering, The University of Tokyo, Tokyo 113-8656, Japan*

² *Materials Research Center for Element Strategy, Tokyo Institute of Technology
Yokohama 226-8503, Japan*

The roles of transition metal cluster as the catalyst are significantly important during the growth of single-walled carbon nanotubes (SWNTs). To analyze their catalytic activity, classical molecular dynamics (MD) [1] has been applied. MD simulation is an effective method to investigate the dynamic growth model, such as initial cap formation and SWNT extension. However, it has difficulty to deal with chemical reactions such as adsorption and dissociation on the catalyst. On the other hand, density functional theory (DFT) is a strong simulation tool to evaluate these processes. Therefore, we performed both MD and DFT calculations to understand the SWNT synthesis.

We analyzed the quality of SWNTs and local chirality obtained by MD simulation. Then we found excessive carbon supply (which corresponds to high pressure) suppresses the quality and chiral uniformity. Figure 1 shows the formation of new six-membered ring of SWNT which occurs in the region where the catalyst surface is not covered with carbon atoms. This ring formation area becomes unstable and suppressed when the carbon pressure is high.

Chemical reactions on the catalyst surface are also needed to study for the evaluation of carbon supply rate. We applied DFT calculation to the reaction of ethanol and small cobalt cluster which can be compared with the experimental results of FT-ICR (Fourier transform ion cyclotron resonance) spectroscopy [2]. An obtained stationary point of the system is shown in Fig. 2, in which oxygen atom of the ethanol approaches to top of the cluster.

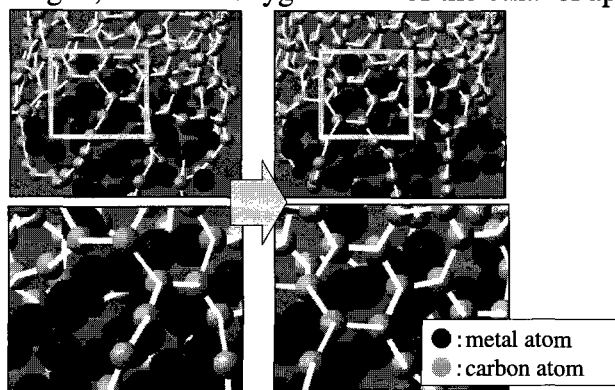


Fig. 1 Six membered ring formation during growth process in MD simulation.(total: 0.2 ns). Carbon atoms inside the metal cluster are not visualized.

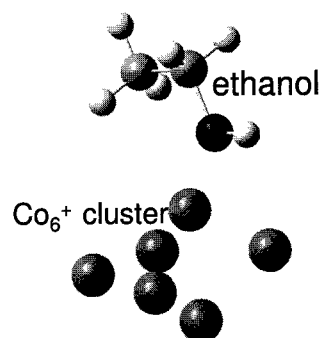


Fig. 2 The stable structure of a Co_6^+ cluster and an ethanol molecule obtained by DFT calculation.

[1] Y. Shibuta and S. Maruyama, *Chem. Phys. Lett.*, **382** (2003) 381.

[2] S. Inoue and S. Maruyama, *Jpn J. Appl. Phys.*, **47** (2008) 1931.

Corresponding Author: Shigeo Maruyama

Tel: +81-3-5841-6421, Fax: +81-3-5800-6983,

E-mail: maruyama@photon.t.u-tokyo.ac.jp

Chirality Analysis of Horizontally Aligned Single-Walled Carbon Nanotubes by Raman Spectroscopy

○Taiki Inoue, Daisuke Hasegawa, Shohei Chiashi, Shigeo Maruyama

Department of Mechanical Engineering, The University of Tokyo, Tokyo 113-8656, Japan

Chirality controlled growth of single-walled carbon nanotubes (SWCNTs) has been studied extensively and some groups have reported the enrichment of near-armchair SWCNTs in certain growth conditions [1]. This selectivity is considered to derive from the chirality-dependent cap stability [2] and/or the chirality-dependent growth rate [3]. Although chirality distribution of SWCNTs is evaluated by several methods, it is impossible to obtain separate information about populations and lengths of SWCNTs with different chiralities by measurement of bulk SWCNTs or randomly oriented individual SWCNTs. Detailed analysis of chirality-dependent population and length distribution of SWCNTs would be helpful to understand the mechanism of the selective growth.

Here, we investigated the population distribution of chiralities utilizing individual aligned SWCNTs and Raman spectroscopy. Horizontally aligned SWCNTs with moderate density were grown by alcohol chemical vapor deposition on r-cut quartz substrates using photolithographically patterned iron catalysts. For Raman measurement, SWCNTs were transferred onto SiO₂/Si substrates and metal markers were fabricated on the substrates (Fig. 1 (a)). We used four excitation wavelengths and acquired radial breathing mode (RBM) peaks of individual SWCNTs with scanning laser spot positions perpendicular to the alignment direction (Fig. 1 (b)). The well-organized structure of horizontally aligned SWCNTs and the systematic investigation enable us to obtain Raman spectra of all resonant SWCNTs in the specific area without multiple counting. RBM peaks with wavenumbers higher than ~180 cm⁻¹ were used for chirality assignment. Figure 1 (c) shows chiral angle distribution of SWCNTs obtained from 49 RBM peaks. Additional correlation of chirality-assigned SWCNT positions to scanning electron microscope (SEM) observation would yield information about length distribution of SWCNTs depending on chirality.

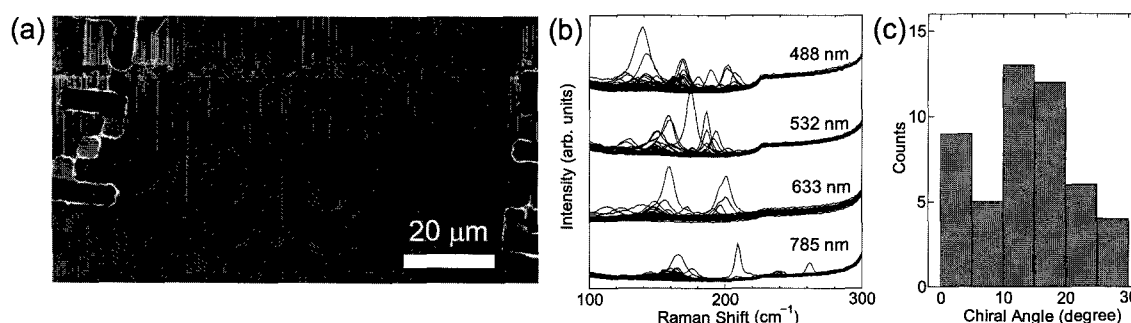


Fig. 1 (a) SEM image of horizontally aligned SWCNTs and marker structures on an SiO₂/Si substrate. (b) RBM peaks of individual SWCNTs, excited at the indicated laser wavelengths. (c) Chiral angle distribution of SWCNTs.

- [1] Y. Miyauchi *et al.*, Chem. Phys. Lett. 387, 198 (2004).
 [2] S. Reich *et al.*, Chem. Phys. Lett. 421, 469 (2006).
 [3] F. Ding *et al.*, Proc. Natl. Acad. Sci. U.S.A. 106, 2506 (2009).

Corresponding Author: S. Maruyama

Tel: +81-3-5841-6421, FAX: +81-3-5800-6983,

E-mail: maruyama@photon.t.u-tokyo.ac.jp

Growth kinetics of narrow-chirality distributed single-walled carbon nanotube under pulse plasma CVD

○Bin Xu, Toshiaki Kato, Koshi Murakoshi, and Toshiro Kaneko

Department of Electronic Engineering, Tohoku University, Sendai, 980-8579 Japan

One dimensional single-walled carbon nanotubes (SWNTs) with various novel characteristics are potential materials for future nanoelectronics. Since the electronic and optical properties of SWNTs strongly depend on their diameter and chirality, the selective synthesis of SWNTs with desired chiralities is one of the major challenges in nanotube science and applications. We realized a narrow-chirality distributed growth of SWNTs by time-programmed plasma CVD [1]. In this method, we used very short time growth of SWNTs. Based on the systematic investigations, it has been revealed that there is a close correlation between incubation time (t_i) and SWNT structures. Since t_i of the small diameter (or specific chirality) SWNTs is shorter than that of the larger (or other chiralities) one, selective growth of narrow-chirality distributed SWNTs has been realized by adjusting the growth time during plasma CVD. Recently, a new strategy to realize the mass production of narrow-chirality distributed SWNTs using pulse plasma CVD is also demonstrated [2]. In the pulse plasma CVD, multiple short time growth of SWNTs is possible by repeating the plasma generation. It is found that the amount of SWNTs increases with an increase in the total growth time. Interestingly, it is also revealed that the initial narrow-chirality distribution of SWNTs can be maintained even after the long time pulse plasma CVD.

In this study, we have investigated the growth kinetics of SWNTs under pulse plasma CVD. The chirality distribution of SWNTs is found to be very sensitive to the off time of pulse plasma generation. Large diameter SWNTs growth can be suppressed and chirality distribution becomes narrow with an increasing in the off time up to 30 sec (Fig.1). This can be explained by the combination of t_i difference between small and large diameter SWNTs and changing of catalyst particle size due to Ostwald ripening during pulse plasma CVD.

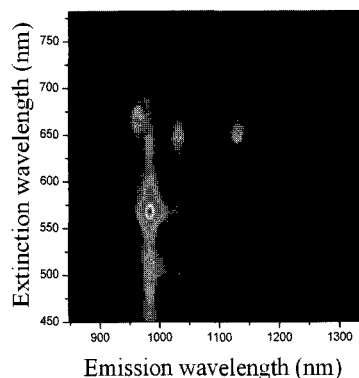


Fig.1: Photoluminescence-excitation mapping of narrow-chirality distributed SWNTs grown by pulse plasma CVD.

[1] T. Kato and R. Hatakeyama, ACS Nano 4, 7395 (2010).

[2] K Murakoshi, T. Kato, R. Hatakeyama and T. Kaneko, Abstracts of the 44th Fullerenes-Nanotubes-Graphene General Symposium, 63 (2013).

Corresponding Author: X. Bin

Tel: +81-22-795-7046, Fax: +81-22-263-9225,

E-mail: xu12@ecei.tohoku.ac.jp

Optical properties of vertically aligned CNT forests formed at various growth temperatures

○Hiroshi Furuta^{1,2}, Kazuki Sekiya¹, Keisuke Takano³, Masanori Hangyo³, Akimitsu Hatta^{1,2}

¹ *Electronic and Photonic Systems Engineering, Kochi University of Technology, Kochi 782-0003, Japan*

² *Institute for Nanotechnology, Kochi University of Technology*

³ *Institute of Laser Engineering, Osaka University, Osaka 565-0871, Japan*

Unique optical properties of carbon nanotube forests have been reported on the extremely high absorption of vertically aligned CNT forests [1, 2], and on the angle dependent absorption for the polarized incident light [3]. We previously reported [4, 5] that the vertical alignment of CNT forests are quantitatively evaluated as vertical the alignment factor ($Va = (002) \text{ diffraction beam} / ((000) \text{ Initial beam} - (000) \text{ Transmitted beam})$) utilizing a cross-sectional XRD in $2\theta/\varphi$ scan [4]. Figure 1(a) shows plots of vertical alignment factor (Va) as a function of position from the substrate in the forest, measured from the side-wall of CNT forests [5]. Peak located at 4.5eV is attributed to π plasmon. As shown in Fig. 1(a), the Va for CNT forest grown at 690°C was lower than those of 580 and 630°C. Figure 1(b) shows the reflectance spectra at 5° for each forests. These CNT forests showed very low reflectance lower than $4 \times 10^{-3} \%$ in visible region. The reflectance of forests grown at 690°C was higher than those of 580 and 630°C, due the higher reflectance of lateral CNTs [7].

As a quantitative index of vertical alignment of CNT forest, the vertical alignment factor (Va) was closely correlated to the optical reflectance of vertically aligned CNTs.

This work was supported by Japan Society for the Science (JSPS) KAKENHI (No. 24560050), Grant-in-Aid for Scientific Research (C).

- [1] Z. -P. Yang *et al.*, Nano lett. 8(2), 446 (2008). [2] K. Mizuno *et al.* PNAS **106**, 6044 (2009).
 [3] Y. Murakami *et al.*, Carbon **43**(13), 2664 (2005). [4] H. Furuta *et al.* APEX **3**, 105101(2010).
 [5] H. Furuta *et al.*, 43th FNTG Sympo. (Sendai, 2012). [6] Y. Murakami *et al.*, PRL **94**, 087402(2005). [7] T. Saleh *et al.*, APL **101**, 061913(2012).

Corresponding Author: H. Furuta

Tel: +81-887-57-2211, E-mail: furuta.hiroshi@kochi-tech.ac.jp

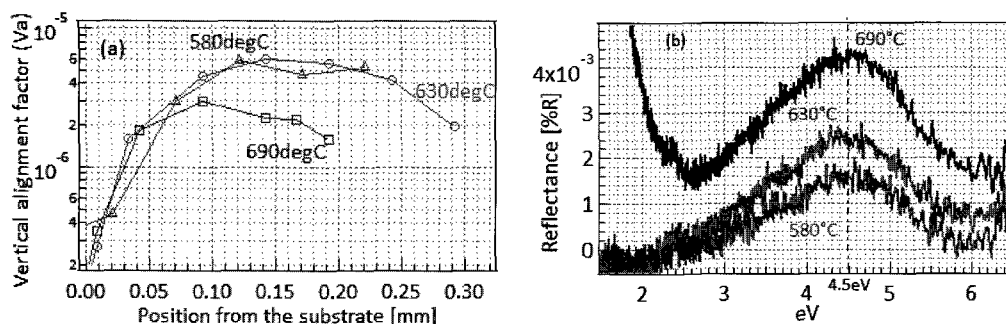


Fig.1. (a) vertical alignment factor plot [5] and (b) reflectance spectra of CNT forests, which has been grown at various temperature of 580, 630, and 690°C. Highly vertically aligned CNT forest of 580 and 630°C showed lower reflectance than that of 690°C.

Coherent phonon spectroscopy of semiconducting single-wall carbon nanotubes

Yuki Honda¹, Elizabeth Maret¹, Atsushi Hirano², Takeshi Tanaka², Kotaro Makino³,
Muneaki Hase¹

¹ *Institute of Applied Physics, University of Tsukuba, Tsukuba 305-8573, Japan*

² *Nanosystem Research Institute, National Institute of Advanced Industrial Science and Technology, Tsukuba 305-8562, Japan*

³ *Nanoelectronics Research Institute, National Institute of Advanced Industrial Science and Technology, Tsukuba 305-8562, Japan*

Coherent phonon spectroscopy, based on impulsive stimulated Raman scattering by using ultrafast pulse lasers, has been used to study sub-picosecond carrier-phonon nonequilibrium dynamics of single-walled carbon nanotubes (SWCNTs). It is well known that the coherent phonon spectroscopy exhibits a large anisotropic phonon response dependent upon the polarization of excitation light [1]. However, little is known about the behavior of pure (metal/semiconductor separated) SWCNT samples excited at resonant and off-resonant conditions. In this study, we have investigated the anisotropic properties of two pure and separated semiconducting SWCNTs (*s*-SWCNT) samples [2], one as an aligned film and the other as a dispersed solution.

The samples were produced by HiPco process and SDS was used to disperse SWCNTs. The aligned *s*-SWCNTs films were prepared by immersing a glass sample slide into the separated *s*-SWCNTs solution. Time-resolved transient transmission and reflection of the sample were measured by employing a pump-probe technique with Ti:sapphire laser (20 fs, 80 MHz repetition rate, 800 – 850 nm central wavelength) to measure coherent phonons.

Coherent phonon spectra for the radial breathing mode (RBM) exhibit the different monochromatic frequency between the film (7.2 THz) and solution (6.4 THz) samples because of the presence of differing exciton resonances. By varying the incident pump polarization on the aligned SWCNT film, we found that the anisotropy of the coherent RBM excitation depends on the laser wavelengths, we consider to be associated with the resonant and off-resonant behavior of RBM excitation [3].

[1] J. -H. Kim *et al.*, *J. Appl. Phys.* **105**, 103506 (2009).

[2] A. Hirano, T. Tanaka, and H. Kataura, *ACS Nano*, **6**, 10195 (2012).

[3] Y. Honda and E. Maret *et al.*, *Appl. Phys. Lett.* **102**, 222109 (2013).

Interplay of wall number and diameter on the electrical conductivity of carbon nanotube thin films

○Guohai Chen¹, Don N. Futaba^{1,2}, Shunsuke Sakurai^{1,2}, Motoo Yumura^{1,2}, and Kenji Hata^{1,2}

¹ *Technology Research Association for Single Wall Carbon Nanotubes (TASC), Tsukuba
305-8565, Japan*

² *National Institute of Advanced Industrial Science and Technology (AIST), Tsukuba
305-8565, Japan*

When carbon nanotubes (CNT) are used in practical applications, they are in the form of assemblies as opposed to individual CNTs. Many CNT-based macroscopic assemblies with diverse configurations, compositions, and composed of different CNT structures have been developed as represented by CNT thin films, CNT fibers, CNT mats, CNT composites, and buckypapers to meet the specific demands of the target application [1-2]. There are two crucial factors which determine the properties of the assemblies: the CNT structure itself and the assembly structure. Variation in the diameter, length, crystallinity, wall number of the CNTs greatly influences the properties of the assembly [3-4]. In reality, changes in the individual CNT structure also results in changes to the assembly structure, which increases the complexity of this matter. This interdependency might result in an unexpected and interesting dependence of the CNT assembly performance on the CNT structure, although this aspect, to the best of our knowledge, has not been greatly pursued in the literature.

Here, we report the interplay between the CNT structure (wall number and diameter) and assembly structure (packing density) on the electrical conductivity of CNT thin films. By controlling the average wall number of CNTs from 1 to 5.5 (and inevitably changing of the diameter from 3 to 8.7 nm), the electrical conductivity of CNT films showed a unique and unexpected phenomenon, i.e. peaking at ~2.7 walls that was ~3-times higher than that of single-walled CNTs and ~1.6-times higher than that of 5.5-walled CNTs. By developing a simple model, the individual contributions of individual CNT structure and assembly structure were estimated, and we found that the peak arose from offsetting factors: increase in the effective CNT conductivity and decrease in the packing density with increased wall number. This represents the first finding of the synergetic effect between the CNT structure and assembly structure on the performance would provide a scientific framework to deeply understand CNT assemblies.

[1] L. Ericson *et al.* *Science* **305**, 1447(2004).

[2] M. Engel *et al.* *ACS Nano* **2**, 2445(2008).

[3] L. Zhang *et al.* *Nano Lett.* **12**, 4848(2012).

[4] S. Ata *et al.* *Nano Lett.* **12**, 2710(2012).

Corresponding Author: Don N. Futaba

Tel: +81-29-861-4656, Fax: +81-29-861-4851,

E-mail: d-futaba@aist.go.jp

Effect of lattice vibration on the geometry of carbon nanotubes

○Takashi Koretsune, Koichiro Kato, Susumu Saito

¹*Department of Physics, Tokyo Institute of Technology, Tokyo 152-8551, Japan*

The geometrical structure is fundamental information to discuss the property of materials such as electronic, mechanical and optical properties. In carbon nanotubes, however, it is difficult to determine the geometrical parameters precisely from experiments. Thus, it is of great importance to clarify the geometry of carbon nanotubes from first principles. So far, our group has performed a first-principles electronic structure study for all types of carbon nanotubes and found that the deviation of bond lengths and angles from those of the rolled-up graphene can be classified well by the so-called chiral indices of carbon nanotubes [1,2]. Interestingly, the chiral nanotubes are predicted to have intrinsic twisting and therefore they do not possess the exact translational symmetry [3].

To compare the predicted geometrical parameters with experiments in detail, however, we have to pay attention that the effect of lattice vibration such as thermal expansion can play a significant role. Particularly, in carbon nanotubes, the radial and axial extension due to lattice vibration may be different. Thus, we investigate the effect of lattice vibration by computing the phonon frequencies using first-principles calculations. We clarify the contributions of the zero-point motion and the thermal expansion and discuss how the lattice vibration affects the electronic structures as well as geometrical structures.

[1] K. Kato and S. Saito, *Physica E* **43** 669-672 (2011).

[2] K. Kato, T. Koretsune and S. Saito, *J. Phys: Conf. Ser.* **302** 012007 (2011).

[3] K. Kato, T. Koretsune and S. Saito, *Phys. Rev. B* **85** 115448 (2012).

Corresponding Author: T. Koretsune

E-mail: koretune@stat.phys.titech.ac.jp

Temperature Dependence of Stokes and anti-Stokes photoluminescence from oxygen-doped carbon nanotubes

○Yuhei Miyauchi^{1,2}, Naoto Akizuki¹, Munechiyo Iwamura¹,
Shinichiro Mouri¹, and Kazunari Matsuda¹

¹*Institute of Advanced Energy, Kyoto University, Gokasho, Uji, Kyoto 611-0011, Japan*

²*PRESTO, Japan Science and Technology Agency, 4-1-8 Honcho Kawaguchi, Saitama 332-0012, Japan*

In contrast to intensive studies over the past decade on the intrinsic one-dimensional (1D) exciton photophysics in single-walled carbon nanotubes (SWNTs) [1], there have been limited number of reports [2-5] on the impact of local quantum states on excitonic properties in SWNTs. If a well-organized 0D-like local luminescent state is generated in an intrinsic 1D SWNT, such a complex nanostructure can be viewed as nearly ideal 1D-0D hybrid low dimensional system where novel exciton photophysics may emerge [4]. Additionally, the modifications originating from the additional local states may exert changes on the intrinsic optical properties of SWNTs that are favorable for their optoelectronics applications. In this study, we explore exciton photophysics in local quantum states in SWNTs through the observations of temperature dependence of photoluminescence (PL) from carbon nanotubes with 0D-like local luminescent states generated by atomic oxygen doping [3, 4]. Figure 1 shows the Stokes PL spectra from the intrinsic and localized excitons in oxygen-doped SWNTs measured at different temperatures. We found that the temperature-dependent variation of PL intensities from both 1D intrinsic and 0D-like localized excitons are well reproduced by considering the exciton diffusional transport and the reduction of the bright exciton population due to the existence of lower lying dark states [6] not only in the intrinsic states but also in the localized states. We also observed a reduction of the Stokes PL intensity of the localized excitons at higher temperature range more than 200K. This temperature dependent variation indicates the existence of phonon-assisted exciton upconversion process from the local state to the 1D state, as we have confirmed by observations of anti-Stokes PL induced by the direct photoexcitation of the local states. We will discuss the detailed mechanisms responsible for the observed temperature-dependent changes in the Stokes and anti-Stokes PL intensity.

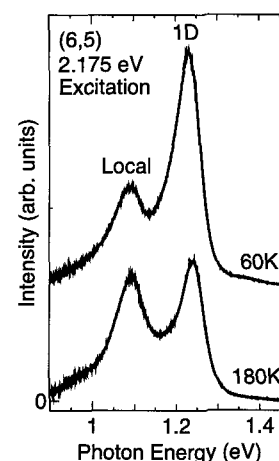


Fig. 1. Stokes PL spectra of oxygen-doped carbon nanotubes measured at 60 and 180 K. Peaks at 1.07 and 1.25 eV correspond to PL from localized and intrinsic excitons, respectively.

- [1] Y. Miyauchi *et al.*, Phys. Rev. B **80**, 081410(R) (2009).
- [2] K. Iakoubovskii *et al.*, Appl. Phys. Lett. **89**, 173108 (2006).
- [3] S. Ghosh *et al.*, Science **330**, 1656 (2010).
- [4] Y. Miyauchi *et al.*, Nature Photon., in press.
- [5] S. Kilina *et al.*, Nano Lett. **12**, 2306 (2012).
- [6] R. Matsunaga *et al.*, Phys. Rev. Lett. **101**, 147404 (2008).

Corresponding Author: Y. Miyauchi

Tel: +81-774-38-3463, Fax: +81-774-38-3467

E-mail: miyauchi@iae.kyoto-u.ac.jp

Highly Sensitive Detection of Oxygen Gas by Perovskite Materials Decorated Single-Walled Carbon Nanotubes

○H. Fukuda¹, K. Matsushita¹, H. Tabata¹, O. Kubo¹, M. Katayama¹, R. Shimazaki², H. Tanjo², and M. Horiuchi²

¹ Department of Electronic Engineering, Graduate School of Engineering, Osaka Univ.
2-1 Yamadaoka, Suita, Osaka 565-0871, Japan

² New Cosmos Electric Co., Ltd., Osaka, Japan

The monitoring of airborne contaminants is becoming increasingly important in semiconductor manufacturing processes as CMOS devices are scaled down to nanometers. For this purpose, safety, low cost, and simple gas sensor is required, which has sufficient sensitivity to trace amount (of the order of ppb) of oxygen.

In this study, we fabricated chemiresistive sensors using single walled carbon nanotubes (SWNTs) covered with various perovskite-type metal oxides, and subjected to evaluation for detecting trace levels of oxygen in vacuum.

SWNTs were directly grown on a conventional sensor platform [1] by thermal chemical vapor deposition method. The SWNTs were then covered with CaTiO₃, BaTiO₃, and SrTiO₃ layer, respectively by pulsed laser deposition. The sensitivity of the sensors was evaluated in vacuum (base pressure : 10⁻⁵ Pa) by monitoring the conductance change after injecting trace amount of O₂.

Figure 1 shows transmission electron microscopy (TEM) image of a SrTiO₃-SWNT. It revealed that the covered SrTiO₃ layer was amorphous. Figure 2 shows sensor responses of the various metal-oxide SWNT to 1 × 10³ Pa of O₂ gas, with the response of as-grown SWNT, for comparison. By covering the metal oxides, the responses of SWNTs to oxygen were largely enhanced. These results indicate that the metal oxides work as active layers for O₂ sensing. Figure 3 shows the reproductibility of the sensor responses of BaTiO₃ and SrTiO₃-SWNT. In both sensors, the variation of the sensor responses was within 20 % during 18 cycles.

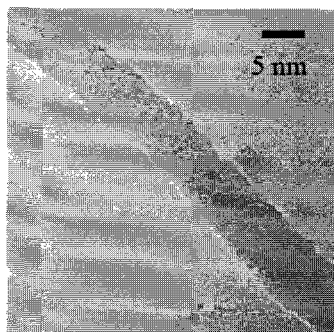


Figure 1. HRTEM image of SrTiO₃-SWNT.

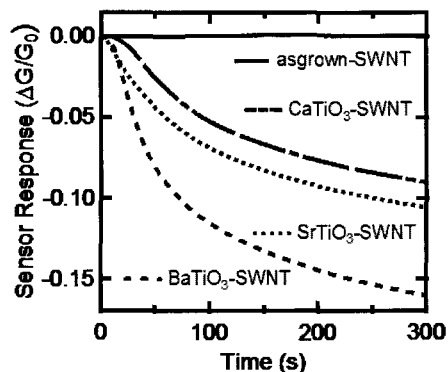


Figure 2. Sensor responses of SWNTs coated with various perovskite materials to O₂ gas.

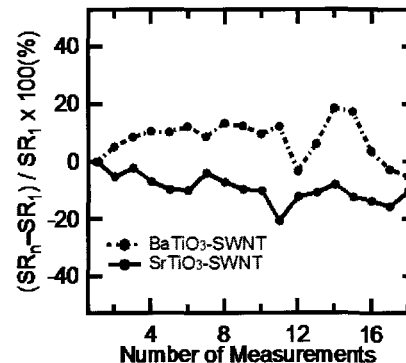


Figure 3. Variations of sensor responses of BaTiO₃ and SrTiO₃-SWNTs versus number of measurements.

Corresponding Author: Mitsuhiro Katayama

Tel: 06-6879-7775, Fax: 06-6876-4564

E-mail: katayama@nmc.eei.eng.osaka-u.ac.jp

[1] W. Wongwiriyanpan *et al.* : Jpn. J. Appl. Phys. 44 (2005) 457.

Gas Sensing using Semiconducting Single-Walled Carbon Nanotubes Thin Film

○Y. Suzuki¹, R. Nomoto¹, N. Matsutake¹, H. Tabata¹, O. Kubo¹, M. Katayama¹,
T. Ueda², R. Shimazaki², H. Tanjo², and M. Horiuchi²

¹ *Department of Electronic Engineering, Graduate school of Engineering, Osaka Univ.
2-1 Yamadaoka, Suita, Osaka 565-0871, Japan*
² *New Cosmos Electric Co., Ltd., Osaka, Japan*

Gas sensors using a single walled carbon nanotube (SWNT) film as an active material have received considerable attention because of their outstanding properties such as fast response, high sensitivity, operating room temperature and good reproducibility. However, the sensor performance has been limited by the metallic SWNTs (m-SWNTs) included in as-grown SWNTs. Recent progress of the sorting technology extracting semiconducting SWNTs (s-SWNTs) from mixture of m- and s-SWNTs makes available semiconducting-enriched SWNT film for SWNT-based sensors.

In this study, we investigated the sensor response properties of s-SWNT film to oxidizing and reducing gases. The s-SWNT film was deposited on a conventional sensor platform [1] by dipping the substrate in s-SWNT (99%) solution. For comparison, we also prepared unsorted, as-grown-SWNTs film directly grown on the sensor substrate by chemical vapor deposition. Figure 1 shows sensor response upon exposure of the s-SWNT film to NO₂ (1ppm) compared with that of the as-grown-SWNT film, which are plotted in terms of sensor response $((G-G_0)/G_0)$ as a function of time. The s-SWNT film exhibited double digit or more improvement in sensitivity compared with the unsorted SWNT films. Figure 2 shows sensor response upon exposure of the s-SWNT film to NH₃ (100ppm) compared with that of the as-grown-SWNT film. The s-SWNTs exhibited four times higher response than as-grown-SWNTs. These results indicate that the usage of s-SWNTs effectively improves the sensitivity of the SWNT sensor to both oxidizing and reducing gases.

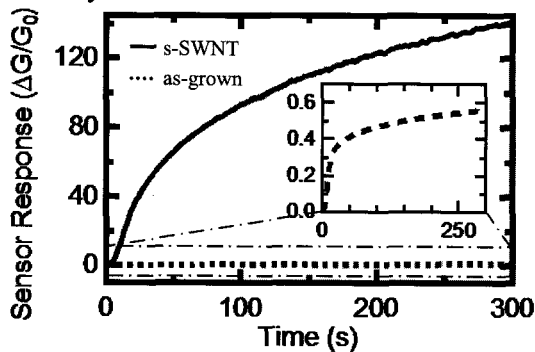


Figure 1. Sensor responses of s-SWNT film and as-grown SWNT film to NO₂ (1 ppm) exposure in N₂.

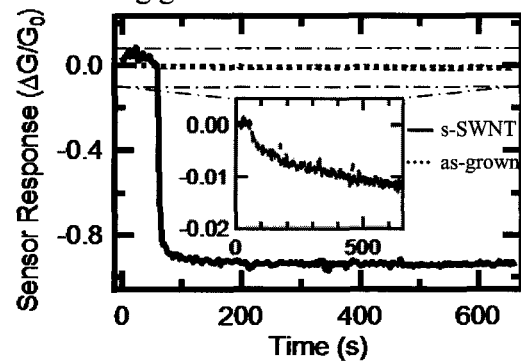


Figure 2. Sensor responses of s-SWNT film and as-grown SWNT film to NH₃ (100 ppm) exposure in N₂.

[1] W.Wongwiriyapan *et al.* :Jpn. J. Appl. Phys. 44 (2005) 457

Corresponding Author: Katayama Mitsuhiro
Tel: 06-6879-7775, Fax: 06-6876-4564,
E-mail: katayama@nmc.ei.eng.osaka-u.ac.jp

Interaction between Carbon Nanotubes and Neurons Studied With High-Density Microelectrode Arrays

Florent Seichepine^a, Kosmas Deligkaris^a, Urs Frey^a,

^a *Frey Initiative Research Unit, RIKEN QBiC, Kobe, Hyogo 650-0047, JAPAN*

Carbon nanotube (CNT) have been successfully tested has neuronal cell culture scaffold. The properties of CNT layers, such as chemical stability, nano-roughness and electrical conductivity are very suitable to engineer a large number of biointerfaces, and especially neuro-interfaces. CNTs have been shown to have a direct influence on the plasticity of several types of cells, but also a direct influence on the neuronal electrophysiological activity, such as changes of the firing rates and excitability[1]. The interactions between CNTs and neurons have become a subject of high interest[2]. Several hypotheses have been formulated to explain such a functional coupling. An explanation could be direct shortcuts in the network through the CNTs[3]. In order, to precisely study the effect of CNTs on neuronal networks, we are using high-density microelectrode arrays (HDMEA)[4] to electrically image the neuronal activity at subcellular resolution and we are studying the influence of CNT layers on the action potentials of cultured neurons.

To pattern and control the CNT layers on ours HDMEA interfaces, we are using a technique based on spray assisted micro-contact printing. Neuronal cells are than cultured on this CNT micro-structured scaffold and are forming networks. The patterning of the CNT layer allows the comparison of the electrical behavior of cells on a CNT layer and directly on the chips during a single experiment. This approach coupled with the sub-cellular resolution and some new techniques to precisely follow the electric signals in narrow path will lead to a better understanding of the mechanism behind the interactions between CNTs and neurons.

- [1]T. Chen, J. *et al.* Toxicology letters,217, 121 (2013)
 [2]E. Heister, E. *et al.* ACS applied materials & interfaces, (2013)
 [3]G. Cellot *et al.* Nature nanotechnology, 4, 126 (2009)
 [4]U.Frey *et al.* IEEE J. of Solid-State Circuits, 45, 467,(2010)

Corresponding Author: Florent Seichepine
 Frey Initiative Research Unit, RIKEN QBiC, Kobe Institute
 2-2-3 Minatojima-minamimachi, Chuo-ku, Kobe, Hyogo
 650-0047, JAPAN
 e-mail: f.seichepine@riken.jp

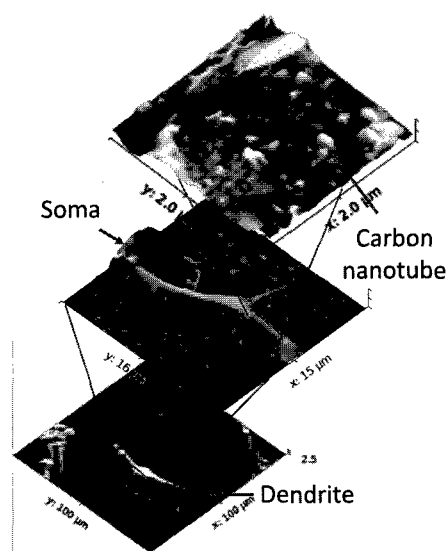


Fig.1. AFM study of neuronal cells cultured on a thin CNT layer.

Oxygen Reduction Reaction of Nitrogen-doped Graphitic Structure Using Single-walled Carbon Nanotubes as a Catalyst Support

Junichi Morita¹, Tsuyohiko Fujigaya^{1,2}, and Naotoshi Nakashima^{1,2,3}

¹Department of Applied Chemistry, Graduate School of Engineering, Kyushu University, 744 Motooka, Fukuoka 819-0395, Japan

²World Premier International (WPI), International Institute for Carbon-Neutral Energy Research, Kyushu University 744 Motooka, Nishi-ku, Fukuoka 819-0395, Japan

³Japan Science and Technology Agency, CREST, 5 Sanbancho, Chiyoda-ku, Tokyo, 102-0075, Japan

Polymer electrolyte fuel cell (PEFC) systems using Pt-free catalyst are the strong request from industry side because Pt is expensive and exhaustive metal. One of the promising approaches for the Pt-free cathode catalyst is the use of nitrogen-doped graphite structure (N-doped Carbon) (Fig. 1), which has oxygen reduction reaction (ORR) activity.

We have reported the novel preparation method to prepare N-doped Carbon on carbon nanotube (CNT) for ORR catalyst in acidic condition (Fig. 2) [1]. The composite (CNT/N-doped Carbon) was fabricated by a coordination of cobalt (II) onto pyridine containing polybenzimidazole (PyPBI) wrapped around CNT, and this composite (CNT/PyPBI(Co)) was calcined at 600 °C for 1.5 h in N₂. After metal-leaching by acid, the CNT/N-doped Carbon was obtained. In this composite, the use of CNT as a supporting material leads a smooth electron conduction due to the fibrous network morphology.

In this study, we investigated a relationship between catalytic activity and difference of CNT type. As a CNT, single-walled carbon nanotubes (SWNT) and multi-walled carbon nanotubes (MWNT) was employed.

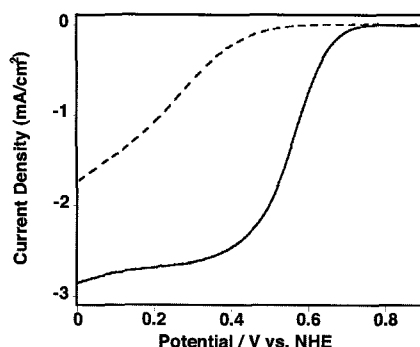


Fig. 3 Linear sweep voltamograms for MWNT/N-doped Carbon (dotted line) and SWNT/N-doped Carbon (solid line) under O₂. Rotating speed, 1600 rpm; catalyst loading, 0.5 mg/cm².

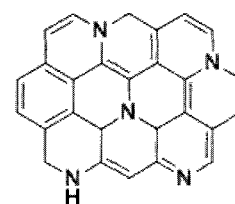


Fig. 1 Chemical structure of N-doped Carbon.

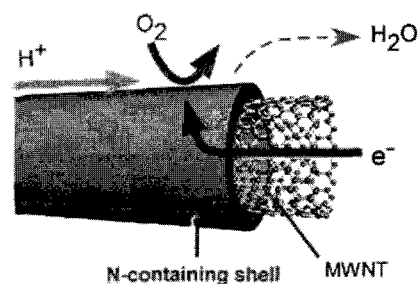


Fig. 2 Schematic illustration of CNT/N-doped Carbon and mass transfer upon ORR.

The ORR activities were evaluated using rotating disc electrode in a O₂ saturated 0.5 M H₂SO₄ aqueous solution (Fig. 3). As a result, a higher onset potential was observed for the composite having SWNT as a supporting material. We studied the mechanism of the higher ORR activity for SWNT.

[1] T. Fujigaya et al., *Chem. Commun.* 2011, 47, 6843.

Corresponding Author: Naotoshi Nakashima

E-mail: nakashima-tcm@mail.cstm.kyushu-u.ac.jp

Tel & Fax: +81-92-802-2842

Air-Stable High-Efficiency Nanotube-Si Heterojunction Solar Cells

○Kehang Cui¹, Olivier Reynaud², Takaaki Chiba¹, Erik Einarsson¹, Albert G. Nasibullin²,
Shohei Chiashi¹, Esko I. Kauppinen², Shigeo Maruyama¹

¹*Department of Mechanical Engineering, The University of Tokyo, Tokyo 113-8656, Japan*

²*Department of Applied Physics, Aalto University, Aalto FI-00076, Finland*

The present energy needs would be satisfied by only 0.1% coverage of the Earth's surface with 10%-efficiency solar cells [1]. Various efforts have been focused on the improving both the efficiency and stability of solar cells, among which, single-walled carbon nanotubes (SWNTs) with outstanding electronic and optical properties as well as chemical stability have drawn intensive attention. Here we present the air-stable SWNT-Si heterojunction solar cells with the efficiency exceeding 10%.

The SWNTs were synthesized by the thermal decomposition of ferrocene vapor in a carbon monoxide atmosphere [2], with the average diameter of approx. 2 nm. The SWNT films showed a sheet resistance of 117 Ω /sq. at the transmittance of 91% over the AM1.5G spectrum. The heterojunction solar cell was fabricated by dry depositing the SWNT film to the 3 mm by 3 mm n-type silicon substrate [3]. Our test result shows that the power conversion efficiency (PCE) of 10.12% is achieved, with short-circuit current, open-circuit voltage and fill factor of 30.9 mA/cm², 540 mV and 60%, respectively. The result was stable after three-week exposure in ambient condition. The Raman spectra demonstrate the pristine state of SWNTs.

Part of this work was financially supported by Grant-in-Aid for Scientific Research (22226006, 23760180, 23760179, 25630063). This work was also supported by the VLSI Design and Education Center (VDEC), The University of Tokyo, in collaboration with Cadence Corporation.

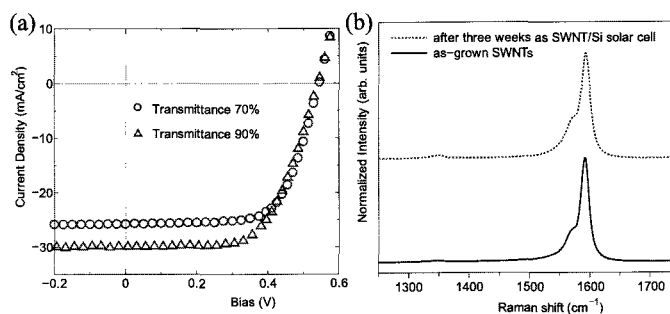


Fig.1 (a). Solar test under 100mA/cm² AM1.5G illumination.
(b) Raman spectra of as-grown SWNTs and after one month fabrication of solar cell.

[1] M. Grätzel. *Phil. Trans. R. Soc. B* **365**, 993 (2007).

[2] A. Kaskela et al. *Nano Lett.* **10**, 4349 (2010).

[3] K. Cui et al. submitted.

Corresponding Author: S. Maruyama

Tel: +81-3-5841-6408, Fax: +81-3-5841-6421, E-mail: maruyama@photon.t.u-tokyo.ac.jp

Influence of dispersion state of long SWCNTs on the electrical conductivity of composites

○Howon Yoon¹, Seisuke Ata^{1,2}, Takeo Yamada^{1,2}, Motoo Yumura^{1,2}, Kenji Hata^{1,2}

¹ *Technology Research Association for Single Wall Carbon Nanotubes (TASC), Tsukuba, Ibaraki, 305-8565, Japan*

² *Nanotube Research Center, National Institute of Advanced Industrial Science and Technology (AIST), Tsukuba, Ibaraki, 305-8565, Japan*

The superior mechanical, electrical, and thermal properties of CNTs and their high aspect ratio make an excellent filler material of them for advanced composites. Although the potential of CNTs is well-recognized, it is not easy to disperse them while retaining the intrinsic properties of the pristine CNTs. Therefore, ever-increasing interest in applying CNTs in many different fields has led to continued efforts to develop dispersion technique. In order to select a proper method for CNT dispersion, various types of dispersion methods should be evaluated and compared. However, most of studies have been focused on the optimum dispersion condition employing only one or two types of methods. It is still not established that which dispersion methods is appropriated for which kinds of CNTs.

Here, we focused primarily on the use of many types of dispersion methods, as a new approach for exploring the appropriated dispersion method of aligned long SWCNTs (length from 500 to 1,000 μm). We have compared three general classes of dispersion mechanisms, such as turbulent flow, cavitation, and mechanical force, which encompassed 11 different dispersion methods. From this work, we have found that the mechanism of turbulent flow showed unique and superior dispersion ability for long SWCNTs that was advantageous to make highly conductive rubber and polymer composites. The dispersed long SWCNTs by turbulent flow show the higher G/D ratio (Fig. 1a) in spite of the smaller particle size (Fig. 1b) than mechanical force. This result indicates that less damage was introduced on the SWCNTs during turbulent flow dispersion. In addition, turbulent flow method showed higher electrical conductivities than that for mechanical force (Fig. 1c), which was comparable at ~ 10 min dispersion, ~ 4 -times higher at its peak (60 min), and still ~ 4 -times higher when it dropped (120 min). We interpret that the biaxial shearing force caused an exfoliation effect to homogeneously disperse the long SWCNTs while suppressing damage.

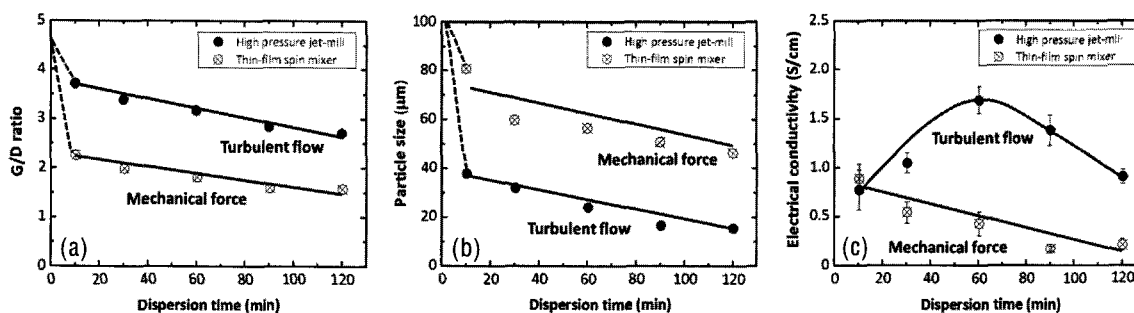


Fig. 1. (a) Particle size and (b) G/D ratio of long SWCNTs dispersed for different time. (c) Electrical conductivity of 1 wt% long SWCNT/fluorinated rubber composites.

Corresponding Author: K. Hata

Tel: +81-29-861-4654, Fax: +81-29-861-4851,

E-mail: kenji-hata@aist.go.jp

Fabrication and characterization of inverted-type organic thin-film solar cells using [60]fullerene-diamine assembly films

○Shoto Banya¹, Taisuke Matsumoto¹, Takeo Oku¹, Tsuyoshi Akiyama^{1*}

¹ Department of Materials Science, School of Engineering, The University of Shiga Prefecture, Hikone, Shiga 522-8533, Japan.

Fullerenes are highly attractive π -electron systems as electron acceptor and organic n-type semiconductor. Indeed, fullerenes are widely used for artificial photosynthetic models, organic solar cells, organic transistors and so on. Adjacent or aggregated fullerene structures are expected as efficient electron-transfer components; therefore, the development of a facile method for the preparation of fullerene aggregates is important for organic electronic materials.

In particular, formation of fullerenes thin films is basically important for their electronic applications. One of the simplest chemical modification methods for the preparation of fullerene derivatives is an addition reaction between fullerenes and amines.^[1,2] From these backgrounds, in this research, we investigated fabrication of multilayer films of C₆₀ fullerene on the surface of amino-substituted substrate using the addition reaction between fullerene-diamine.^[3] In addition, photoelectrochemical properties of the C₆₀ assembly films ([Assem-C₆₀]_n) demonstrates photovoltaic cells composed of [Assem-C₆₀]_n and poly(3-hexylthiophene) (P3HT), which n is the number of alternate immersions into the C₆₀ toluene solution. Schematic structure of the photovoltaic cells is shown in Figure 1.

Current density-voltage characteristic of photovoltaic cells using [Assem-C₆₀]_n is shown in Figure 2. The results strongly suggest that the fabricated [Assem-C₆₀]_n worked as an n-type semiconductor for P3HT. In the symposium, most recent developments and characteristics about C₆₀ assembly film materials will be presented.

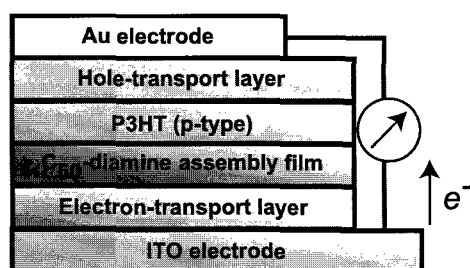


Figure 1. Device structure of the photovoltaic cell.

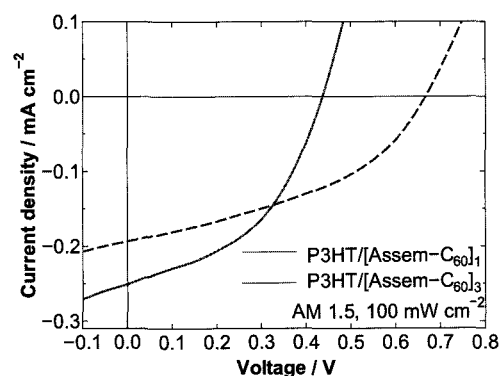


Figure 2. Current density-voltage characteristic of the photovoltaic cells using [Assem-C₆₀]_n.

[1] Matsuoka, K.-i.; Matsumura, S.; Akiyama, T.; Yamada, S., *Chem. Lett.*, **37**, 932–933 (2008).

[2] Matsuoka, K.-i.; Akiyama, T.; Yamada, S., *Langmuir*, **26**, 4274–4280 (2010).

[3] Banya, S.; Matsumoto, T.; Oku, T.; Akiyama, T., *J. Phys. Conf. Ser.*, **433**, 012007 (2013).

Corresponding Author:

E-Mail: akiyama.t@mat.usp.ac.jp, Tel : +81-749-28-8358, Fax : +81-749-28-8583

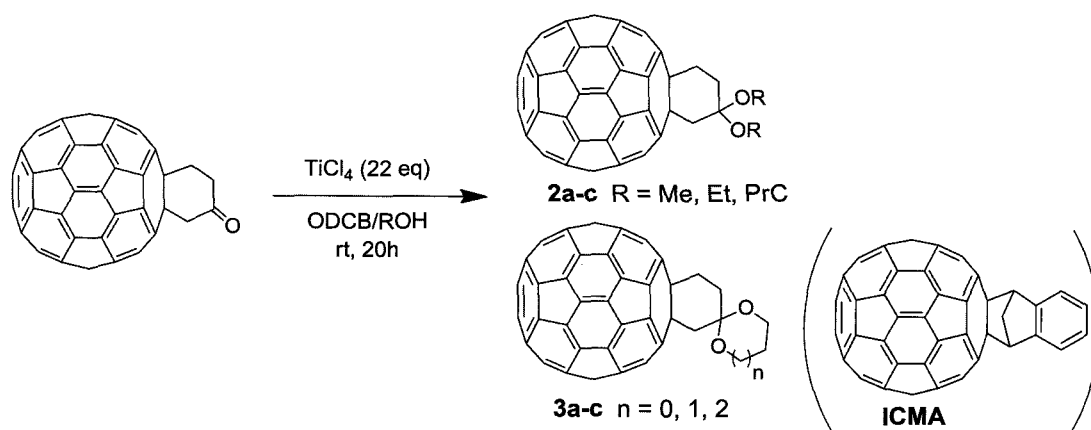
Synthesis and evaluation of spiro-acetalized [60]fullerenes toward organic photovoltaic devices

○Hiroyuki Masuda, Ken Kokubo, Naohiko Ikuma, Tsubasa Mikie,
Akinori Saeki, Shu Seki, Takumi Oshima

*Division of Applied Chemistry, Graduate School of Engineering, Osaka University,
2-1 Yamadaoka, Suita, Osaka 565-0871, Japan*

Chemical functionalization of fullerenes as n-type semiconductor materials in organic photovoltaic (OPV) devices has recently attracted much attention. Slightly higher LUMO energy level than that of C₆₀ and the improved solubility for co-mixing with p-type materials enable to improve the Photo Conversion Efficiency (PCE) depending on their structure.

As compared with the structure of representative n-type derivatives indene-C₆₀ monoadduct (ICMA) and bisadduct (ICBA), acetal group can be easily introduced by a simple nucleophilic attack of various alcohols to carbonyl group. In this study, we report a facile synthesis of new acetalized [60]fullerenes **2** and **3** by TiCl₄-mediated reaction of cyclohexanone-fused fullerene **1** with several alcohols as well as their thermal and electronic properties[1]. The evaluation of OPV device based on P3HT/ spiro-cyclic-acetalized fullerene **3b** showed PCE of 2.3%, while acyclic compounds **2a-c** did not.



[1] Kokubo, K. *et al.*, *Tetrahedron Lett.* 2013, *54*, 3510.

Corresponding Author: Ken Kokubo

TEL: +81-6-6879-4592, FAX: +81-6-6879-4593, E-mail: kokubo@chem.eng.osaka-u.ac.jp

Preparation and microscopic analysis of fullerene-diamine adducts as organic electronic material

○Yuji Ono, Tsuyoshi Akiyama, Takeo Oku

Department of Materials Science, School of Engineering, The University of Shiga prefecture, Hikone, Shiga 522-8533, Japan

Fullerene and its derivatives have been considered as a promising electron acceptor and n-type organic semiconductor. This has been demonstrated by photoinduced electron transfer systems, organic transistors, photoelectric conversion molecular based devices and so on. Intensive investigations have been made to explore functionalization of fullerenes. As one of the way to create organic electronic material based on the fullerene structure, assembling of fullerene have been attracted from various points of view.

From this background, we have focused on the C_{60} and diaminoethylene (DAE) adduct as an novel organic electronic material, which is obtained by the assembling of fullerene molecules via covalent bond formation between C_{60} and amino group. The shapes and properties of these microparticles were varied by the reaction conditions.

Control of the shapes and properties of the C_{60} -DAE seems to be basically important for optimization of the electronic properties of the adducts. Systematic investigation of the C_{60} -DAE preparation condition was performed. In the present work, possible mechanism of the C_{60} -DAE adduct formation will be discussed, which is based on the microscopic analysis of the adducts.

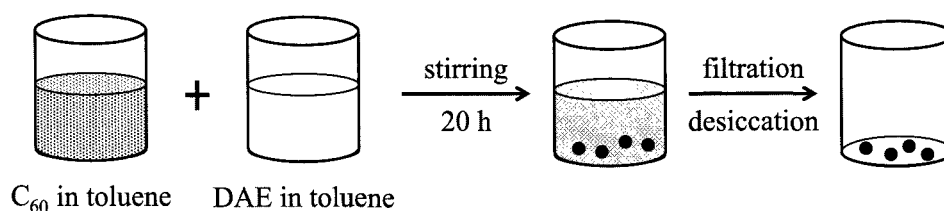


Fig.1. Synthesis of C_{60} -DAE microparticles.

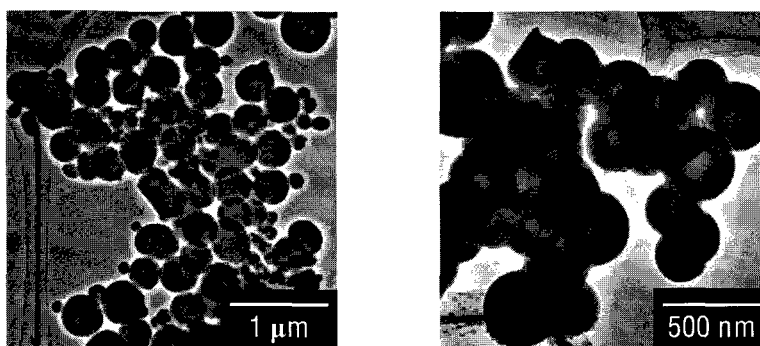


Fig.2. TEM images of C_{60} -DAE microparticles.

- [1] P. V. Kamat, S. Barazzouk, K. G. Thomas and S. Hotchandani, *J. Phys. Chem. B* 104, 4014 (2000).
- [2] S. Barazzouk, S. Hotchandani and P. V. Kamat, *Adv. Mater.* 13, 1614 (2001).
- [3] K. Matsuoka, H. Seo, T. Akiyama and S. Yamada, *Chem. Lett.* 36, 934 (2007).
- [4] K. Matsuoka, S. Matsumura, T. Akiyama and S. Yamada, *Chem. Lett.* 37, 932 (2008).
- [5] K. Matsuoka, T. Akiyama and S. Yamada, *Langmuir* 26, 4274 (2009).

Corresponding Author: T. Akiyama

Tel: +81-749-28-8358, Fax: +81-749-28-8583, E-mail: akiyama.t@mat.usp.ac.jp

Electrical transport properties of polymerized C₆₀ thin film using focused optical vortex

○Wataru Akiyama¹, Daiki Momiyama¹, Naoto Toriumi¹, Katsuhiko Miyamoto¹, Takashige Omatsu^{1,2}, Jonathan P. Bird³, Yuichi Ochiai¹, Nobuyuki Aoki^{1,4}

¹ Graduate School of Advanced Integration Science, Chiba University,
Chiba, 263-8522 Japan

² JST-CREST, 4-1-8 Honcho Kawaguchi, Saitama 332-0012, Japan

³ Department of Electrical Engineering, University at Buffalo, SUNY, Buffalo, NY
14260-1920, USA

⁴ JST-PREST, 4-1-8 Honcho Kawaguchi, Saitama 332-0012, Japan

Recently, a state of the art photo-polymerization of a C₆₀ thin film has been realized by irradiation of topological laser beam namely optical vortex (OV). Since the beam has a helical wavefront and a torque appears along the tangential direction, a confinement force can be expected along the peripheral direction of the beam and the polymerization takes a progress with a compressive photon-pressure under a high-beam-power density. Therefore, it can be expected to achieve a highly-packed and uniform photo-polymerization in a C₆₀ thin film. Moreover, combining with circular polarization, total angular momentum of light can be controlled [1].

In our study, thermally evaporated C₆₀ thin film was deposited 100 nm on a SiO₂ layer on top of a heavily doped Si substrate. A continuous-wave 532 nm laser beam was used for the optical source. The OV was produced by using a spiral phase plate and irradiated onto the sample through an objective lens. The photo-polymerization was done at high-vacuum condition.

We observed characteristics of a field effect transistor composed of a C₆₀ thin film polymerized by OV irradiation without exposing to the atmosphere. The currents at ON state decrease with increasing the dosage by successive irradiations. On the other hand, the threshold voltages is shifted in the positive direction under a dose of ~1 MJ/cm² however they begin to shift toward the negative direction over the critical dose value. The most negative threshold voltage, -5.8 V, was observed at a dose of 50 MJ/cm². The mechanism of the change of the characteristic will be discussed with results of the in-situ observation of the Raman scattering spectrum.

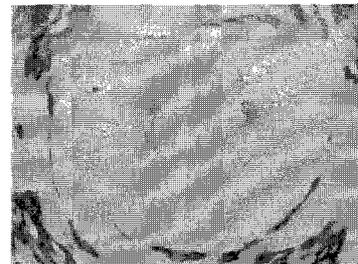


Fig. 1. Optical image of a C₆₀ thin film around electrodes after OV irradiation. Circular pattern reflects the beam profile.

[1] T. Omatsu *et al.*, Opt. Express 18 (2010) 17967.

[2] S. J. Duclos *et al.*, Solid State Commun. 80 (1991) 481.

Corresponding Author: N. Aoki

Tel: +81-43-290-3430, Fax: +81-43-290-3427,

E-mail: n-aoki@faculty.chiba-u.jp

Efficiency improvement of PTB7:PC₇₁BM organic solar cells by inserting LiF cathode buffer layer

○Shunjiro Fujii¹, Tatsuki Yanagidate², Masaya Ohzeki², Yuichiro Yanagi², Yuki Arai², Takanori Okukawa², Akira Yoshida², Takeshi Tanaka¹, Yasuhiro Nishioka², and Hiromichi Kataura¹

¹Nanosystem Research Institute, National Institute of Advanced Industrial Science and Technology (AIST), Ibaraki 305-8562, Japan

²Nihon University, Funabashi, Chiba 274-0851, Japan

Organic solar cells are of special interest owing to the advantages of low-cost and solution-processable fabrications. Recently, a bulk-heterojunction (BHJ) solar cell with a high power conversion efficiency (PCE) of 9.2% has been reported by using a benzodithiophene polymer of PTB7* and phenyl-C₇₁-butyric-acid-methyl-ester (PC₇₁BM) [1]. It is also known that insertion of a lithium fluoride (LiF) buffer layer between the active layer and the electrode effectively improves the efficiencies of the solar cells [2]. However, the effect of LiF buffer layer on the PCE and its stability of PTB7:PC₇₁BM solar cells have not been investigated.

In this work we fabricated PTB7:PC₇₁BM-based BHJ solar cells on a glass substrate using LiF as a cathode buffer layer (Figure 1). The PCE extracted from the current density-voltage curve (Figure 2) was increased from 2.1% to 3.6% by inserting the LiF layer. The stability of the PCE of the device with LiF was also improved (Figure 3). In this presentation, the detailed characteristics will be discussed.

*PTB7; poly[[4,8-bis[(2-ethylhexyl)oxy]benzo[1,2-b:4,5-b']dithiophene-2,6-diyl][3-fluoro-2-[(2-ethylhexyl)carbonyl]thieno[3,4-b]-thiophenediyl]

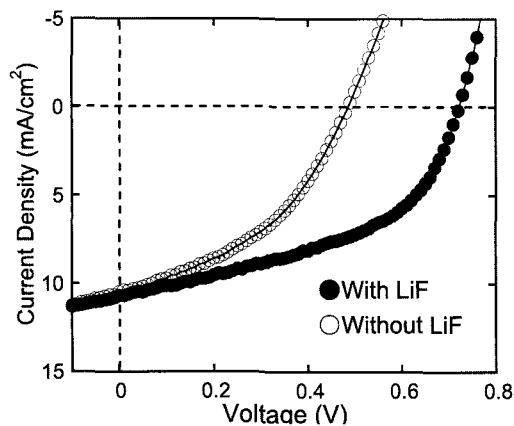
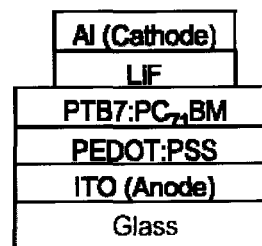


Figure 2 Relationships between the current density and the voltage of the solar cells under simulated AM 1.5 irradiation (100 mW/cm²) in air.

Figure 1 Schematic illustration of the solar cell.

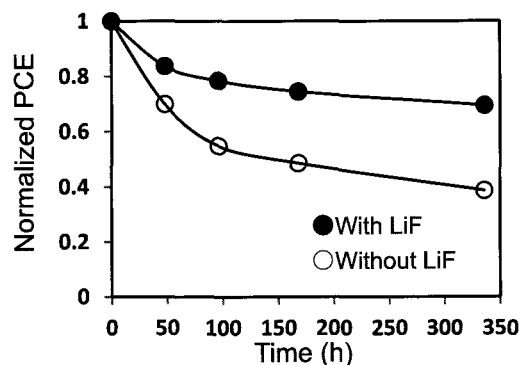


Figure 3 Normalized PCE as a function of time. The un-encapsulated devices were stored in vacuum and periodically tested in air.

[1] Z. C. He et al., Nat. Photonics, 6 (2012) 591

[2] S. E. Shaheen, et al., Appl. Phys. Lett., 13 (2001) 841

Corresponding Author: Hiromichi Kataura

E-mail: h-kataura@aist.go.jp

Energetics and Electronic Structure of C₆₀ doped Bulk Si

Susumu Okada

*Graduate school of Pure and Applied Sciences, University of Tsukuba, Tsukuba 305-8571,**Japan**Japan Science and Technology Agency, CREST, 7 Gobancho, Chiyoda-ku, Tokyo 102-0076,**Japan*

Vacancies in semiconductors are the subject of the cluster sciences as an inversion of the conventional semiconductor clusters. Many works showed that there is magic numbers and stable conformation of vacancies (V_n) those are determined by their electronic structure and strain energy as in the case of usual clusters. Furthermore, the electronic structures of the vacancies strongly depends on their detailed atomic arrangements of the vacancies. In the technological view, the vacancies in semiconductors can be applicable for the semiconductor electronic devices. In the devices, atom-scale control of size and morphologies of vacancies are desired. For such purposes, recently, experimental works reported interesting hybrid structures consisting of vacancies in conventional semiconductors and C₆₀. In the hybrid structure, C₆₀ is expected to control the size and morphology of vacancies due to its spherical cage structure of sp² C atoms with 1 nm diameter. However, the detailed geometric and electronic structures of such hybrid structure are still unknown. In the present work, we studied the geometric and electronic structures of C₆₀ doped bulk Si by performing the first-principle total energy calculation based on density functional theory. Our calculations showed the optimum size and geometry of the vacancies for C₆₀ incorporation. Electronic properties of the hybrid structure will be discussed.

Corresponding Author: Susumu Okada

E-mail: sokada@comas.frsc.tsukuba.ac.jp

FAX: +81-2-9853-5924

Synthesis and Characterization of Fullerene Derivatives with a Thiophene Moiety in Organic Photovoltaic Devices†

○Tatsuya Hayashi¹, Jaebuem Oh², Haeseong Lee^{2,3}, Jong Jun Ann³, Hee Jae Lee⁴, Jin Jang⁴, Chyongjin Pac^{1,5}, and Hiroshi Moriyama¹

¹Department of Chemistry, Toho University, Miyama 2-2-1, Funabashi 274-8510, Japan

²TAKOMA Technology Co., Ltd., Nosung-myeon, Nonsan-city, Chungnam 320-922, Korea

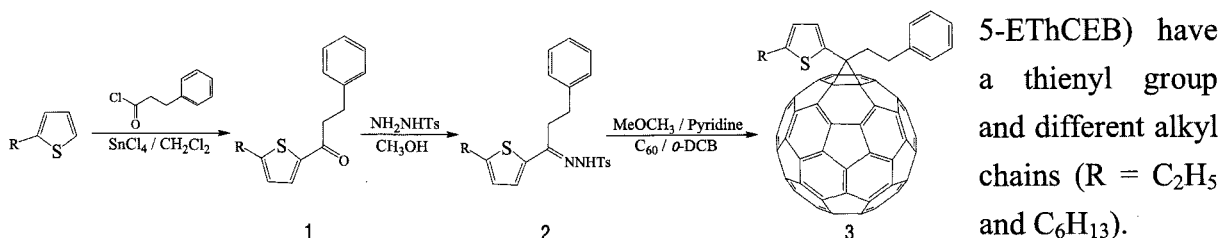
³Department of Advanced Materials Jeonju University, Wansangu Jeonju 560-759, Korea

⁴Department of Information Display, Kyung Hee University, Dongdaemun-ku, Seoul 130-171, Korea

⁵Department of Materials Chemistry, Korea University, Sejong Jochiwon, Chung-Nam 339-700, Korea

Bulk heterojunction (BHJ)-type organic photovoltaic (OPV) cells have attracted significant attention for next-generation solar cells because of their light weight, solution process construction and flexibility. One of the most representative OPVs is the device based on a blend of poly(3-hexyl thiophene) (P3HT) as an electron donor and a C₆₀ derivative, [6,6]phenyl-C₆₁-butyric acid methyl ester (PCBM), as an electron acceptor.

In this study, we synthesized a new series of fullerene derivatives with a thienyl group that has potential affinity with the P3HT donor. The synthetic scheme for these fullerene derivatives is based on that of PCBM [1], as shown below. The two fullerene derivatives (5-HThCEB,



We fabricated OPV cells using P3HT as the donor and the newly designed fullerene derivatives as the acceptor. The performance of the novel fullerene derivatives was found to be lower than that of PCBM, although the V_{OC} of **3** is slightly higher than that of PCBM. The electron-donating property of thiophene might be assumed to increase V_{OC} .

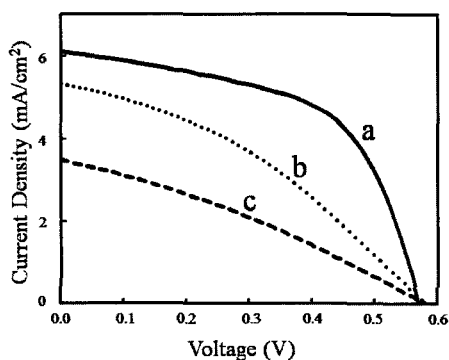


Figure 1. J - V characteristics of the devices fabricated with P3HT and the new C₆₀ derivatives.

Table 1. Photovoltaic parameters using the new C₆₀ derivatives.

		J_{SC} (mA/cm ²)	V_{OC} (V)	FF (%)	PCE (%)
PCBM	(a)	6.10	0.571	56.1	1.95
5-HThCEB	(b)	5.32	0.583	36.0	1.12
5-EThCEB	(c)	3.49	0.583	31.0	0.63

[1] J. C. Hummelen, B. W. Knight, F. LePeq, F. Wudl, J. Yao, C. L. Wilkins, *J. Org. Chem.* 1995, *60*, 532–538.

† This work is supported by Bilateral International Collaborative R&D Program (Project number: G1-2009-CL-OT-0058, Ministry of Knowledge Economy, Republic of Korea and a MEXT-Supported Program for the Strategic Research Foundation at Private Universities, Japan.

Structural Effect of Fullerene Derivatives with a Cyano Group in Organic Photovoltaic Devices[†]

○Kana Matsumoto¹, Jaebuem Oh², Haeseong Lee^{2,3}, Jong Jun Ann³, Hee Jae Lee⁴,
Jin Jang⁴, Chyongjin Pac^{1,5}, and Hiroshi Moriyama¹

¹ Department of Chemistry, Toho University, Miyama 2-2-1, Funabashi 274-8510, Japan,

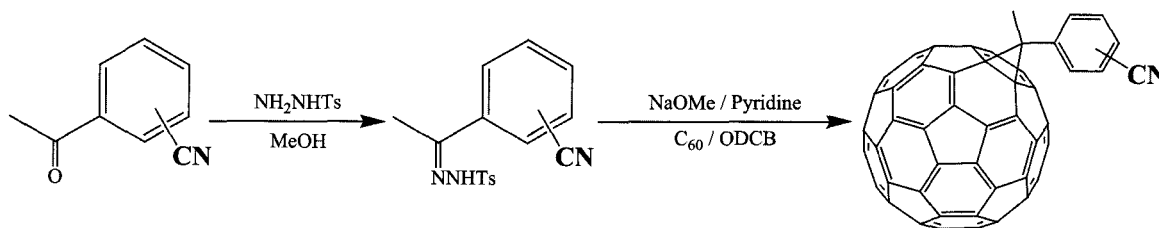
² TAKOMA Technology Co., Ltd., Nosung-myeon, Nonsan-city, Chungnam 320-922, Korea,

³ Department of Advanced Materials Jeonju Univ. Wansang Jeonju 560-759, Korea,

⁴ Department of Information Display, Kyung Hee University, Dongdaemun-ku Seoul 130-171, Korea,

⁵ Department of Materials Chemistry, Korea University, Sejong Jochiwon Chung-Nam 339-700, Korea,

Organic photovoltaic devices (OPVs) have attracted attention because of low cost, light weight, the advantages of easy fabrication and the possibility to fabricate flexible devices in comparison with conventional inorganic semiconductor photovoltaic devices. OPVs are commonly composed of a photoactive blend film (Bulk heterojunction; BHJ) of a conjugated polymer donor and a soluble fullerene derivative acceptor sandwiched between a PEDOT:PSS-coated ITO positive electrode and a low-work-function metal negative electrode. In the BHJs of the photoactive blend film, the polymer electron donor and the fullerene electron acceptor materials form an interpenetrating network to optimize the exciton dissociation and charge transport.



Scheme

In this study, we synthesized three PCBM [1]-like C₆₀ derivatives, (*p*-MCPN, *m*-MCPN, *o*-MCPN), by adding a cyano group to the phenyl ring in different positions. The derivatives with a cyano group have high solubility, facilitating the synthesis and purification. In addition, a cyano group on the phenyl ring should be in close proximity to the fullerene cage when connected to the 2-position of the phenyl ring (*o*-MCPN). A possible direct through-space effect between the cyano group and the carbon cage can be expected. We tested OPVs with the new fullerene electron-acceptor materials. The V_{OC} , J_{SC} and PCE of the OPVs based on P3HT/*p*-MCPN were found to be 0.48 V, 5.61 mA cm⁻² and 1.57%, respectively. The OPVs based on P3HT/*p*-MCPN show poorer photovoltaic performance than that of the OPVs using PCBM as acceptors.

[1] J. C. Hummelen, B. W. Knight, F. LePeq, F. Wudl, J. Yao, C. L. Wilkins, *J. Org. Chem.* **1995**, *60*, 532–538.

[†] This work is supported by Bilateral International Collaborative R&D Program (Project number: GF2009-CL-OT-0058, Ministry of Knowledge Economy, Republic of Korea and a MEXT-Supported Program for the Strategic Research Foundation at Private Universities, Japan.

Corresponding Author : Hiroshi Moriyama

TEL: +81-47-472-1211, FAX: +81-47-476-9449, E-mail: moriyama@chem.sci.toho-u.ac.jp

Controlling the number of layers of graphene by binary metal catalyst

○Yuichiro Takesaki¹, Masaharu Tsuji^{1,2}, Hiroki Ago^{*,1,2}

¹ Graduate School of Engineering Sciences, Kyushu University, Fukuoka 816-8580

² Institute for Materials Chemistry and Engineering, Kyushu University, Fukuoka 816-8580

For electronic applications of graphene, it is essential to control the number of layers. Double-layer graphene is useful for field-effect transistors, as the band gap can be opened by applying a vertical electric field [1]. Three- and four-layer graphene is useful for transparent electrodes and touch panels, because multi-layers can significantly reduce the sheet resistivity while maintaining high optical transparency [2]. In spite of the importance of controlling the number of layers, few studies have been reported on the chemical vapor deposition (CVD) growth of graphene with controlled layer numbers [3-5].

Here, we demonstrate the graphene growth by ambient-pressure CVD using two types of metal catalysts, Ni and Cu, with different carbon solubilities. The [Ni]/[Cu] ratio was systematically investigated by the successive sputtering onto c-plane sapphire, and graphene was grown at 1000 °C with CH₄ feedstock. We found that the crystallinity of the bimetal catalyst and the quality of graphene are strongly dependent on the order of metal deposition. The Cu-on-Ni film (Cu/Ni/sapphire) showed more flat metal surface than Ni-on-Cu film (Ni/Cu/sapphire), and the former gave graphene with much higher quality than the latter. Furthermore, a clear dependence of the [Ni]/[Cu] ratio on graphene's layer number was observed. For the low Ni concentration, below 10%, single-layer graphene covered the metal surface (Fig. 1(a)). Increase of the Ni concentration assists double-layer growth, and the 30% Ni produces a double-layer film with 80% coverage (Fig. 1(b)). When we increased the Ni ratio up to 40%, three-layer graphene was formed together with complete coverage of double-layer (Fig. 1(c)). We think that the diffusion of Ni atoms into the Cu film increases the carbon solubility, resulting in the increase of the layer number. This work is expected to contribute to future development of graphene-based electronic devices.

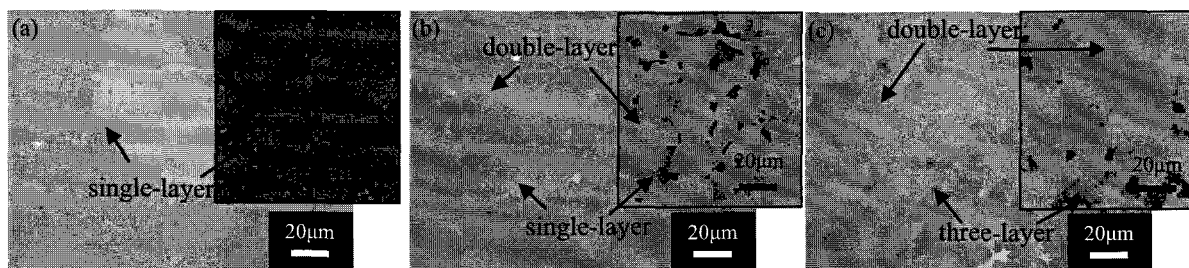


Fig. 1 Optical microscope images of transferred graphene grown on Cu/Ni catalyst with (a) Ni 10%, (b) Ni 20%, (c) Ni 30% concentrations. Insets show the distribution of the layer number determined from color contrast of the microscope images.

[1] Y. Zhang *et al.*, *Nature*, 459, 820 (2009). [2] T. H. Han *et al.*, *Nat. Photon.*, b, 105 (2012).

[3] Y. Wu *et al.*, *ACS Nano*, 6, 7731 (2012). [4] X. Liu *et al.*, *J. Phys. Chem. C*, 115, 11976 (2011).

[5] Z. Sun *et al.*, *ACS Nano*, 6, 9790 (2012).

Corresponding Author: Hiroki Ago, Tel&Fax: +81-92-583-7817, E-mail: ago@cm.kyushu-u.ac.jp

Direct Growth of Graphene on Insulating Substrates by Annealing of Amorphous Carbon

○Yohei Hasebe, Hitoshi Nakahara, Koji Asaka, and Yahachi Saito

Department of Quantum Engineering, Nagoya University, Nagoya 464-8603, Japan

Chemical vapor deposition (CVD) has been intensively investigated as an efficient method of synthesizing graphene films. However, graphene films grown by CVD must be transferred from metal substrates to insulating ones for their applications to electronic devices. The transfer processes are complicated and chemical adsorptions, contaminations and cracks often remain in the graphene. Therefore, transfer-free processes are desired for the fabrication of electronic devices. In this study, an amorphous carbon (a-C) layer was sandwiched between an iron (Fe) layer and SiO₂/Si substrate, and then graphene layers were synthesized on SiO₂ directly by annealing.

As shown in Figure 1(a), films with Fe (60 nm) / a-C (10 nm) / SiO₂ (30 nm) / Si were prepared by electron-beam deposition. The films were annealed at 950 °C for 30 min to graphitize (Fig. 1(b)). After annealing, the films were investigated by cross-sectional transmission electron microscopy (TEM) and Raman spectroscopy.

Figure 2 shows a cross-sectional TEM image of the film after annealing. Multilayer graphene was formed at the interface between Fe and SiO₂ layers. The above-mentioned result suggests that graphene layers grew up on SiO₂ directly.

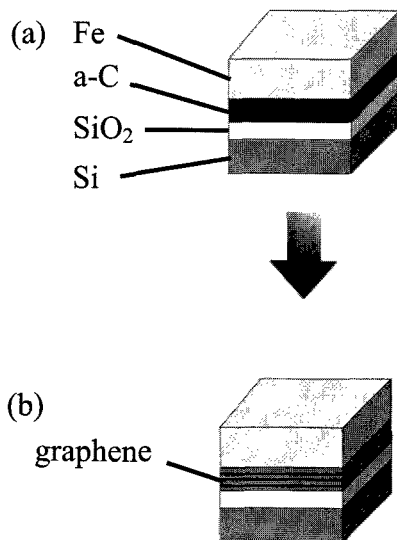


Fig. 1. (a) SiO₂, a-C and Fe layers are deposited on a Si by electron-beam deposition. (b) The films are annealed to graphitize.

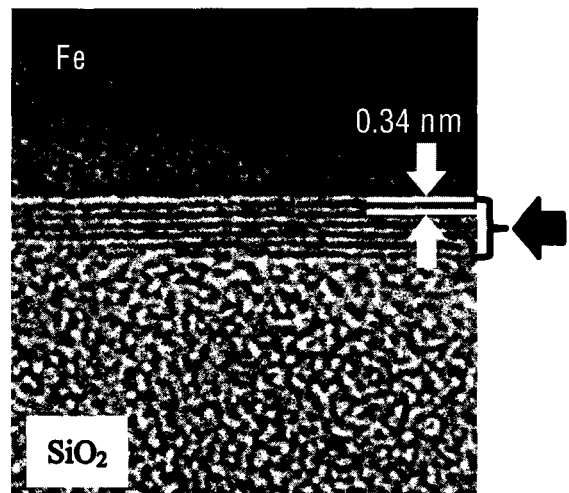


Fig. 2. Cross-sectional TEM image of the interface between Fe and SiO₂ layers. Multilayer graphene is indicated by an arrow.

Corresponding Author: Y. Hasebe

Tel&Fax&E-mail: +81-52-789-3714, +81-52-789-3703, hasebe@surf.nuqe.nagoya-u.ac.jp

Shape-controlled synthesis of graphene and h-BN heterostructures

○Eriko Maeda, Yasumitsu Miyata, Ryo Kitaura, and Hisanori Shinohara*

Department of Chemistry & Institute for Advanced Research, Nagoya University, Nagoya

Atomic-layer lateral heterostructures of graphene and hexagonal boron nitride (hBN) have attracted much attention because of their unique interface-originated properties as well as applications in electronics. Recently, the synthesis of in-plane heterostructures has been reported by several groups including the present authors [1-3]. These works demonstrate that firstly-grown graphene can behave as a nucleation site of secondary-grown hBN in a successive chemical vapor deposition (CVD) [1].

Here, we report our recent progresses in the shape-controlled growth of graphene/hBN heterostructure. Individual grains of single-layer graphene are first grown from methane on a copper foil, and then the graphene is etched under hydrogen atmosphere to enhance the hBN growth. Besides, ribbon-shape graphene is formed from firstly-grown hBN grain edges. The samples obtained are characterized by using optical imaging, scanning and transmission electron microscope observations, and electrostatic force microscopy. As shown in Fig.1, we have obtained various heterostructures including hexagonal-shape hBN grains in graphene (Fig.1a,b) and graphene nanoribbons around hBN grains. In the presentation, the detail of graphene/hBN interface structure will be discussed.

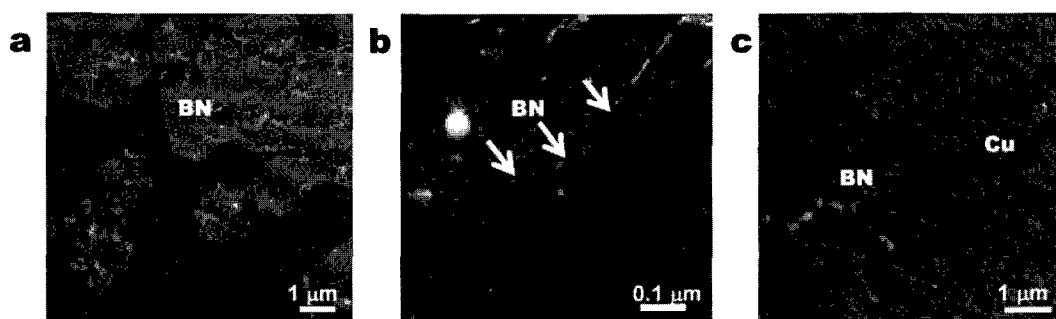


Fig.1 (a) SEM image of hexagonal-shape hBN grains formed in graphene. (b) Dark-field TEM image of hBN/graphene interface. (c) SEM image of graphene nanoribbons grown from hBN edges.

[1] Y. Miyata et al. Appl. Phys. Express 5 (2012) 085102.,

[2] M. Levendorf et al. Nature, 488 (2012) 627., [3] P. Sutter et al. Nano Lett., 12 (2012) 4869.

Corresponding Authors: Yasumitsu Miyata, Hisanori Shinohara

Tel: 052-789-2482, Fax: 052-747-6442, E-mail: ymiyata@tmu.ac.jp, noris@nagoya-u.jp

Decreasing growth rate of graphene layers on graphene nanoribbons

^oH. Kitakawa¹, R. Negishi¹, H. Tanaka², M. Fukumori², T. Ogawa², Y. Kobayashi¹

¹Department of applied physics, Osaka University, 2-1 Yamadaoka Suita 565-0871, Japan

²Department of Chemistry, Osaka University, 1-1 Matikaneyama-cho, Toyonaka 560-0043, Japan

Nanometer-width graphene nanoribbons (GNRs) have recently attracted considerable attention because the energy gap is created by the width direction confinement [1]. However, the electrical properties of field effect transistors (FETs) using monolayer GNR channel have the problem of a low on-current due to its nanometer-width channel. On the other hand, theoretical calculation predicts that the multilayer GNRs with weak interlayer coupling is the best candidates for channel materials in high-performance graphene-based FETs because of the increasing on-current due to the multi-channel [2]. Moreover, the weak interlayer coupling leads the carrier transport properties of the multilayer GNRs behave as if monolayer GNR. In the present work, we report that the multilayer GNRs are synthesized by the growth of graphene layers on the GNR as template using alcohol chemical vapor deposition (CVD).

GNRs as the growth template were obtained from unzipping of carbon nanotubes [1]. Graphene layers were grown by CVD using a furnace with three temperature zones, in which temperatures for carbon feedstock decomposition and graphene growth can be controlled individually[3]. The temperatures used in the experiments were 900 °C and 720-735 °C for thermal decomposition and graphene growth, respectively. After the growth, the film thickness of the grown graphene was evaluated by atomic force microscopy (AFM).

Figure 1 shows the AFM images obtained from the GNR (a) before and (b) after growth. Before the growth, the layer numbers of the GNR estimated from the AFM image is mono or bilayer [1]. The most remarkable feature is that the height of the GNR increases from ~ 1.2 to ~ 2.0 nm after CVD growth. This result indicates that the multilayer GNR with 4 ~ 5 layers is formed by the CVD growth. Figure 2 shows the growth thickness of graphene layers on the GNR and the mechanically exfoliated graphene flake (MEG) as a comparison. Note that the growth thickness of graphene layers on the GNR is thinner than that on the MEG. In previous work [4], we observed that the growth thickness of graphene layers on the MEG is independent of the sizes in the range from $0.5 \sim 50 \mu\text{m}^2$, and this means that the graphene layers on the MEG grow by the multiple nucleation. However, the growth rate of the graphene layer on the GNR is obviously slower than that on the MEG. The possible reasons are as follows: (1) the nucleation process changes from multiple to single because the size of GNR is extremely small ($\sim 0.01 \mu\text{m}^2$) in comparison to the MEG, and/or (2) the lateral growth from the GNR edge site restricts the growth rate of graphene layers because the area ratio of the edge site to GNR is extremely high. More works are necessary for elucidation of the growth mechanism of the multilayer GNRs to control the layer number and structure.

Acknowledgement: Authors would like to thank prof. K. Matsumoto (Osaka Univ.) for supporting AFM measurements. [1] X. Li, et al., Science 319 (2008)1229. [2] Y. Ouyang, et al., Nano Research 3 (2010)8. [3] R. Negishi, et al., Thin Solid Films 519 (2011)6447. [4] R. Negishi, et al., The 39th FNTG (2010). Corresponding Author: E-mail: kitakawa@ap.eng.osaka-u.ac.jp

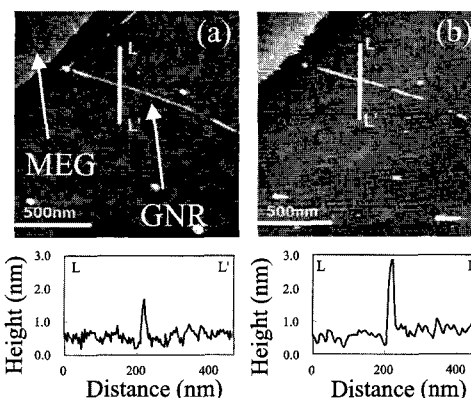


Fig.1 AFM images of GNR and MEG (a) before growth and (b) after growth.

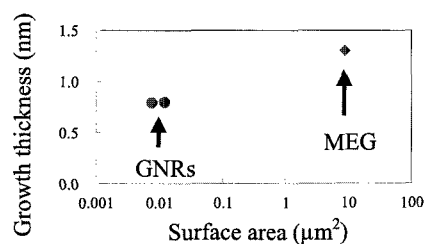


Fig.2 Growth thickness of the graphene layers on the GNR and MEG.

Growth mechanism for graphene and graphene nanoribbon under rapid-heating plasma CVD

○Hiroo Suzuki, Toshiaki Kato and Toshiro Kaneko

Department of Electronic Engineering, Tohoku University, Sendai 980-8579, Japan

Graphene is a monolayer carbon sheet including high carrier mobility, flexibility, and high optical transmittance. These properties are advantageous if graphene is to be used as a component in electrical devices such as field effect transistors, solar cells, and various gas and chemical sensors. Chemical vapor deposition (CVD) is one of the most promising methods of growing graphene, which can produce large, relatively high-quality graphene sheets. However, the graphene growth by CVD is limited only to the metal catalyst surfaces such as Ni, Cu, or Co, which is one of the most serious problems for the practical application of graphene as electronic devices. Thus, the development of the method for the direct growth of graphene on the insulating substrate, especially on a SiO₂ substrate, is highly required.

Recently, we have established a novel, simple, and scalable method for the direct growth of graphene on the insulating substrate by rapid-heating plasma CVD (RH-PCVD). It is revealed that by adjusting the growth parameters, the graphene layer can be grown along the interface of the Ni layer and the SiO₂ substrate instead of on top of the Ni layer. After removing the top Ni layer, high-quality single- or few-layer graphene sheets are found to be directly grown on the entire substrate area in large scale. Interestingly, at the initial growth stage, the hexagonal domain structure of graphene can be observed in our method (Fig.1) [1]. We have also realized the site- and alignment-controlled growth of graphene nanoribbon with Ni nanobar as a catalyst in RH-PCVD [2]. Since graphene nanoribbon can be directly grown between source and drain electrodes on the SiO₂ substrate, graphene nanoribbon grown by our method can be directly used as a conductive channel of field effect transistors. Actually, high-performance graphene nanoribbon transistors (on/off ratio > 10⁴) has been demonstrated [2].

In this study, the growth kinetics of graphene and graphene nanoribbon under RH-PCVD is systematically investigated by adjusting the growth parameters such as growth temperature, Ni structures, gas pressure, mixture gas ratio of methane to hydrogen, heating speed, plasma generation power, plasma irradiation time, and so on. It is found that the combination of growth temperature, initial Ni structures (film thickness and/or nanobar width), and plasma irradiation time is very important to realize growth of graphene and graphene nanoribbon with RH-PCVD.

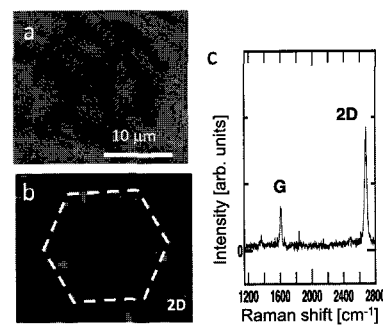


Fig. 1: (a) Scanning electron microscope, (b) 2D Raman peak mapping, and (c) raw Raman scattering spectrum of high quality graphene directly grown on SiO₂ substrate by RH-PCVD.

[1] T. Kato and R. Hatakeyama, *ACS Nano* 6, 8508 (2012).

[2] T. Kato and R. Hatakeyama, *Nature Nanotechnology* 7, 651 (2012).

Corresponding Author: H. Suzuki

Tel: 022-795-7046, Fax: 022-263-9225,

E-mail: suzuki12@ecei.tohoku.ac.jp

The effect of adding N-containing compounds on the eDIPS-CVD synthesis of SWCNTs

○Shigekazu Ohmori¹, Masaharu Kiyomiya¹, Takayoshi Hirai¹, Yuki Kuwahara^{1,2}, Takeshi Saito^{1,2}

¹ *Technology Research Association for Single Wall Carbon Nanotubes (TASC), Tsukuba 305-8562, Japan*

² *National Institute of Advanced Industrial Science and Technology (AIST), Tsukuba 305-8562, Japan*

Single-wall carbon nanotube (SWCNT) has potential for the application in printed electronics in terms of their unique electronic properties as well as chemical robustness. In the application for SWCNT transistors, the fineness of tube diameter is important, because the thinner diameter brings the larger band gap to SWCNTs. We have developed an efficient floating-catalyst chemical vapor deposition (CVD) method named the enhanced direct injection pyrolytic synthesis (eDIPS) with precise diameter controllability within 1–2 nm [1].

Recently, it has been reported that the adoption of N(nitrogen atom)-containing compounds results in the narrower SWCNT production in the substrate-type CVD synthesis [2]. The mechanism was suspected that nitrogen atoms would be absorbed and strongly bind to the surface of Cobalt nanoparticles and make frustration for producing wall of nanotubes. Similar narrowing effect was also reported on the floating catalyst technique using carbon mono-oxide as a carbon source, however the detail of the thinning mechanism was not discussed [3]. Although the modulation of the catalyst activity by adding N-containing compounds is proposed as the origin of the narrowing effect, the detailed mechanism is still an open question.

In this work, we have investigated the effect of adding N-containing compounds into the feedstock in the eDIPS method. As a result, the variety in terms of the diameter distribution, yield, and optimum thermal condition in the CVD reaction has been observed according to the molecular structure of N-containing compounds. For example, in the case of using pyrazine as a N-containing compound, slight narrowing effect in the diameter of grown SWCNTs was observed by Raman scattering spectroscopy measurements. Furthermore, although the yield was decreased comparing with that obtained without the addition of pyrazine, the same quality of SWCNTs (G/D ratio and impurity level) was confirmed. On the other hand, replacing thiophene molecule, which is commonly used as a promoter in eDIPS method, to thiazole or 1,3-benzothiazole causes broadened diameter distribution rather than thinning. These results might contradict the suggested simple mechanism for the effect of N-containing compounds in the CVD production of SWCNTs. This work has been supported by NEDO.

[1] T. Saito *et al.* *J. Nanosci. Nanotechnol.* 8 6153 (2008).

[2] T. Thurakitseree, *et al.* *ACS nano.* 7 2205 (2013).

[3] T. Susi *et al.* *Chem. Mater.* 23 2201 (2011).

Corresponding Author: T. Saito

Tel: +81-29-861-4863, Fax: +81-29-861-4413,

E-mail: takeshi-saito@aist.go.jp

Preparation and structural properties of BN-doped carbon nanohorn aggregates

○Ryota Yuge¹, Takashi Manako¹, Shunji Bandow⁴, Masako Yudasaka², Kiyohiko Toyama¹, Takashi Yamaguchi³, Sumio Iijima⁵, and Kentaro Nakahara¹

¹ *Smart Energy Research Laboratories, NEC Corporation, Tsukuba 305-8501, Japan*

² *Nanotube Research Center, National Institute of Advanced Science and Technology (AIST), Tsukuba, 305-8565, Japan*

³ *Institute for Advanced Research, Nagoya University, Nagoya, 464-8602, Japan*

⁴ *Department of Applied Chemistry, Meijo University, Nagoya 468-8502, Japan*

⁵ *Faculty of Science Technology, Meijo University, Nagoya 468-8502, Japan*

Single-wall carbon nanohorns (SWNHs) [1] are a kind of nano-carbon materials such as carbon nanotubes, and graphenes, which are attractive due to their excellent properties of their composites with metal nanoparticles [2]. Recently, it has been reported that non-metallic nitrogen-doped carbon nanotubes have the intrinsic catalytic properties for oxygen reduction reaction (ORR) [3]. This achieves not only the potentially low cost as they are noble metal free but also their better stability toward CO poisoning compared to traditional platinum catalysts [3]. Here, we tried binary doping of heteroatoms such as nitrogen and/or boron in SWNHs to extend their application possibility.

SWNHs were prepared by the CO₂ laser ablation, which was operated at 3.5 kW at room temperature. The graphite target with or without boron was used. The buffer gases were Ar and N₂. The gas flow rate and pressure were 10 L/min and 760 Torr, respectively. The boron-, nitrogen, and boron/nitrogen-implanted SWNHs are denoted as B-, N-, and BN-SWNHs, respectively.

Shapes of B-SWNHs, N-SWNHs, and BN-SWNHs observed by a scanning electron microscopy and scanning transmission electron microscopy were almost the same. Although the obtained SWNHs were mainly dahlia type, the petal-type structure has also been contained for B- and BN-SWNHs. This tendency did not depend on the buffer gas types. From Raman spectra and X-ray photoelectron spectroscopy results, we found that the nitrogen, boron, and BN atoms were incorporated in the graphene networks and B- and BN-SWNHs behaved as P-type dopants. The details are shown in the presentation.

[1] S. Iijima *et al.* Chem. Phys. Lett. 309, 165 (1999).

[2] T. Yoshitake *et al.* Physica B 323, 124 (2002).

[3] K. Gong *et al.* Science 323, 760 (2009).

Corresponding Author: R. Yuge

Tel: +81-29-850-1566, Fax: +81-29-856-6137

E-mail: r-yuge@bk.jp.nec.com

Dynamic whole-body imaging of radiolabelled carbon nanohorns in mice

○Minfang Zhang¹, Dhifaf Jasim², Antonio Nunes², Cécilia Ménard-Moyon³, Alberto Bianco³, Sumio Iijima¹, Masako Yudasaka^{1*}, Kostas Kostarelos^{2*}

¹ Nanotube Research Center, AIST, Tsukuba 305-8565, Japan

² Nanomedicine Laboratory, UCL School of Pharmacy, University College London, Brunswick Square, London WC1N 1AX, United Kingdom

³ Institute of Molecular and Cellular Biology, CNRS, 67000 Strasbourg, France

For future practical uses of carbon nanohorns (CNHs) in the field of nanomedicine as well as for safety assessment, clarification of their kinetic biodistribution in living animals is an important issue. Recently, we have quantitatively-analyzed the biodistribution of CNHs in mice by using Gd-labels through ICP measurement. This method is invasive, including body dissection and tissue extraction. In order to perform detailed studies to reveal the tissue distribution kinetics of CNHs, non-invasive visualization of CNHs in the living body is required. To do that, we performed single photon emission tomography (SPECT) imaging of CNHs conjugated with ¹¹¹In.

Oxidized CNHs were reacted with amino diethylenetriaminepentaacetic acid (NH₂-DTPA) to allow chelation of the ¹¹¹In. The obtained [¹¹¹In]DTPA-CNHS were intravenously administered in mice by tail vein injection. At 0.5-48 hr post-injection, the whole body imaging was obtained with SPECT/CT (Figure 1), in which the CNH distribution kinetics were clearly visible.

In addition, [¹¹¹In]DTPA-CNHS in each organ and blood were quantified, showing accumulation of CNHs in liver and spleen and short retention period in blood vessels, less than one hour. These tendencies were similar to those of the Gd-CNHS coated with glucose [1] but not to those coated with DSPE-PEG that showed the longer retention period in blood (ca. 6 h) [2]. The tissue distribution and accumulation of CNHs is expected to play a role in determining their overall safety profile.

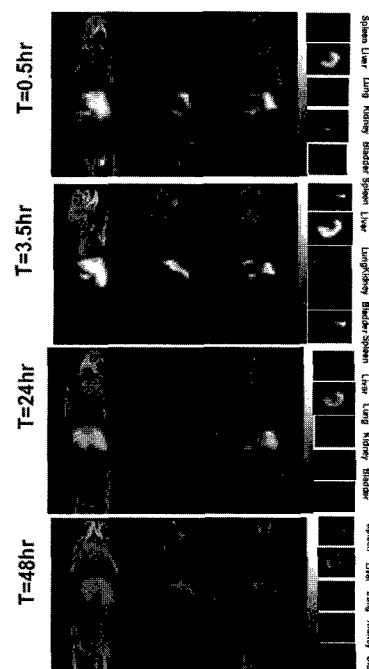


Figure 1. Whole-body SPECT/CT imaging of [¹¹¹In]-DTPA-CNHS after i.v. injection in mice.

[1] J. Miyawaki *et al.* ACS Nano, 3, 1399(2009).

[2] M. Zhang *et al.* Adv. Healthcare Mat. (2013), in press.

Corresponding Authors: K. Kostarelos, M. Yudasaka

E-mail: k.kostarelos@ucl.ac.uk, m-yudasaka@aist.go.jp

Electrical resistance measurement of single carbon nanocoil

○Ryuji Kunimoto¹, Taiichiro Yonemura¹, Yoshiyuki Suda¹, Hideto Tanoue¹, Hirofumi Takikawa¹, Hitoshi Ue², Kazuki Shimizu³, Yoshito Umeda⁴

¹ Department of Electrical and Electronic Information Engineering, Toyohashi University of Technology, Toyohashi 441-8580, Japan

² Fuji Research Laboratory, Tokai Carbon Co., Ltd., Oyama 410-1431, Japan

³ Development Department, Shonan Plastic Mfg. Co., Ltd., Hiratsuka 254-0807, Japan

⁴ Toho Gas Co., Ltd., Tokai, Aichi 476-8501, Japan

Carbon nanocoil (CNC) is a fibroid nanocarbon material that has a helical structure. CNC is predicted to have a high mechanical strength^[1], and we focus on the elongation behavior of CNC. The purpose of this study is to measure the electrical resistance of CNC when it is elongated under a tensile load. CNC was synthesized in our laboratory by chemical vapor deposition^[2]. Fig. 1 shows a schematic of measurement system used in this study. We have fixed the end of CNC to Au film on SiO₂/Si substrate using focused ion beam (FIB). Silver paste was used to bond the Au film with a stage of SEM. The stage of SEM was connected to the manipulator tip through a source meter. We approached the manipulator tip to the CNC and measured the electrical resistance of CNC.

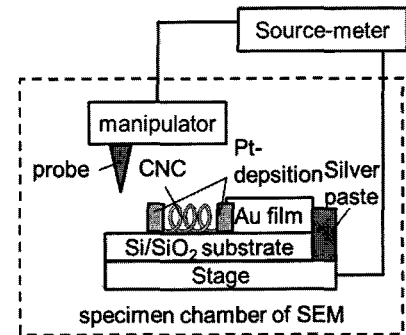


Fig. 1 Schematics of the measurement systems

Table 1 shows the measurement results of CNC electrical resistances. It was shown that the average electrical resistivity of CNC is about $4.28 \times 10^{-2} [\Omega / \text{cm}]$.

Table 1. Measurement of electrical resistance of five CNC samples.

	Sample 1	Sample 2	Sample 3	Sample 4	Sample 5
Fiber diameter [nm]	692	551	407	407	352
Coil diameter [nm]	1385	854	889	889	1340
Electrical resistivity [$\Omega \cdot \text{cm}$]	1.08×10^{-2}	8.55×10^{-2}	4.03×10^{-2}	3.37×10^{-2}	4.36×10^{-2}

This work has been partly supported by the EIIRIS Project from Toyohashi University of Technology (TUT); the Core University Programs (JSPS-CAS program in the field of "Plasma and Nuclear Fusion") from the Japan Society for the Promotion of Science (JSPS); JSPS KAKENHI Grant Number 24360108 and 25630110; and MEXT KAKENHI Grant Number 24110708.

[1] S. Motojima, et al. Diamond and Related Materials 13, 1989 (2004)

[2] M. Yokota, et al. The Journal of Nanoscience and Nanotechnology 11, pp.2344-2348 (2011)

Corresponding Author: Yoshiyuki Suda

Tel: +81-532-44-6726, Fax: +81-532-44-6757, E-mail: suda@ee.tut.ac.jp

Efficient synthesis of fullerenes in multi-phase ac arc plasma

○Hiroshi Sano¹, Ryoji Nakaya², Norio Maki¹, Masaaki Ashihara¹,
Hiroyuki Magara¹, Mikihiro Ueno¹, Masanori Takeuchi¹ and Eiji Saji¹

¹ Industrial Technology Center of Fukui Prefecture, Fukui 910-0102, Japan

² Fukui Health and Welfare Center, Fukui 918-8004, Japan

The synthesis of fullerenes was efficiently carried out in multi-phase ac arc discharge plasma. The experimental equipment for multi-phase ac arc system consists of the water-cooled vacuum chamber that is radially inserted plural carbon electrodes connecting with multiple phase ac power supplies as illustrated in Figure 1. The advantage of this system is that the number of discharging paths among the electrodes larger than the case of single-phase or dc arc, and it can lead to a stable arc plasma generation [1].

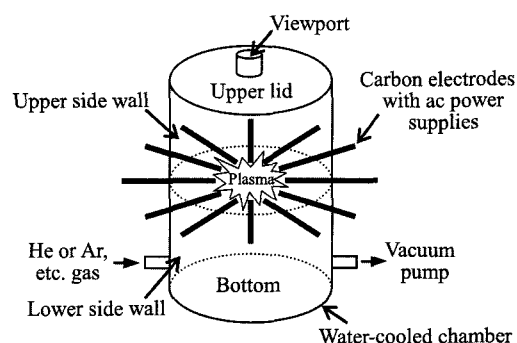


Fig.1. Schematic illustration of the multi-phase ac arc reactor.

One of the experimental results of synthesizing fullerenes in the three-phase ac plasma is shown in Table 1 when He-gas pressure and current density of the carbon electrode are 300Torr and 4A/mm² respectively. The yields of fullerenes from soot in the chamber were mainly obtained at the upper lid and the side wall i.e. above the electrodes in the chamber. And on the other parts including the bottom in the chamber we could hardly find fullerene.

Table 1. Yield of fullerenes in three-phase ac plasma.

	Upper lid	Upper side wall	Others	Total
Weight of soot	292mg	109mg	45mg	446mg
Yield of fullerenes	17.3%	13.7%	-	14.7%

The influence of current density on synthesis of fullerene is shown in Figure 2. The high yield of fullerene at 3A/mm² was remarkably attained to more than 22% on the upper side wall.

The synthesis of fullerene by multi-phase ac arc system involves no other chemical solvents e.g. benzene and is relatively easy. Therefore, this method is considered that it can be suitable for the efficient production of fullerenes.

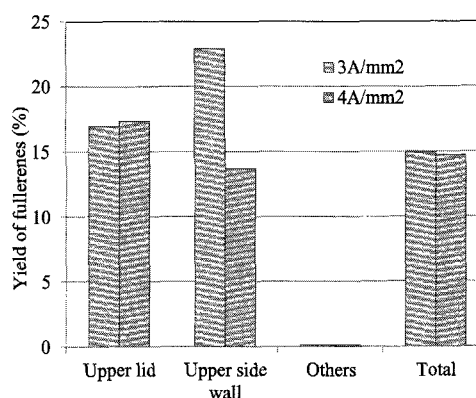


Fig.2. Influence of electrode current density on synthesis of fullerenes.

[1] T. Matsuura *et al.* Proc. 19th Int. Symp. Plasma Chem. 157 (2009).

Corresponding Author: H. Sano

Tel: +81-776-55-0664, Fax: +81-776-55-0665,

E-mail: sano@fklab.fukui.fukui.jp

Direct CVD Synthesis of Suspended Double-walled Carbon Nanotubes and Their Characterization by TEM and Optical Spectroscopy

○Sihan Zhao¹, Tomoya Kitagawa¹, Yuhei Miyauchi^{2,3}, Kazunari Matsuda², and Hisanori Shinohara¹ and Ryo Kitaura¹

¹ *Department of Chemistry & Institute for Advanced Research, Nagoya University, Nagoya 464-8602, Japan*

² *Institute for Chemical Research, Kyoto University, Uji, Kyoto 611-0011, Japan*

³ *Japan Science and Technology Agency, PRESTO, Saitama 332-0012, Japan*

The physical properties of CNTs strongly depend on chirality, defects, the number of walls and encapsulated chemical species. Double-wall carbon nanotube is one of the most fundamental systems to examine the effect of inter-layer interactions on the electronic transitions. To study the inter-layer coupling in double-wall CNTs in detail, it is necessary to develop a direct preparation method of long and clean suspended individual double-wall CNTs on an open slit, which enables us to apply two complementary experimental techniques, Rayleigh scattering and TEM observations, on the same double-wall CNTs for characterizations of electronic transition energies in double-wall CNTs with defined inner and outer wall structures. Here, we report a preparation of suspended double-wall CNTs using the chemical vapor deposition (CVD) and also a characterization of their structure and optical properties.

Fe catalyst nanoparticles supported by MgO were deposited on the substrate with an open slit (~10 m×1.5 mm). After the deposition of Fe/MgO, suspended DWCNTs were grown by the alcohol catalytic chemical vapor deposition (ACCVD) method. The suspended DWCNTs have been characterized by TEM and Rayleigh scattering spectroscopy, and their chiral indexes and optical transition energies were identified. At presentation, we will discuss the detailed experimental procedures and the interlayer coupling effects on the electronic transition energies in detail.

[1] K. Liu, et al., *Nature Nanotech.* 7, 325 (2012).

Corresponding Author: H. Shinohara and R. Kitaura

Tel: +81-52-789-2482, Fax: +81-52-747-6442,

E-mail: noris@nagoya-u.jp and r.kitaura@nagoya-u.jp

Evaluation method of reliable specific strength of ultra-light MWCNT fiber based on uncertainty

○Hikaru Nishizaka¹, Yoshinori Sato¹, Kenichi Motomiya¹, Kazuyuki Tohji¹

¹*Graduate School of Environmental Studies, Tohoku Univ., Sendai, 980-8579 Japan*

Carbon nanotubes (CNTs) possess extraordinary mechanical properties. CNT fibers have a flexible structure and consist of highly aligned CNTs [1], which is an advantage in fabricating macroscale CNT materials capable of fully utilizing the excellent mechanical properties of individual CNTs. However, the mechanical properties of CNT fibers are much lower than those of individual CNTs. The load transfer between CNTs in a fiber has currently been transferred by increasing fiber density [2] and introducing polymer chains adjacent CNTs [3]. The specific strength of a fiber (S) is calculated using the following formula [4]:

$$S = \frac{F}{L}$$

where F is a breaking force on the tensile test curve and L is the linear density of the CNT fiber in tex (1 tex = 1 mg/m). Reliability is relatively low at lower linear density, because the error of the linear density mainly depends on the accuracy of a microbalance. Hence, the error of S is relatively large at lower L . In order to precisely evaluate the specific strength of an ultra-light CNT fiber, assessing the reliability of S and its error is of great significance.

Here, we quantitatively expressed the reliability of specific strength based on uncertainty. Uncertainty of specific strength was calculated using the law of propagation of uncertainty. Multi-walled carbon nanotube (MWCNT) fibers were spun from vertically aligned MWCNT arrays synthesized by chemical vapor deposition. The mass per unit length and breaking tensile load of fibers then were measured by an electric microbalance (UMX2, METTLER TOLEDO) and tensile tester (model5848, INSTRON), respectively. Additivity of variance was employed and the combined standard uncertainty (CSU) of each reading was equal to the root-mean-square of standard uncertainties, which were attributed to certain factors such as repeatability and linearity. The CSU of specific strength was then calculated using the CSU of each reading and the law of propagation of uncertainty. The reliability of specific strength is inversely proportional to the CSU. Additionally, the breaking forces were normally distributed due to a slight difference between test specimens. The standard uncertainty attributed to this distribution was expressed as a standard error of distribution of specific strengths. The reliable specific strength was finally expressed as the mean of specific strengths, except for those that possessed lower reliability.

[1] K. L. Jiang *et al.* Nature, 419, 801 (2002)

[2] K. Liu *et al.* Nanotechnology, 21, 045708 (2010)

[3] K. Liu *et al.* ACS Nano, 4, 5827 (2010)

[4] M. Miao *et al.* Carbon, 48, 2802 (2010)

Corresponding Author: Y. Sato

Tel & Fax: +81-22-795-3215

E-mail: hige@ncsimd.kankyo.tohoku.ac.jp

Gas adsorption properties of gel-immobilized ultrathin carbon nanotubes

○Eri Inukai¹, Yasumitsu Miyata², Ryo Kitaura¹, Hisanori Shinohara¹

¹*Department of Chemistry, Nagoya University, Nagoya, 464-8602*

²*Department of Physics, Tokyo Metropolitan University, Hachioji, 192-0397*

Because of their superior tunability of surface and inner morphology, carbon nanotubes (CNTs) are expected as an ideal material for gas sensing and separation. To expand their practical applications, the enhancement of gas selectivity is one of the most important challenges. For this purpose, we focus our attention on ultrathin CNTs with one-atom-thick inner diameter and widely-varied surface curvature. However, the nature of interactions between gas atoms/molecules and such ultrathin nanotubes are still unknown due to their limited availability.

In this work, we have investigated the gas adsorption properties of small-diameter nanotubes enriched and immobilized effectively by using gel beads. An improved gel filtration method is applied to enrich ultrathin CNTs smaller than 0.75 nm in diameter. We have found that some nanotubes can be immobilized by the gel beads (Fig. 1a) and exhibit stable photoluminescence even under vacuum at temperatures from 300 K to 77 K. Interestingly, a clear shift of emission peak is observed between atmospheric and vacuum conditions as presented in Fig.1b. This result indicates that the present immobilized process provides an effective system for gas adsorption study of ultrathin nanotubes.

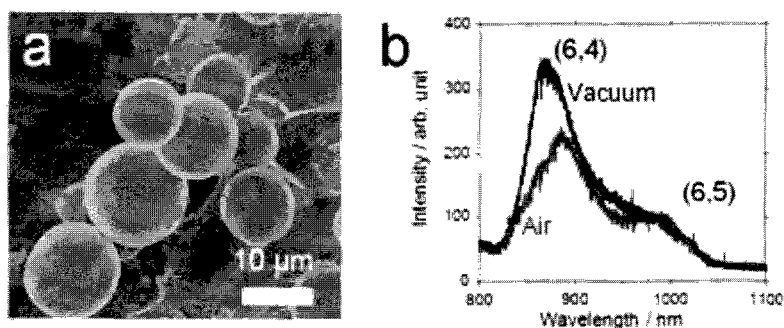


Fig. 1. (a) SEM image of the gel beads used in this study. (b) Photoluminescence spectra of gel-immobilized CNTs in vacuum and air.

Corresponding Authors: Yasumitsu Miyata, Hisanori Shinohara

TEL : +81-52-789-2482, FAX : +81-52-747-6442,

E-mail : ymiyata@tmu.ac.jp, noris@nagoya-u.ac.jp

Coulomb Blockade Effect at Quantum Dots Formed in SWNTs Network FET Studied via Scanning Gate Microscopy

○Masahiro Matsunaga¹, Xiaojun Wei¹, Kenji Maeda¹, Tatsuro Yahagi¹, Jonathan P. Bird², Koji Ishibashi³, Yuichi Ochiai¹ and Nobuyuki Aoki¹,

¹ Graduate School of Advanced Integration Science, Chiba University, Chiba 263-8522, Japan

² Department of Electrical Engineering, University at Buffalo, SUNY, Buffalo, New York 14260-1920, USA

³ Advanced Device Laboratory, RIKEN, 2-1 Hirosawa, Wako, Saitama 351-0198, Japan

Field effect transistors (FETs) whose channel is composed of a network of single wall carbon nanotubes (SWNTs) have been studied for the practical applications as flexible FETs. However, the mechanism of device operation has not been well evaluated yet. Scanning gate microscopy (SGM) is one of such techniques to establish a spatially resolved local gate study in semiconductor nano-structures [1]. By using the technique, electrostatic characteristics of each SGM-active regions can be evaluated individually.

In our previous study [2], we reported concentric-multiple rings were observed in the SGM images within the network of semiconducting enriched SWNTs prepared by density gradient ultracentrifuge (DGU) process and such responses would be related to transport through discrete energy levels of quantum dots due to defects in the SWNT.

Here, we demonstrated an observation of local current-voltage characteristics at SGM-active region within the channel and a depiction of diamond-shape characteristics from the SGM response. The AFM tip was fixed at the center of the response with applying ac- (V_{tip-ac}) and dc- (V_{tip-dc}) tip voltage. This allows that an observation of the local differential conductance (Δg_m) as a function of the back gate voltage (V_{bg}) and the source-drain voltage (V_{sd}). Fig. 1 (a) shows clear change of slope of ac component of source current (i_{sd})- V_{tip-ac} characteristics at different V_{bg} and then some of steps can also be confirmed. The slopes of i_{sd} - V_{sd} curves oscillate with increasing V_{bg} . The characteristics as a function of V_{bg} and V_{sd} are shown as a contour plot in Fig. 1 (b). Clear diamond-shaped structures are resolved even at room temperature. Modulating one of the SGM-active regions, the local characteristics are revealed. Step-like current-voltage characteristics and diamond-shaped contour plots are successfully visualized using the local SGM responses. It can be suggested that these responses would be attributed to the presence of Coulomb blockade effect at quantum dots formed in SWNTs.

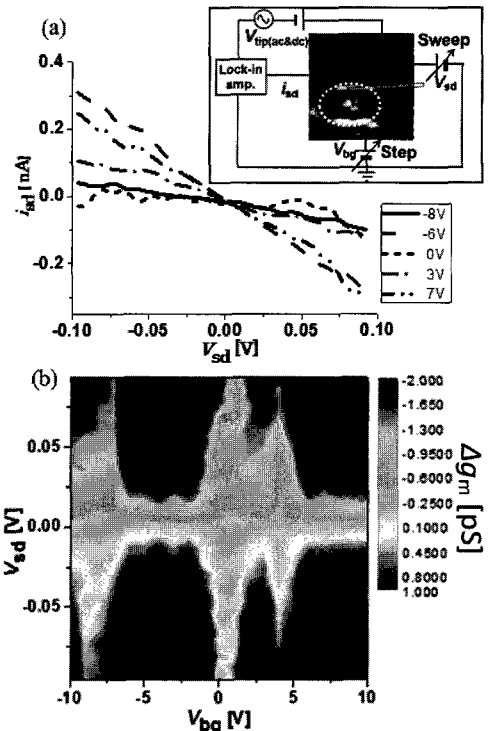


Fig. 1 (a) i_{sd} was plotted as a function of V_{sd} . The inset shows the schematic diagram of SGM experiments. (b) Contour plot of i_{sd} as a function of V_{bg} and V_{sd} at room temperature.

[1] D. Mann *et al.*, Nano Lett. 3 (2003) 1541, [2] X. Wei *et al.*, The 44th FNTG General Symposium (2012) 1P-9
Corresponding Author: M. Matsunaga

Tel: +81-43-290-3430, Fax: +81-43-290-3427, E-mail: m-matsunaga@chiba-u.jp

Mechanistic Studies on the Helicity-Selective Photoreaction of Single-Walled Carbon Nanotubes with Organosulfur Compounds in the Presence of Oxygen

○Yuri Amagai¹, Yutaka Maeda¹, Kei Ohkubo², Shunichi Fukuzumi², Michio Yamada¹, Tadashi Hasegawa¹, Takeshi Akasaka^{1,3}

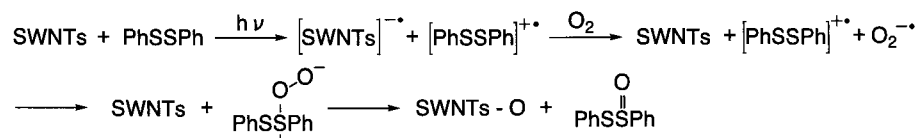
¹Department of Chemistry, Tokyo Gakugei University, Koganei 184-8501, Japan

²Department of Material and Life Science, Division of Advanced Science and Biotechnology, Graduate School of Engineering, Osaka University, ALCA, Japan Science and Technology Agency, Osaka 565-0871, Japan

³Foundation for Advancement of International Science, Ibaraki 305-0821, Japan

Chemistry of Single-walled carbon nanotubes (SWNTs) with organosulfur functional groups has received great deal of attention. Self-assembly and drug delivery systems are constructed using SWNTs and thiols or disulfides. The thiol and disulfide groups are used for the introduction of functionality on the SWNT sidewall via photochemical and thermal reactions. Recently, we developed the helicity selective photoreaction of SWNTs with disulfide in the presence of oxygen. In the present work, we report the mechanistic studies on the photoreaction in detail [1].

A THF solution of SWNTs containing diphenyl disulfide was sonicated, and then irradiated under saturated oxygen with a 500W halogen lamp. The XPS spectra of the SWNTs before and after the photoreaction showed no peaks attributable to sulfur, although peaks related to carbon and oxygen were observed around 285 eV (C 1s) and 531 eV (O 1s). Recently, Weisman et al. reported that the photoluminescence spectra of semiconducting SWNTs were red-shifted by the small amount of oxygenation [2]. After the photoreaction of SWNTs with diphenyl disulfide in the presence of oxygen, similar red shifts were observed. These results suggest that oxidation of SWNTs occurred. Lacombe et al. reported that the photoreaction of sulfides and disulfides under oxygen in the presence of a photosensitizer afforded persulfoxide and thiopersulfinate intermediates, which act as nucleophilic oxidizing agents [3]. To clarify the detailed reaction mechanism, the femtosecond laser flash photolysis transient absorption measurement was conducted. The thianthrene radical cation was observed, which is formed from rearrangement of diphenyl disulfide radical cation [4]. The radical species were also detected using ESR measurements conducted under photoirradiation in the O₂-saturated frozen THF glass at 100 K. These experimental results suggest one plausible reaction mechanism via electron transfer as shown in the scheme below.



[1] Y. Maeda *et al.* J. Am. Chem. Soc. **135**, 6356 (2013).

[2] S. Ghosh *et al.* Science **330**, 1656 (2010).

[3] S. Lacombe *et al.* Photochem. Photobiol. Sci. **1**, 247 (2003). Y. Maeda *et al.* Chem. Lett. **40**, 1431 (2011).

[4] G. Jones, II *et al.* J. Org. Chem. **58**, 2035 (1993). J. Giordan *et al.* Chem. Ber. **115**, 2548 (1982). P. S. Lakkaraju *et al.* J. Chem. Soc., Perkin Trans. 2, 1119 (1998).

Corresponding Author: Y. Maeda

Tel&Fax: +81-42-329-7512

E-mail: ymaeda@u-gakugei.ac.jp

Thermal annealing effect of X-ray irradiation defect in carbon nanotube

○Mitsuaki Matsuda¹, Yuki Yamamoto¹, Toshiya Murakami¹, Kenji Kisoda²,
and Chihiro Itoh¹

¹ *Department of Materials Science and Chemistry, Wakayama University, Wakayama
640-8510, Japan*

² *Department of Physics, Wakayama University, Wakayama 640-8510, Japan*

Single walled carbon nanotube (SWNT) has many attractive properties due to its unique structure. For developing future nanoscale devices using SWNT, the control of electronic properties is required. The electric properties of SWNT strongly depended on their geometric structures, so-called chirality. X-ray irradiation technique is a promising tool for modifying the structure of SWNT. X-ray irradiation results in formation of defect and eventually structural change.[1] Recently, we have found that the X-ray induced defects are Frenkel pairs, vacancy and interstitial pairs, because the defect was healed by thermal annealing.[2] In this report, we demonstrate the thermal annealing effect of X-ray induced defect by resonant Raman scattering spectroscopy.

SWNTs were synthesized by chemical vapor deposition. The defects were formed in SWNTs by X-ray (1254 eV) irradiation. The irradiated samples were subsequently annealed at 100~700 °C. The resonant Raman spectra were measured with the probe laser of 532 nm.

Figure 1 shows the radial breathing modes (RBMs) of the unirradiated, irradiated, and annealed samples. The Raman intensities were normalized with respect to the G band at 1590 cm⁻¹. After the X-ray irradiation, the intensity of the RBM peaks were greatly reduced. The intensities of several RBM peaks were retrieved by the annealing at 600°C. However, the peaks of (10, 0), (6, 5) tubes were not recovered even by the annealing at 700 °C. Moreover, the temperature of the intensity recovery is different by peak. Based on these results, we suggested that the structure of the X-ray induced defect varies depending on the tube geometry.

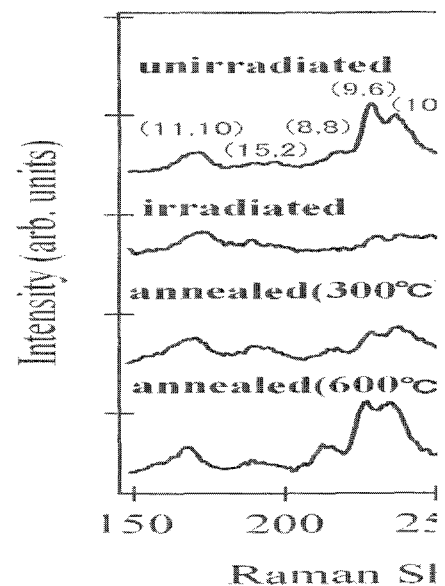


Fig.1 RBM spectra of unirradiated, irradiated and annealed (300, 600 °C) SWNTs.

[1] C. Itoh *et al.* Nucl. Instr. Meth. B **266** (2008) 2772,

[2] T. Murakami, *et. al.*, Eur. Phys. J. B **86** (2013) 187

Corresponding Author: M.Matsuda, Tel: +81-73-457-8532 E-mail: s143052@center.wakayama-u.ac.jp

Electric and electronic properties of CNT/n-type 4H-SiC interface formed by surface decomposition of SiC

○Takatoshi Yajima¹, Toyokazu Nomoto², Takahiro Maruyama^{1,3}

¹ *Department of Materials Science and Engineering, Meijo University, Nagoya 468-8502, Japan*

² *Aichi Synchrotron Radiation Center, Seto 489-0965, Japan*

³ *Department of Applied Chemistry, Meijo University, Nagoya 468-8502, Japan*

Carbon nanotube (CNT) growth by surface decomposition of SiC is a unique synthesis method, since vertically aligned, high-density CNTs can be obtained only by heating SiC in a vacuum [1]. In addition, this method is catalyst-free, and CNTs are directly bonded to SiC at the interface, as a result, CNT/SiC heterojunctions are self-organizedly formed. So far, we have investigated the electronic structure of the CNT/n-type 6H-SiC heterojunction, where Schottky junctions was formed at the interface [2]. In this study, we formed CNT/SiC heterojunction using n-type 4H-SiC and investigated the electric and electronic properties at the CNT/SiC interfaces, since the band gap of 4H-SiC (3.2 eV) is larger than that of 6H-SiC and the interface properties might be different from that for 6H-SiC.

After 4H-SiC(0001)(n-type) (CREE) substrates were cleaned with acetone and methanol by the ultrasonic cleaning, they were etched by immersing in 10% HF for 10 min. Then, they were heated in a vacuum to form CNTs. To characterize the CNT/SiC heterojunction, we carried out the current-voltage (I-V) and photoemission (PES) measurements. The PES measurements were carried out at BL6N1 of the Aichi Synchrotron Radiation Center.

From the I-V measurements, rectifying behavior was observed at the CNT/SiC heterojunction: when a positive voltage was applied to the CNTs, the current from the CNTs to SiC increased linearly with bias voltage (forward bias). On the other hand, when a positive voltage was applied to SiC, only small current flowed from SiC to the CNTs (reverse bias). This leakage current was strongly dependent on the growth condition of CNTs, which might be due to the crystalline quality of CNTs at the interface. We also carried out PES measurements for CNT/SiC interface. From the C 1s spectra at the CNT/SiC interface, the energy separation in C 1s between CNTs and SiC was estimated to be 1.5 eV. These results suggest the formation of Schottky barrier, leading to the rectifying behavior at the interface.

This work was supported in part by JSPS KAKNEHI (Grant-in-Aid for Scientific Research © 21510119 and Challenging Exploratory Research 25600031) and the Nanotechnology Platform Program (Molecule and Material Synthesis) of the Ministry of Education, Culture, Sports, Science and Technology (MEXT), Japan.

[1] M. Kusunoki *et al.* Appl. Phys. Lett. **77** (2000) 531.

[2] T. Maruyama *et al.* Appl. Phys. Lett. **101** (2012) 092106.

Corresponding author: Takahiro Maruyama

Phone: +81-52-838-2386, Fax: +81-52-832-1179

E-mail: takamaru@meijo-u.ac.jp

Precise Probing of Local Thermal Elevation of Metal Nanostructure during Laser Illumination Utilizing Surface-enhanced Raman Scattering from a Single-Walled Carbon Nanotube

○Satoshi Yasuda^{1,2}, H. Nabika¹, Mai Takase¹, S. Hoshina¹,
M. Nara¹, R. Shito¹, Kei Murakoshi¹

¹ Department of Chemistry, Hokkaido University, Sapporo, 060-0810, Japan

² JST-PRESTO, Kawaguchi, Saitama 332-0012, Japan

Precise temperature measurement around laser-heated metal nano structure has been fascinating issue in recent years for novel photochemical, medical and engineering applications in the field of plasmonic science. Laser illumination of plasmonic nano-metal structures gives rise to a local thermal elevation of the metal nanostructure due to the absorption of light. However, despite the importance of the local heating effect in terms of the applications, we know little about the degree of temperature rise at the metal nano-gap. Therefore, a precise estimation of the temperature of individual metal nanostructures under laser illumination has been regarded as a significant issue to further develop the field of plasmonic science. Recently, carbon nanotubes have been found to possess a clear temperature dependence on the Raman frequency, prompting speculation of their potential usage as a nanoscopic thermometer.¹ In this work, we have employed an isolated single-walled carbon nanotube (SWNT) supported at the nano-metal gap of an Au nano dimer as a thermometer and measured the laser-heating temperature rise of the Au nano dimer in different environments via surface-enhanced Raman scattering (SERS) measurements. The local thermal elevation on the metal surface was measured by evaluating the frequency shift of the SERS spectra. We observed a clear local thermal elevation from an analysis of the Raman spectra. It was found that a smaller power dependence of the band position in aqueous solution results in a large dissipation through high thermal conduction of water compared with air (Fig. 1). The results demonstrate the probing of the laser heating effect on the metal nanostructure using the SERS spectra of an individual SWNT. The present finding is expected to contribute to the understanding and controlling of novel photochemical, medical and engineering applications in the field of plasmonic science.²

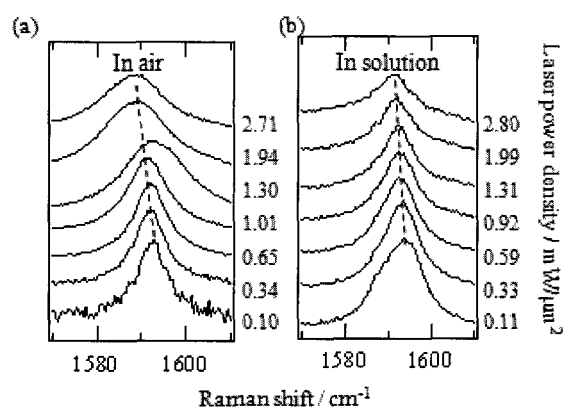


Figure 1. SERS spectra of the supported SWNT in the metal gap in air (a) and in aqueous solution (b) at seven different laser power density between 0.10 and 2.80 mW / μm^2 . (c) Laser power density dependence of the G-band frequency (left axis) in air and aqueous solution. Right axis is estimated temperature calculated from a coefficient of $-0.024 \text{ cm}^{-1} / \text{K}$ previously reported.

[1] S. Chiashi, Y. Murakami, Y. Miyauchi and S. Maruyama, *Jpn. J. Apl. Phys.*, 2008, **47**, 2010.

[2] M. Takase, H. Nabika, S. Hoshina, M. Nara, K. Komeda, R. Shito, S. Yasuda, K. Murakoshi, *Phys. Chem. Chem. Phys.*, 2013, **15** (12), 4270.

Corresponding Author: K. Murakoshi

TEL & FAX: +81-(0)11-706-2704

E-mail: kei@sci.hokudai.ac.jp

UV, X-ray and e-beam irradiation effects of IR absorption bands in single-walled carbon nanotubes

○Masao Ichida¹, Yasumitsu Miyata², Chihiro Ito³, Toshiya Murakami³, Yuka Ikemoto⁴, Akira Kawakami⁵, Kazuhiro Yanagi², Hiromichi Kataura⁶, Hiroaki Ando¹

¹ Department of Physics, Konan University, Kobe 658-8501, Japan

² Department of Physics, Tokyo Metropolitan University, Hachioji 192-0397, Japan

³ Faculty of Systems Engineering, Wakayama University, Wakayama 640-8510, Japan

⁴ JASRI/SPRING-8, Hyogo 679-5198, Japan

⁵ KARC/NICT, Kobe 651-2492, Japan

⁶ NRI/AIST, Tsukuba 305-8568, Japan

In the absorption spectra for semiconducting (S) and metallic (M) single-walled carbon nanotubes (SWNTs), the intrinsic absorption bands can be observed between near infrared to ultra-violet region. Although, there are no corresponding intrinsic electronic states, the broad absorption bands appear in infrared region for both S- and M-SWNTs[1]. The origins of these infrared absorption bands have not been understood. In this study, we have irradiated UV light, X-ray, and e-beam to high purity S- and M-SWNTs thin film samples, and investigated the irradiation effects in the infrared absorption spectra.

Figure 1 shows the Raman spectra for pristine and after e-beam irradiation for S-SWNTs sample. After e-beam irradiation, G/D ratio decreases from 13.8 to 7.6. This result indicates that many defects are introduced in the S-SWNTs.

The solid curve in Fig. 2 shows the absorption spectrum for pristine S-SWNTs thin film. The exciton absorption (S1) band is observed at 0.7 eV. Broad absorption band is also observed in infrared energy region of 0.02 eV – 0.2 eV. As seen in broken curve, after e-beam irradiation, the intensity of S1 band decreases, and the infrared band shows the decrease of intensity and shift to the high energy side. These results suggest that the origin of infrared band is due to the optical resonance of finite-length SWNT, often called antenna effects[2].

[1] M. Ichida *et al.* Solid State Commun. **151**, 1696 (2011).

[2] T. Nakanishi *et al.* J. Phys. Soc. Jpn. **78**, 114708 (2009).

Corresponding Author: Masao Ichida

Tel: +81-78-435-2679, Fax: +81-78-435-2679,

E-mail: ichida@konan-u.ac.jp

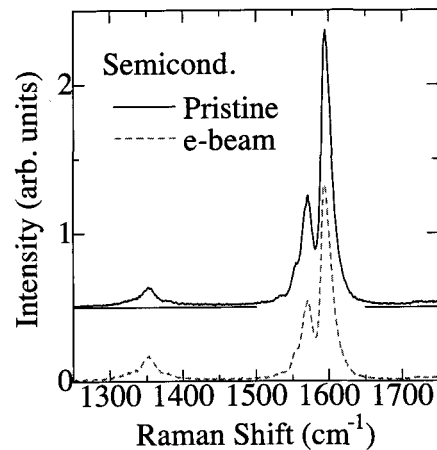


Fig.1. Raman spectra for pristine (solid) and e-beam irradiated (broken) S-SWNTs thin film.

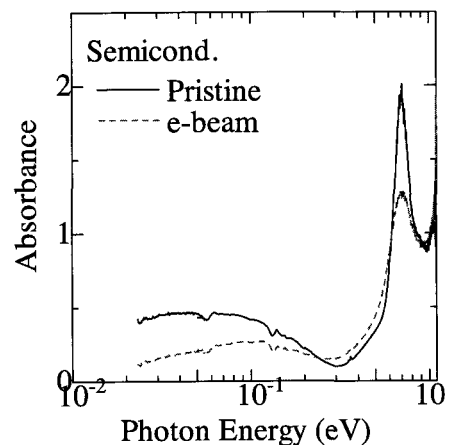


Fig.2. Absorption spectra for pristine (solid) and e-beam irradiated (broken) in S-SWNTs.

Charge transfer between polyoxometalates and SWNTs by means of photoluminescence spectroscopy

○ Liu Hong, Naotoshi Nakashima

Department of Applied Chemistry, Kyushu University, Fukuoka, 819-0395, Japan

Hybridization of single-walled carbon nanotubes (SWNTs) with molecules enables the emergence of new functionalities to afford important components for molecular-scale electronics [1]. Here, we describe charge transfer behavior between the SWNTs and phosphododecamolybdic acid (PMo_{12} , Fig.1), which is one of well-known polyoxometalates (POMs) behaved as electron reservoir to carbon nanotubes [2], by means of photoluminescence (PL) spectroscopy.

After sonication with carboxymethylcellulose sodium salt (Na-CMC) and ultracentrifugation, we obtained individual SWNT aqueous solution, to which PMo_{12} aqueous solution (1 mg/mL) was added. As shown in PL mapping, PL of the SWNTs quenched by the addition of PMo_{12} . We found that the PL quenching rates of several chiralities in SWNTs were different, which was considered as a result induced by different electrochemical band gaps of SWNT chiralities [3]. Furthermore, new PL peaks due to charged excitons were observed in the PL spectra [4]. Details will be reported at the meeting.

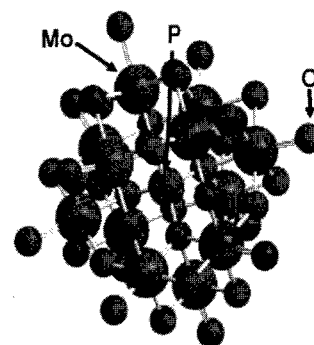


Fig.1 molecular structure of PMo_{12}

[1] X. Z. Bo *et al.* Appl. Phys. Lett. 87, 203510 (2005); T. Takenobu *et al.* Nat. Mater. 2, 683 (2003); A. K. Feldman *et al.* Acc. Chem. Res. 41, 1731 (2008).

[2] L. Hong *et al.* J. Mater. Chem. C. 1, 1137 (2013).

[3] Y. Hirana *et al.* J. Am. Chem. Soc. 132, 13072 (2010).

[4] J. S. Park *et al.* J. Am. Chem. Soc. 134, 14461 (2012)

Corresponding Author: N. Nakashima

Tel: +81-92-802-2840, Fax: +81-92-802-2840,

E-mail: nakashima-tcm@mail.cstm.kyushu-u.ac.jp

Determination of Hyperfine Coupling Constants of Cycloparaphenylene Cation Radical

○Takahiko Koyama¹, Eiichi Kayahara², Shigeru Yamago², Tatsuhisa Kato^{1,3}

¹ *Department of Interdisciplinary Environment, Graduate School of Human and Environmental Studies, Kyoto University, Kyoto 606-8501, Japan*

² *Institute for Chemical Research, Kyoto University, Uji 611-0011, Japan*

³ *Institute For Liberal Arts and Sciences, Kyoto University, Kyoto 606-8501, Japan*

Yamago group of author succeeded to synthesize [n]CPPs (n=6, 8, 10, 12) cations as SbCl_6^- salts. The cation radicals exhibited ESR spectra with equally split multiplet due to ^1H hyperfine coupling (hfc) in CH_2Cl_2 solution, which indicated that the spin and charge were equally delocalized over the entire benzene rings of CPPs. The ^1H hfc constants decreased with the number of repeating paraphenylene units of CPPs. Furthermore these findings were also supported by theoretical calculations and UV-vis-NIR spectra.

Typical line width alternation effect was exhibited by the highly resolved CW-ESR spectra of [6] and [8]CPP cation radicals in solution, as shown in Fig. 1. It suggested that [6] and [8]CPPs formed a belt like structure with the dihedral angle between the two benzene rings being not zero. Four different ^1H hfc constants were confirmed by ENDOR measurements, as shown in Fig. 2. The intra-molecular motion around the dihedral angle reflected on the line width alternation effect.

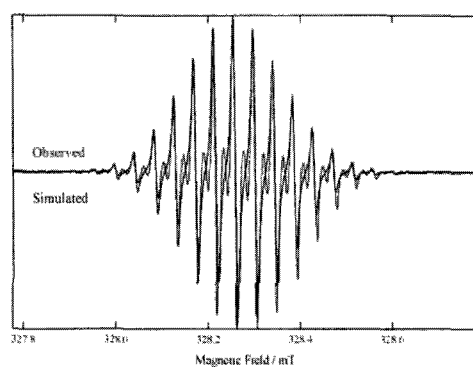


Fig. 1. ESR spectrum of [6]CPP cation radical in CH_2Cl_2 solvent at 273 K.

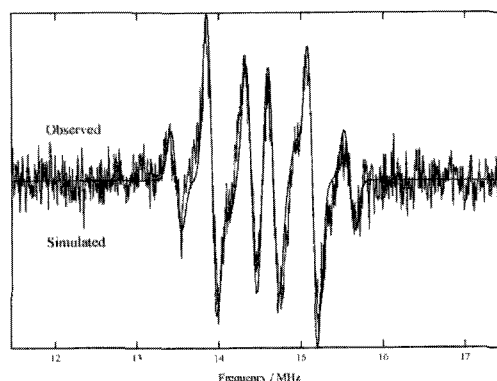


Fig. 2. ENDOR spectrum of [6]CPP cation radical in CH_2Cl_2 solvent at 213 K.

Corresponding Author: T. Kato

Tel: +81-75-753-6695, Fax: +81-75-753-6695,

E-mail : kato.tatsuhisa.6e@kyoto-u.ac.jp

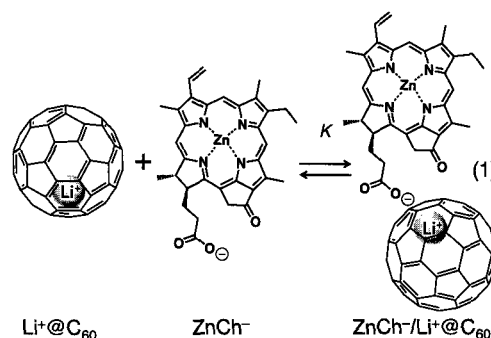
Photoinduced Charge Separation in Supramolecules between $\text{Li}^+\text{@C}_{60}$ and Chlorins

○Yuki Kawashima¹, Kei Ohkubo¹, Shunichi Fukuzumi^{1,2}

¹ Department of Material and Life Science, Graduate School of Engineering, Osaka University, ALCA, Japan Science and Technology Agency, Osaka 565-0871, Japan

² Department of Bioinspired Science, Ewha Womans University, Seoul, 120-750, Korea

Porphyrins and fullerenes that have highly delocalized π systems are suitable for efficient electron transfer because the uptake or release of electrons results in minimal structural and solvation changes upon electron transfer.[1] Thus, they are suitable electron donor and acceptor for formation of the long-lived charge separated states. Therefore, there have been many reports of photoinduced charge separation in porphyrin-fullerene linked- and supramolecular systems. In natural systems, however, reduced porphyrins, namely chlorins are the electron donor pigments of the electron transfer processes. It is of great interest to examine the use of chlorophyll-like molecules such as chlorins. However, there has been no report of photoinduced charge separation using chlorin/fullerene supramolecular system in polar solvent. We report herein construction of chlorin/fullerene supramolecular system and photoinduced charge separation in a polar benzonitrile (PhCN) solution.



UV-vis absorption spectra of an anionic zinc chlorin (ZnCh^-) in PhCN at 298 K are changed upon addition of a cationic lithium encapsulated C_{60} ($\text{Li}^+\text{@C}_{60}$), where the Soret band at 665 nm and an absorption band at 617 nm are blue-shifted to 661 nm and 620 nm, respectively. The formation constant (K) determined from the titration to be $7.7 \times 10^4 \text{ M}^{-1}$. This results exhibit that strong supramolecular binding between ZnCh^- and $\text{Li}^+\text{@C}_{60}$ occur by ionic interaction in PhCN (eq 1). The transient absorption spectra of $\text{ZnCh}/\text{Li}^+\text{@C}_{60}$ supramolecular complex were measured by nanosecond laser flash photolysis are shown in Fig. 1. The band of 470 nm observed at $2 \mu\text{s}$ is assigned to the $^3[\text{ZnCh}^-]^*$. The absorption band of the triplet excited state of ZnCh , $^3[\text{ZnCh}^-]^*$ decays with increasing the absorbances at 790 and 1035 nm, which can be assigned to $[\text{ZnCh}^-]^{++}$ and $\text{Li}^+\text{@C}_{60}^{--}$, respectively.[2,3] It clearly indicating the formation of the CS state between $[\text{ZnCh}^-]^{++}$ and $^3[\text{Li}^+\text{@C}_{60}]^*$. The lifetimes of the triplet CS state in the supramolecular complex is $170 \mu\text{s}$ at 298 K. The quantum yield of the CS state is determined to be 0.62.

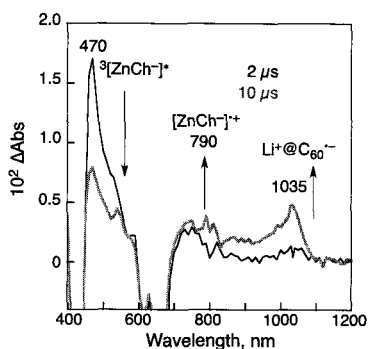


Fig. 1 Transient absorption spectra of ZnCh^- ($2.5 \times 10^{-5} \text{ M}$) with $\text{Li}^+\text{@C}_{60}$ ($5.0 \times 10^{-5} \text{ M}$) in PhCN measured at $2.0 \mu\text{s}$ (black) and $10 \mu\text{s}$ (red) after laser excitation at 450 nm.

[1] Fukuzumi, S.; Guldi, D. M. in *Electron Transfer in Chemistry*, Balzani, V., Ed.: Wiley-VCH, Weinheim, 2001, Vol. 2, pp. 270-337. [2] Fukuzumi, S. *et al. J. Am. Chem. Soc.* **2001**, *123*, 10676-10683. [3] Kawashima, Y.; Ohkubo, K.; Fukuzumi, S. *J. Phys. Chem. A* **2012**, *116*, 8942-8948.

Corresponding Author: S. Fukuzumi, Tel: +81-6-6879-7369, Fax: +81-6-6879-7370, E-mail: fukuzumi@chem.eng.osaka-u.ac.jp

A trend in the hyperfine constant for the series of N@C_n endofullerenes

○Tomonari Wakabayashi, Tatsuya Kanemoto, Ryuki Imamura

Department of Chemistry, Kinki University, Higashi-Osaka 577-8502, Japan

Nitrogen-doped fullerenes, N@C₆₀ and N@C₇₀, have enjoyed a unique story among many other endofullerenes [1-3]. The hyperfine constant (hfc) of atomic nitrogen in a fullerene cage was directly compared to the gas-phase constant, revealing that, for N@C₆₀, it was ~1.5 times as large as in the gas phase [1]. The hfc for N@C₇₀ was slightly smaller than that for N@C₆₀, indicating some differences in the spin-cage interaction [2]. The extraordinarily long coherence time, ~0.2 ms, observed for N@C₆₀ [3] lead to an idea of possible applications of the electron-nuclear spin system to quantum computing and quantum information processing (QC/QIP) [4].

We produced N@C₆₀ and N@C₇₀ in order to compare hfc in relation to the spin-cage interaction. Figure 1 shows ESR spectra from which the hfc can be deduced. The hfc is 15.8 MHz for N@C₆₀, while 15.0 MHz for N@C₇₀, approaching slowly to the gas-phase constant of 10.6 MHz. Since no anisotropic splitting is discernible in the ESR spectrum for N@C₆₀, it is believed that the nitrogen atom is located at the center of the cage or that it moves rapidly around the center within a “free space” inside the C₆₀ cage. The difference in hfc for N@C₆₀ and N@C₇₀ may be explainable in terms of volume or size of the hosting fullerene cage. Therefore, it will be interesting to study a trend in the hfc of atomic nitrogen trapped inside different isomers of fullerenes as hosting cages. We discuss on the size dependence of the hfc for the series of N@C_n (n=60, 70, 84, ...).

[1] T. Almeida-Murphy *et al.* Phys. Rev. Lett. **77**, 1075 (1996).

[3] B. Piezak *et al.* in Endofullerenes, Chapter 2, T. Akasaka and S. Nagase Eds. Kluwer, 13 (2002).

[2] J. J. L. Morton *et al.* J. Chem. Phys. **124**, 014508 (2006).

[4] T. Wakabayashi in Molecular Realizations of Quantum Computing, M Nakahara Ed. World Scientific, 163 (2009).

Corresponding Author: T. Wakabayashi

Tel: +81-6-4307-3408,

Fax: +81-6-6723-2721,

E-mail: wakaba@chem.kindai.ac.jp

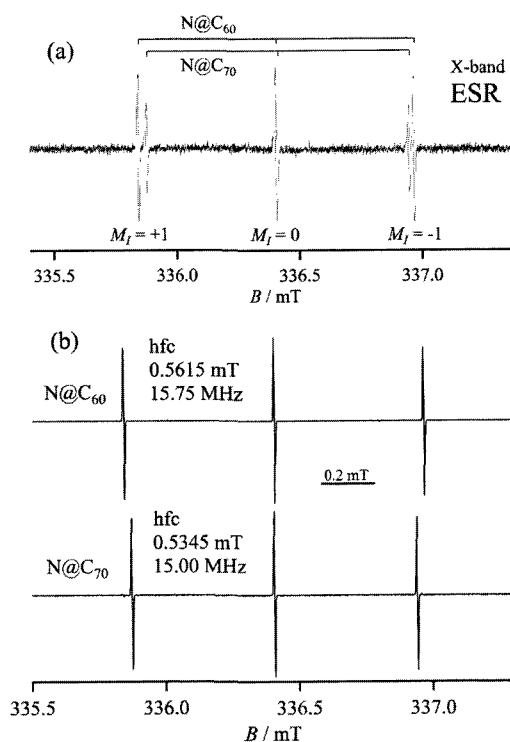


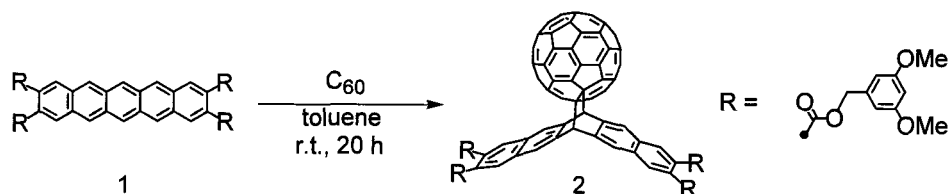
Fig. 1. ESR spectra for (a) the mixture of N@C₆₀ and N@C₇₀ and (b) separate samples of N@C₆₀ and N@C₇₀.

Synthesis, structure, and properties of a highly soluble fullerene-pentacene adduct

○Takuya Nishihama, Tomoyuki Tajima, Yushi Ozawa, Keitaro Fukuda, Yutaka Takaguchi

*Graduate School of Environmental and Life Science, Okayama University,
Okayama 700-8530, Japan*

C_{60} -pentacene adducts have attracted much attention because of unique photo and electronic properties. From the viewpoint of solution-processable semiconductor materials, a highly soluble fullerene-pentacene adduct is of interest. On the other hand, fullerene reacts as a dienophile in a [4+2] fashion with acene. Murata and Komatsu reported the [4+2] cycloaddition reaction of pentacene with C_{60} affording various adducts by the use of HSVM technique.[1] Miller et al reported the unique molecular arrangement of fullerene-pentacene adduct in solid state.[2] Meanwhile, we have reported the synthesis and characterization of 2,3,9,10-substituted pentacene.[3] In marked contrast to pristine pentacene, the pentacene derivative was very soluble in various organic solvents. In addition, we have found that regiospecific [4+2] cycloaddition of the pentacene with dienophiles proceeded at the central ring of the pentacene in good yields. This paper describes synthesis, structure, and photo and electronic properties of a new fullerene-pentacene adduct showing solubility in various organic solvents.



Scheme 1. Synthesis of C_{60} -pentacene adduct **2**.

C_{60} -pentacene adduct **2** was synthesized in good yield (70%) by the use of a Diels-Alder reaction of C_{60} with pentacene **1** (Scheme 1). The structure of **2** was satisfactorily confirmed by mass spectrometry and NMR spectroscopy, and the molecular structure was finally determined by X-ray crystallographic analysis. Fig.1 shows the crystal packing of **2** in the solid state. The redox behavior of the C_{60} -pentacene adduct **2** was investigated by the use of cyclic voltammetry in benzonitrile with $\text{Bu}_4\text{N}^+\text{BF}_4^-$ as a supporting electrolyte. Details of semiconducting properties will be also described.

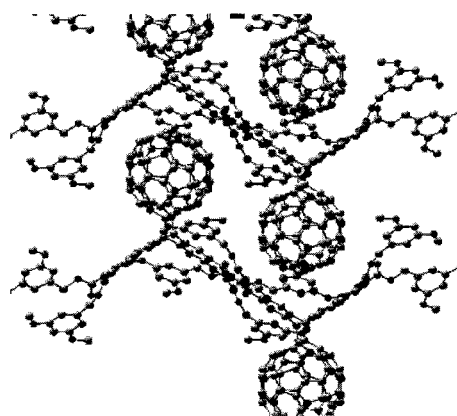


Fig.1. Crystal packing of **2**.

[1] Y. Murata and K. Komatsu *et al.* *J. Org. Chem.* **64**, 3483 (1999). [2] G. P. Miller *et al.* *Org. Lett.* **25**, 3979 (2012). [3] Y. Takaguchi *et al.* *Chem Lett.* **41**, 1622. (2012).

Corresponding Author: Y. Takaguchi

Tel: +81-86-254-8903, Fax: +81-86-254-8903, E-mail: yutaka@cc.okayama-u.ac.jp

Solid-State Reaction of $\text{H}_2\text{O}@C_{60}$ and X-Ray Structure of the [2+2] Dimer

○Rui Zhang,¹ Michihisa Murata,¹ Atsushi Wakamiya,¹ Yasujiro Murata^{1,2}

¹ Institute for Chemical Research, Kyoto University, Uji, Kyoto 611-0011, Japan

² JST, PRESTO, 4-1-8 Honcho, Kawaguchi, Saitama 332-0012, Japan

It is well known that chemical reactivities of endohedral metallofullerenes are very different from those of empty fullerenes because the electronic structure of them are different from those of empty ones due to electron transfer from the encapsulated metals to the outer fullerene cages in the ground state. However, in the case of endofullerenes encapsulating electrically neutral molecule(s), there are only a few studies on the chemical reactivity of outer fullerene cages.

Recently, we have reported the macroscopic synthesis of $\text{H}_2\text{O}@C_{60}$.¹ Although the reduction potential of $\text{H}_2\text{O}@C_{60}$ was found to be almost the same as that of empty C_{60} , it is interesting to study the chemical reactivity of the outer carbon cage as well as the physical properties, which are expected to be potentially affected by an intrinsic polarity of the water molecule. Here we report the reaction of $\text{H}_2\text{O}@C_{60}$ and X-ray structure of the dumbbell shaped C_{60} dimer encapsulating two molecules of water.

The cross dimerization of $\text{H}_2\text{O}@C_{60}$ and empty C_{60} gave the three dimers of C_{60} ,² two of which encapsulate one or two molecules of water (Scheme 1). The similar reactivity toward the dimerization was observed for $\text{H}_2\text{O}@C_{60}$ and empty C_{60} . The encapsulation of water molecules affected the elution order upon the HPLC analysis. The structure of **3** was unambiguously determined with encapsulated water molecules located at the center of each of the C_{60} cages (Figure 1).

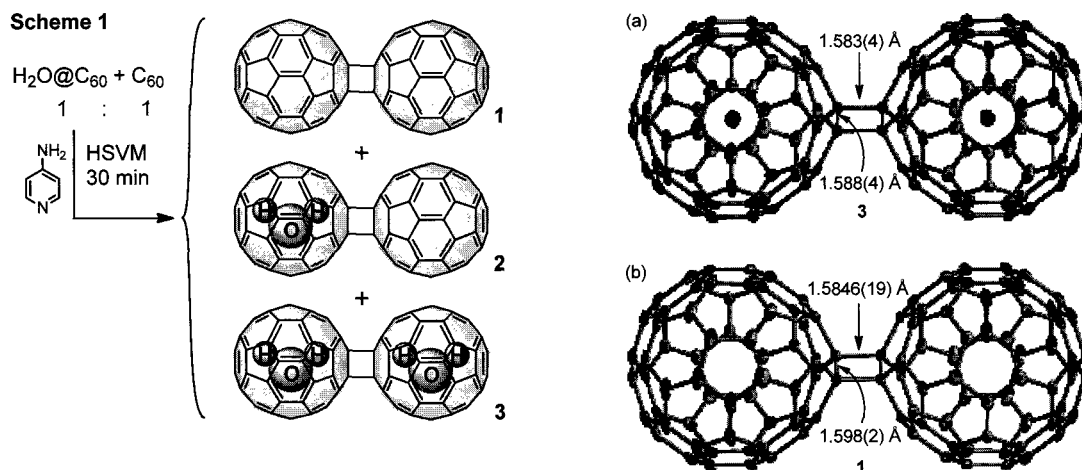


Figure 1. X-ray structure of dimers determined at 170 °C; (a) dimer **3** and (b) dimer **1**. The solvent molecules and hydrogen atoms were omitted for clarity.

[1] Kurotobi, K.; Murata, Y. *Science* **2011**, *333*, 613.

[2] Wang, G.-W.; Komatsu, K.; Murata, Y.; Shiro, M. *Nature* **1997**, *387*, 583.

[3] Zhang, R.; Murata, M.; Wakamiya, A.; Murata, Y. *Chem. Lett.* **2013**, *42*, in press. DOI:10.1246/cl.130358.

Corresponding Author: Y. Murata

Tel: +81-774-38-3172, Fax: +81-774-38-3178,

E-mail: yasujiro@scl.kyoto-u.ac.jp

Photoinduced electron transfer in a porous organic salt composed of 9-(4-sulfophenyl)anthracene and triphenylmethylamine and fullerene.

○Tetsuya Hasegawa^{1,2}, Kei Ohkubo^{1,2}, Norimitsu Tohnai^{1,3}, Ichiro Hisaki¹, Mikiji Miyata¹, Shunichi Fukuzumi^{1,2}

¹ Graduate School of Engineering, Osaka University, Suita 565-0871, Japan

² ALCA, JST, ³ PRESTO, JST

The control of fullerene array by using porous materials that have regularly-ordered pore channels is of significant interest in organic electronics. Thus, we have constructed porous organic salts by using triphenylmethylammonium (TPMA) sulfonates, which have flexible porous structure by weak intermolecular interaction such as hydrogen bond and π - π interaction.[1] However, fullerenes have yet to be included because the channel size of porous organic salts was too small to accommodate fullerenes.

We report herein construction of porous structure with large spherical spaces that can include C₆₀ and C₇₀ by using 9-(4-sulfophenyl)anthracene (SPA) and TPMA. Inclusion crystals were obtained by recrystallization of SPA, TPMA and fullerene. Single-crystal X-ray analysis revealed that C₆₀ and C₇₀ were arranged one dimensionally (shown in Figure 1) and the host structure in each crystal composed of SPA and TPMA remained virtually the same. A flexible porous material that can include different fullerenes is useful. Moreover, each fullerene strongly interacted with anthracene moieties of SPA in the crystals.

No emission was observed from C₆₀/SPA/TPMA crystal under photoirradiation. This suggests that efficient electron or energy transfer from SPA to C₆₀ occurs in the crystal. To clarify the emission quenching mechanism, time-resolved transient absorption spectral measurements of C₆₀ inclusion crystal were performed by femtosecond laser flash photolysis as shown in Figure 2.

The absorption band at 570 nm observed at 0.70 ps is assigned to singlet excited state of SPA (¹SPA*). This band decayed with increasing the absorbance at 690 nm, which can be assigned to SPA^{•+}. This clearly indicates the photoinduced electron transfer from the anthracene moieties to fullerenes occurs in the crystal.

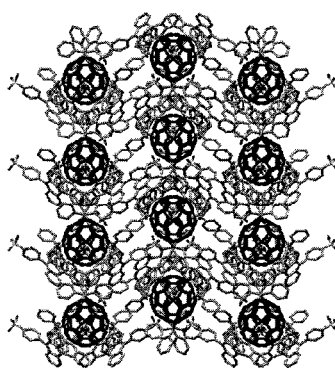


Fig.1. Structure of fullerene inclusion crystal. (C₆₀/SPA/TPMA)

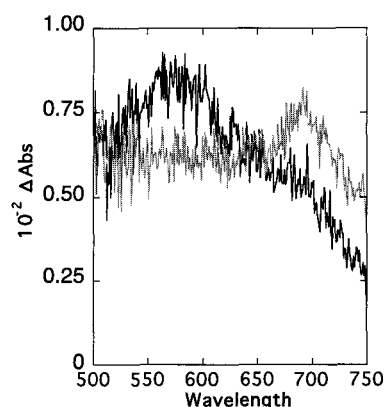
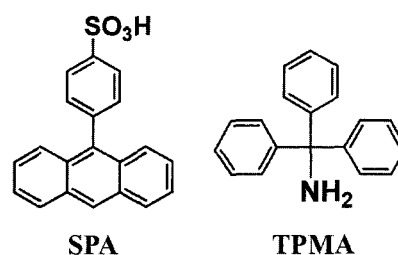


Fig.2. Transient absorption spectra of C₆₀ inclusion crystal with KBr measured at 0.70 ps (black), 1.7 ps (gray) after excitation at 393 nm.

[1] A. Yamamoto, T. Hamada, I. Hisaki, M. Miyata, N. Tohnai, *Angew. Chem. Int. Ed.* **2013**, *52*, 1709.

Corresponding Author: S. Fukuzumi

Tel: +81-6-6879-7369, Fax: +81-6-6879-7370,

E-mail: fukuzumi@chem.eng.osaka-u.ac.jp

Evaluation of Thermal Stability of Nanocomposite Polymers with Multiarylated Fullerenes

○Ryo Takahashi¹, Ken Kokubo¹, Akio Harada², Naohiko Ikuma¹, Takumi Oshima¹

¹ Division of Applied Chemistry, Graduate School of Engineering, Osaka University,
2-1 Yamadaoka, Suita, Osaka 565-0871, Japan

² Totai Co., Ltd., 5-24-17 Ueno, Taito-ku, Tokyo 110-0005, Japan

High reactivity of fullerenes toward radical species has attracted much attention for the application to polymer stabilizing agents. Recently, we have prepared nanocomposite of polycarbonate or poly(vinyl alcohol) with C₆₀ and C₆₀(OH)_n and mainly focused on the thermal stability of C₆₀ nanocomposites regardless of its poor solubility and aggregation behavior [1]. However, only a few examples have been reported on the polymer nanocomposites of chemically modified fullerene derivatives.

In this study, we have prepared new nanocomposite films of polystyrene (PS) and poly(methyl methacrylate) (PMMA) by loading PCBM and multiarylated [60]fullerenes bearing tolyl and phenol groups (*i.e.*, C₆₀(tolyl)_n and C₆₀(phenol)_n) as highly compatible fullerene derivatives with polymers. The thermal analysis of the PMMA nanocomposites by use of TGA and DSC showed no appreciable change in the degradation temperature as well as the glass transition temperature for the C₆₀(tolyl)_n composite as compared to C₆₀, while the improved stability was performed for PCBM and C₆₀(phenol)_n even under air (Figure 1).

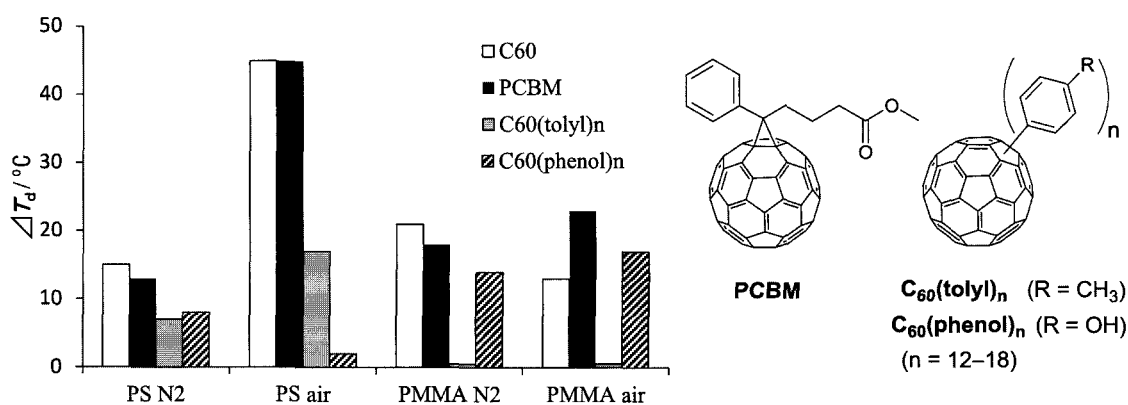


Figure 1. Difference in degradation temperature at 15 wt% loss of polymer/fullerene nanocomposite films relative to those of the corresponding polymer films under N₂ and air.

[1] T. Saotome, K. Kokubo, S. Shirakawa, T. Oshima, H. T. Hahn, *J. Compos. Mater.* 45, 2595 (2011).

Corresponding Author: Ken Kokubo

TEL: +81-6-6879-4592, FAX: +81-6-6879-4593, E-mail: kokubo@chem.eng.osaka-u.ac.jp

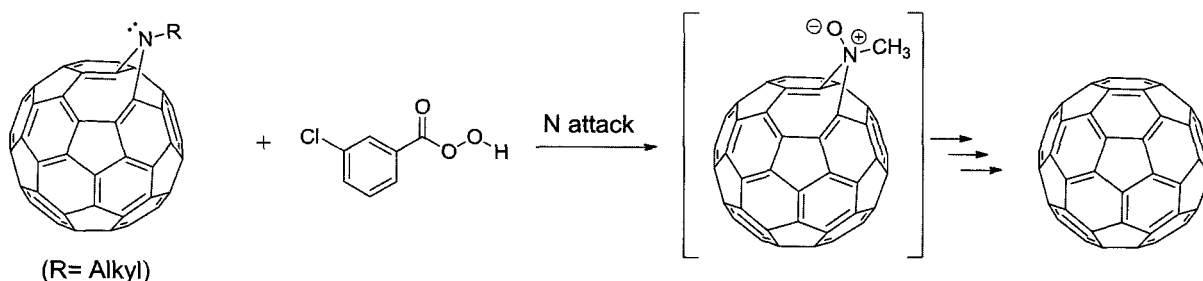
C₆₀ regeneration by oxidative deamination of azafulleroids with peracids and substituent effects of azafulleroids

○Koichi Fujioka, Naohiko Ikuma, Yusuke Misawa, Ken Kokubo, Takumi Oshima

*Division of Applied Chemistry, Graduate School of Engineering, Osaka University,
2-1 Yamadaoka, Suita, Osaka 565-0871, Japan*

Azafulleroids have a bridged nitrogen atom at the [5,6]-open ring junctions and adjacent strained double bonds, so-called anti-Bredt double bonds. Because these sites are highly reactive, it is expected that reactions of azafulleroids with various reagents can occur regioselectively in contrast to low regioselective reactions of C₆₀. Previously, we reported that the reaction of fulleroid with *m*CPBA occurred at the anti-Bredt double bond, and did not produce epoxides but regioselective esterified adducts [1]. On the contrary, it is likely that azafulleroids undergo two types of electrophilic attacks, N attack or C=C attack, depending on the substituents of the N atom. Here, we present the oxidative deamination of azafulleroid with electrophilic peracids such as *m*CPBA and peracetic acid, and their substituent effects on the reaction site-selectivity.

The reaction of alkyl-substituted azafulleroid regenerated C₆₀ probably because of the oxidation of intrinsically basic N atom, followed by the elimination of nitroso unit [2], whereas the reaction of electron-withdrawing substituent such as tosyl group and the π -conjugated substituent such as phenyl group probably brought about epoxidation or esterification at the anti-Bredt double bond due to the reduced basicity of N atom. As a result of oxidation of azafulleroid (R = Me) with *m*CPBA, the isolated yield of C₆₀ was 61%. On the other hand, the yield was 20% at most for the reaction with peracetic acid because of the weaker oxidizability than *m*CPBA.



[1] (a) N. Ikuma, S. Sumioka, H. Asahara, T. Oshima, *Tetrahedron Lett.*, 53, 3581 (2012). (b) G. W. Gribble *et al.*, *Tetrahedron Lett.*, 41, 3673 (1976)

[2] H. W. Heine, J. D. Myers, E. T. Peltzer, *Angew. Chem. Int. Ed.*, 9, 374 (1970).

Corresponding Author: Naohiko Ikuma

TEL: +81-6-6879-4593, FAX: +81-6-6879-4593, E-mail: ikuma@chem.eng.osaka-u.ac.jp

Activation Energies of C₂ Elimination from C₆₂ Isomers

Dai Nagashima¹, Tohru Sato^{1,2}, Kazuyoshi Tanaka¹

¹*Department of Molecular Engineering, Kyoto University, Kyoto 615-8510, Japan*

²*Elements Strategy Initiative for Catalysts and Batteries Kyoto University*

The formation mechanism of fullerene C₆₀ is still an open problem[1]. According to the mechanism proposed by S. Irlé *et al.*, "Shrinking Hot Giant" road [2], C₆₀ is formed by the shrink of giant fullerenes which formed from carbon vapor with a few hundreds of carbon atoms. The final stage of the formation mechanism should include the formation of C₆₀ itself, however, the final stage has not been published yet.

According to the mechanism, the shrinking process is assumed as C₂ elimination from giant fullerenes. Therefore the final stage is considered as the C₂ elimination from C₆₂. In this work, we investigate the transition energies of the C₂ elimination from C₆₂ isomers to form C₆₀.

The initial structures of the C₆₂ isomers were obtained by putting C₂ on C₆₀ in various orientations. All the structures of the reactants, products, and transition states were optimized, and confirmed to be a local minimum or a saddle point by using vibrational analysis. Intrinsic reaction coordinate calculations were also performed for all the path. All the calculations were performed at the B3LYP/3-21G level of theory by using Gaussian09.

The optimized structures C₆₂ are shown in Fig. 1. C_s:7mbr is the most stable structure of all the C₆₂ isomers[3]. Figure 2 shows that energy profile of the C₂ elimination from the C₆₂ isomers. We found that the C₂ elimination consists of the two steps. For the first step, the transition energy from the cage isomers to the intermediates, Im1 and Im2 ranges from 4.75 eV to 5.28 eV. For the second step, on the other hands, the calculated transition energy is 5.23 eV.

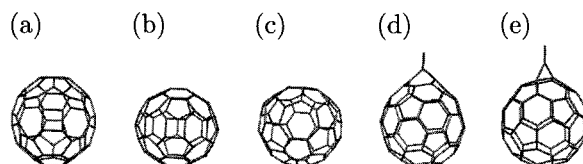


Fig. 1: The optimized structure of C₆₂ isomers:
(a) C₁:7+4; (b) C_{2v}:4mbr; (c) C_s:7mbr; (d) Im1; and (e) Im2.

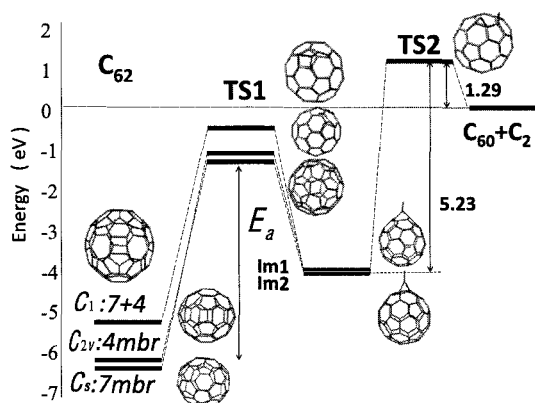


Fig. 2: Energy profile of the reaction C₆₂ → C₆₀ + C₂.

Table 1: Activation energies for the first steps of the C₂ elimination paths.

Initial structure	Activation energy / eV
C ₁ :7+4	4.75
C _{2v} :4mbr	4.85
C _s :7mbr	5.28

[1] E. Osawa *J. Comput. Chem. Jpn.* **10**, A31 (2011).

[2] S. Irlé *et al.*, *J. Phys. Chem. B.* **110**, 14531 (2006).

[3] Y. Cui *et al.*, *J. Phys. Chem. A.* **111**, 7933 (2007).

Tel:+81-75-383-2803,Fax:+81-75-383-2555,

E-mail:tsato@moleng.kyoto-u.ac.jp

One-pot Synthesis of Periconjugated Fullerotriazolium and its Aggregation Behavior

○Naohiko Ikuma, Saori Inaba, Ken Kokubo, Takumi Oshima

Division of Applied Chemistry, Graduate School of Engineering, Osaka University, Suita, Osaka, 565-0871, Japan

Ionic fullerenes are useful for medical applications such as antibacterial and anti-HIV agents, and for self-assembly nanocarbon materials owing to the amphiphilic intermolecular ionic, π/π as well as hydrophobic interactions [1]. For instance, widely investigated fulleropyrrolidinium ion is formally constructed by the methylene-conjunction of quaternary ammonium moiety and the fullerene sphere, and thus the ionic center is almost localized on the nitrogen atom on account of the less favorable hyperconjugation. On the other hand, fullerotriazolium is characterized by the possible high delocalization of positive charge on N_1 - N_2 - N_3 linkage suitable for the periconjugation with fullerene *cis*-1 π -orbital [2]. Hence, fullerotriazolium would exhibit novel self-assembly behavior and biological activity in contrast to the conventional fulleropyrrolidinium.

Here, we report the synthesis and self-assembly of diphenylfullerotriazolium hexafluorophosphate $2^+ \cdot \text{PF}_6^-$. This compound was prepared by the one-pot reaction of *in situ* generated 1,3-diaza-2-azoniaallene salt 1^+ [2] with fullerene (Figure 1a). By a DFT calculation (B3LYP/6-31G*), LUMO of 2^+ was found to expand to the triazolium and fullerene moieties by the periconjugation (Figure 1b). After casting the THF solution of 2^+ on Si-plate, formation of nanocrystal or vesicle was observed by SEM (Figure 1c).

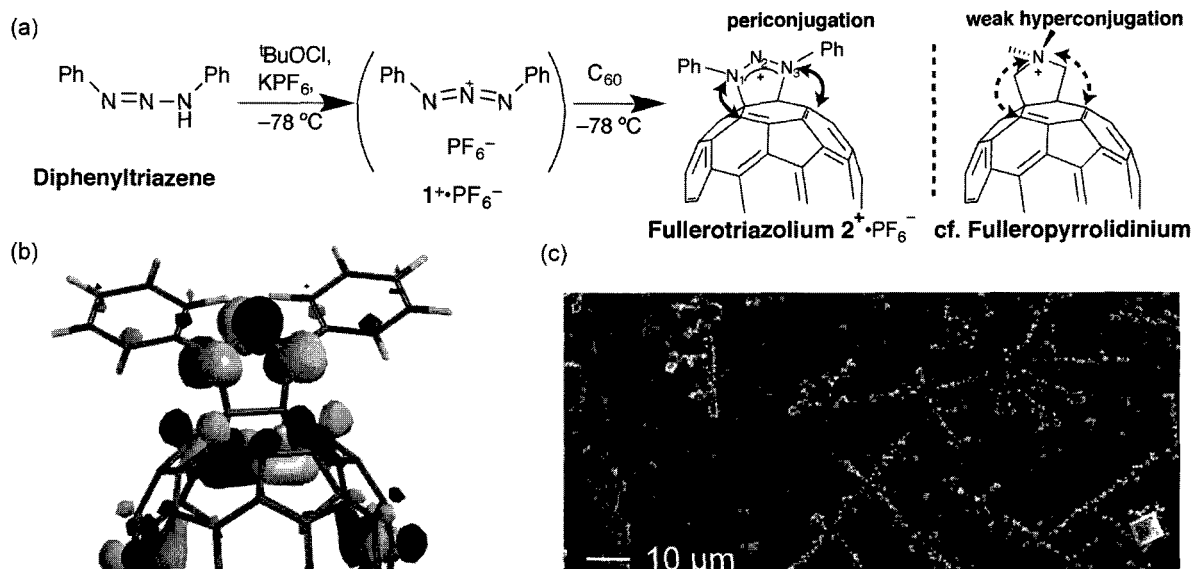


Figure 1

[1] D. M. Guldi, M. Prato *et al.*, *Acc. Chem. Res.*, 2005, **38**, 38.

[2] F. Wudl *et al.*, *Angew. Chem. Int. Ed.*, 1995, **34**, 1591. (b) F. Wudl *et al.*, *J. Am. Chem. Soc.*, 1997, **119**, 9871.

[3] (a) J. C. Jochims *et al.*, *Synthesis*, 1997, **1997**, 233. (b) R. H. Grubbs *et al.*, *Organometallics*, 2011, **30**, 2617.

Corresponding Author: N. Ikuma

Tel&Fax: +81-6-6879-4593,

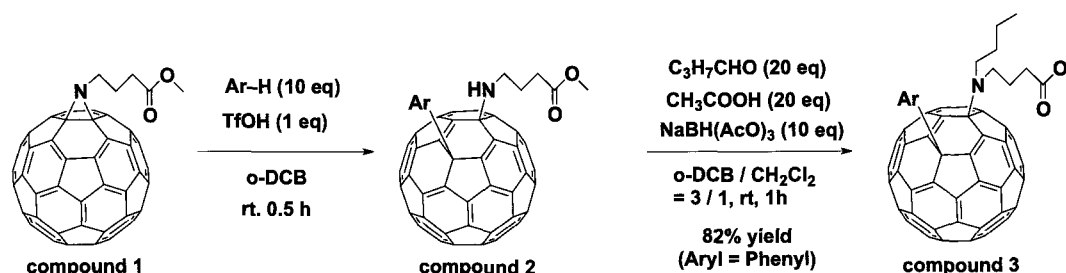
E-mail: ikuma@chem.eng.osaka-u.ac.jp

Synthesis and Properties of 1-Aryl-4-(N-alkylamino)fullerenes

○Tsubasa Mikie*, Akinori Saeki, Naohiko Ikuma, Ken Kokubo, Takumi Oshima, and Shu Seki.

Department of Applied Chemistry, Graduate School of Engineering, Osaka University, 2-1 Yamadaoka, Suita, Osaka 565-0871, Japan

Whilst functionalized fullerene derivatives are the most promising electron acceptor materials in organic photovoltaic devices, only a limited number of fullerene derivatives such as [6,6]-phenyl-C₆₁-butyric acid methyl ester (PC₆₁BM) have been successfully employed. Because most reactions of fullerene C₆₀ have difficulty on the control of reaction condition to inhibit side reaction due to their 30 equivalent double bonds. In order to solve this problem, we have focused on aziridinofullerene containing a basic nitrogen atom and a strained triangular ring, which expects useful synthetic intermediate.¹⁾ Herein, we report the efficient arylation of aziridinofullerene based on Friedel-Crafts reaction to obtain 1,4-asymmetrically-substituted fullerene. The arylation proceeded smoothly on various aromatic nucleophile remaining amino group with excellent yield. Next, we carried out reductive amination of compound **2** (Ar = Ph) with the purpose of the control of solubility and polar.²⁾ The properties and the performances of the photovoltaic devices of compound **2** and **3** are currently in progress.



Scheme 1. Synthesis of 1,4-asymmetrically-substituted fullerene derivatives using acid-triggered reaction and subsequently reductive amination.

[1] M. Nambo, Y. Segawa, K. Itami, *J. Am. Chem. Soc.* **133**, 2402 (2011).

[2] S. Xiao, Y. Li, Y. Li, H. Liu, H. Li, J. Zhuang, Y. Lu, D. Zhang, D. Zhu, *Tetrahedron Lett.*, **45**, 3975 (2004).

Corresponding Author: Shu Seki

Tel: +81-6-6879-4587, Fax: +81-6-6879-4586,

E-mail: seki@chem.eng.osaka-u.ac.jp

Thermal Silylation Reactions of C₆₀ Using Three-membered Ring Organosilicon Compounds

○Daiki Inaba¹, Ryosuke Iida¹, Masahiro Kako¹, Tadashi Hasegawa²,
Yutaka Maeda², Michio Yamada², Takeshi Akasaka³

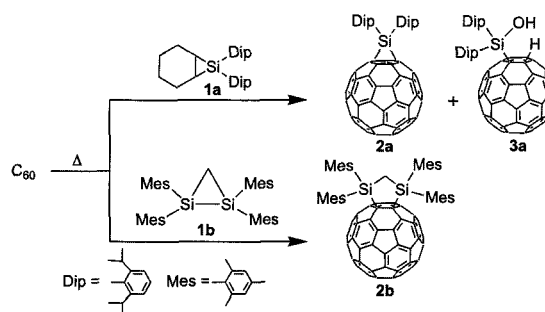
¹Department of Engineering Science, The University of Electro-Communications, Chofu,
Tokyo 182-8585, Japan

²Department of Chemistry, Tokyo Gakugei University, Koganei, Tokyo 184-8501, Japan

³Life Science Center of Tsukuba Advanced Research Alliance, University of Tsukuba,
Tsukuba, Ibaraki, 305-8577, Japan

Chemical derivatization of fullerenes has been developed as useful tools to modify the physical and chemical properties of fullerenes for various applications such as molecular electronics. It has been demonstrated that exohedral functionalization using electropositive silicon-based groups induces remarkable changes in the electronic characteristics of hollow fullerenes and endohedral metallofullerenes. The photoreactions of fullerenes with reactive organosilicon compounds such as silylenes, disiliranes, silyl radicals, and siliranes proceeded readily to afford the corresponding silylated fullerene derivatives. In those cases, electrochemical analyses and theoretical calculations confirmed the negatively charged electronic structures of the cages. However, ultraviolet irradiation, and nucleophilic addition of silyl anion reagents have been long employed for silylation of C₆₀ and C₇₀. For the synthesis of silylated fullerenes that are labile under photolytic or anionic conditions, it is worthwhile to develop alternative and convenient procedures without lights or organometallic reagents. Recently, bis-silylation and carbosilylation of endohedral metallofullerenes have been accomplished by thermal additions of disiliranes [1] and siliranes [2], respectively. Moreover, thermally generated silylenes have been found to be applicable for the mono-silylation of Lu₃N@I_h-C₈₀ [3]. These results naturally prompted us to investigate the thermolysis of siliranes and disiliranes with C₆₀ for alternative silylation procedures. We now report the thermal reactions of C₆₀ with siliranes and disiliranes, providing the examples of formal [2+3] cycloaddition and silylene addition to C₆₀ under thermolytic conditions.

When a toluene solution of C₆₀ and silirane **1a** was heated at 110°C for 40h, a silylated product **2a** and hydrosilylated product **3a** were obtained in 30 % and 2 % yields, respectively. In a similar procedure, the reaction of disilirane **1b** and C₆₀ afforded the corresponding bis-silylated adduct **2b** in 12 % yield. The details of the properties of silylated derivatives obtained will be also presented.



Scheme 1.

[1] Y. Iiduka *et al.* J. Am. Chem. Soc. **127**, 9956 (2005).

[2] M. Yamada *et al.* J. Am. Chem. Soc. **132**, 17953 (2010).

[3] K. Sato *et al.* J. Am. Chem. Soc. **134**, 16033 (2012).

Corresponding Author: M. Kako Tel: +81-42-442-5570

E-mail: kako@e-one.uec.ac.jp

The density functional theory (DFT) calculations of $\text{Sc}_2\text{C}_2@\text{C}_{82}$

○Yuma Seino, Takahiro Hinoishi, Hajime Yagi, Miyazaki Takafumi, Shojun Hino

Department of Materials Science and Biotechnology, Graduate School of Science and Engineering, Ehime University, Matsuyama 790-8577, Japan

[Introduction] Electron transfer from the entrapped metal atom(s) to the fullerene cage takes place in endohedral metallofullerenes. They could be used as molecular memories or molecular electronic devices when the amounts of transferred electrons can be controlled. Combination of the theoretical calculation and ultraviolet photoelectron spectrum (UPS) measurements is one of the effective methods to estimate the amounts of transferred electrons. We present the DFT calculation of $\text{C}_{2v}\text{-Sc}_2\text{C}_2@\text{C}_{82}$ and discussed its molecular geometry in conjunction with the UPS.

[Calculations] DFT calculations were performed using Gaussian 09 program module at the B3LYP level. After placing the Sc_2C_2 cluster in the $\text{C}_{2v}\text{-C}_{82}$ cage its geometry was optimized. Then Kohn-Sham orbital energies of the optimized geometry were calculated using the DZP basis set for carbon atoms and TZP sets for scandium atoms.

[Results and discussion] Geometry optimization yielded three different structures (Isomers 1 to 3). The most stable structure was Isomer 1. Other structures, Isomer 2 and 3 were less stable by +4.04 kcal/mol and +16.0 kcal/mol, respectively. Their simulated spectra (SS) obtained by broadening the K.S energies with Gaussian functions and the UPS of $\text{Sc}_2\text{C}_2@\text{C}_{82}$ are shown in Fig.1. The SS of Isomer 1 reproduced the UPS of $\text{Sc}_2\text{C}_2@\text{C}_{82}$ very well, and that of Isomer 2 gave reasonably good correspondence. The SS of Isomer 3 showed poor correspondence. Comparison between the SS and the UPS is favor to Isomer 1 as the actual geometry of $\text{Sc}_2\text{C}_2@\text{C}_{82}$. However, small formation energy difference and reasonably good correspondence of SS of Isomer 2 cannot completely deny the possibility that $\text{Sc}_2\text{C}_2@\text{C}_{82}$ takes the structure of Isomer 2. The calculation suggests that the amounts of transferred electrons were 4.

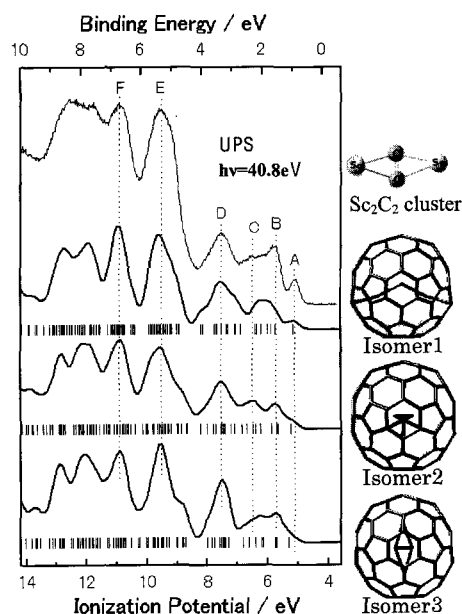


Fig. 1 UPS obtained by He II and the SS of Isomer 1-3 structures

Corresponding Author: S. Hino Tel: 089-927-9924 E-mail: hino.shojun.mk@ehime-u.ac.jp

Photoelectron spectroscopy of $\text{Er}_3\text{N@C}_{80}$

○Takahiro Hinoishi¹, Yuma Seino¹, Hajime Yagi¹, Takafumi Miyazaki¹,
Tatsuhiko Nishi², Hisanori Shinohara³, Shojun Hino¹

¹Graduate School of Science and Engineering, Ehime University ²Institutes for Molecular Science, Okazaki ³Graduate School of Science, Nagoya University

[Introduction] While stable structure of C_{80} is $(80 : 2)$ after the nomenclature of Fowler and Manolopoulos, namely D_2 symmetry, stable structure of trimetal nitride fullerenes $\text{M}_3\text{N@C}_{80}$ is $(80 : 7)$ is I_h symmetry. One of the reasons why the structures of empty and endohedral fullerenes are different can be the electron transfer from the entrapped atoms to the cage. Electron transfer seems to play an important role in the formation of endohedral fullerenes. We will present the UPS and XPS of $\text{Er}_3\text{N@C}_{80}$ and discuss the electronic structure and electron transfer in it.

[Experimental] UPS was measured at the beamline 8B of UVSOR of IMS. MgK α XPS was measured with a SCIENTA SES 100 electron energy analyzer equipped with a Thermo Electron XR3 X-ray gun.

[Results and Discussion] Fig. 1 shows the UPS of $\text{Er}_3\text{N@C}_{80}$ and $\text{Gd}_3\text{N@C}_{80} - (I_h)$ obtained with $h\nu = 40$ eV photon. Both UPS resembles each other, which suggests that $\text{Er}_3\text{N@C}_{80}$ has I_h symmetry as $\text{Gd}_3\text{N@C}_{80}$. Minute differences between these UPS can be attributed to the energy difference of the MO's to which electrons from the entrapped metal atoms are to be situated.

Fig. 2 shows the XPS of the Er4d level of $\text{Er}_3\text{N@C}_{80}$ as well as those of erbium metal and Er_2O_3 . The Er4d_{5/2} level of $\text{Er}_3\text{N@C}_{80}$, Er and Er_2O_3 appeared at 169.4, 167.6 and 170.1 eV, respectively. Since the Er4d_{5/2} of $\text{Er}_3\text{N@C}_{80}$ appeared between those of Er^0 and Er^{+3} , the oxidation state of Er atoms in the C_{80} cage must be between 0 and +3. Assuming the linear relation between the oxidation state and the Er4d_{5/2} level binding energy, the oxidation state of entrapped Er might be +2. That is, $(\text{Er}_3\text{N})^{6+}\text{@C}_{80}^{6-}$ is the possible electron configuration.

Corresponding Author: S. Hino Tel: 089-927-9924 E-mail:hino.shojun.mk@ehime-u.ac.jp

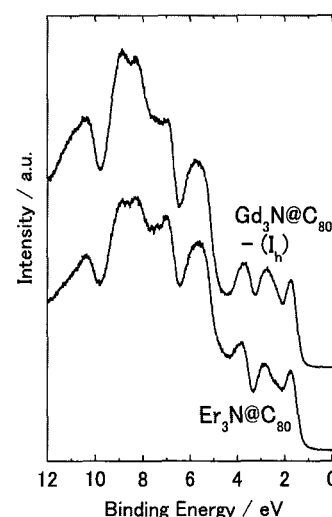


Fig. 1 The UPS of $\text{Er}_3\text{N@C}_{80}$ and $\text{Gd}_3\text{N@C}_{80} - (I_h)$

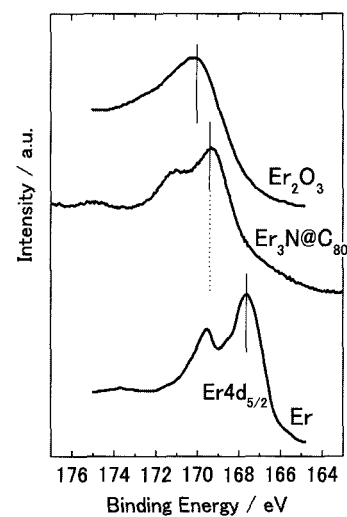


Fig. 2 The XPS Er4d core level of pure erbium, $\text{Er}_3\text{N@C}_{80}$ and Er_2O_3

Definite molecular structures of $M@C_{2v}(9)-C_{82}$ ($M = Sc, Y, \text{ and } Ce$)

○Mitsuaki Suzuki,^{1,2,3} Zdenek Slanina,^{3,4} Naomi Mizorogi,³ Xing Lu,^{3,5} Michio Yamada,² Yutaka Maeda,² Tadashi Hasegawa,² Shigeru Nagase,⁶ Marilyn M. Olmstead,⁷ Alan L. Balch,⁷ and Takeshi Akasaka^{1,2,3,5}

¹ *Foundation for Advancement of International Science, Ibaraki 305-0821, Japan*

² *Department of Chemistry, Tokyo Gakugei University, Tokyo 184-8501, Japan*

³ *Life Science Center of Tsukuba Advanced Research Alliance, University of Tsukuba, Ibaraki 305-8577, Japan*

⁴ *Department of Chemistry and Biochemistry, National Chung-Cheng University, Chia-Yi 62117, Taiwan – ROC*

⁵ *School of Materials Science and Engineering, Huazhong University of Science and Technology, Wuhan 430074, China*

⁶ *Fukui Institute for Fundamental Chemistry, Kyoto University, Kyoto 606-8103, Japan*

⁷ *Department of Chemistry, University of California, Davis, California 95616, United States*

Endohedral metallofullerenes (EMFs) have special properties and structures because of the electron transfer from encapsulated species (metal-atom, metallic cluster, etc.) to fullerene cages. $M@C_{2v}(9)-C_{82}$ ($M = Sc, Y, \text{ or lanthanide}$) are the most abundantly extracted as representative monometallic EMFs. The molecular structures of $M@C_{2v}(9)-C_{82}$ were initially predicted by theoretical calculation.^[1] Experimentally, the cage structures of $M@C_{2v}(9)-C_{82}$ have been determined by ¹³C NMR spectroscopy.^[2] However, such ¹³C NMR studies could not show the metal-atom positions. To reveal the metal-atom positions, single-crystal X-ray structure analyses of EMF derivatives have been performed because such derivatized forms tend to crystallize more easily than pristine forms.^[3] However, we should notice that the metal-atom positions could be affected by the chemical modification of the outer surface. In this context, single-crystal X-ray structure analysis of pristine EMFs is of particular importance. The cocrystallization with Ni^{II}(OEP) (OEP = octaethylporphyrin) is an alternative solution to provide more accurate information relating to the pristine structures of EMFs.

This poster describes a systematic single-crystal X-ray structure analysis of the molecular structures of three $M@C_{82}$ -EMFs, i.e. $Sc@C_{2v}(9)-C_{82}$, $Y@C_{2v}(9)-C_{82}$, and $Ce@C_{2v}(9)-C_{82}$, through cocrystallization with Ni^{II}(OEP), providing new insights into metal–cage interactions in monometallic EMFs.

References

- [1] K. Kobayashi *et al. Chem. Phys. Lett.* 282, 325 (1998).
 [2] (a) T. Akasaka *et al. J. Am. Chem. Soc.* 122, 9316 (2000). (b) T. Akasaka *et al. J. Phys. Chem. B* 105, 2971 (2001). (c) L. Feng *et al. Chem. Phys. Lett.* 405, 274 (2005). (d) T. Wakahara *et al. J. Am. Chem. Soc.* 126, 4883 (2004). (e) T. Wakahara *et al. Chem. Phys. Lett.* 360, 235 (2002).
 [3] (a) M. Hachiya *et al. J. Am. Chem. Soc.* 134, 15550 (2012). (b) X. Lu *et al. J. Am. Chem. Soc.* 131, 12066 (2009). (c) Y. Takano *et al. J. Am. Chem. Soc.* 131, 9340 (2009). (d) T. Akasaka, *et al. J. Am. Chem. Soc.* 130, 12840 (2008). (e) Y. Maeda *et al. J. Am. Chem. Soc.* 126, 6858 (2004).

Corresponding Author: T. Akasaka

Tel: +81-42-329-7512, Fax: +81-42-329-7512,

E-mail: akasaka@fais.or.jp

Synthesis of new $[\text{Li}^+@C_{60}]$ salts for improved solubility

○Hiroshi Okada, Yutaka Matsuo

¹ *Department of Chemistry, School of Science, The University of Tokyo, Tokyo, 113-0033, Japan*

Good solubility of materials is one of the prerequisites for application of solution-processable organic semiconductor devices such as organic thin film photovoltaics. Chemical modification and introduction of solubilizing groups are common method to prepare materials having high solubility. Recently, we synthesized Li^+ -endohedral fullerene $[\text{Li}^+@\text{PCBM}]$ ([6,6]-phenyl- C_{61} -butyric acid methyl ester) and observed improved solubility from pristine $[\text{Li}^+@C_{60}]\text{PF}_6^-$.

One of peculiarities of $[\text{Li}^+@C_{60}]$ is its ionic character. Solubilities of ionic materials depend heavily on their counter ions. We tried to improve the solubility of $[\text{Li}^+@C_{60}]$ salt by counter-anion exchange.

Anion exchange of $[\text{Li}^+@C_{60}]\text{PF}_6^-$ was successfully achieved to produce new $[\text{Li}^+@C_{60}]$ salts having OTf^- (trifluoromethanesulfonate), NTf_2^- (bis(trifluoromethylsulfonyl)imide), and TFPB^- (tetrakis{3,5-bis(trifluoromethyl)phenyl}borate, $\{3,5-(\text{CF}_3)_2\text{C}_6\text{H}_3\}_4\text{B}$) as counter anions. These salts had 2- to 10-fold solubility of $[\text{Li}^+@C_{60}]\text{PF}_6^-$. X-ray crystal structure analysis was performed for the TFPB salt, which revealed that the cationic $[\text{Li}^+@C_{60}]$ part was surrounded by six TFPB⁻ anions (Figure 1). Bulkiness of the TFPB⁻ anion increased inter-fullerenes and cation-anion distances. These structural features contributed toward improving the solubility of this ionic compound. Based on these results, further molecular design of soluble endohedral [60]fullerenes containing Li^+ can be performed for application to various solution-processed devices.

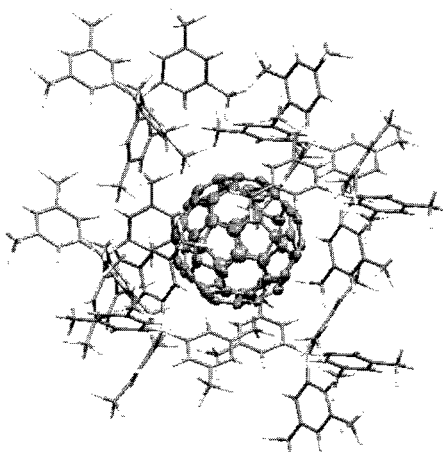


Figure 1. $[\text{Li}^+@C_{60}]$ surrounded by six large TFPB anions

[1] Y. Matsuo *et al. Org. Lett.* **2012**, *14*, 3784–3787.

Corresponding Author: H. Okada

Tel: +81-3-5841-1371, Fax: +81-3-5841-1371

E-mail: h_okada@chem.s.u-tokyo.ac.jp

Solid State Lithium NMR Studies on Complexes Composed of Lithium and C₆₀ Fullerene

○Tomoaki Endo¹, Shin-ichiro Yoshida², Ken-ichiro Komatsu³, Kazuhiko Kawachi³,
Yasuhiko Kasama³, Eunsang Kwon²

¹*Sendai National College of Technology, Natori 981-1239, Japan*

²*Research and Analytical center for Giant Molecules, Graduate School of Science,
Tohoku University, Sendai 980-8578, Japan*

³*Idea International Co. Ltd., Sendai 981-0922, Japan*

Lithium clusters circumscribed by fullerene would be shaped during the formation process of the lithium ion-encapsulated fullerene (Li⁺@C₆₀) by the low energy ion bombardment method [1]. Recently, applying to the lithium plasma radiation to vaporized fullerene, it is possible to produce a large scale production of Li⁺@C₆₀ [2] and it was prepared to Li⁺@C₆₀ salt using chemical treatment. We need to elucidate that the cluster not only form the view point of scientific research but also aspects of engineering. In this study, we investigate the lithium clusters using ⁷Li solid state NMR spectroscopy.

The chemical shifts of lithium clusters circumscribed by fullerene have four different values at under LiCl standard. To elucidate the lithium and fullerene cluster structure corresponding to those chemical shifts, we have to understand the basic nature of chemical shift of lithium nuclei, which the case means lithium atom exist in the outside of fullerene cage or inside of fullerene cage and how the lithium atom attached with fullerene.

In the case of lithium ion-encapsulated fullerene, the chemical shift of lithium nuclei was observed high field shift (about 10ppm)[3]. On the other hand, the chemical shifts of lithium nuclei of simple complex of lithium and fullerene have not made clear. To measure such chemical shifts, we synthesized lithium and fullerene complexes to fix the ratio of lithium and fullerene [4].

The exact chemical shift values are now measuring. To compare those chemical shifts, it will achieve a complete understanding of lithium clusters circumscribed by fullerene. Those of knowledge may become an important key to prepare a large scale Li⁺@C₆₀ preparation. The result of ⁷Li solid state NMR study will be presented.

[1] "Production and LDMS characterisation of endohedral alkali-fullerene films", E.E.B. Campbell, R. Tellgmann, N. Krawez, I.V. Hertel, J. of Phys. and Chem. of Solids, **58**, 1763-1769 (1997).

[2] S. Aoyagi *et al.* Nature. Chem. **2**, 678 (2010).

[3] E.Kwon *et al.* FNTG-43 予稿集 (2013).

[4] S. N. Titova *et al.* Physics of the Solid State. **123**, 456 (2011).

Corresponding Author: T. Endo

Tel: +81-22-291-7410, Fax: +81-22-291-7410,

E-mail: tendo@sendai-nct.ac.jp

Preparation and Properties of Surface Modified Graphene Oxide by Grafting of Polymers

○Tetsuo Sumiyoshi¹, Kazuhiro Nagata¹, Yusuke Yagi¹, Kazuhiro Fujiki²,
Takeshi Yamauchi¹, Norio Tsubokawa¹

¹ *Graduate School of Science and Technology, Niigata University, 8050, Ikarashi 2-no-cho,
Nishi-ku, Niigata 950-2181, Japan*

² *Department of Environmental Science, Niigata Institute of Technology, 1719, Fujihashi,
Kashiwazaki, Niigata 945-1195, Japan*

We have reported that nanocarbons, such as carbon black, fullerene and carbon nanotubes, act as a strong radical scavenger [1]. Therefore, when these nanocarbons are reacted with azo-polymers, polymer radicals formed by the thermal decomposition of the azo-polymer were grafted onto these carbon material surfaces. In addition, we have reported that ligand-exchange reaction of polymers bearing ferrocene moieties with polycondensed aromatic rings of nanocarbons, such as carbon black, carbon nanotube, and nano-diamond, successfully proceeded to give polymer-grafted nanocarbons [1].

In this paper, grafting of polymers onto graphene oxide (GO) by polymer radical trapping and ligand-exchange reaction was investigated to improve the dispersibility of GO in solvents.

The grafting of polymers, such as hydrophilic poly(ethylene oxide) was successfully grafted onto GO by radical trapping of the corresponding polymers formed by the thermal decomposition of the azo-polymer, which contains azo groups in the main chain: the percentage of grafting (weight percent of grafted polymer to GO) was determined to be 10-15%. In addition, the effect of molecular weight of azo-polymers on the grafting was investigated. As a result, it was found that the percentage of grafting onto GO decreased with increasing molecular weight of azo-polymers. The results suggest that steric hindrance of polymer to the surface increased with increasing molecular weight of polymer radicals.

The grafting of polymers onto GO was also achieved by a ligand-exchange reaction of ferrocene moieties of copolymers, poly(vinyl ferrocene-*co*-methyl methacrylate) (poly(Vf-*co*-MMA)) and poly(Vf-*co*-styrene) with polycondensed aromatic rings of GO in the presence of AlCl₃ and Al powder as catalysts: the percentage of grafting of poly(Vf-*co*-MMA) and poly(Vf-*co*-styrene) was determined to be 54.2% and 61.1%, respectively. On the contrary, no grafting of polymer was observed in the absence of catalysts. The grating of polymers onto GO was confirmed by FT-IR, thermal decomposed gas GC-MS, and TGA.

The dispersibility in solvents was investigated. The dispersion of untreated GO in organic solvents completely precipitated immediately, but poly(ethylene glycol)-grafted GO gave a stable dispersion in THF and water. On the other hand, poly(Vf-*co*-MMA)-grafted and poly(Vf-*co*-styrene)-grafted GO readily dispersed in organic solvents, such as toluene: no precipitation of GO was observed even after one month.

Acknowledgement: This study was supported in partly by a Grant in Aid for Scientific Research form Ministry of Education, Culture, Sports, Science and Technology of Japan (No. 24560836).

[1] N. Tsubokawa, Polym. J., Polym. J. **39**, 938 (2007).

Corresponding Author: N. Tsubokawa

Tel: +81-25-262-6779, Fax: +81-25-262-6779

E-mail: ntsuboka@eng.niigata-u.ac.jp

Hybrid Graphene –Titanium Surface for Sensing Applications

○Yousuke Kakimi, Gemma Rius, Osamu Eryu

Nagoya Institute of Technology, Gokiso, Showa, Nagoya 466-8555, Japan

The use of graphene for sensing applications is among the feasible examples of nanodevices and nanostructured surfaces benefiting from the introduction of graphene as a key functional element [1]. As graphene is very stable electrically and mechanically it guarantees the sensor operation reliability. Its chemical sensitivity to the local environment (liquid and gas) makes graphene an ideal large surface area transducer, with potential for beating sensing detection limits, and may contribute to a faster response. Selectivity can be tuned additionally by using growth of hierarchical nanostructures on graphene [2]. Hybrid nanostructures, such as flexible biochemical and pressure sensors, emission devices and battery electrodes based in graphene have already shown remarkable performance [3]. We propose a capacitive sensor based on a compound interface consisting of ultraflat pure Ti decorated with graphene.

For the device construction we are working in, 1) the development of a polishing technique for obtaining a very flat surface of ultrapure Ti, and 2) optimization of the transfer of graphene onto the target Ti support. An example of Raman scattering characterization of graphene, synthesized by CVD on a Cu foil and transferred onto Ti foil is shown in Figure 1, left. Transfer has been successfully performed using PMMA-assisting media, but establishing a direct transfer processing is under consideration.

As the study of the sensor device is still in its early stage of technology development, we complement the conventional characterization of the graphene growth products and its transfer efficiency and quality - typically done by SEM and Raman spectroscopy - for example, with the assessment of contact angle measurements. Contact angle measurements would assist the understanding of both the status of the surface (polishing) and pre-transfer heat annealing (Figure 1, Right), as well as the graphene transfer process. The wettability is highly determined by the roughness of the surface and distinctive hydrophobicity - hydrophilicity of each material [4]. Also wettability can play a dominant role applied to the chemical sensor performance. In brief, the present work aims developing graphene-based surfaces on versatile substrates using simple or simplified fabrication routes.

[1] Q. He , S. Wu , Z. Yin and H. Zhang. *Chem. Sci.* **3**, 1764 (2012).

[2] A. Gutés *et al.* *Nanoscale* **4**, 438 (2012).

[3] M. Arif, K. Heo, B. Y. Lee, J. Lee, D. H. Seo, S. Seo, J. Jian, S. Hong. *Nanotechnology* **22**, 355709 (2011).

[4] J. Grodzka, A. Pomianowski. *Physicochemical Prob. Min. Proc.* **40**, 5 (2006).

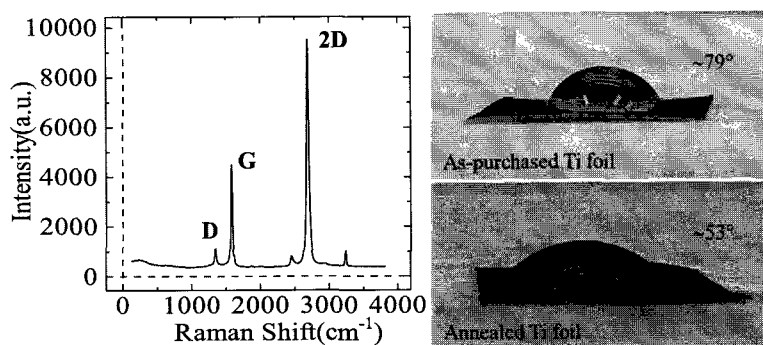


Figure 1. (Left) Raman scattering spectrum of graphene transferred onto a Ti foil, grown by CVD at 950 °C using CH₄ as the carbon precursor. (Right) Contact angles for as-purchased Ti foil (upper image) and heat annealed Ti foil (bottom image).

Corresponding Author: Y. Kakimi
Tel: +81-52-735-5909
E-mail: cjk19508@stn.nitech.ac.jp

Substrate effects on chemical doping of graphene in tris buffer

Katsuya Masuda, ◯Masahito Sano

*Department of Polymer Science and Engineering, Yamagata University
Yonezawa, Yamagata 992-8510, Japan*

Nano-carbon materials based on hexagonal structures can be both electron- and hole-doped easily by either external electric fields or chemical compounds. Unlike carbon nanotubes, which can be nearly isolated by standing freely on a solid surface or suspended in solution, graphene often requires a solid substrate to be held, with one face almost completely in contact with the solid surface. This implies that graphene is more susceptible to substrate effects. It becomes serious with chemical doping, since the doping level cannot be tuned like an external electric field and the compound itself may interact with the substrate.

Graphene offers an excellent platform for biochemical studies, for its atomic flatness, chemical inertness, and simple van der Waals adsorption. In many studies, tris is often used as buffer to control solution pH. Previously, we have shown that single-walled carbon nanotubes dispersed in tris buffer are electron-doped by tris molecules [1]. The doping level is so significant that the doped nanotubes reduce cytochrome c by simply mixing in the solution. Thus, it is important to know the doping behavior of graphene in tris buffer, especially any dependences on the substrate that the graphene is held.

Raman microscopy was used to follow the chemical doping of a particular graphene flake. A single layer graphene was produced by the mechanical method using HOPG. All graphene samples had a single Lorentzian 2D band and the 2D/G intensity ratios around 3-4 in air. After the microscope was fixed on a particular graphene, pure water was added to confirm the absence of contaminants that might dope graphene without tris, followed by tris buffers with increasing concentrations. Figure 1 shows a result of 2D band shifts for eight independent samples, each on a different oxidized silicon substrate. Whereas some samples are hardly affected by tris, others react unpredictably. Similar results were observed on 2D FWHM as well as those of G band. Thus, the commonly used oxidized silicone is not a suitable substrate for biochemical studies. We will discuss the similar experiments using polymers as substrate.

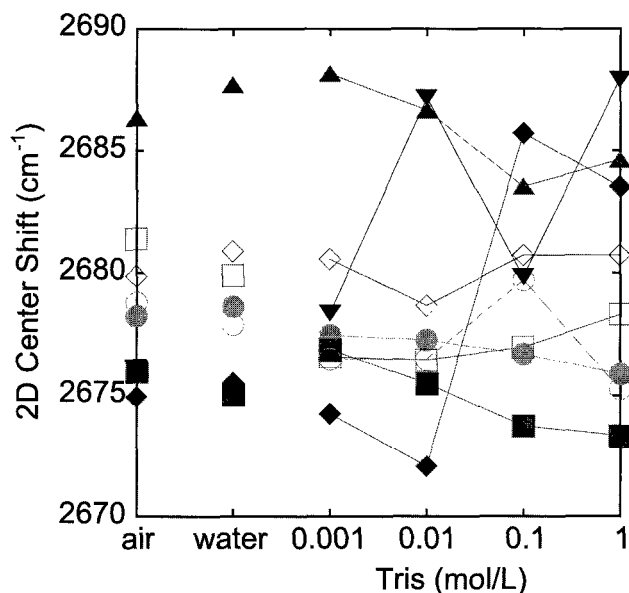


Figure 1. Raman 2D shift of the same graphene in air, in water, and in tris buffer. 8 different samples are plotted.

[1] T. Nakashima, M. Sano, *J. Phys. Chem. C* **115**, 20931 (2011).

Corresponding Author: M. Sano

Tel: +81-238-26-3072

E-mail: mass@yz.yamagata-u.ac.jp

Anomalous behavior of Raman signals from carbon nanotube-graphene hybrid structures

○T. Kusumoto, H. Kokame, R. Negishi, and Y. Kobayashi

Department of Applied Physics, Osaka University, Suita, 565-0871, Japan

Graphene and single-walled carbon nanotubes (SWCNTs) are low-dimensional nanocarbon materials which have attracted great attention for their extraordinary physical properties and potential applications. Recently, research activities on hybridizing SWCNT and graphene are widely stimulated in order to improve their physical performance for these applications [1]. We have reported the growth of metal-free SWCNTs from nanodiamond nuclei and the formation of graphene by efficient structural restoration of graphene oxides (GOs) under the condition of chemical vapor deposition (CVD) [2]. In this work, we fabricate the hybrid structures of SWCNT and graphene and analyze their structures by Raman spectroscopy.

The hybrid structures were fabricated by the CVD treatments of GOs deposited on SWCNT films grown from nanodiamonds. Figure 1 shows SEM images of the hybrid structures, in which the reduced GO (=graphene) flakes are observed as dark regions, and the SWCNT films as bright networks. Close view of their boundary indicates that the SWCNT networks are tightly coupled with a reduced GO flake. The strong interaction between SWCNT and graphene is also indicated in Raman spectra as distinct variation in the radial breathing mode (RBM) signals. As shown in Fig. 2, the RBM signals, which are observed from SWCNT films without GO overlayers (Fig.2(a)) completely disappear in the spectrum from SWCNT-graphene hybrids treated under the CVD conditions with ethanol vapor (Fig.2(e)). G peak shape and D to G peak intensity ratio observed from SWCNT-graphene hybrids correspond to the combined spectra of SWCNT and rGO (Fig.2(d)). This means that drastic change of the RBM signal intensities should not be caused by shift of resonance condition in Raman scattering, but by specific interaction between graphene sheets of SWCNTs and reduced GO flakes. Additionally, sheet resistance of the SWCNT-graphene hybrid films was significantly improved due to a low contact resistance via the interactions. These findings indicate that the hybrid structures are quite promising approach for the application of nanocarbons as electronic materials.

[1] M. Zhao et al., ACS Nano 6(2012)10759, D. D. Nguyen et al., Nanoscale 4(2012)632 and refs. therein.

[2] D. Takagi, Y. Kobayashi, Y. Homma, J. Am. Chem. Soc., 131(2009)6922; R. Negishi et al., Int. Conf. Solid State Devices and Materials, C-4-4, 2012.9.25-27, Kyoto.

Corresponding Author: T. Kusumoto

Tel: +81-6-6879-7833, Fax: +81-6-6879-7863,

E-mail: kusumoto@ap.eng.osaka-u.ac.jp

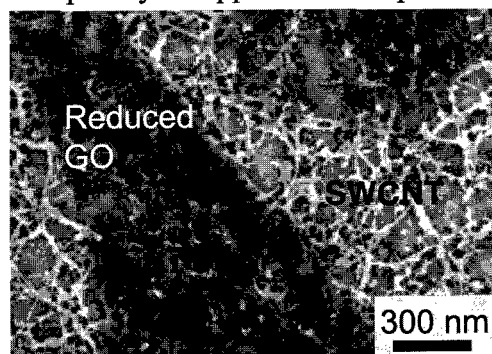


Fig.1 SEM images of SWCNT-graphene (reduced GO) hybrid structures.

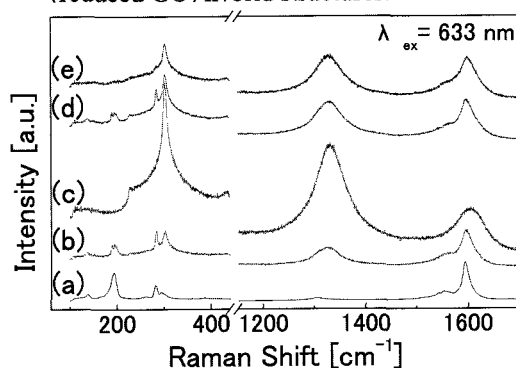


Fig.2 Raman spectra observed from (a)SWCNT, (b)SWCNT after reduction, (c)rGO, (d)combined spectra of SWCNT and rGO, (e)SWCNT/rGO hybrid structure

Synthesis and characterization of Pt-Ru nanoparticles on carbon nanosheets by one-step electrodeposition

o¹Shohei Hayase, ¹Haruhiko Yoshitake, ²Wang Zhipeng ^{1,3}Hironori Ogata

¹ *Department of Chemical Science and Technology, Hosei University Koganei 184-8584 Japan*

² *Institution for Sustainability Research and Education, Shinshu University Nagano 380-8553, Japan*

³ *Research Center for Micro-Nano Technology, Hosei University, Koganei 184-0003, Japan*

Direct methanol fuel cells (DMFCs) are one of the most promising have attracted great attention. The basic operation principle of DMFCs involves methanol oxidation and oxygen reduction on the precious metal catalysts, which are loaded on the support surfaces. As is well-known, the dispersion of Pt-based alloys on carbon supports as well as catalyst particle size and shape plays a dominant role in the electrochemical performance for fuel cells. In this study, we explore the carbon nanosheets (CNSs) by microwave plasma-enhanced chemical vapor deposition (MPECVD) method as a catalyst support for Pt-based nanoparticles by one-step electrodeposition. The morphology, microstructure, chemical composition, and electrochemical properties of the CNS-supported Pt-based nanoparticles were investigated.

CNS films were deposited on Cu substrates by 2.45 GHz MPECVD method. The microwave power, base pressure, working pressure, reaction time, initial temperature are 900 W, 23 mTorr, 380 mTorr, 60 min., 400°C, respectively. A mixture of CH₄(2.5sccm)-Ar(20sccm) was used as the source gas. After deposition, CNS film was peeled from Cu substrate. Then, the cleaned Pt electrode with some ethanol on its surface was covered completely by the as-synthesized CNS film. Finally, the CNSs-modified Pt electrode was dried by a 150 W halogen lamp for 10 min. Electrodeposition of Pt-Ru on modified Pt electrodes was prepared according to a one-step process. Cyclic voltammetry was carried out in an electrolyte solution including 5 mM K₂RuCl₆, 5mM K₂PtCl₆ and 0.5 M H₂SO₄ above the potential from -0.25 to 0.4 V with a scan rate of 50 mV s⁻¹ for 10 cycles.

Figure.1 shows the TEM images of CNSs after electrodeposition. The detailed results on the relationship between the condition of electrodeposition, the chemical composition of nanoparticles and their electrocatalytic performance for methanol oxidation will be presented.

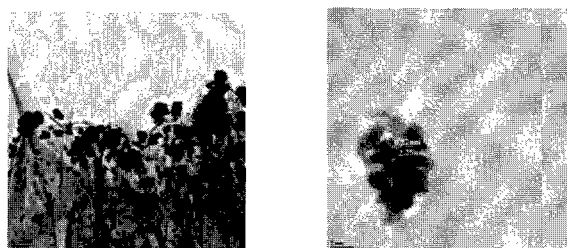


Figure 1. TEM images of Pt-Ru/CNSs.

1) Zhipeng Wang, Mao Shoji and Hironori Ogata, *Appl. Surf. Sci.*259(2012)219-224.

Corresponding Author: Hironori Ogata,

Tel: +81-42-387-6229, Fax: +81-42-387-6229, E-mail: hogata@hosei.ac.jp

Suppressed mobility degradation in large-area graphene oxide films by alcohol vapor treatments

°M. Matsuzaki¹, R. Negishi¹, Y. Ohno², K. Maehashi², K. Matsumoto², Y. Kobayashi¹
¹*Department of applied physics, Osaka University, 2-1 Yamadaoka Suita 565-0871, Japan*
²*ISIR, Osaka University, 8-1 Mihogaoka, Ibaraki 567-0047, Japan*

Reduced graphene oxide (rGO) is one of the promising candidates for the scalable integration of the graphene-based field effect transistors (FETs) toward the device applications such as biosensor. However, the electrical performance of GO thin film such as carrier mobility is insufficient, considering intrinsic properties of graphene, due to the carrier scattering at the interface between the GO flakes [1] and defects created by oxidation process. In this work, we find that the reduction and restoration of GO using alcohol vapor treatment is good for the suppression of carrier scattering at the interface between GO flakes from analyzing the channel-length (L_c) dependence of carrier mobility in the rGO-FET.

GO (Graphene Lab. Inc.) thin films on SiO₂ (290 nm)/Si substrate, were prepared by spin-coating method, and FETs were fabricated by conventional lithography techniques. Reduction of GO thin film was carried out under alcohol vapor and Ar/H₂ (3%) annealing.

Figure 1 shows the L_c dependence of carrier mobility in the rGO-FETs prepared by Ar/H₂ annealing (■) and alcohol vapor (ACV) treatment (●). We confirmed that the average size of single graphene flake is $\sim 1\mu\text{m}$ by atomic force microscopy. Therefore, when the L_c is longer than $\sim 1\mu\text{m}$ (shorter than $\sim 1\mu\text{m}$), the carrier transport properties reflect multiple flakes (single flake). For the single flake region ($L_c < \sim 1\mu\text{m}$), the carrier mobilities in the rGO-FETs by Ar/H₂ annealing and ACV treatment are ~ 0.4 and $6.3\text{ cm}^2/\text{Vs}$, respectively. The improving carrier mobility indicates that the π -electron system is recovered due to the restoration of graphitic structure in a single flake by ACV treatment. The most remarkable feature is that the carrier mobilities in the rGO-FETs prepared by ACV treatment show an almost constant value between single and multiple regions. It has reported that the carrier mobility with the GO thin films prepared by usual reduction process such as hydrazine vapor soaking without carbon feedstock dramatically drops due to the carrier scattering at the interface between GO flakes when L_c is over a single GO flake size [1]. Actually, the carrier mobility in the rGO-FETs prepared by Ar/H₂ annealing deteriorates at multiple GO flakes region as indicated by arrow in Fig. 1. On the other hand, from the fact that the carrier mobility in the rGO-FETs prepared by ACV treatment is independent of L_c , it is considered that the ACV treatment has an effect of suppressing the carrier scattering at the interface between the GO flakes. It means that the restoration of graphitic structure in each GO flake by ACV treatment promotes π - π stacking interaction between GO flakes and/or activated dangling bonds at edge sites of GO flake combine with another GO flake, and these lead to reducing the barrier height between GO flakes. This result indicates that rGO thin films prepared by ACV behave as if they are large single graphene flake.

[1] T. Kobayashi, et al., Small 6(2010)1210.

Corresponding Author: M. Matsuzaki
 E-mail: negishi@ap.eng.osaka-u.ac.jp

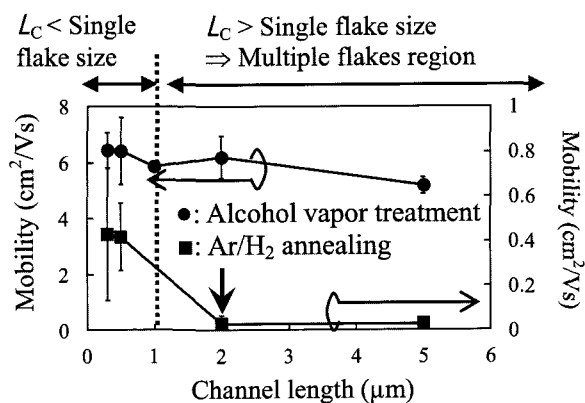


Fig. 1 Channel length (L_c) dependence of rGO-FET mobilities prepared by alcohol vapor treatment (●) and Ar/H₂ annealing (■) at 850 °C.

Water-Soluble Graphene through Polyglycerol Grafting

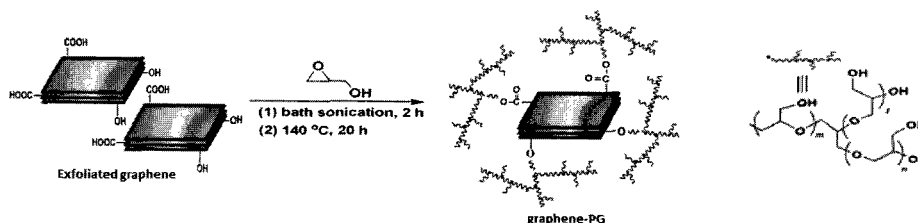
oToku Yasuda^{1,2}, Li Zhao¹, Liu Gang¹, Shuji Aonuma², Takahide Kimura¹, Naoki Komatsu¹

¹ Department of Chemistry, Shiga University of Medical Science, Otsu 520-2192, Japan

² Department of Materials Science, Osaka Electro-Communication University, Osaka 572-8530, Japan

For applications of nanocarbons in biology and medicine, such as imaging probe and drug carrier, they have to be well dispersed in a physiological environment. In this context, surface chemical functionalization has been extensively investigated to impart strong hydrophilicity to nanocarbons. We found recently that polyglycerol (PG) grafting on the surface of nanodiamond (ND) made ND to be highly dispersed in phosphate buffer [1]. The aqueous dispersion is very stable for months and the dispersibility of the PG-functionalized ND (PG-ND) is as high as 16 mg/mL in phosphate buffer saline (PBS), which is 400 times larger than that of the PEG-functionalized ND [2].

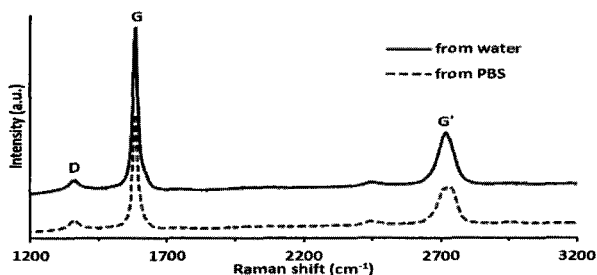
In this paper, we will present our recent result of PG grafting at the periphery of exfoliated graphene through ring-opening polymerization of glycidol to prepare PG-functionalized graphene (PG-G) dispersed in PBS (Scheme 1). We carried out the PG-functionalization of



Scheme 1 Synthesis of graphene functionalized with hyperbranched polyglycerol through the ring - opening polymerization of glycidol.

exfoliated graphene under similar reaction conditions to those of the PG-ND [1], but used graphene prepared through wet-process of graphite exfoliation as a starting material. The strong Tyndall effects were observed in the aqueous dispersions, suggesting that PG-G is dispersed both in the water and PBS. The existence of PG-G in these dispersions was confirmed by UV and Raman spectroscopies (Fig. 1). Aqueous dispersions have UV

absorption around 270 nm. Since it is well known that graphene exhibits absorption at similar wavelength, we conclude that the dispersions contain graphene. The Raman spectra shown in Fig. 1 support the above conclusion; both G and G' bands are detected in the dried samples from water and PBS solutions. From the



ratio of G' / G and the symmetrical shape of G' band, a few-layer graphene is considered to be dominant in the PG-G. In addition, the intensity of the D band is very low, indicating that the PG-G does not have number of defects and that the process to prepare PG-G causes little damage to graphene.

[1] L. Zhao, T. Takimoto, M. Ito, N. Kitagawa, T. Kimura, N. Komatsu, *Angew. Chem. Int. Ed.*, 50, 1388 (2011).

[2] T. Takimoto, N. Komatsu, *et al. Chem. Mater.*, 22, 3462 (2010).

Corresponding Author: Naoki Komatsu

Tel: +81-77-548-2102, Fax: +81-77-548-2405, E-mail: nkomatsu@shiga-med.ac.jp

Fabrications of Fullerene-Graphene and Fullerene-Nanotube-Graphene Composites

○Tomokazu Umeyama^{1,2}, Jinseok Baek¹, Noriyasu Tezuka¹, Kazuki Morita¹, Hiroshi Imahori^{1,3}

¹ Graduate School of Engineering, Kyoto University, Kyoto, 615-8510, Japan

² PRESTO, Japan Science and Technology Agency (JST), Kawaguchi, 332-0012, Japan

³ Integrated Cell-Material Sciences (WPI-iCeMS), Kyoto University, Kyoto, 615-8510, Japan

The large specific surface area intrinsically associated with the two-dimensional (2D) graphene sheets offers an advantage for anchoring other functional materials to form novel hybrid nanostructures with synergetic effects. In this study, we conducted a two-step methodology,¹ i.e., i) rapid injection of poor solvent (acetonitrile) to a mixed solution on *o*-dichlorobenzene (ODCB) and ii) subsequent electrophoretic deposition, for fabricating novel binary nanocarbon composite films of fullerene C₆₀ and functionalized chemically converted graphene (f-CCG) on semiconducting electrodes (i.e., FTO/SnO₂) (Figure 1). FE-SEM images of the FTO/SnO₂/(C₆₀+f-CCG)_m electrode showed dispersed C₆₀ clusters on the f-CCG basal plane as well as the closely packed C₆₀ clusters that coincide with the deposited film of single-component C₆₀ in a similar manner. The photoelectrochemical device with the f-CCG–C₆₀ composites with an optimized weight ratio exhibited a higher incident photon-to-current efficiency (IPCE) value (6.0% at 400 nm) than that with the C₆₀ single-component cluster (5.1%). Electronic communication between C₆₀ clusters and f-CCG may facilitate the electron transport to the SnO₂ electrode.

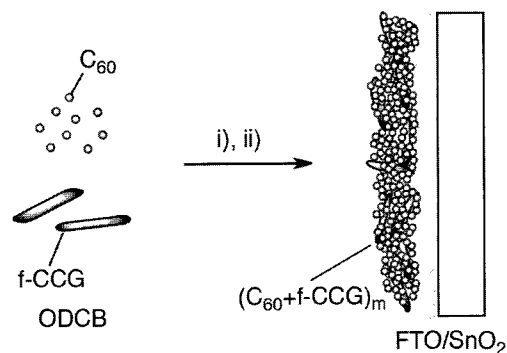


Figure 1. Formation of binary composite films of C₆₀ and f-CCG onto the FTO/SnO₂ electrode. i) Rapid injection of acetonitrile, ii) electrophoretic deposition.

On the other hand, we also conducted a three-step procedure, i.e., i) clusterization of fullerene C₇₀ and functionalized single-walled carbon nanotube (f-SWNT) by the rapid injection of acetonitrile into the mixed solution in ODCB, ii) addition of f-CCG solution in ODCB to the C₇₀–f-SWNT composite cluster solution, and iii) electrophoretic deposition onto the FTO/SnO₂ electrode to obtain the ternary composite film of C₇₀, f-SWNT, and f-CCG. Observation of the surface morphology of FTO/SnO₂/(C₇₀+f-SWNT+f-CCG)_m by FE-SEM revealed that coalescent fibrous network structure of (C₇₀+f-SWNT)_m is partially covered with the graphene sheet. Contrary to the above case, the introduction of f-CCG into the binary composite of C₇₀ and f-SWNT showed an adverse impact on the photocurrent generation properties because f-CCG inhibited formation of the porous network structure constructed by the f-SWNT–C₇₀ clusters. These results obtained here will provide valuable information on the design of optoelectronic devices composed of all-nanocarbon materials.

[1] T. Umeyama and H. Imahori, *J. Phys. Chem. C*, **117**, 3195 (2013).

Corresponding Author: T. Umeyama

Tel: +81-75-383-2568, Fax: +81-75-383-2571

E-mail: umeyama@scl.kyoto-u.ac.jp

Layer Number Determination using Raman Spectroscopy for Graphene Films Grown on SiC Substrate

◦Hitoshi Nakahara, Daisuke Maeta, Yahachi Saito

Department of Quantum Engineering, Nagoya University, Nagoya 464-8603, Japan

Because of its unique electronic structure, graphene is an important candidate for next-generation high-speed electronic devices and high-sensitivity sensors. It is also well known that graphene characteristics largely depend on its number of layers. Therefore, layer number measurement and growth control is inevitable for device applications of graphene. For graphene films on transparent substrate, optical transmittance is the most suitable and reliable method of layer number measurement. For opaque substrate, several methods were already reported for layer number determination, however, none of them has both capabilities of non-destructive large area measurement and easy to use for in-line inspection. In this study Raman spectroscopy and XRD measurements were carried out for graphene films grown on 6H-SiC substrate using thermal decomposition method. G/2D intensity ratio of a Raman spectrum and a XRD result were carefully compared and the ratio dependence on graphene thickness was delivered.

6H-SiC(000 $\bar{1}$) substrate was cleaned by hydrogen etching followed by annealing in Ar pressure of 0.05 atm at 1670-1750 °C for 15-420 sec to obtain samples with various thickness. The XRD measurements were carried out at beam line of PF BL-3a in High Energy Accelerator Research Organization (KEK). The measurement area of the XRD was about 1 mm square. The XRD results were analyzed by using a multi-term Laue function to obtain layer number distribution of measured area. For the Raman spectroscopy, 532 nm laser was used. The measurement area of the Raman spectroscopy is about 10 μm square, so that mapping measurement was carried out for 1 mm square area and all spectra was averaged over the area. SiC peaks in the measured spectra were subtracted, and graphene peaks were fitted by Lorentz functions to obtain integrated intensities of respective peaks.

Figure 1 shows G/2D integrated intensity ratio dependence on average graphene layers obtained by XRD analysis. A broken line in the figure indicates G/2D ratio of bulk graphite (HOPG). As shown in the figure, G/2D ratio is usable for layer number determination up to 10-20 layers. This dependence can be derived from a simple calculation with optical transmittance with assumption that 2D peak is mostly originated in the topmost layer. The experimental result was fitted with optical transmittance of graphene (T) as a parameter, and the fitting result $T = 0.943 \pm 0.003$ (a solid line in the figure) was in relatively-good agreement with its known value 0.97.

Corresponding Author: Hitoshi Nakahara
Tel: +81-52-789-4659, Fax: +81-52-789-3703
E-mail: nakahara@nagoya-u.jp

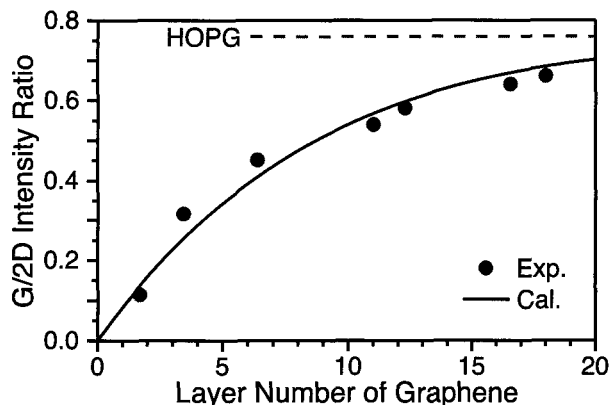


Figure 1: G/2D integrated intensity ratio versus layer number of graphene film. A broken line denoted as HOPG is a ratio for bulk graphite. A solid curve in the figure is a calculated result (see text).

A Two-dimensional Carbon Network of Fused Pentagons: All Carbon Magnetic Sheet

○Mina Maruyama and Susumu Okada

Graduate School of Pure and Applied Sciences, University of Tsukuba, 1-1-1 Tennodai, Tsukuba, Ibaraki 305-8571, Japan

Carbon molecules are known to form various polygonal conformations due to flexibility of its bonding angle and length. These polygons can be a constituent unit for the various molecular patchworks by sewing these polygons. Graphene is an interesting example for the possible two-dimensional carbon allotropes consisting of carbon polygons. Among the polygons, in the present work, we focus on pentagon that can cover a two-dimensional plane with dodecagons. We study the geometric and electronic structures of a two-dimensionally carbon sheet fused of pentagon trimer (acepentalene structure) based on the density functional theory (DFT). To express the exchange-correlation potential among the interacting electrons, we use the local spin density approximation (LSDA). We adopt the ultrasoft pseudopotential for describing electron-ion interactions. The valence wave function is expanded in terms of plane wave basis set with cutoff energy of 25 Ry.

Figure 1 (a) shows optimized structure of the fused pentagon network which consists of pentagons and dodecagons. We find that the stable sp^2 carbon sheet of which lattice parameters are $a=0.71$ nm. Figure 1 (b) shows the electron structure of the fused pentagon network under the optimum lattice constant. We find that the sheet is a metal in which flat dispersive band at the Fermi level that leads to the spin polarization on the sheet. The polarized electron spin is ferromagnetically aligned and extended through the sheet with the spin moment of $0.62 \mu_B/\text{nm}^2$.

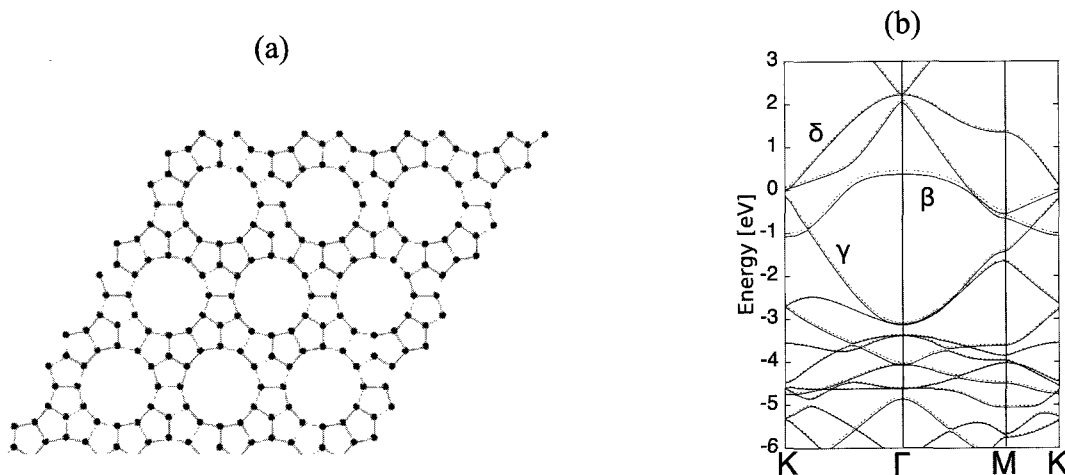


Fig. 1 (a) Geometric structures of the fused pentagon network with $a=0.71$ nm. (b) Electronic energy structure of the fused pentagon network.

Corresponding Author: Mina Maruyama

E-mail: mmaruyama@comas.frsc.tsukuba.ac.jp

Tel: +81-29-853-5600(ext: 8233)

Fermi energy dependence of G' band of graphene and single wall carbon nanotubes

○Kentaro Sato ¹, Riichiro Saito ²

¹ Sendai National College of Technology, Sendai 989-3128, Japan

² Department of Physics, Tohoku University, Sendai 980-8578, Japan

Raman spectra give us rich information for understanding physical properties of graphene related materials and for characterizing the stacking structure of graphene and the chirality of single wall carbon nanotubes (SWNTs) [1]. Additionally, gate-modulated Raman spectroscopy shows the distinguishable and characteristic Raman feature of each Raman peak in the Raman spectra by changing the Fermi energy [2]. The Fermi energy dependence of Raman intensity, line width, and Raman shift shows us information for the phonon mode assignment and for understanding the optical processes and the electron-phonon interaction. For example, phonon softening phenomena of longitudinal-optical (LO), and transverse-optical (iTO), and radial breathing phonon modes at the Brillouin zone center Γ point ($q=0$) in metallic SWNTs have been reported [3]. Gate-modulated Raman spectroscopy is useful for sample characterization and for understanding physical properties of graphene and SWNTs.

Several groups have demonstrated the Fermi energy dependence of Raman feature for the combination and overtone of non-zero wavevector ($q \neq 0$) phonon modes of graphene and SWNTs by using gate-modulated Raman spectroscopy. Araujo *et al.* reported the Fermi energy dependence of the G^* band, which appears at 2450 cm^{-1} , and the G' (2D) band of monolayer graphene [4]. Here the Raman shift of G band increases with increasing the absolute value of the gate voltage $|V_G|$, while the Raman shift of G' band decreases with increasing $|V_G|$. The opposite behavior was discussed by considering the phonon self-energy with $q \neq 0$. Furthermore, the technique reveals that the G^* band is composed of both the combination mode of iTO and LA phonon modes and the overtone mode of iTO phonon mode around K point. The technique can assign the phonon modes when the Raman shifts are close each other. Since gate-modulated Raman spectroscopy can distinguish complex Raman peaks of graphene and SWNTs, it is important to reveal a relation between the Raman feature and the Fermi energy.

In this paper, we calculate the Fermi energy dependence of G' band Raman shift of monolayer graphene and SWNTs to evaluate the phonon renormalization effects of the G' band. The Raman intensity is given by calculating electron-photon, electron-phonon matrix elements, and phonon self-energy corrections based on the tight binding scheme [1,3]. We compare our calculations with experiments. The Fermi energy dependence of G^* band will be discussed.

[1] A. Jorio *et al.*, Raman Spectroscopy in Graphene Related Systems, Wiley-VCH (2011).

[2] R. Saito *et al.*, Solid State Commun., in press, doi:10.1016/j.ssc.2013.05.010.

[3] K. Sasaki *et al.*, Physica E **42**, 2005 (2010).

[4] P. T. Araujo *et al.*, Phys. Rev. Lett. **109**, 046801 (2012).

Corresponding Author: K. Sato

Tel: +81-22-391-5575, E-mail: kentaro@sendai-nct.ac.jp

Electronic Properties of Graphene under an Electric Field

○Ayaka Yamanaka, Susumu Okada

*Graduate School of Pure and Applied Sciences, University of Tsukuba, Tennodai, Tsukuba
305-8577, Japan*

In recent years, graphene is attracting much attention due to its possible application for semiconductor electronic devices. In particular, graphene is regarded as the one of promising emerging materials in the next generation. Therefore it is urging us to unravel fundamental properties of graphene under an electric field for designing and fabricating graphene-based electronic devices. In this work, we study the electronic properties of graphene under a parallel electric field to simulate the effect of the electric field by source-drain electrodes.

All calculations are performed by using the density functional theory. To express the exchange correlation potential among interacting electrons, we apply the local density approximation. We use an ultrasoft pseudopotential to describe the interaction between valence electrons and ions. The effective screening medium (ESM) method is applied to investigate behaviors of graphene under the electric field in the framework of the first-principles calculations.

We applied the electric field on the graphene nanoribbons whose edges are terminated by H atoms in parallel direction to their axes as shown in Fig. 1. Under the external electric field, we investigate the electrostatic potential on each C atomic site to uncover how the electric field affects on the electronic properties of graphene. In the case of graphene nanoribbon with armchair edges, we find that the potential modulation strongly depends on the atomic site. The fact indicates that the electric field inside the nanoribbon is nonuniformly screened by the electrons on C atoms on the nanoribbons (Fig. 2). The structural analyses unravel that this unusual screening is ascribed to the bond alternation in graphene nanoribbons.

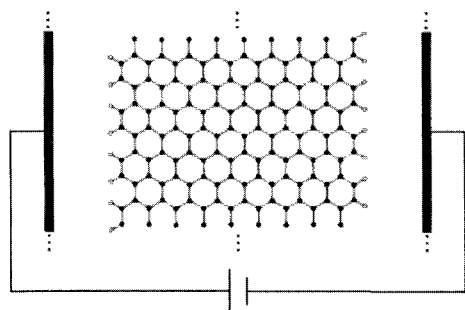


Fig.1. A structural model of nanoribbons under the electric field.

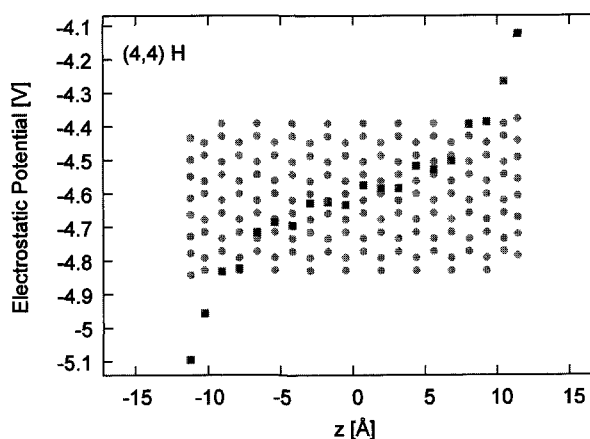


Fig.2. Electrostatic potential at each C atomic site of nanoribbons.

Corresponding Author: A. Yamanaka

Tel: +81-29-853-5600 (ext. 8233), Fax: +81-29-853-5924,

E-mail: ayamanaka@comas.frsc.tsukuba.ac.jp

Collective excitations in superconducting graphene

○Daisuke Inotani¹, Yoji Ohashi², Susumu Okada¹¹ *Graduate School of Pure and Applied Sciences, University of Tsukuba, Tsukuba, Ibaraki 305-8571, Japan*² *Faculty of Science and Technology, Keio University, 3-14-1 Hiyoshi, Kohoku-ku, Yokohama 223-8522, Japan*

The possibility of superconductivity in graphene has theoretically been discussed by many researchers [1]. Although the superconductivity in graphene has not been observed experimentally, it was pointed out that the superconductivity could be realized when the strength of the pairing interaction is sufficiently large even in undoped regime. Collective excitations are one of the most fundamental phenomena in superconductivity. Recently, the collective modes in the superfluid state of *neutral* Dirac fermions have theoretically been discussed [2]. In this neutral system, the linear dispersion of the Dirac fermions stabilizes a collective mode due to the preformed Cooper pairs in the semi-metal state near the superfluid critical temperature. Thus the observation of this collective mode in graphene could be used as a clear signature of the precursor of superconductivity.

However, because of the long range Coulomb interaction between the electrons, the properties of the collective excitations in graphene are expected to exhibit unusual feature. In this talk, we theoretically investigate electronic collective excitations in the superconducting graphene. For this purpose, we calculate the density-density correlation function within the framework of the generalized random phase approximation [2]. Using this, we reveal the properties of the collective excitations in graphene near the superconducting transition temperature.

[1] B. Uchoa and A. H. Castro Neto, Phys. Rev. Lett. **98**, 146801 (2007).

[2] S. Tsuchiya, R. Ganesh, T. Nikuni, arXiv: 1303.3343 (2013).

[3] Y. Ohashi and S. Takada, J. Phys. Soc. Jpn. **66**, 2437 (1997).

Corresponding Author: D. Inotani

Tel: +81-29-853-4030, Fax: +81-29-853-5924,

E-mail: dinotani@comas.frsc.tsukuba.ac.jp

Structural transformation of iron oxide nanotubes by the heat treatment

○Shunji Bandow, Yuki Shiraki

Department of Applied Chemistry, Meijo University, Nagoya 468-8502, Japan

An enhancement of photo-induced current for the complex of iron-oxide nanotubes (Fe-ox NTs) and fullerenols was reported at the last meeting of FNTG44 [1]. However, structural information about Fe-ox NTs used was not clearly understood. We only guess the structure similar to the FeO from the electron diffraction. This uncertainty makes an explanation for the observed enhancement of photo-current difficult. Here we carried out the heat-treatment of as-prepared Fe-ox NTs and studied by x-ray diffraction and transmission electron microscopy.

Figure 1 is TG-DTA curves taken under 20 % of oxygen containing Ar flow. At around 200 °C, a huge exothermic reaction followed by the weight loss can be seen. This is due to a burning of residual surfactant which is used for rolling up to form the nanotubes in the sol-gel process. Another remarkable endothermic anomaly like a glass transition is started at ~400 °C without weight change. This may be caused by the structural transformation or the morphological change. Hence we prepared the sample heat-treated at 185, 250, 350 and 400 °C. Figure 2 is the x-ray diffraction profiles. As seen in this figure, it is reasonable to consider that the structural transformation occurred between the temperature 250 and 350 °C, and therefore the thermal anomaly at ~400 °C should stem from the morphological change. Figures 3 a, b and c are the TEM images taken for, respectively, the heat-treated samples at 250, 350 and 400 °C. They evidently indicated that the nanotube structure was destroyed by the 400 °C heating. Details of the structural analyses and further photo-induced current information in the complex with the fullerenols will be reported.

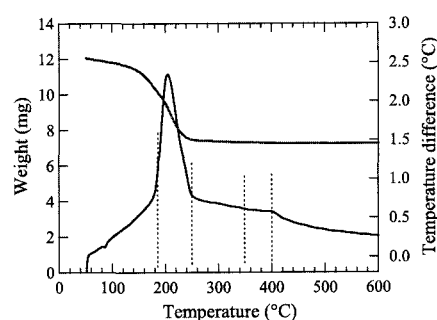


Fig. 1. TG-DTA curves taken for Fe-ox NTs.

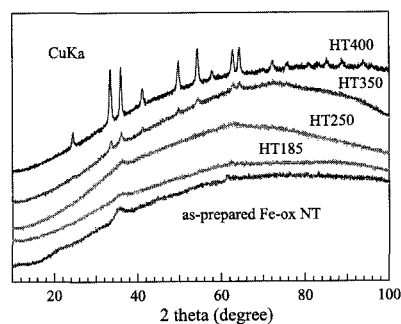


Fig. 2. XRD profiles taken for Fe-ox NTs heat-treated.

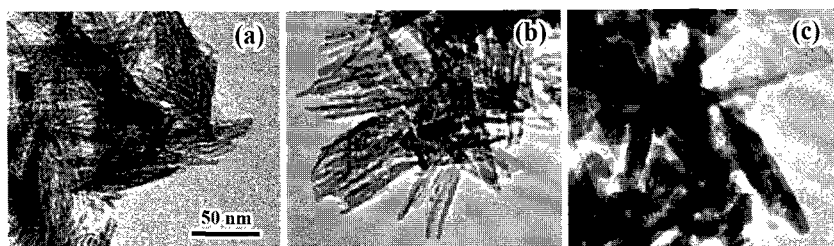


Fig. 3. TEM images taken for Fe-ox NTs heat-treated at (a) 250 °C, (b) 350 °C and (c) 400 °C.

[1] Y. Shiraki *et al.*, The 44th FNTG (March, 2013), **2P-45**.

Corresponding Author: S. Bandow, Tel: +81-52-838-2404, E-mail: bandow@meijo-u.ac.jp

Improvement of synthesis conditions for high yield of carbon nanocoils

○Koji Maruyama¹, Yoshiyuki Suda¹, Hideto Tanoue¹, Hirofumi Takikawa¹,
Hitoshi Ue², Kazuki Shimizu³, Yoshito Umeda⁴

¹ Department of Electrical and Electronic Information Engineering,
Toyohashi University of Technology, Toyohashi 441-8580 Japan

² Fuji Research Laboratory, Tokai Carbon Co., Ltd., Sunto, Shizuoka 410-1431, Japan

³ Shonan Plastic Mfg. Co., Ltd., Hiratsuka, Kanagawa 254-0807, Japan

⁴ Toho Gas Co., Ltd., Tokai, Aichi 476-8501 Japan

Carbon nanocoil is a helical carbon nanofiber and its fiber diameter is 100-500 nm. High yield production method of CNC is required for application to capacitor electrode and electromagnetic wave absorbers. In chemical vapor deposition (CVD) of our laboratory, high purity CNC was synthesized on one surface of the sheet-like compounds with a catalyst molar ratio, Fe: Sn = 5:2. The authors have succeeded in synthesizing almost 100%-purity CNC on both sides of the compound sheet with a Fe:Sn=3:1 catalyst ratio. We investigated the factor which CVD conditions affect growth of CNC by observing the surface area of high-purity CNC.

Synthesized compounds on graphite substrate is shown in Fig. 1 (a). The compound has a sheet-like structure. Fig. 1 (b) and (c) are surface and fracture of the sheet-like compounds, respectively. CNC was observed with a purity of almost 100% on both sides of the surface of sheet-like composite. CNC prepared in this study had higher purity than made by conventional methods⁽¹⁾. In the fracture surface of the sheet-like composite (Fig. 1(c)), linear or irregular shaped carbon nanofibers (CNFs) and a small amount of CNCs were observed. CNC is grown on carbon deposit layer⁽²⁾. In this study, CNC is grown from carbon deposit layer (Fig. 1 (c))

This work has been partly supported by the EIIRIS Project from Toyohashi University of Technology (TUT); the Core University Programs (JSPS-CAS program in the field of "Plasma and Nuclear Fusion") from the Japan Society for the Promotion of Science (JSPS); JSPS KAKENHI Grant Number 24360108 and 25630110; and MEXT KAKENHI Grant Number 24110708.

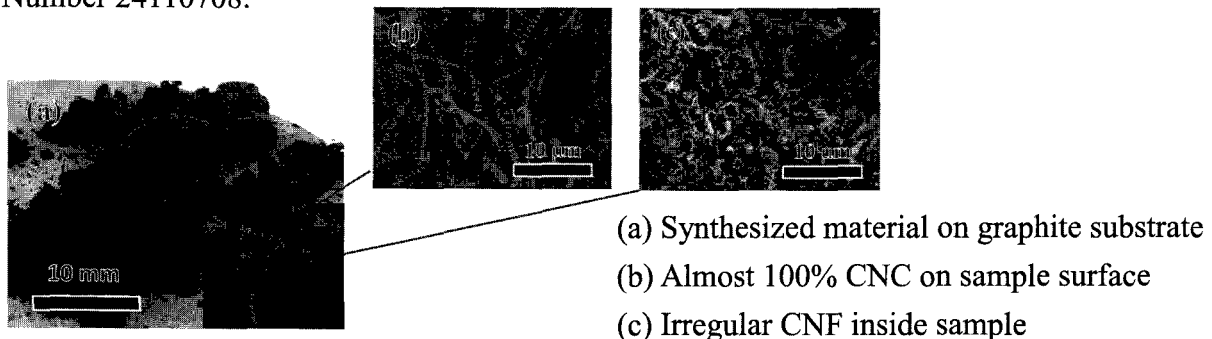


Fig. 1 Synthesized CNCs.

(1) M. Yokota *et al.* *J.Nanosci. Nanotechnol.* 10, 3910-3914 (2010).

(2) K. Hirahara *et al.* *Carbon.* 56, 264-270 (2013).

Corresponding Author: Yoshiyuki Suda

Tel: +81-532-44-6726, Fax: +81-532-44-6757, E-mail: suda@ee.tut.ac.jp

Electromagnetic wave absorption properties of carbon nanocoils

○Ryo Kato¹, Shingo Yasudomi¹, Yoshiyuki Suda¹, Hideto Tanoue¹, Hirofumi Takikawa¹,
Hitoshi Ue², Kazuki Shimizu³, Yoshito Umeda⁴, Usaburo Eguchi⁵

¹ Department of Electrical and Electronic Information Engineering,
Toyohashi University of Technology, Toyohashi 441-8580, Japan

² Fuji Research Laboratory, Tokai Carbon Co., Ltd., Oyama 410-1431, Japan

³ Shonan Plastic Mfg. Co., Ltd., Hiratsuka 254-0807, Japan

⁴ Toho Gas Co., Ltd., Tokai, Aichi 476-8501, Japan

⁵ Tsuruoka National College of Technology, Tsuruoka, Yamagata 997-8511, Japan

Carbon nanocoil (CNC) is a carbon nanofiber with helical shape. The electromagnetic wave absorption properties of carbon microcoil (CMC) with larger coil diameter than CNC has been already reported by S. Motojima, et al.⁽¹⁾ We fabricated electromagnetic wave absorbers from CNC which was synthesized in our laboratory, and evaluated its electromagnetic wave absorption properties.

CNC was prepared from acetylene gas by chemical vapor deposition using Fe and SnO₂ as catalysts. The electromagnetic wave absorption properties of CNCs/epoxy and CNCs/paraffin composites with different additive ratios were measured by the free space method using lens antennas in frequency ranges of 5.6 - 40 and 67 - 110 GHz. Fig. 1 shows the electromagnetic wave absorption properties of CNCs/epoxy composites and CNCs/paraffin composites. The CNCs/epoxy composites of 0.1 - 1.0 wt.% showed poor reflection losses (Fig. 1 (a)). The 10 wt.% CNCs/paraffin composite achieved a reflection loss of -32 dB at 79.2 GHz (Fig. 1 (b)). Its bandwidth corresponding to the reflection loss below -20 dB was 4.85 GHz. It was found that CNCs/paraffin composite shows a good absorption property in W band frequencies (75 - 110 GHz).

This work has been partly supported by the EIIRIS Project from Toyohashi University of Technology (TUT); the Core University Programs (JSPS-CAS program in the field of "Plasma and Nuclear Fusion") from the Japan Society for the Promotion of Science (JSPS); JSPS KAKENHI Grant Number 24360108 and 25630110; and MEXT KAKENHI Grant Number 24110708.

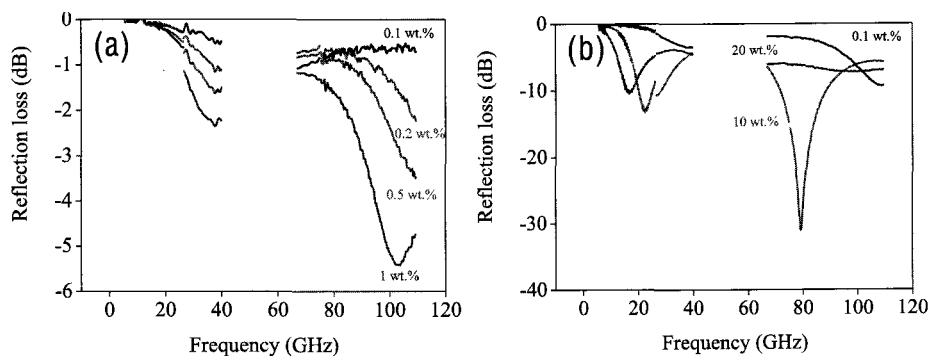


Fig. 1 Electromagnetic wave absorption properties of
(a) CNCs/epoxy and (b) CNCs/paraffin composites

(1) S. Motojima, *et al.*: *Journal of Applied Physics*, 77, 457-465 (2007)

Corresponding Author: Yoshiyuki Suda

Tel: +81-532-44-6726, Fax: +81-532-44-6757, E-mail: suda@ee.tut.ac.jp

Spring Constant Measurement of Carbon Nanocoils

○Taiichiro Yonemura¹, Yoshiyuki Suda¹, Hideto Tanoue¹, Hirofumi Takikawa¹,
Hitoshi Ue², Kazuki Shimizu³, Yoshito Umeda⁴

¹ Department of Electrical and Electronic Information Engineering,
Toyohashi University of Technology, Toyohashi, 441-8580, Japan

² Fuji Research Laboratory, Tokai Carbon, Co., Ltd., Oyama, 410-1431, Japan

³ Development Department, Shonan Plastic Mfg. Co., Ltd., Hiratsuka, 254-0807, Japan

⁴ Toho Gas Co., Ltd., Tokai, 476-8501, Japan

Carbon nanocoil (CNC) is a carbon nano-fiber which has a helical shape. CNC is predicted to have a high mechanical strength. Several groups have studied the physical properties and electrical characteristics of tiny helical-shaped elements [1][2]. It is necessary to study CNC fracturing mechanism under tensile loads for nano-spring application. In this study, we study the CNC fracturing properties [3] using a focused ion beam (FIB) technique for applying uniaxial loads.

A CNC was pasted on a substrate which was attached to a spring table. The spring table has two leaf springs which has a specific spring constant of 12 N/m. The spring table moves with the substrate. Because this phenomenon is accordance with Hooke's law, we could calculate applied force by observing the substrate displacement. Hooke's law can be expressed as follows:

$$F = kx$$

where F is the applied force, k is the spring constant of spring table, and x is the displacement of substrate.

We observed the elongation of CNC until it fractured by gradually changing the substrate height at a constant speed in the FIB chamber. We obtained experimental results of the tensile deformation of CNC. Fig. 1 shows Force-Elongation curve of the CNC. From this figure, we can see that the CNC was applied under an uniaxial load, approximately 100 μ N until fracturing. Furthermore, this CNC has fractured after elongated 190% of its original length. We used Hooke's law for even estimating the spring constant of the CNC. In this case, we can replace x as the elongation of the CNC. We estimated the spring constant by the slope of Fig. 1. We found that the CNC had spring constant of 13 N/m.

This work has been partly supported by the EIRIS Project from Toyohashi University of Technology (TUT); the Core University Programs (JSPS-CAS program in the field of "Plasma and Nuclear Fusion") from the Japan Society for the Promotion of Science (JSPS); JSPS KAKENHI Grant Number 24360108 and 25630110; and MEXT KAKENHI Grant Number 24110708.

[1] X. Chen, et al: *Nano Lett.*, 3 (2003) 1299.

[2] K. Nakamatsu, et al: *Jpn. J. Appl. Phys. Part 1*, 48 (2009) 105001.

[3] T. Yonemura, et al: *J. Appl. Phys.*, 112 (2012) 084311

Corresponding Author: Yoshiyuki Suda

Tel: +81-532-44-6726, Fax: +81-532-44-6757, E-mail: suda@ee.tut.ac.jp

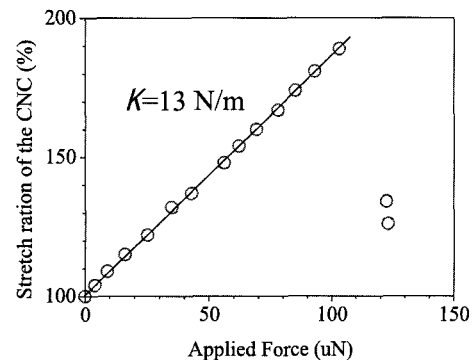


Fig. 1 Force—Elongation curve.

In-situ observation of carbon nanocoil growth by optical microscope

○Takehiro Gohara, Takayuki Arie, and Seiji. Akita

Department of Physics and Electronics, Osaka Prefecture University, Osaka 599-8531, Japan

Carbon nanocoils (CNCs) are carbon fibers which have nanometer scale coiled structure. Due to their peculiar helical morphologies, CNCs are widely expected for applications including electromagnetic wave absorber. To apply CNCs to practical applications, large-scale CNC synthesis should be established. However, the detailed mechanism of CNC growth is still an open subject. In this study, we investigate the initial stage of individual CNC growth by in-situ observation using an optical microscope. The activation energy for growth of individual CNCs is also investigated.

To observe the initial stage of CNC growth, we prepared a small reactor and furnace with an optical microscope for in-situ observation (Fig. 1). CNCs were synthesized by catalytic CVD method using C_2H_2 as a source gas, where Fe-Sn oxidized particles were used as the catalyst.

Figures 2(a)-2(c) show a series of optical microscope images of CNC growth. Initially, the catalyst color was changed to dark black and then filament-like structures were observed around the edge of the catalyst particle after a few ten seconds as shown in Fig. 2(b). Excess feeding of C_2H_2 causes the bloat of non-coiled structure around the catalyst particles as shown in Fig. 2(c). We measured the temperature dependence of growth rate of individual CNCs, when the growth temperature was varied from 770 to 800 °C. Figure 3 shows an Arrhenius plot of the growth rate, where the each point was obtained from the average growth rate of 4 individual CNCs. The activation energy, E_a , estimated from the slope was 0.51 eV. Since C_2H_2 is decomposed at temperatures higher than 650 °C in gas phase, the contribution of the decomposition energy to E_a can be ignored. Thus, the obtained E_a is most likely due to the combination of the surface reaction energy of decomposed C_2H_2 and the formation energy of the coiled structure on the catalyst.

Acknowledgement: This work was supported by the Osaka Prefecture Collaboration of Regional Entities for the Advancement of Technological Excellence, JST.

Corresponding Author: S. Akita

Tel: +81-72-254-9261, Fax: +81-72-254-9261,

E-mail: akita@pe.osakafu-u.ac.jp

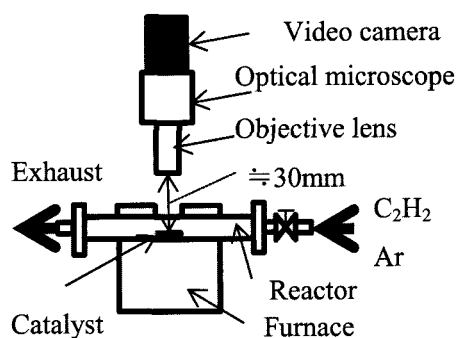


Fig. 1 Schematic of experimental setup.

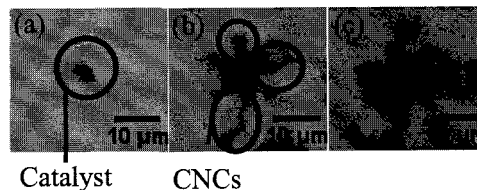


Fig. 2 Optical microscope images (a) before (b) after 2 min. and (c) 10 min. CVD process.

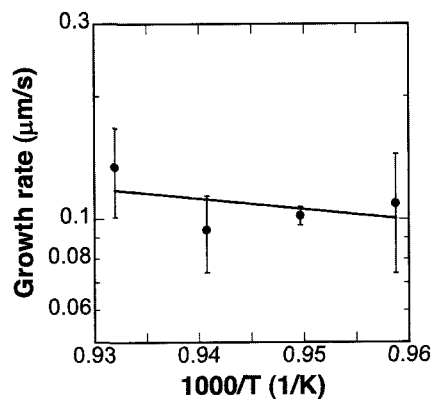


Fig. 3 Arrhenius plot of the temperature dependence of the growth rate.

Electrically Induced P-N Junction in WSe₂ Monolayer Film

○Ryo Shimizu¹, Jiang Pu¹, Yijin Zhang², Lain-Jong Li³, Yoshihiro Iwasa², Taishi Takenobu¹

¹ Department of Applied Physics, Waseda University, Shinjuku 169-8555, Japan

² Department of Applied Physics, The University of Tokyo, Tokyo 113-8656, Japan

³ Institute of Atomic and Molecular Sciences, Academia Sinica, Taipei, 10617, Taiwan

Two-dimensional (2D) layered nanomaterials have attracted much attention due to their unusual physical properties. For example, graphene, a single-layer 2D carbon material with honeycomb lattice structure, is the most widely studied 2D nanomaterial owing to its exceptional electronic, thermal, and mechanical properties [1]. However, because graphene is a zero-bandgap semiconductor, graphene transistor exhibits a very low on/off current ratio, which limits the use of these material for applications in logic electronics and optoelectronics. On the other hand, other 2D layered inorganic graphene analogues, such as WSe₂ which belongs to transition-metal dichalcogenides (TMDC) have energy bandgap corresponding to visible region ($E_g \sim 1.6$ eV) (Fig. 1). So they are prospective materials for optoelectronics [2,3]. The fundamental optoelectronic elements require p-n junction. Here, we realized pseudo stable p-n junction on the channel of WSe₂ ambipolar electric double layer transistor (EDLT) by fixing ions in liquid-gate insulator with low temperature. This method can't be duplicated in conventional transistors with solid gate dielectrics.

First we fabricated WSe₂ EDLT device. For the source and drain electrodes, Au contacts with Ni adhesion layers were thermally deposited onto the surface of CVD grown WSe₂ monolayer film. Second we dropped gel electrolyte called "ion gel" onto them. Finally, the transistor channel was covered with a thin Pt foil to form the top-gate electrode. This EDLT shows ambipolar transport behavior. Then in order to form p-n junction in the channel of the transistor, we controlled electric voltage of each terminals and froze ion gel with keeping applying voltages. Fig. 2 represents rectification characteristics of this device. Importantly, we do not apply gate voltage for these measurements. This rectification behavior was maintained until ion gel melted.

In summary, we have demonstrated pseudo stable p-n junction on the channel of WSe₂ EDLT by coinstantaneous accumulation of holes and electrons. This p-n junction is expected to play an important role in developing next-generation optoelectronic devices.

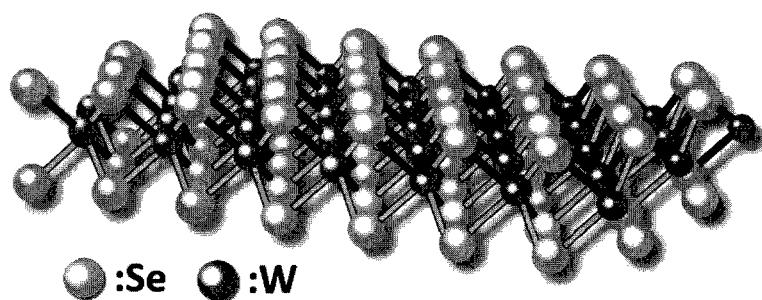


Fig.1 Crystalline structure of WSe₂

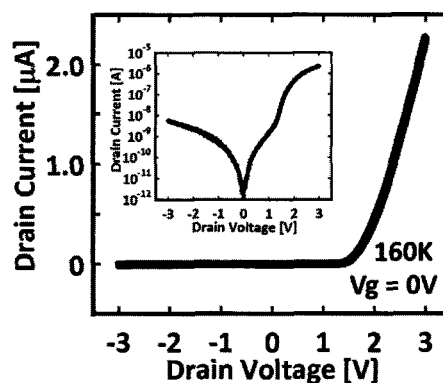


Fig.2 Rectification behavior of p-n junction

[1] A. K. Geim, Science 324, 1530 (2009).

[2] W. Zhao *et al.*, ACS Nano 7, 791 (2013).

[3] P. Tonndorf *et al.*, Opt. Express 21, 4908 (2013).

Corresponding Author: Taishi Takenobu

Tel&Fax : +81-3-5286-2981

E-mail: takenobu@waseda.jp

Layer Number Dependence of Optical Properties of MoS₂

○Yasunori Ogawa¹, Yuka Tsuboi¹, Zhou Lizhong¹, Shinichiro Mouri¹,
Yuhei Miyauchi^{1,2}, Kazunari Matsuda¹

¹*Institute of Advanced Energy, Kyoto University, Uji, Kyoto 611-0011, Japan*

²*Japan Science and Technology Agency, PRESTO, 4-1-8 Honcho Kawaguchi, Saitama
332-0012, Japan*

Atomically thin two-dimensional (2D) molybdenum disulfide (MoS₂) has attracted much attention for its remarkable optical properties and optoelectronic applications [1]. It has been reported that the optical properties of MoS₂ strongly depend on the number of layer [2]. Thus, it is required the simple and exact method to identify the layer number of MoS₂. In the previous studies, the methods by using the optical contrast [3], the ratio of the Raman intensity between MoS₂ and Si substrate [4] were suggested to identify the layer number of MoS₂. In this study, we investigate the layer number dependence of optical properties of MoS₂ and suggest a new method to identify a layer number using photoluminescence (PL) and Raman spectra.

MoS₂ with various thickness was prepared by the mechanical exfoliation and deposited on SiO₂/Si substrate. Raman and PL spectra of MoS₂ were measured using a cw solid-state laser (2.33 eV). Figure 1(a) shows the Raman spectra of MoS₂ with various layer numbers, and two phonon modes of E_{2g} and A_{1g} are observed. With decreasing the layer number, the frequency difference and Raman intensity of two phonon modes change. Figure 1(b) shows the PL spectra of MoS₂ with various layer numbers. The PL spectral shape and PL intensity change with decreasing the layer number. With decreasing the layer number, the Raman intensity decreases, while the PL intensity increases. Thus, it is possible to identify the layer number in MoS₂ from the intensity ratio of the Raman and PL intensity. Moreover, the layer number dependence of PL properties in MoS₂ and other transition metal dichalcogenides will be discussed.

[1] Q. H. Wang, *et.al. Nature Nanotech.* 7, 699 (2012).

[2] K. F. Mak, *et.al., Phys. Rev. Lett.* 105, 136805 (2010).

[3] M. M. Benameur, *et.al., Nanotechnology* 22, 125706 (2011).

[4] Li. Song-Lin *et.al., ACS Nano.* 6, 7381 (2010).

Corresponding Author: Yasunori Ogawa
Tel: +81-774-38-3465,
Fax: +81-774-38-3467,
E-mail: yasunori.o@ax5.ecs.kyoto-u.ac.jp

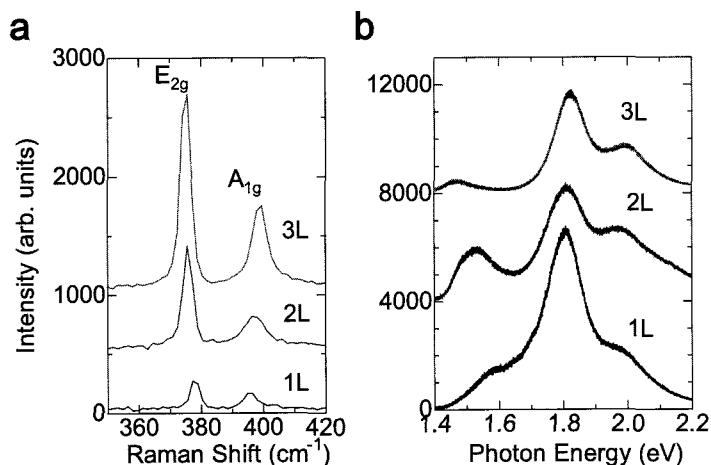


Figure 1 (a)Raman, and (b)PL spectra of MoS₂ with various thickness.

Preparation of Diamond Particle Decorated with Carbon Nanotube

○Wataru Kimura¹, Kazuhiro Fujiki², Takeshi Yamauchi¹, Norio Tsubokawa¹

¹ Graduate School of Science and Technology, Niigata University, 8050, Ikarashi 2-no-cho, Nishi-ku, Niigata 950-2181, Japan

² Department of Environmental Science, Niigata Institute of Technology, 1719, Fujihashi, Kashiwazaki, Niigata 945-1195, Japan

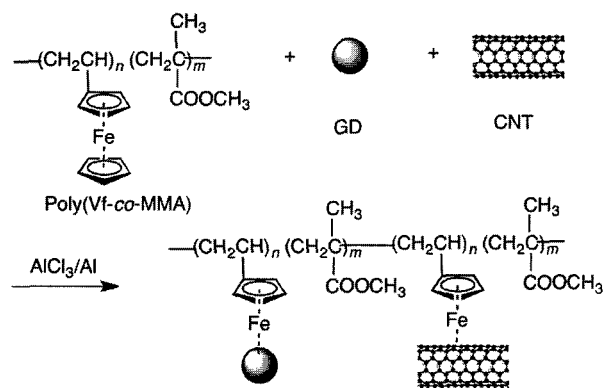
We have reported that ligand-exchange reaction of polymers bearing ferrocene moieties with polycondensed aromatic rings of nanocarbons, such as carbon black, carbon nanotube, and nano-diamond, successfully proceeded to give polymer-grafted nanocarbons [1].

In this paper, the preparation of diamond micro particle decorated with carbon nanotube (CNT) was investigated by use of the ligand exchange reaction of polymers bearing ferrocene moieties in the co-existence of CNT and diamond particles as shown in Scheme 1.

In this study, surface graphitized diamond (GD) and multi walled CNT was used. The average particle size of GD was determined to be 15 μm .

It was confirmed that grafting of poly(Vf-co-MMA) onto GD successfully proceeds by ligand-exchange reaction of ferrocene moieties of poly(Vf-co-MMA) with polycondensed aromatic rings of GD in the presence of AlCl_3 and Al powder as catalysts: the percentage of grafting of poly(Vf-co-MMA) onto GD was determined to be 32.2%. On the contrary, the no grafting of polymer onto GO was observed in the absence of AlCl_3 and Al powder.

Then the reaction of poly(Vf-co-MMA)-grafted GD with CNT in the presence of the catalysts was examined. As a result, CNT was immobilized on the GD surface to give GD decorated with CNT was obtained as shown in Figure 1. In addition, GD decorated with CNT was also obtained both by the reaction of poly(Vf-co-MMA)-grafted CNT with GD and by one-step reaction of poly(Vf-co-MMA) in the co-existence of GD and CNT (Scheme 1) in the presence of the catalysts.



Scheme 1 Preparation of diamond particle decorated with CNT

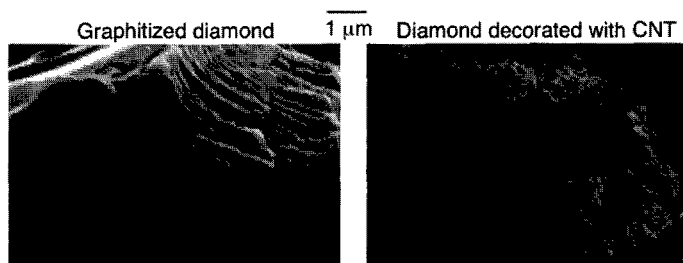


Figure 1 SEM aspect of GD decorated with CNT

Acknowledgement: This study was supported in partly by a Grant in Aid for Scientific Research form Ministry of Education, Culture, Sports, Science and Technology of Japan (No. 24560836).

[1] N. Tsubokawa, Polym. J., Polym. J. **39**, 938 (2007).

Corresponding Author: N. Tsubokawa

Tel: +81-25-262-6779, Fax: +81-25-262-6779

E-mail: ntsuboka@eng.niigata-u.ac.jp

Synthesis of ordered carbon nanotube network using pillar molecules

○Kosuke Tashiro, Hayong Song, Yosuke Ishii, Shinji Kawasaki*

Nagoya Institute of Technology, Gokiso, Nagoya 466-8555, Japan

For the application of nanocarbons, several kinds of chemical modification techniques have been developed. Among them, the network construction to connect the isolated nanocarbons by introducing chemical bonds between two nanocarbons is fascinating because it can produce a new category of ordered porous carbon. Recently, Matsuo reported the synthesis of pillared graphite and its superior hydrogen storage property^[1]. In this work, we tried to apply the modification strategy of pillared graphite to single-walled carbon nanotubes (SWCNTs). By using pillar modification method for SWCNTs, ordered SWCNT networks would be prepared as shown in Fig1. In this process, a two-step reaction is required. The first step is oxidation of SWCNTs surfaces. The second step is connecting functional groups on SWCNTs surfaces to each other using pillar molecules.

We used ethylenediamine (EDA) as pillar molecules to bridge SWCNTs. EDA are symmetrical molecules with amine groups at both ends. The nanostructures and chemical structures of the obtained functionalized graphite and SWCNTs were characterized using XRD, TG, FT-IR, and elemental analysis. Detailed discussion will be presented at the conference.

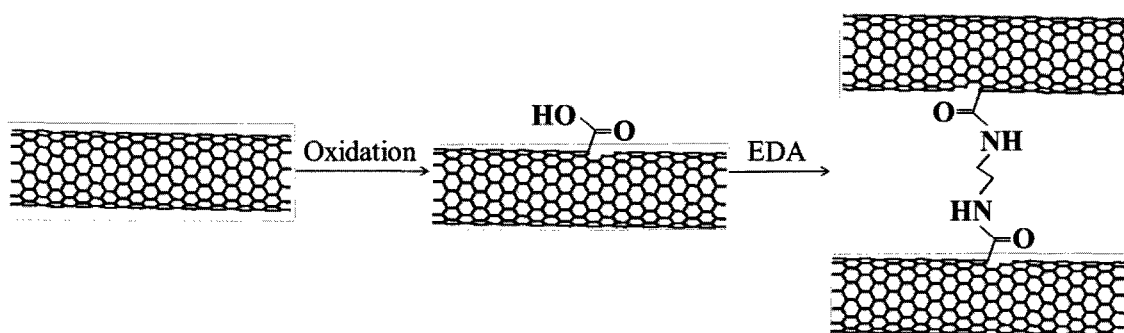


Fig1. Synthesis procedure of pillared SWCNTs.

[1] Y. Matsuo *et al.*, Carbon. 37, 10702 (2012)

*Corresponding Author: S. Kawasaki
E-mail: Kawasaki.shinji@stn.nitech.ac.jp

Carbon nanotubes functionalized with carboxylic acid dispersed in 3D polymeric microstructures

○A. J. G. Otuka¹, V. Tribuzi¹, D. S. Corrêa², A. R. Zanatta¹, C. R. Mendonca¹

¹ Instituto de Física de São Carlos, Universidade de São Paulo, CP.369, 13560-970, São Carlos, SP, Brazil

² Laboratório Nacional de Nanotecnologia para o Agronegócio (LNNA), Embrapa Instrumentação, Rua XV de Novembro, 1452, CP.741, 13560-970, São Carlos, SP, Brazil

Carbon nanotubes are known for their extraordinary thermal conduction, mechanical and electrical properties [1]. When used combined with other materials, nanotubes can provide improvements and function to structures made from various materials.

In this work we fabricated polymeric microstructures containing single-walled carbon nanotubes (SWCNTs) functionalized with carboxylic acid. The microstructures were fabricated by direct laser writing, using two-photon polymerization. This is a powerful fabrication method that allows obtaining complex structures with high spatial resolution.

An SEM image of a set of fabricated structures is presented in Fig 1a. To confirm that carbon nanotubes were in fact incorporated in polymeric structures we carried out Raman spectroscopy measurements, whose result is displayed in Fig. 1b.

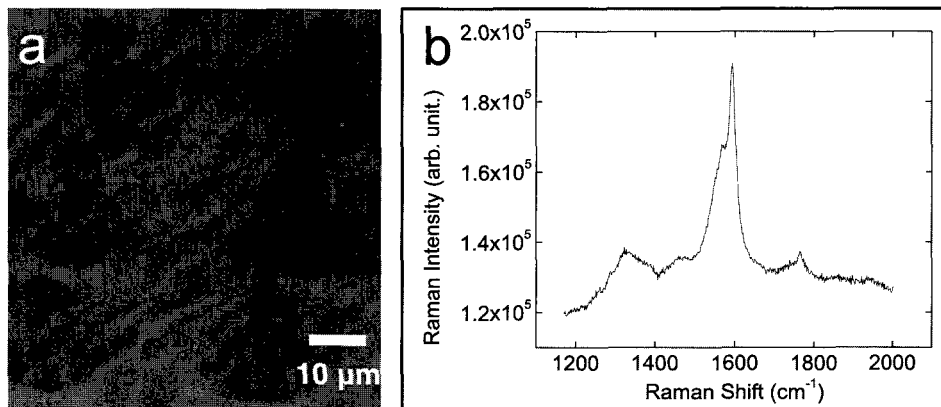


Fig. 1. (a) Microstructures containing SWCNTs. (b) Raman spectrum of the microstructures.

As it can be seen from the SEM results (Fig. 1a) the presence of the nanotubes in the microstructure does not affect the structural quality and the polymerization process if proper experimental conditions are used. In our results, we were able to incorporate carbon nanotubes with a concentration up to 0.01 wt% and the fabrication was performed using 40 mW and a scanning speed of 10 μm/s. The Raman spectrum (Fig. 1b) shows two specific peaks at approximately 1300 and at 1595 cm⁻¹ assigned to D-band and G-band of SWCNTs, respectively, providing evidence for the presence of SWCNTs in the polymeric structures [2]. Such results are very promising to favor the manufacture of technological devices.

[1] A. Jorio, G. Dresselhaus, M. S. Dresselhaus. "Carbon nanotubes – Advanced topics in the synthesis, structure, properties and applications". Springer, 2008. New York.

[2] S. Ushiba, S. Shoji, K. Masui, P. Kuray, J. Kono, S. Kawata. "3D microfabrication of single-wall carbon nanotube/polymer composites by two-photon polymerization lithography", Carbon, v. 59, pp. 283-288 (2013).

Corresponding Author: A. J. G. Otuka

Tel: +55(16) 3373-8085 (241); Fax: +55(16) 3373-8085 (212)

E-mail: otuka@ursa.ifscusp.br

High-Performance fluorinated resin with Low-content Aligned carbon nanotube

○Kentaro Miyoshi¹, Takeru Yajima¹, Toru Sakai¹, Masami Toyoda², Yoshikazu Nakayama²

¹ Carbon Nanotube Project, Yamanashi Laboratories, Taiyo Nippon Sanso Corporation, Yamanashi 408-0015, Japan

² Department of Mechanical Engineering, The University of Osaka, Osaka 565-0871, Japan

We have made Aligned carbon nanotube(CNT), which is Multi-walled CNT(length; 100 μm over) on Silicon wafer(Fig.1). [1] As consistency of an application use, We made High-Performance fluorinated resin with good conductivity by doping 0.01%-1%(w/w) of Aligned carbon nanotube for practical applications of High-Performance fluorinated resin that have electrical and thermal conductivity. In addition, We made a study of production process about High-Performance fluorinated resin and optimized them.

About electrical conductivity, we confirmed volume specific resistance $10^7 \Omega \cdot \text{cm}$ level by doping 0.01%(w/w) of CNT(Fig.2).

About thermal conductivity, it was thermal conductivity 0.64 W/(m·K) by doping 0.05%(w/w) of CNT and 0.69 W/(m·K) by doping 1%(w/w) of CNT. In addition, We could confirm that a characteristic improved as the length of CNT and the thing which had high crystal characteristics.

After performing examination, the cost of the commercial process, We were able to confirm the possibility that We could realize the products cost of the same class level to conventional conductivity fluorinated resin.



Fig.1 Fe-SEM image of Aligned CNT

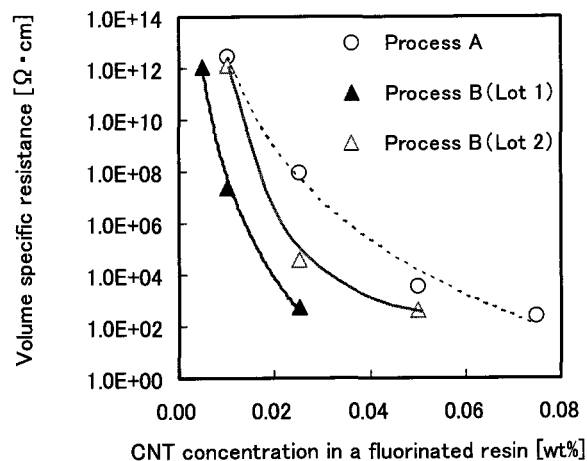


Fig.2 Electric conduction performance of High-Performance fluorinated resin

[1] T. Nagasaka, T. Sakai, K. Hirahara, S. Akita, and Y. Nakayama, *Jpn. J. Appl. Phys.* **48**, 091602 (2009).

Tel: +81-551-42-4897, Fax: +81-3-6866-0461,

E-mail: Kentaro.Miyoshi@tn-sanso.co.jp

***In-situ* TEM study on reaction of silicon nanoparticles with carbon supported on a carbon nanotube heater**

○Koji Asaka, Tomohiro Terada, and Yahachi Saito

Department of Quantum Engineering, Nagoya University, Nagoya 464-8603, Japan

The transformation of silicon (Si) nanoparticles on a multiwall carbon nanotube (MWNT) during Joule heating was studied by *in situ* transmission electron microscopy (TEM). The Si nanoparticles reacted with graphitic layers of the MWNT surface to form silicon carbide (SiC) nanoparticles.

A MWNT produced by arc discharge was attached to an edge of a 50 μm -thick gold (Au) plate by dielectrophoresis using an isopropyl alcohol solution and Si was deposited on the MWNT surface at 773 K by electron beam evaporation. The Au plate was mounted to a movable stage on the specimen holder of TEM. The MWNT protruding from the edge of the plate was manipulated and brought into contact with an opposite Au electrode in the microscope. The structural changes in Si nanoparticles during Joule heating were observed by high-resolution imaging operated at 120 kV using a television system. The bias voltage and current applied to the MWNT were simultaneously measured by the two-terminal method while observing the structural changes.

Figure 1 shows a sequential time series of high-resolution images of the structural changes in a Si nanoparticle on a MWNT. When a current of 73.0 μA passed through the MWNT, the diameter of the Si nanoparticle began to decrease, and the outermost graphitic layer of the MWNT with which the nanoparticle was just in contact disappeared (Figs. 1(a)-1(c)). Finally, the increase of the current up to 75.4 μA led to the disappearance of three graphitic layers near the contact region (Figs. 1(d)-1(f)). After the disappearance, the high-resolution TEM observation of the nanoparticle in Fig. 1(f) showed that the nanoparticle was composed of SiC. The present results demonstrate that the MWNTs can be applicable as carbon sources for the syntheses of nanomaterials.

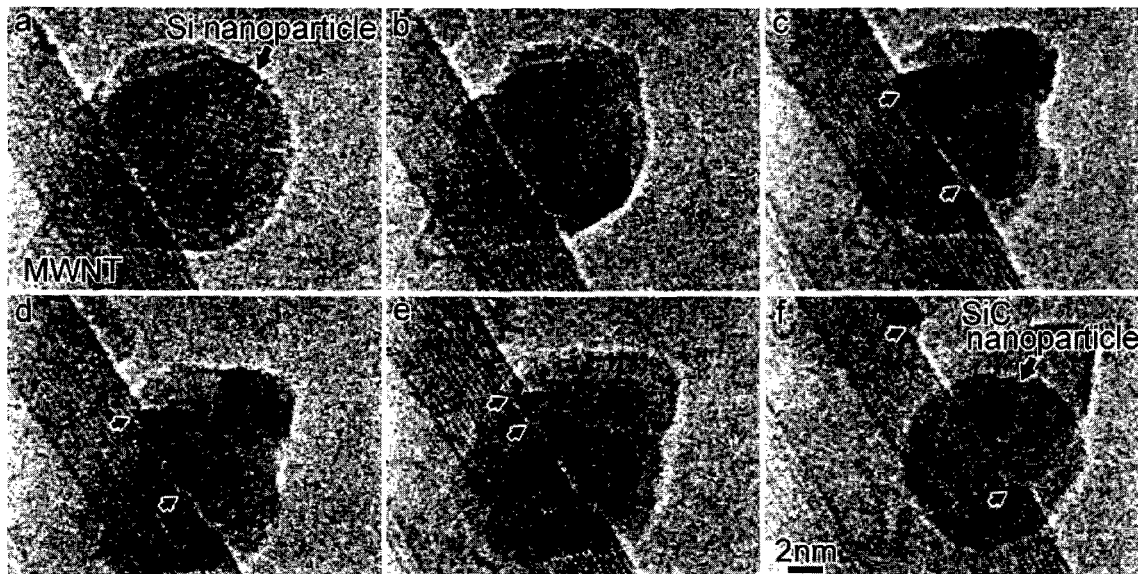


Fig.1. A sequential time series of high-resolution images of the structural changes in a Si nanoparticle on the MWNT.

Corresponding Author: K. Asaka

Tel: +81-52-789-4464, Fax: +81-52-789-3703, E-mail: asaka@nuqe.nagoya-u.ac.jp

Large current controllable solution-gate FET by carbon nanotube forest

○Miho Myodo, Masafumi Inaba, Mikinori Kobayashi,
Yukihiro Shintani, Atsushi Hiraiwa, Hiroshi Kawarada

School of Science and Engineering, Waseda University, Tokyo 169-8555, Japan

1. Electrolyte solution gate FET of CNT:

Semiconducting carbon nanotubes (CNTs) show effective modulation characteristics. In contrast, the electron current of metal CNTs is hardly modulated by field effect. However, graphene, which is used for high-frequency FET[1] and sensor[2], has similar electronic structure to metal CNTs. CNT forest has both metal and semiconducting CNTs, and each tube is highly aligned. Here, we fabricated an electrolyte solution-gate FET (SG-FET) by CNT forest, which is composed of both semiconducting and metal CNTs, and investigated the modulation effect.

2. CNT forest sheet for FET:

The mm-long CNT forest sheets, whose surface density is $\sim 10^{11} \text{ cm}^{-2}$, were synthesized using point-arc microwave plasma CVD [3,4]. With this sheet as mm-long channel, we fabricated the SG-FET. The gate width is $\sim 3 \text{ mm}$ and gate length is $\sim 1 \text{ mm}$ and thickness of sheet is 0.3 mm . Electrolyte solution is used as gate electrode.

3. FET characteristics:

Figure 1 and 2 show the drain current (I_{ds})-the drain voltage (V_{ds}) characteristics, and the I_{ds} and gate voltage (V_{gs}) characteristics of an FET device, respectively. I_{ds} is modulated effectively by V_{gs} through electrolyte solution in the range of $0.5\sim 2 \text{ A}$. Since drain-source electric field is sufficiently small as $\sim 20 \text{ V/cm}$, these devices operate in the linear region and the I_{ds} does not saturate. The maximum transconductance normalized by the gate width at $V_{ds} = 2 \text{ V}$ is $\sim 1 \text{ S/mm}$. This high transconductance indicates the possibility of application to the large current amplification and the high sensitivity sensing.

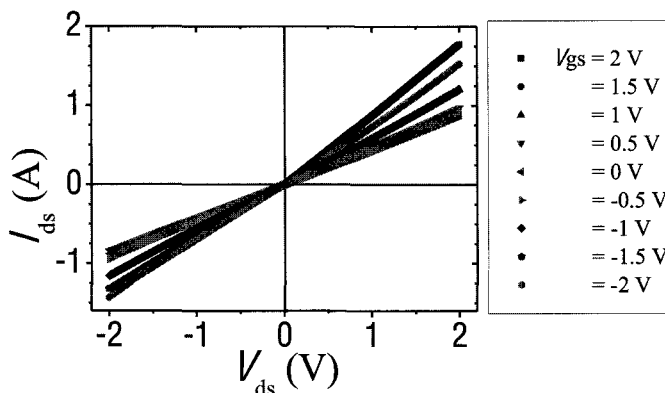


Fig.1 I_{ds} - V_{ds} characteristic of a CNT SG-FET

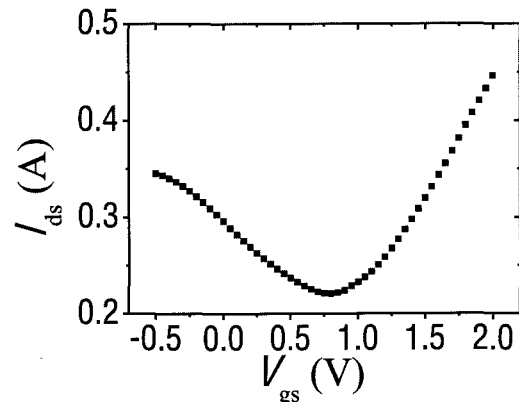


Fig.2 I_{ds} - V_{gs} characteristic of a CNT SG-FET

[1] J. S. Moon *et al.*, *IEEE Electron Device Lett.* 30, 6 (2009)

[2] Y. Ohno, K. Matsumoto *et al.*, *Nano Lett.* 9, 9 (2009)

[3] G. Zhong, H. Kawarada *et al.*, *J. Phys. Chem. B*, 111, 8 (2007)

[4] T. Iwasaki, H. Kawarada *et al.*, *Nano Lett.* 8, 3 (2008)

Corresponding Author: M. Myodo

Tel: +81-3-5286-3391, Fax: +81-3-5286-3391,

E-mail: foreverfriends@ruri.waseda.jp

Limiting factors of photovoltaic efficiency in semiconducting Single-walled Carbon Nanotubes/Si heterojunction cells: Correlation between cell structure, morphology, interface states and photovoltaic properties

○Atsushi Nakano¹, Jiyou Kim², Mao Shoji¹, Hironori Ogata^{1,2}

¹ Graduate School of Engineering, Hosei University, Tokyo 184-8584, Japan

² Department of Faculty of Bioscience and Applied Chemistry, Hosei University, Tokyo 184-8584, Japan

Single-Walled Carbon Nanotubes(SWNTs) are expected to the application to the various kinds of the electronic devices. Especially, semiconducting SWNTs(S-SWNTs) are direct and tunable band gap materials and expected to be useful for photonic and optoelectronic applications. Recently, several research groups reported on the properties of S-SWNT/Si heterojunction solar cells[1-4]. However, their photovoltaic properties were greatly depend on the purity of S-SWNTs, the morphology(coverage or loading) of S-SWNTs film, and the structure of heterojunction interface between Si and S-SWNTs film. So the intrinsic photovoltaic properties of S-SWNT/Si heterojunction solar cells are not fully understood yet. In this study, we investigated the photovoltaic properties in S-SWNTs/n-Si heterojunction cells by several kinds of the fabrication procedure of S-SWNTs films. We also investigated the effects of doping on the photovoltaic properties in S-SWNTs/Si devices. The SWNTs (CoMoCAT method, 0.8 ± 0.1 nm in diameter, ratio of the S-SWNTs:90 % or 98 %) was dispersed in several kinds of liquid(1,2-dichlorobenzene, dimethylformamide, ethanol or chlorosulfonic acid). The S-SWNTs films were prepared by using a nitrocellulose filter or glass sliding method. The S-SWNTs film was transferred to the Si substrate in deionized water. The schematic of SWNTs/Si device is showed in Figure 1. We found that the cell structure and morphology of S-SWNTs film had a great influence on the value of V_{oc} and J_{sc} . The detailed results on the cell structure, morphology, interface states and photovoltaic properties will be presented.

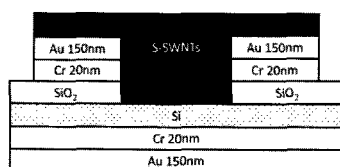


Fig. 1 The schematic illustration of the cross sectional view of S-SWNTs/Si cell.

References:

- [1] Y.Jia, P.Li, J.Wei, A.Cao, K.Wang, C.Li, D.Zhuang, H.Zhu,D.Wu, *Mater. Res. Bull.* 45 (2010) 1401-1405.
- [2] P.-L.Ong, W.B.Euler, I.A. Levitsky, *Nanotechnology* 21 (2010)105203/1-7.
- [3] D.Kozawa, K.Hiraoka, Y.Miyauchi, S.Mouri, K.Matsuda, *Appl.Phys.Exp.*5(2012)042304/1-3.
- [4]Y.Jung, X. Li, N. K. Rajan, A. D. Taylor, M. A. Reed, 13(2013)95-99.

Corresponding Author: H.Ogata

Tel: +81-42-387-6229, Fax: +81-42-387-6229, E-mail: hogata@hosei.ac.jp

Effect of the Structure of Single-Walled Carbon Nanotube Counter Electrode on Dye-Sensitized Solar Cells

○Takaaki Chiba, Hidenori Kinoshita, Kehang Cui,
Eric Einarsson, Shohei Chiashi, Shigeo Maruyama

Department of Mechanical Engineering, The University of Tokyo, Tokyo 113-8656, Japan

Dye-sensitized solar cells (DSSCs), invented by O'Regan and Grätzel in 1991 [1], have advantage of relatively high power conversion efficiency (PCE) and low production cost. Because Pt, which is often used as the counter electrode, is expensive and dissolved in the electrolyte, the alternative of Pt is necessary. The counter electrodes demand high conductivity and catalytic activity, and carbon materials such as graphene [2] or carbon nanotube [3] are good candidates. In this study, vertically aligned single-walled carbon nanotube (VA-SWNT) films and honeycomb-structured SWNT films are used as the counter electrode. VA-SWNTs were grown by ACCVD with Co/Mo catalyst on Si substrates, and then they were transferred on FTO substrates with hot water method. Honeycomb-structured SWNTs were obtained by water vapor exposure. The DSSCs are analyzed based on the measurements of I-V characteristics and impedance spectra. Moreover, the impedance spectra of symmetry cells, consisted of two identical counter electrodes, were measured to evaluate only counter electrodes.

The I-V characteristics of DSSCs under AM1.5G illumination are shown in Fig. 1(A). The PCE of DSSCs with VA-SWNT counter electrodes was lower than those with Pt counter electrodes. The PCE and fill factor (F. F.) of the DSSCs with VA-SWNT electrodes increased from 3.49% to 3.90%, from 0.56 to 0.61, respectively (Fig. 1(A)) and the internal resistance decreased after the vapor treatment (Fig. 1(B)). The impedance spectra of the symmetry cells in Fig. 2 show that the catalytic activity of FTO electrodes was extremely low. It indicates that the sufficient coating the FTO substrate surface with SWNT films and the structure of SWNT films are essential to the performance of the DSSCs with SWNTs counter electrodes.

[1] B. O'Regan and M. Grätzel, *Nature*, **353**, 737 (1991).

[2] K. Ladislav, *et al.*, *Nano Lett.*, **11**, 5501 (2011).

[3] Z. Yang, *et al.*, *Chem. Phys. Lett.*, **549**, 82 (2012).

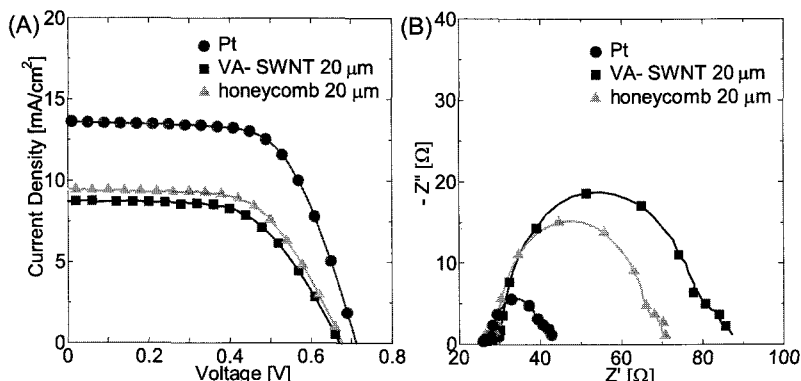


Fig.1 (A) I-V characteristics and (B) impedance spectra of DSSCs with Pt, VA-SWNT and honeycomb SWNT counter electrodes.

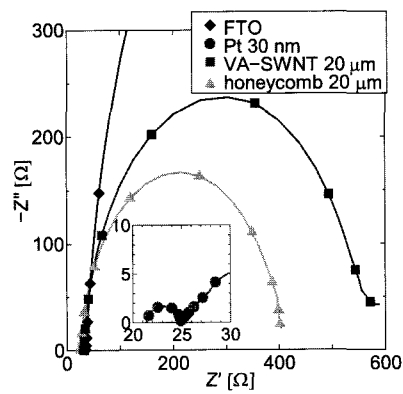


Fig. 2 Impedance spectra of symmetry cells with FTO, Pt, VA-SWNT and honeycomb SWNT electrodes.

Fabrication of flexible and transparent capacitance-type touch panel with single-walled carbon nanotubes based on simple transfer process

○Norihiro Fukaya¹, Shigeru Kishimoto¹, Suguru Noda², and Yutaka Ohno¹

¹*Department of Quantum Engineering, Nagoya University, Nagoya 464-8603, Japan*

²*Department of Applied Chemistry, Waseda University, Tokyo 169-8555, Japan*

Carbon nanotubes (CNTs) are promising material for transparent conductive films (TCFs) without resource problems because of their various advantages such as good flexibility and chemical stability, less haze, and so on. The patterning of CNT films on a plastic substrate is one of key processes for the device applications. In the previous study, we have proposed the simple and rapid transfer process to form patterned CNT films, and demonstrated high-performance TCFs with a grid structure [1]. In this study, we have applied this technique to fabricate the flexible and transparent capacitive-type touch sensors.

CNTs were grown by the floating-catalyst chemical vapor deposition (FC-CVD) [2] and collected with the membrane filter on which the patterns of electrodes for the touch sensor was formed by the photoresist as shown in Fig 1. Figure 2 shows the fabrication process for the touch sensor. CNT films were transferred from the patterned membrane filter onto the both sides of a plastic film. We carried out a densification of the CNT films with isopropanol and chemical doping with nitric acid. Leads were formed with silver paste by the screen printing technique. Finally, the protection films were attached to the both sides. All fabrication processes were carried out at the ambient condition. We have confirmed the normal operation of the fabricated touch sensor.

Acknowledgment: This work was supported by JST/ALCA.

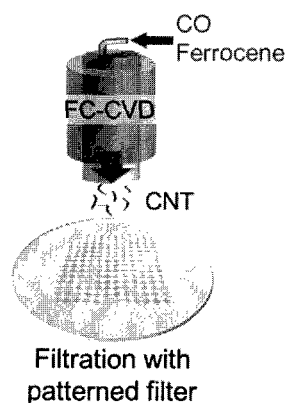


Fig.1 Schematic filtration process with patterned membrane filter.

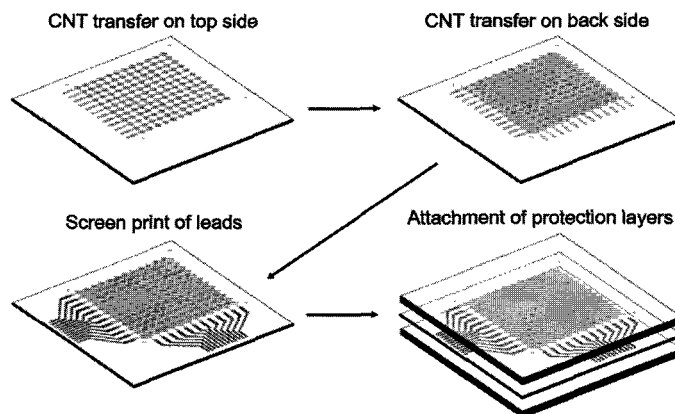


Fig.2 Schematic fabrication process for touch sensors based on simple transfer technique.

[1] N. Fukaya *et al.*, The 45th Fullerenes-Nanotubes-Graphene General Symposium, 2P-19 (2013).

[2] A. Kaskela *et al.*, Nano Lett. **10**, 4349 (2010).

Corresponding Author: Y. Ohno

Tel: +81-52-789-5387, Fax: +81-52-789-5387,

E-mail: yohno@nuee.nagoya-u.ac.jp

Charge state of capsule prepared by coalescence of $\text{Sc}_3\text{N}@C_{80}$ molecules in a carbon nanotube

○Yuki Yonetani¹, Ahmadreza Fallahgilvaei¹, Ryosuke Senga¹, Kaori Hirahara¹, Ryo Kitaura², Hisanori Shinohara², Yoshikazu Nakayama¹

¹ Department of Mechanical Engineering, Osaka University, Osaka 565-0871, Japan

² Department of Chemistry and Institute for Advanced Research, Nagoya University, Aichi 464-8602, Japan

Endhedral metallofullerenes have attracted interest due to electronic polarization between encapsulating metal atoms and their cages, since it may realize new nano-devices. It is known that when fullerene molecules are encapsulated in a carbon nanotube (CNT), charge transfer occurs between the fullerene molecules and CNT, namely the fullerene molecules are electrically charged [1]. One can expect that a capsule-like short CNT prepared by coalescence of such charged fullerene molecules still has an electric charge and is applicable to a GHz oscillator [2]. In this work, we prepared capsules containing Sc atoms by coalescence of $\text{Sc}_3\text{N}@C_{80}$ in CNTs and examined the electronic state of the capsules by electron energy loss spectroscopy (EELS).

In order to coalesce $\text{Sc}_3\text{N}@C_{80}$ molecules encapsulated in a CNT, $\text{Sc}_3\text{N}@C_{80}$ molecules were exposed to electron beams through the host CNT in a transmission electron microscope (TEM). An electron dose of 5×10^9 electrons/nm² with an acceleration voltage of 90 kV formed capsules in the CNT. Dark spots pointed by arrows in a TEM image shown in Fig.1 indicate clusters of Sc or Sc_3N that remain in a newly formed capsule.

We examined an electric charge state of such capsules by EELS. Figure 2 shows EELS spectra taken from the capsules and other reference samples. Two peaks are assigned to Sc L_{23} -edge from their position corresponding to the valence state of Sc atoms. The peak positions for $\text{Sc}_3\text{N}@C_{80}$ molecules and $\text{Sc}_2@C_{80}$ crystals are close, which indicate that the valence state of Sc in $\text{Sc}_3\text{N}@C_{80}$ is similar to that of $\text{Sc}_2@C_{80}$. Inserting $\text{Sc}_3\text{N}@C_{80}$ into CNTs induces a slight shift of the peaks i.e. a shift of the oxidation state of the Sc atoms towards +3, because of the transfer of electrons from the cage to the host CNTs. Observation of no change in the peak position before and after coalescence of $\text{Sc}_3\text{N}@C_{80}$ molecules in the CNTs suggests that the capsule containing Sc atoms is positively charged.

The existence of Sc atoms in the capsules can be exploited for realizing new nano-devices.

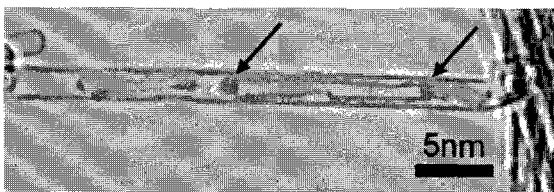


Fig.1 TEM image of capsules prepared by coalescence of $\text{Sc}_3\text{N}@C_{80}$. Arrows point to metal.

[1] Jhinhwan Lee *et al.*, Nature. **415**, 1005-1008 (2002)

[2] S. B. Legoas *et al.*, Phys. Rev. Lett. **90**, 5 (2003)

Corresponding Author: Yuki Yonetani

Tel & Fax: +81-6-6877-5111 (ex. 3355),

E-mail: yonetani@ne.mech.eng.osaka-u.ac.jp

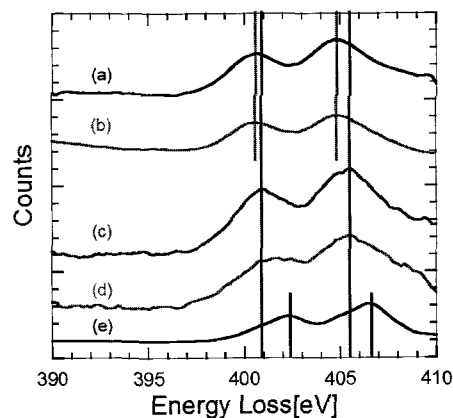


Fig.2 EELS spectra taken from (a) $\text{Sc}_2@C_{84}$ crystal (Sc^{2+}), (b) $\text{Sc}_3\text{N}@C_{80}$, (c) $\text{Sc}_3\text{N}@C_{80}$ in SWCNT, (d) Sc_3N contained in capsule in SWCNT, (e) Sc_2O_3 crystal (Sc^{3+}).

Energetics of Formation Process of C₆₀ included [n]Cyclacene

○Shota Kigure and Susumu Okada

*Graduate School of Pure and Applied Sciences, University of Tsukuba,
1-1-1 Tennodai, Tsukuba, Ibaraki 305-8571, Japan*

Hydrocarbon polymers with hoop-like conformation inherently possess nanometer scale space inside and could be a potential candidate for the host materials of inclusion complexes. Indeed, recent experiments reported that cycloparaphenylene (shortest armchair nanotubes)[1] and cyclochrysenylene (the shortest chiral nanotubes)[2] accommodate a C₆₀ molecule inside. Such complexes are expected to exhibit interesting physical properties those are not simple sum of that of each constituent unit by analogy with the fact that is observed in conventional peapods. In our previous work, we certainly demonstrated that the electronic structure and energetics of the inclusion complex consisting of cyclacene and C₆₀ exhibit interesting diversity depending on the diameter of the host cyclacene molecule [3]. In the present work, we aim to elucidate further theoretical insight on the physical properties of the inclusion complexes consisting of [n]cyclacenes (n=16,17,18,19,20) and C₆₀ based on density functional theory with local density approximation. Figure 1 shows the total energy of complex along a reaction coordinate that corresponds to the insertion process of C₆₀ inside [17]cyclacene. We find that the insertion process is exothermic without any reaction barriers. However, by focusing near the equilibrium position, we found that the anomalous potential energy profile associated to the steric hindrance of edge C-H bonds. We also found that included C₆₀ can oscillate with the frequency of about 1 THz around their equilibrium position,

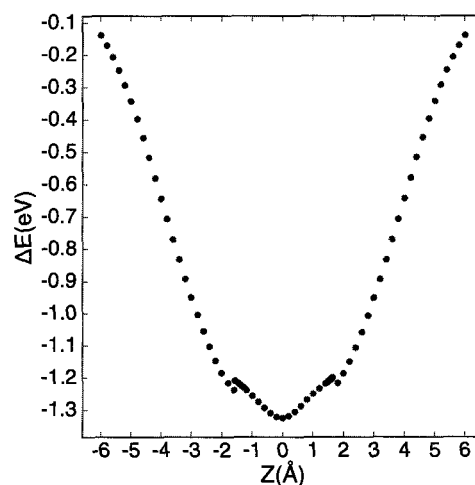


Fig 1: Reaction energy of C₆₀ as a function of C₆₀ position

[1] T.Iwamoto *et al.* *Angew. Chem. Int. Ed.* **50**, 8342 (2011)

[2] H.Isobe *et al.* *Chem. Sci.* **4**,1293 (2013)

[3] S.Kigure and S.Okada, *J. Phys. Soc. Jpn.*, Submitted.

Corresponding Author : S.Kigure

Tel: +81-29-853-5600(ext. 8233,) Fax: +81-29-853-5924,

E-mail: skigure@comas.frsc.tsukuba.ac.jp

Effect of the catalytic activity of catalyst nanoparticles on different types of carbon supports

○Masahiro Ozaki¹, Yoshiyuki Suda¹, Hirofumi Takikawa¹, Hideto Tanoue¹,
Hitoshi Ue², Kazuki Shimizu³

¹ Toyohashi University of Technology, ² Tokai Carbon Co., Ltd.,
³ Shonan Plastic Mfg. Co., Ltd.

Direct methanol type fuel cell (DMFC) has been attracting attention as a power source for mobile devices. It is necessary to increase the output and power generation efficiency. We have developed a carbon electrode for DMFC by supporting a metal catalyst on carbon supports of various shapes. In this study, we examined the effect of the activity of catalyst metal on the shape of carbon support. We used five carbon nanomaterials; particulate cluster types are Vulcan XC-72 (Vulcan), and arc black (AcB)⁽¹⁾, fiber types are carbon nanocoil (CNC) and VGCF-X (CNT), and sheet type is graphene oxide (GO).

We supported metal catalysts, Pt and Ru by the reduction method using sodium borohydride. The supported catalyst metals were observed by transmission electron microscope (TEM). For each sample, 70 nanoparticles in the TEM micrographs were counted⁽²⁾. Particle size distributions of the catalyst metals supported on AcB, Vulcan, and rGO had two peaks. On the other hand, those on CNC and CNT had one peak. The average diameters of particles on AcB, Vulcan, rGO, CNC, and CNT were 2.2 nm, 2.8 nm, 2.3 nm, 3.9 nm, and 3.7 nm, respectively.

This work has been partly supported by the EIIRIS Project from Toyohashi University of Technology (TUT); the Core University Programs (JSPS-CAS program in the field of "Plasma and Nuclear Fusion") from the Japan Society for the Promotion of Science (JSPS); JSPS KAKENHI Grant Number 24360108 and 25630110; and MEXT KAKENHI Grant Number 24110708.

References

- [1] S. Oke, et al.: Chem. Eng. J., 143, 225-229 (2008).
[2] Y. Suda, et al: J. Phys.: Conf. Ser., 433, 012008 (2013)

Corresponding Author: Yoshiyuki Suda

Tel: +81(0)532 44 6726, Fax: +81(0)532 44 6757,

E-mail: suda@ee.tut.ac.jp

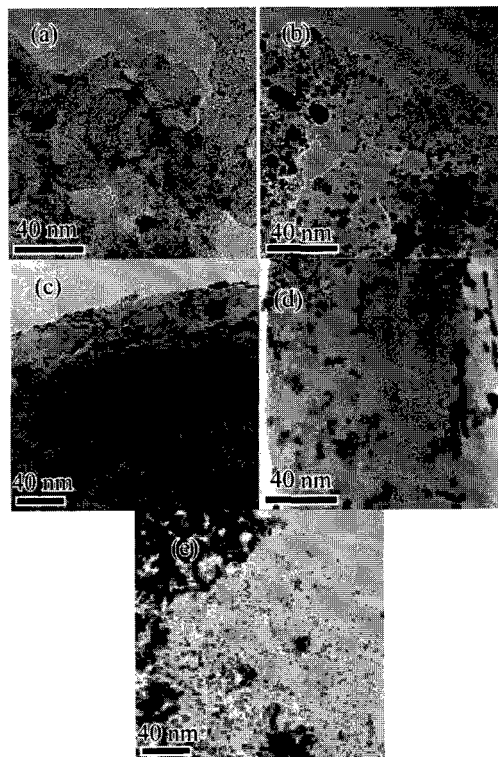


Fig. 1. TEM images of (a) PtRu/AcB, (b) PtRu/Vulcan, (c) PtRu/CNC, (d) PtRu/CNT, (e) PtRu/rGO

Production of carbon nano-capsules and sack-like nano-carbons by impact reaction in nitrogen gas

○Tetsu Mieno, Kazuhiko Kondo ¹, Sunao Hasegawa ², Kosuke Kurosawa ²

Graduate School of Science & Technology, Shizuoka University, Shizuoka 422-8529

¹ Department of Physics, Shizuoka University, Suruga-ku, Shizuoka 422-8529

² Inst. Space Astronautical Science, JAXA, Chuou-ku, Sagamihara 252-5210

Chemical reactions in the interstellar medium are making various kinds of carbon clusters. We are interested in the impact production of carbon clusters and carbon molecules on planets and satellites, especially on Titan satellite. By this motivation, the model experiment has been carried out using a 2-staged light-gas-gun ($v=6.5$ km/s) at JAXA. By the impact reactions under 1 atm. of nitrogen gas, where a polycarbonate bullet hits an iron target (a water + iron target, *etc.*), many types of carbon clusters, like fullerenes, carbon nanotubes, carbon nano-capsules, and balloon-like carbons are produced.

[1] Effects of adding water in the target and cooling the target are also examined. Produced samples are carefully analyzed by a TEM, a LD-TOF-MS, *etc.* As a result, production of carbon nano-capsules including polymer-like material and sack-like nano-carbons is observed as shown in Fig. 1. In the left figure, polymers are encapsulated in the carbon shell (position A). There is minor production of these carbons, which are often imperfect carbon capsules. Mass spectra from the LD-TOF-MS show masses of amino acids (asparagine acid, *etc.*)

[1] T. Mieno, S. Hasegawa, K. Mituishi: Jpn. J. Appl. Phys. **50** (2011) 125102.

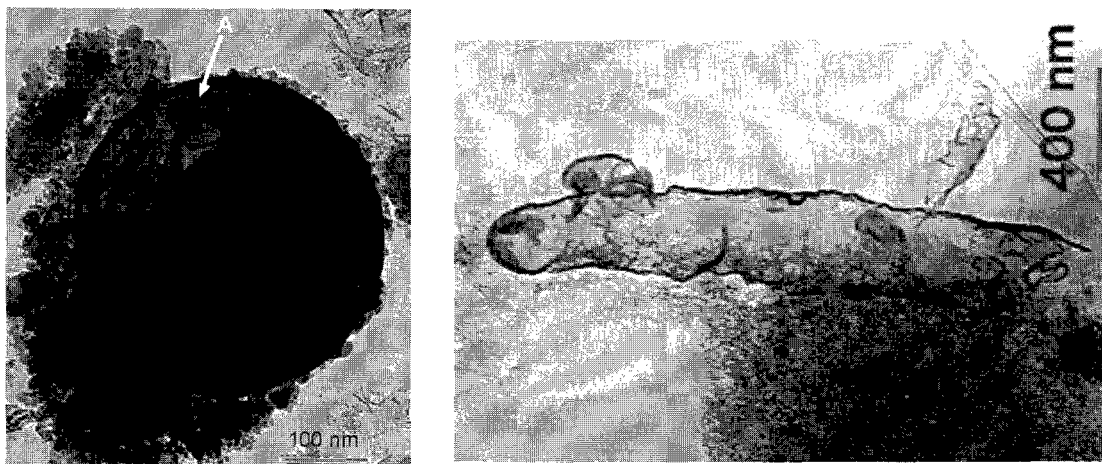


Fig. 1. Carbon capsules storing polymers and a metal particle (left figure), where a polycarbonate bullet hits an ice + hexane + iron target. A carbon sack with graphite-wall and a mouth (right figure), where a polycarbonate bullet hits an ice + iron target (- 60 C). *E-mail: sptmien@ipc.shizuoka.ac.jp

Formation of LaCO_3OH in the oxidation process of carbon nanocapsules encaging LaC_2

○Kazunori Yamamoto¹, Kenji Yamaguchi¹, Shin-ichi Shamoto¹, Takeshi Akasaka²

¹*Nano-Structure Synthesis Research Group, Quantum Beam Science Directorate,
Japan Atomic Energy Agency, Tokai-mura, Naka-gun, Ibaraki 319-1195, Japan*

²*Life Science Center of Tsukuba Advanced Research Alliance, University of Tsukuba, Ibaraki
305-8577, Japan*

The discovery of “endohedral” carbon nanostructures, such as fullerenes [1, 2], nanocapsules [3, 4] and nanotubes [5], has triggered new exciting field of research. Pure metals, alloys and carbides have been nanoencapsulated in carbon. Although rare-earth carbides are hygroscopic and readily hydrolyze in moist air, they did not degrade even after a decade of exposure in the capsules. Due to their high chemical stability, carbon materials are widely used such as electrodes in batteries. Moreover, empty nanocapsules and nanotubes are more resistant to oxidation than other forms of carbon (such as diamond, soot, graphite, and C_{60} fullerene) [6, 7]. Higher oxidation resistance was, therefore, expected for these endohedral multi-wall nanoencapsulates. In this study oxidation of LaC_2 nanocrystallites encaged in carbon nanocapsules has been examined by transmission electron microscopy (TEM) and X-ray diffraction (XRD).

Nanocapsules encaging LaC_2 were synthesized by conventional DC-arc discharge method [3, 4]. They were heated in thermogravimetric (TG) analyzer in the range of 20 – 950 °C at a heating rate of 10 °C/min in excess air. The TG profile showed two remarkable exothermic peaks around 500 – 550 and 650 – 750 °C. The latter peak corresponds to combustion of carbon materials and La_2O_3 was obtained after the TG measurement, although La_2O_3 was rapidly converted to $\text{La}(\text{OH})_3$ after the exposure in moist air. Below 460 °C essentially no weight loss was observed, suggesting no oxidation of LaC_2 in the nanocapsules. One of runs was stopped at 460 °C and the sample was examined by energy dispersive X-ray spectroscopy (EDS) as well as TEM and XRD. TEM observation showed that all carbon nanocapsules including filled and empty nanocapsules seen in the sample were completely unchanged, suggesting no degradation of nanocapsules up to 460 °C, which was confirmed by XRD. On the other hand no undamaged nanocapsules were observed in the heating run stopped right after the first exothermic peak at 580 °C. The XRD profile of this sample showed new peaks which were not assigned to LaC_2 or $\text{La}(\text{OH})_3$, but LaCO_3OH . This means that the former exothermic peak around 500 – 550 °C on the TG profile corresponds to oxidation of the nanoencapsulated LaC_2 . The origin of the new species, LaCO_3OH , will be discussed in the presentation.

- [1] J.R. Heath *et al.*, *J. Am. Chem. Soc.*, **107**, 7779 (1985). [2] Y. Chai *et al.*, *J. Phys. Chem.*, **95**, 7561(1991).
[3] R.S. Ruoff *et al.*, *Science*, **259**, 336(1993). [4] M. Tomita *et al.*, *Jpn. J. Appl. Phys.*, **32**, L280(1993).
[5] S. Seraphin *et al.*, *Appl. Phys. Lett.*, **63**, 2073(1993). [6] L. S. K. Pang, *et al.*, *J. Phys. Chem.*, **97**, 6941(1993).
[7] N. Yao, *et al.*, *J. Mater. Res.*, **13**, 2432(1998).

Corresponding Author: K. Yamamoto,

Tel: +81-29-282-6474,

E-mail: yamamoto.kazunori@jaea.go.jp

Improvement in specific capacitance of electric double-layer capacitors by oxidization of carbon nanoballoon

○Y. Okabe¹, Y. Suda¹, H. Takikawa¹, H. Tanoue¹, H. Ue², K. Shimizu³

¹*Department of Electrical and Electronic Information Engineering,
Toyohashi University of Technology,*

²*Tokai Carbon Co., Ltd.,*

³*Shonan Plastic Mfg. Co., Ltd.*

Carbon nanomaterials are used as an electrode of electric double layer capacitors (EDLC). EDLC performs charge and discharge by the electric double layer which is formed between electrode and electrolyte [1]. In this research, we used carbon nanoballoon (CNB) as the electrode material. CNB is graphitic, and the particle shape is hollow. In order to increase the specific capacitance of EDLC, CNB was oxidized at 625 °C in the air. We call this material oxidized carbon nanoballoon (Ox-CNB). Ox-CNB forms particle and hollow structure. Furthermore, Ox-CNB has some pinhole at its shell. When we used Ox-CNB as an electrode material, Ox-CNB had twice larger specific capacitance than CNB. This result suggests that electrolyte could penetrate inside the particles through pinhole which formed by oxidization and the specific surface area became twice of CNB. Thus, it was demonstrated that double specific surface area makes double specific capacitance. Fig. 2 shows the results of electric impedance spectra. In this figure, real impedance of Ox-CNB is smaller than that of CNB although Ox-CNB includes defective structure by oxidization. This suggests that ion which penetrated into hollow space also reduced real impedance.

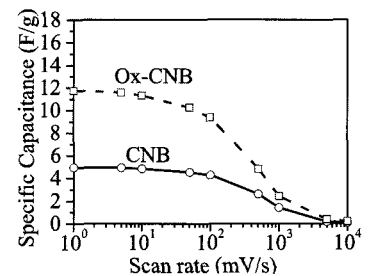


Fig. 1 Specific capacitance

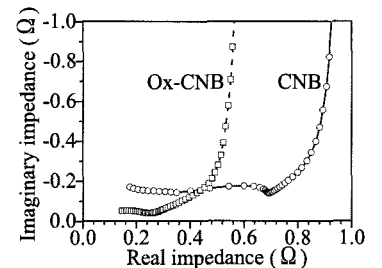


Fig. 2 Nyquist plots

This work has been partly supported by the EIIRIS Project from Toyohashi University of Technology (TUT); the Core University Programs (JSPS-CAS program in the field of "Plasma and Nuclear Fusion") from the Japan Society for the Promotion of Science (JSPS); JSPS KAKENHI Grant Number 24360108 and 25630110; and MEXT KAKENHI Grant Number 24110708.

[1] Pawan Sharma, *et al.*: *Energy Conversion and Management*, 51, 2901-2912 (2010)

Corresponding Author: Yoshiyuki Suda

E-mail: suda@ee.tut.ac.jp, Tel: 0532-44-6726

発表索引
Author Index

Author Index

< A >

Achiba Yohji	3-8
Ago Hiroki	3-1
Akasaka Takeshi	3P-34 2P-15 2P-32 2P-35
Akinori Saeki	1P-31
Akira Ono	1P-3
Akita Seiji	3P-18
Akiyama Tsuyoshi	1P-32
Akiyama Wataru	1P-33
Akizuki Naoto	1-4 1P-23
Akutagawa Tomoyuki	3-7
Amagai Yuri	2P-15
Ando Hiroaki	2P-19
Ann JongJun	1P-36 1P-37
Aoki Nobuyuki	1P-33 2P-14
Aonuma Syuji	3P-7
Aoyagi Shinobu	3-7
Arai Yuki	1P-34
Araki Takumi	1-1
Arie Takayuki	3P-18
Arifuku Tatsuji	1P-14
Asaka Koji	3P-25 2P-2
Ashihara Masaaki	2P-10
Ata Seisuke	1-9 1P-29 1-10
Atsushi Nakano	3P-27

< B >

Baba Keisuke	3-4
Baek Jinseok	3P-8
Balch Alan	2P-35
Bandow Shunji	3P-14 2P-7
Bianco Alberto	2P-8
Bird Jonathan P.	1P-33 2P-14
Bissett Mark	3-1

< C >

Chen Guohai	1P-21
Chiashi Shohei	1P-13 1P-16 3P-28
Chiba Takaaki	3P-28
Correa D. S.	3P-23
Cui Kehang	1P-28 3P-28
Cuong Nguyen Thanh	2-7

< D >

Daisuke Inotani	3P-13
Deligkaris Kosmas	1P-26

< E >

Ebrahimi Afshin J.	2-8
Eguchi Usaburo	3P-16
Einarsson Eric	3P-28
Endo Morinobu	1-1 1-11
Endo Tomoaki	2P-37

< F >

Fallah Gilvaei Ahmadreza	3P-30
Frey Urs	1P-26
Fugetsu Bunshi	1-1
Fujigaya Tsuyohiko	2-4 1P-27
Fujii Shunjiro	1P-34
Fujiki Kazuhiro	3P-21 3P-1
Fujimori Toshihiko	1-11
Fujimoto Kazuki	1P-14
Fujimoto Yoshitaka	2-5
Fujioka Koichi	2P-28
Fukaya Norihiro	3P-29
Fukumori Minoru	2P-4
Fukunishi Nobuhisa	1-7
Fukuzumi Shunichi	2P-22 2P-15 2-1 2-10 2P-26
Furuta Hiroshi	1P-18 1P-12
Futaba Don N.	1P-21 1-10
Futamura Ryusuke	1-11

< G >

Gemma Rius	3P-2
Ghosh Ranajit	1P-10
Gohara Takehiro	3P-18

< H >

Hangyo Masanori	1P-18
Harada Akio	2P-27
Hase Muneaki	1P-20
Hasebe Hiroo	1-7
Hasebe Yohei	2P-2
Hasegawa Daisuke	1P-16
Hasegawa Kai	1P-4
Hasegawa Sunao	3P-33
Hasegawa Tadashi	2P-32 2P-15 2P-35 2P-26
Hashimoto Kenro	3-8
Hasobe Taku	2-1
Hata Kenji	1P-21 1P-29 1-9 1-10
Hatta Akimitsu	1P-12 1P-18
Hayashi Takuya	1-11 1P-36
Hayashida Takuya	1-2

Hayong Song	3P-22			Ito Yusuke	1-2		
Hibino Hiroki	3S-5			Itoh Chihiro	1-3	2P-16	
Hideto Tanoue	3P-15			Iwamura Munechiyo	1P-23		
Hino Shojun	2P-33	2-9		Iwasa Yoshihiro	3P-19		
Hinoishi Takahiro	2P-34	2P-33		Iwata Nobuyuki	1P-8		
Hirahara Kaori	3P-30			Izumi Noriko	2-9		
Hirai Takayoshi	2P-6						
Hirano Atsushi	1P-6	1P-20		< J >			
Hirohumi Takikawa	3P-15			Jang Jin	1P-36	1P-37	
Hironori Ogata	3P-27			Jasim Dhifaf	2P-8		
Hiroshi Fukuda	1P-24						
Hiroshi Nagasawa	1P-3			< K >			
Hiroshiba Yasuhiro	1-16			Kako Masahiro	2P-32		
Hiroyuki Isobe	1P-1			Kamigaito Osamu	1-7		
Hiroyuki Masuda	1P-31			Kaneko Katsumi	1-11		
Hisaki Ichiro	2P-26			Kaneko Toshiro	2P-5		
Hisama Kaoru	1P-15			Kanemoto Tatsuya	2P-23		
Hitoshi Ue	3P-15			Kase Masayuki	1-7		
Homma Yoshikazu	1P-13	1-2		Kataura Hiromichi	1P-6	2-3	2P-19
HONDA Kazuya	1-5				1P-34	2S-4	
Honda Yuki	1P-20			Kato Koichiro	1P-22		
Hong Liu	2P-20			Kato Ryo	3P-16		
Hoshina Shinji	2P-18			Kato Tatsuhisa	2P-21		
Hoshino Norihisa	3-7			Kato Toshiaki	2P-5	3S-6	
				Kawakami Akira	2P-19		
< I >				Kawakami Hiroki	2-11		
Ichida Masao	2P-19			Kawashima Yuki	2P-22	2-1	
Ichimura Ryota	1P-9			Kayahara Eiichi	2P-21		
Igarashi Miki	3-6			Kazuhiko Kondo	3P-33		
Ihara Kazuki	1-6			Kazuki Shimizu	3P-15		
Iida Ryosuke	2P-32			Ken Kokubo	1P-31		
Iijima Sumio	1P-10	2P-8	1-15	Kihara Hideyuki	1P-11		
Iizumi Yoko	1-8			Kikuchi Yuta	1-6		
Ikehara Yuzuru	1-8			Kimura Hiroe	3-10		
Ikemoto Yuka	2P-19			Kimura Takahide	3P-7	3-9	
Ikuma Naohiko	2P-30	2P-28	2P-31	Kimura Wataru	3P-21		
	2-10	2P-27		Kinoshita Hidenori	3P-28		
Imahori Hiroshi	3P-8			Kishimoto Shigeru	3P-29		
Imamura Ryuki	2P-23			Kisoda Kenji	1-3	2P-16	
Imao Hiroshi	1-7			Kitagawa Tomoya	2P-11		
Inaba Daiki	2P-32			Kitakawa Haruki	2P-4		
Inaba Saori	2P-30			Kitaura Ryo	1-12	2-3	2P-3
Inoue Taiki	1P-16	1P-13			2P-13	3-7	3P-30
Inukai Eri	2P-13				2P-11		
Irle Stephan	2-3			Kiyomiya Masaharu	2P-6		
Ishibashi Koji	2P-14			Kiyoyanagi Noriko	1P-14		
Ishii Koji	1P-8			Kobayashi Keita	1-13		
Itami Kenichiro	1P-2			Kobayashi Tomoki	1-2		
Ito Chihiro	2P-19			Kobayashi Yoshihiro	3P-4	1P-14	2P-4
Ito Masahiro	1-2				3P-6		

Kocabas Coskun	2S-3			Matsuda Mitsuaki	2P-16	1-3		
Kodaira Tetsuya	1P-11			Matsumoto Kana	1P-37			
Kodama Takeshi	3-8			Matsumoto Kazuhiko	3P-6			
Koji Hirofumi	1P-12			Matsunaga Masahiro	2P-14			
Koji Maruyama	3P-15			Matsuo Yutaka	2P-36	2-11		
Kokame Hiraaki	1P-14	3P-4		Matsuoka Yuki	1P-7	2-6		
Kokubo Ken	2-10	1-13	2P-30	Matsuzaki Michihiro	3P-6			
Kokubo Ken	2P-28	2P-31	2P-27	Matsuzawa Yoko	1P-11			
Komatsu Naoki	3P-7	3-9	3S-8	Ménard-Moyon Cécilia	2P-8			
Konabe Satoru	3-3	3-1		Mendonca C. R.	3P-23			
Kondo Hiroki	1P-10			Mikami Ninako	1-16			
Koretsune Takashi	1P-22	2-5	3-2	Mikie Tsubasa	2P-31	1P-31		
Kostarelos Kostas	2P-8			Misawa Yusuke	2P-28			
Kosuke Tashiro	3P-22			Miyamoto Katsuhiko	1P-33			
Koyama Takahiko	2P-21			Miyata Mikiji	2P-26			
Kuboki Hironori	1-7			Miyata Yasumitsu	1-12	2-3	1P-9	
Kunimoto Ryuji	2P-9				2P-3	2P-13	2P-19	
Kurosawa Kosuke	3P-33			MIYATA Yasumitsu	1-5			
Kusumoto Taro	3P-4			Miyauchi Yuhei	1P-23	1-4	2P-11	
Kusumoto Yuji	1P-12			Miyaura Kenshi	1-12			
Kuwahara Yuki	1-6	2P-6		Miyazaki Takafumi	2-9	2P-33		
				Miyoshi Kentaro	3P-24			
< L >				Mizorogi Naomi	2P-35			
Lee Haeseong	1P-36	1P-37		Mizuno Takaaki	1-9			
Lee HeeJae	1P-36	1P-37		Momiyama Daiki	1P-33			
Li Lain-Jong	3P-19			Morelos-Gomez Aaron	1-11			
Li Zhao	2-2			Morita Kazuki	3P-8			
Lim Hong En	2-3			Moriyama Hiroshi	3-5	2-10	3-6	
Liu Gang	3P-7	3-9			1P-36	1P-37		
Lu Xing	2P-35			Motomiya Kenichi	2P-12			
				Mouri Shinichiro	1-4	1P-23		
< M >				Murakami Toshiya	1-3	2P-16	2P-19	
Maeda Eriko	2P-3			Muramatsu Hiroyuki	1-11			
Maeda Kenji	2P-14			Murata Michihisa	2P-25			
Maeda Yutaka	2P-15	2P-32	2P-35	Murata Yasujiro	2P-25	3-7		
Maehashi Kenzo	3P-6			Myodo Miho	3P-26			
Maeta Daisuke	3P-9							
Magara Hiroyuki	2P-10			< N >				
Maki Norio	2P-10			Nabika Hideki	2P-18			
Makino Kotaro	1P-20			Nagamori Takashi	2-6			
Manako Takashi	2P-7			Nagase Shigeru	2P-35			
MANIWA Yutaka	1-5			Nagashima Dai	2P-29			
Maniwa Yutaka	1P-9			Nagata Kazuhiro	3P-1			
Maret Elizabeth	1P-20			Naitou Yasuhisa	1P-4			
Maruyama Mina	3P-10			Nakahara Hitoshi	3P-9	2P-2		
Maruyama Shigeo	1P-16	1P-13	3P-28	Nakahara Kentaro	2P-7			
Maruyama Takahiro	2P-17	1P-10		NAKAI Yusuke	1-5			
Masataka Ueno	2-8			Nakai Yusuke	1P-9			
Masayasu Iida	2-8			Nakamura Hisashi	1-1			
Matsuda Kazunari	1-4	1P-23	2P-11	Nakanishi Yuusuke	2-9			

Nakashima Naotoshi	2-4	2P-20	1P-27	Omachi Haruka	1P-2		
Nakatsu Toru	1P-4			Omatsu Takashige	1P-33		
Nakaya Naoki	3S-7			Ono Yuji	1P-32		
Nakaya Ryoji	2P-10			Ookita Sousuke	2-9		
Nakayama Takuya	1P-2			Osamu Eryu	3P-2		
Nakayama Yoshikazu	3P-24	3P-30		Oshima Takumi	2P-30	2P-27	2P-28
Nakayama Yoshikazu					2P-31	2-10	
Naohiko Ikuma	1P-31			Otani Minoru	2-7		
Naoki Komatsu	2-2			Otuka A. J. G.	3P-23		
Nara Masanobu	2P-18			Ozaki Masahiro	3P-32		
Naritsuka Shigeya	1P-10						
Negishi Ryota	2P-4	3P-6	1P-14	< P >			
	3P-4			Pac Chyongjin	1P-36	1P-37	
Nihey Fumiyuki	1-6			Pu Jiang	3P-19		
Nii Daisuke	1-2						
Nishi Tatsuhiko	2-9			< R >			
Nishihama Takuya	2P-24			Rahman A. F. M. Mustafizur	3-9		
Nishimoto Yoshio	2-3						
Nishimura Yoshifumi	2-3			< S >			
Nishioka Yasuhiro	1P-34			Saeki Akinori	2P-31		
Nishizaka Hikaru	2P-12			Sagara Takumi	1P-8		
Noda Suguru	3P-29			Saito Riichiro	3P-11		
Nomoto Toyokazu	2P-17			Saito Susumu	3-2	2-5	1P-22
Norihiko Miyamoto	2-8			Saito Takeshi	1-6	2P-6	
Numata Hideaki	1-6			Saito Yahachi	3P-9	2P-2	3P-25
Nunes Antonio	2P-8			Saji Eiji	2P-10		
				Sakai Hayato	2-1		
< O >				Sakai Toru	3P-24		
Ochiai Yuichi	1P-33	2P-14		Sakurai Shunsuke	1P-21		
Ogata Hironori	3-4			Sano Hiroshi	2P-10		
Ogawa Takuji	2P-4			Sano Masahito	3P-3		
Ogawa Yasunori	3P-20			Sano Yoshiaki	3-4		
Ogura Mutsuo	1-8			Sasaki Fusako	1-6		
Oh Jaebuem	1P-36	1P-37		Sato Kentaro	3P-11		
Ohkubo Kei	2P-22	2P-26	2-10	Sato Tohru	2P-29		
	2P-15	2-1		Sato Yoshinori	2P-12		
Ohmori Shigekazu	2P-6	1-6		Segawa Yasutomo	1P-2		
Ohno Yasuhide	3P-6			Seichepine Florent	1P-26		
Ohno Yutaka	3P-29	1S-1		Seiichi Sawatani	2-8		
Ohzeki Masaya	1P-34			Seino Yuma	2P-33		
Okabe Yuta	3P-35			Seki Shu	2P-31		
Okada Hiroshi	2P-36	2-11		Sekiya Kazuki	1P-12	1P-18	
Okada Susumu	3-3	3P-10	3P-12	Senga Ryosuke	3P-30		
	2-7	3-1		Shamoto Shin-ichi	3P-34		
Okazaki Toshiya	1-8	3-8		Shimizu Kazuki	3P-17	3P-32	3P-35
Okimoto Haruya	2-9				2P-9	3P-16	
Oku Takeo	1P-32			Shimizu Ryo	3P-19		
Okukawa Takanori	1P-34			Shingo Suzuki	2-8		
Okuno Hiroki	1-7			Shinji Kawasaki	3P-22		
Olmstead Marilyn	2P-35						

Shinohara Hisanori	1-12	2P-3	2P-13	Tetsu Mieno	3P-33			
	3-7	3P-30	2-3	Tezuka Noriyasu	3P-8			
	2-9	2P-11		Tohji Kazuyuki	2P-12			
Shinzo Suzuki	1P-3			Tohnai Norimitsu	2P-26			
Shiozawa Hidetsugu	1S-2			Tokuhiro Chano	2-2			
Shiraki Yuki	3P-14			Tomanek David	1-11			
Shiromaru Haruo	3-8			Toriumi Naoto	1P-33			
Shito Ryukou	2P-18			Toyama Kiyohiko	2P-7			
Sho Kamata	1P-1			Toyoda Masami	3P-24			
Shohei Hayase	3P-5			Tribuzi V.	3P-23			
Shota Kigure	3P-31			Tsubokawa Norio	3P-21	3P-1		
Shoto Banyu	1P-30			Tsuda Yusaku	1P-8			
Shu Seki	1P-31			Tsuji Masaharu	3-1			
Shunpei Hitosugi	1P-1			Tsuyoshi Akiyama	1P-30			
Slanina Zdenek	2P-35							
Subramaniam Chandramouli	1-10	1-9		< U >				
Suda Yoshiyuki	3P-17	3P-32	3P-35	Uchiyama Kouya	3-5			
	2P-9	3P-16		Ue Hitoshi	3P-17	3P-32	3P-35	
Sugai Toshiki	1-16				2P-9	3P-16		
Sugimoto Kunihisa	3-7			Ueno Hiroshi	2-10	1-13	3-6	
Sumiyoshi Tetsuo	3P-1			Ueno Mikihiro	2P-10			
Susumu Okada	1P-35	3P-31	3P-13	Umeda Yoshito	3P-17	2P-9	3P-16	
Suzuki Hiroo	2P-5			Umemura Kazuo	1-2			
Suzuki Mitsuaki	2P-35			Umeyama Tomokazu	3P-8			
Suzuki Seiya	2-6			Umino Takanori	1P-13			
				Urabe Yasuko	1P-6			
				Urita Koki	1-11			
< T >								
Tahara Yoshio	1-15							
Taisuke Matsumoto	1P-30			< W >				
Taisuke Matsuno	1P-1			Wada Yoriko	1-14			
Takada Yuko	1P-11			Wada Yoshihumi	1P-4			
Takagi Yuki	1P-4			Wakabayashi Tomonari	2P-23	1-14		
Takahashi Eri	1P-2			Wakamiya Atsushi	2P-25			
Takahashi Ryo	2P-27			Warner Jamie H.	2-3			
Takano Keisuke	1P-18			Wei Xiaojun	2P-14			
Takase Mai	2P-18							
Takenobu Taishi	3P-19	1P-4		< X >				
Takeo Oku	1P-30			Xiao Chen	2-2			
Takeuchi Masanori	2P-10			Xu Bin	1P-17			
Takikawa Hirofumi	3P-32	3P-35	3P-17					
	2P-9	3P-16		< Y >				
Takumi Oshima	1P-31			Yagi Hajime	2P-33	2-9		
Tanaka Hirofumi	2P-4			Yagi Yusuke	3P-1			
Tanaka Kazuyoshi	2P-29			Yahagi Tatsurou	2P-14			
Tanaka Takeshi	1P-6	1P-20	1P-34	Yajima Hirofumi	1P-8			
Tanoue Hideto	3P-17	2P-9	3P-16	Yajima Takatoshi	2P-17			
	3P-32	3P-35		Yajima Takeru	3P-24			
Tejima Syogo	1-1			Yamada Michio	2P-15	2P-35	2P-32	
Terada Tomohiro	3P-25			Yamada Takeo	1P-29	1-9	1-10	
Terrones Mauricio	1-11			Yamago Shigeru	2P-21			

Yamaguchi Kenji	3P-34		
Yamaguchi Takashi	2P-7		
Yamamoto Hiroshi	1P-8		
Yamamoto Kazunori	3P-34		
Yamamoto Shouhei	3-6		
Yamamoto Yuki	1-3	2P-16	
Yamanaka Ayaka	3P-12		
Yamane Isao	1-7		
Yamauchi Takeshi	3P-21		
YANAGI Kazuhiro	1-5		
Yanagi Kazuhiro	1P-9	2P-19	1P-4
Yanagi Yuichiro	1P-34		
Yanagidate Tatsuki	1P-34		
Yang Mei	1-15		
Yasuda Hidehiro	1-13		
Yasuda Satoshi	2P-18		
Yasuda Toku	3P-7		
Yasuda Yuzuri	1-10		
Yasudomi Shingo	3P-16		
Yohji Achiba	1P-3		
Yoji Ohashi	3P-13		
Yonemura Taiichiro	3P-17	2P-9	
Yonetani Yuki	3P-30		
Yoon Howon	1P-29	1-9	
Yoshida Akira	1P-34		
Yoshida Keisuke	1P-5	1P-8	
Yoshida Masaru	1P-11		
Yoshimura Masamichi	1P-7	2-6	
Yoshito Umeda	3P-15		
Yosiyuki Suda	3P-15		
Yosuke Ishii	3P-22		
Yosuke Kakimi	3P-2		
Yoza Kenji	3-5	3-6	
Yudasaka Masako	2P-7	1-8	1-15
	2P-8		
Yuge Ryota	2P-7		
Yuichiro Takesaki	2P-1		
Yumura Motoo	1-10	1P-21	1P-29
Yuto Suzuki	1P-25		

< Z >

Zaima Takeyuki	2-9		
Zanatta A. R.	3P-23		
Zhang Minfang	2P-8	1-15	
Zhang Rui	2P-25	3-7	
Zhao Li	3P-7		
Zhao Sihan	2P-11		
Zhu Zhen	1-11		

複写をご希望の方へ

フラーレン・ナノチューブ・グラフェン学会は、本誌掲載著作物の複写に関する権利を一般社団法人学術著作権協会に委託しております。

本誌に掲載された著作物の複写をご希望の方は、(社)学術著作権協会より許諾を受けて下さい。但し、企業等法人による社内利用目的の複写については、当該企業等法人が社団法人日本複写権センター((社)学術著作権協会が社内利用目的複写に関する権利を再委託している団体)と包括複写許諾契約を締結している場合にあっては、その必要はございません(社外頒布目的の複写については、許諾が必要です)。

権利委託先：一般社団法人学術著作権協会

〒107-0052 東京都港区赤坂 9-6-41 乃木坂ビル 3階

TEL : 03-3475-5618 FAX : 03-3475-5619 E-mail : info@jaacc.jp

注意：複写以外の許諾(著作物の引用、転載・翻訳等)に関しては、(社)学術著作権協会に委託致しておりません。直接、フラーレン・ナノチューブ・グラフェン学会へお問い合わせください。

Reprographic Reproduction outside Japan

- Making a copy of this publication

Please obtain permission from the following Reproduction Rights Organizations (RROs) to which the copyright holder has consigned the management of the copyright regarding reprographic reproduction.

- Obtaining permission to quote, reproduce, translate, etc.

Please contact the copyright holder directly.

Users in countries and regions where there is a local RRO under bilateral contract with Japan Academic Association for Copyright Clearance(JAACC) are requested to contact the respective PROs directly to obtain permission.

Users in countries or regions in which JAACC has no bilateral agreement are requested to apply for the license to JAACC.

Japan Academic Association for Copyright Clearance (JAACC)

Address : 9-6-41 Akasaka, Minato-ku, Tokyo 107-0052 Japan

Website : <http://www.jaacc.jp/>

E-mail : info@jaacc.jp TEL : 81-3-3475-5618 FAX : 81-3-3475-5619

2013年8月5日 発行

第45回フラーレン・ナノチューブ・グラフェン総合シンポジウム 講演要旨集

<フラーレン・ナノチューブ・グラフェン学会>

〒113-8656 東京都文京区本郷 7-3-1

東京大学 大学院工学系研究科 機械工学専攻

丸山研究室内

TEL / FAX : 03-3830-4848

E-mail : fntg@photon.t.u-tokyo.ac.jp

URL : <http://fullerene-jp.org/>

印刷 / 製本 第一資料印刷株式会社 NBD統括事業部

世界トップクラスの高性能、床置き・卓上、日立なら選べます!

バイオ研究 & ナノ粒子研究 の強い味方

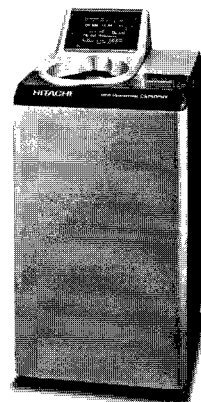
小形超遠心機

エコでスリムな床置きタイプ

himac CS-FNX Series

世界最高速150,000rpm* (CS150FNX)
世界最大遠心加速度1,050,000×g* (CS150FNX)
クラス最静音45dB(A)*
省スペース床置きタイプの小形超遠心機は日立だけ!

- 特長**
- 世界標準の安全規格CEマーキング適合製品
 - サンプルのバランスは目分量でOK!
 - ロータは全て載せるだけ! (ロータクイックセッティング方式)
 - エコ対応省エネモデル
 - 7mlスイングロータ(S50ST)が回せます。
 - 2012年度グッドデザイン賞 受賞!



形名	CS150FNX	CS120FNX	CS100FNX
最高回転速度 (rpm)	150,000	120,000	100,000
最大遠心加速度 (xg)	1,050,000	771,000	604,000
サイズ (W×D×H mm)	440×520×910		
質量 (kg)	105		
標準価格 (税別)	¥5,500,000	¥4,900,000	¥4,300,000

卓上超遠心機

コンパクトなボディに世界トップクラスの性能

himac CS150NX

世界最高速150,000rpm*
世界最大遠心加速度1,050,000×g*
世界最小コンパクトサイズ*
クラス最静音45dB(A)*

- 特長**
- 短い真空待ち時間
 - サンプルのバランスは目分量でOK!
 - ロータは全て載せるだけ!
 - 7mlスイングロータが回せます。



形名	CS150NX
最高回転速度 (rpm)	150,000
最大遠心加速度 (xg)	1,050,000
サイズ (W×D×H mm)	590×582×408
質量 (kg)	97
標準価格 (税別)	¥6,000,000

* (2012年3月現在
当社調べによる)



ロータ仕様

形名	S110AT	S50A	S50ST
最高回転速度 (rpm)	110,000	50,000	50,000
容量 (ml) ×本数 (本)	5.0×8	30.0×6	7.0×4
標準価格 (税別)	¥1,100,000	¥950,000	¥1,500,000
形名	S140AT	S58A	S55A2
最高回転速度 (rpm)	140,000	58,000	55,000
容量 (ml) ×本数 (本)	2.0×10	13.5×8	1.5×12
標準価格 (税別)	¥1,290,000	¥1,000,000	¥750,000

バイオ研究 & ナノ粒子研究 のスタンダード

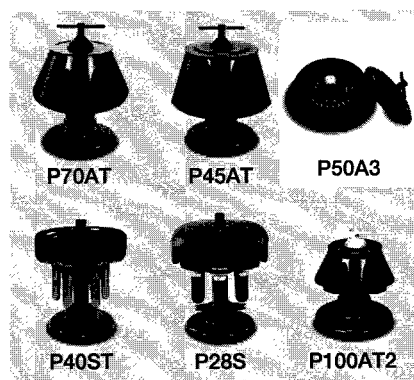
超遠心機

ドライブユニットは安心の完全10年保証!

himac CP-WX Series

クラス最高速100,000rpm* (CP100WX)
クラス最大遠心加速度803,000×g* (CP100WX)
*(2012年6月現在当社調べによる)

- 特長**
- サンプルのバランスは目分量でOK! ●他社ロータが使用可能! (オプション)
 - ロータ寿命自動管理と寿命延長機能搭載 (RLMアダプタ付ロータ)
 - エコ対応省エネモデル ●20Aブレーカにも接続可能!



形名	CP100WX	CP90WX	CP80WX
最高回転速度 (rpm)	100,000	90,000	80,000
最大遠心加速度 (xg)	803,000	700,000	615,000
サイズ (W×D×H mm)	790×690×1,000 (テーブルまでの高さ850)		
質量 (kg)	400		
標準価格 (税別)	¥11,000,000	¥9,500,000	¥8,000,000

ロータ仕様

形名	P70AT	P45AT	P50A3	P40ST	P28S	P100AT2
最高回転速度 (rpm)	70,000	45,000	50,000	40,000	28,000	100,000
容量 (ml) ×本数 (本)	40×8	94×6	1.5×24	13×6	40×6	6.5×8
標準価格 (税別)	¥2,200,000	¥2,350,000	¥1,200,000	¥2,490,000	¥2,350,000	¥2,250,000

※本広告に掲載した以外にもロータを取り揃えております。最奇りの営業所へお気軽にお問い合わせください。

【製造・販売・保守】

日立工機株式会社

東日本地区 03-5733-0202 西日本地区 0798-23-4125

日立遠心機お客様相談センター ☎ 0120-024125

受付時間 9:00~12:00 / 13:00~17:00 (土・日・祝日・弊社休業日除く)

URL <http://www.hitachi-koki.co.jp/himac/>

- この広告に掲載した製品は、改善のため外観または仕様の一部を変更することがあります。
- 印刷の都合上、実際の色と異なる場合があります。
- 標準価格は仕様や構成により異なります。
- 全て税別価格となります。
- 安全のために使用環境、使用条件、据付条件が制限される場合があります。

NANORUPTOR[®] ~サンプル密閉式超音波分散装置~

———— バイオの技術をナノテクへ ————

本装置はカーボンナノチューブや燃料電池用触媒を始めとする
各種ナノ粒子を溶媒に分散させる用途に最適化されています。

実施例：燃料電池用触媒評価、カーボンナノチューブの分散
納入実績：各大学、自動車メーカー、光学機器メーカー、電子部品メーカー



特長

- 分散に最適
各種ナノ粒子(カーボンナノチューブ、フラーレン等)
の分散処理に最適。
- 密閉処理
密閉容器を使用するので溶媒の蒸発・揮散やコンタミがありません。
- 多検体同時処理
1 試料から最大 24 試料を同時に処理できます。
- 再現性良好
回転機構の採用により均一な超音波照射が可能です。
- 低騒音
高性能消音箱により超音波の騒音が低く抑えられます。

NR-350仕様表

品番	NR-350
品名	密閉式超音波分散装置 Nanoruptor
超音波周波数	20 kHz
超音波出力	最大 350 W 可変
電源	100 V、50/60 Hz、5.5 A
最低設置スペース概寸	400 (W) × 300 (D) × 680 (H) mm
発振ユニット概寸	400 (W) × 260 (D) × 160 (H) mm
処理ユニット概寸	170 (W) × 160 (D) × 270 (H) mm
消音箱概寸	400 (W) × 350 (D) × 520 (H) mm
NR-350 全体重量	36 Kg
ランタイマー	1 ~ 60 サイクル
インターバルタイマー (ON)	1 ~ 99 秒
インターバルタイマー (OFF)	30 ~ 99 秒
処理本数	1 本 (50 mL) ~ 24 本 (0.5 mL)
付属品	消音箱、電源ケーブル、接続ケーブル、 排水ポンプ、取り扱い説明書、 ユーザー登録カード
備考	NR-350 は機器のみです。別途処理量に 応じたアクセサリをお買い求め下さい。

メーカー略号：TOS

品名	品番	包装	希望販売価格
超音波密閉式分散装置 Nanoruptor [®]	NR-350	1 UNIT	¥1,950,000
50 mL チューブ用チップ	MM-50WS	1 SET	¥54,000
ギヤー板	NG350-50	1 PC	¥9,000

オプション：冷水循環器

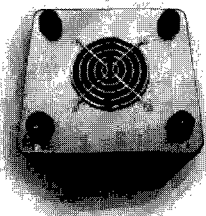
特別仕様品も承ります！

丸形超音波処理槽



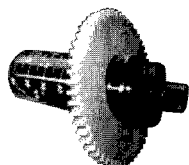
丸形超音波処理槽の採用により分散の効率化を実現。

冷却ファン



冷却ファン及び専用回路の採用により長時間運転が可能。

別売品



50 mL チューブ用チップ
ギヤー板
その他各種

販売



人と科学のステキな未来へ

コスモ・バイオ株式会社

135-0016 東京都江東区東陽2-2-20 東陽駅前ビル

http://www.cosmobio.co.jp

TEL (03) 5632-9622 FAX (03) 5632-9614

製品情報部 栗原 mkurihar@cosmobio.co.jp

製造



東湘電機株式会社

〒253-0101 神奈川県高座郡寒川町倉見 496-1

TEL (0467) 75-1155 FAX (0467) 75-1155

技術部長 伊藤 k-ito@bioruptor.jp



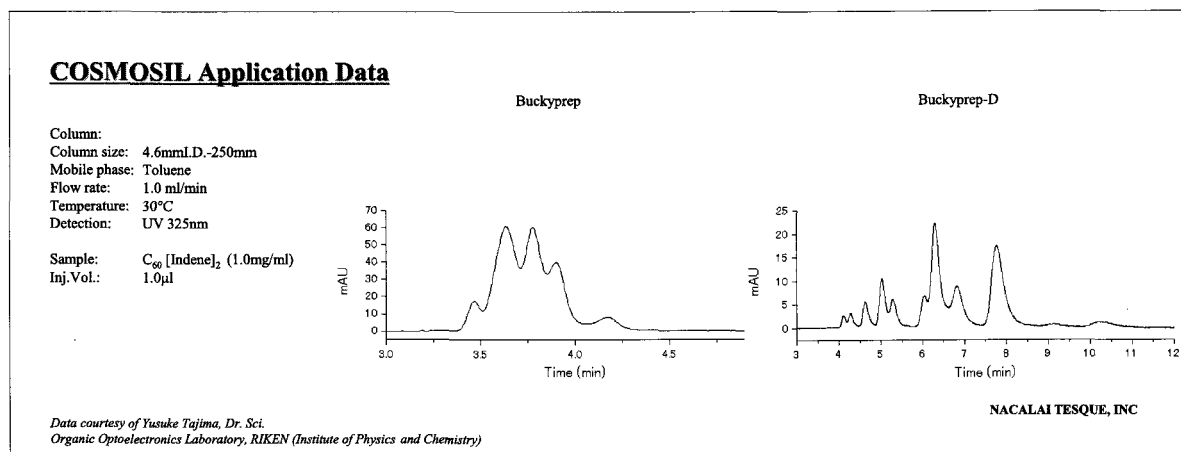
誘導体化フラーレン用HPLCカラム

COSMOSIL[®] Buckyprep-D

- 誘導体化フラーレン用HPLCカラム
- トルエン移動相中で誘導体化フラーレンが分離可能

■C60インデン付加体の分析例

C60インデンは誘導体化フラーレンの一種であり、有機薄膜太陽電池のn型半導体材料として注目されている化合物です。コスモシール Buckyprep-Dを用いることにより高い分離性能が得られます。



■Buckyprepシリーズの用途

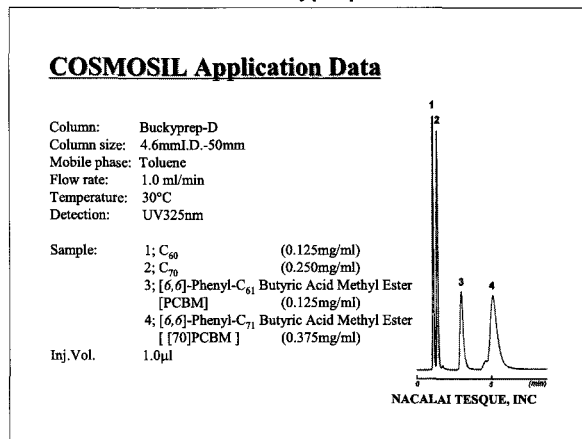
フラーレン分離のスタンダードカラム

誘導体化フラーレンの分離

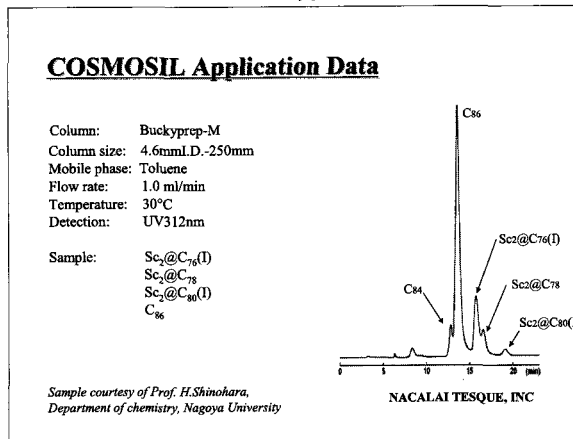
金属内包フラーレンの分離

- ▶ COSMOSIL Buckyprep
- ▶ COSMOSIL Buckyprep-D
- ▶ COSMOSIL Buckyprep-M

・ 誘導体化フラーレン (Buckyprep-D)



・ 金属内包フラーレン (Buckyprep-M)



詳しい情報はWeb siteをご覧ください。

ナカライテスク株式会社

〒604-0855 京都市中京区二条通烏丸西入東玉屋町498

価格・納期のご照会 フリーダイヤル 0120-489-552
製品に関するご照会 TEL:075-211-2746 FAX:075-211-2710

Web site :<http://www.nacalai.co.jp>

分取 HPLC のスタンダード 好評の NEXT シリーズ

JAI のリサイクル分取 HPLC は発売以来40年
特に国内外の有機合成研究室で活躍しています。

高性能

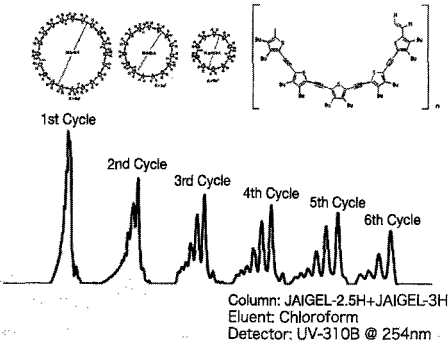
使いやすさ

メンテナンス性能

3つの要素を徹底的に追求したNEXTシリーズが
あなたのラボの作業効率を飛躍的に向上。

コンパクト&スマート
次の時代へ
NEXTシリーズ
JAI

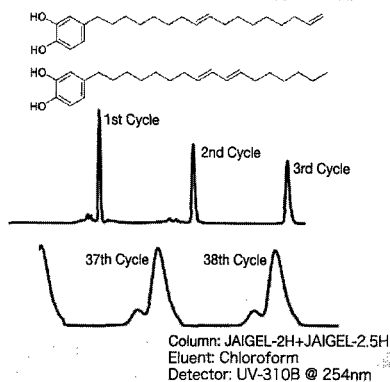
GPCリサイクルによる
Macrocyclic Oligothiophenesの分離



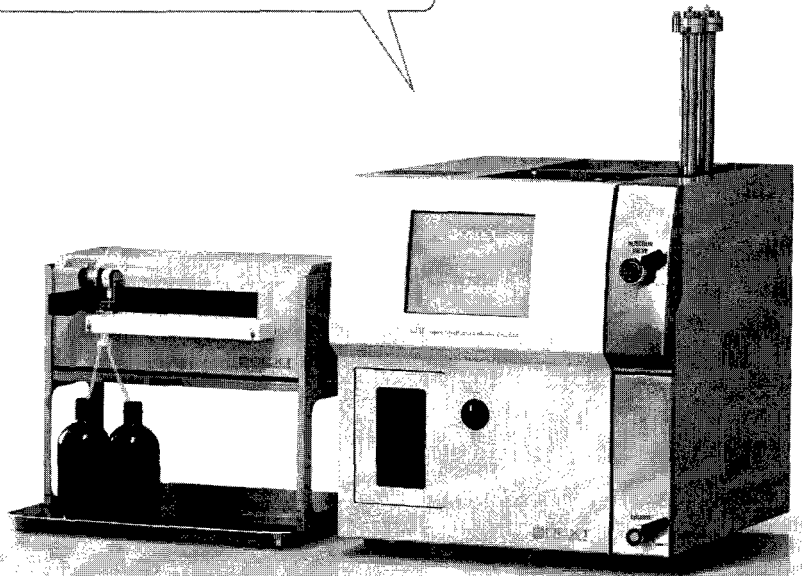
Feature

- ・液晶タッチパネルインターフェイス
- ・溶媒置換に便利な自動洗浄機能
- ・PCコントロールで遠隔操作
- ・同一試料の重ね打ち注入
- ・全自動で繰り返し注入&分取が可能
- ・独自のリサイクル(特許)を標準装備

GPCリサイクルによる位置異性体の分離



最大流量
・LC-9110 II NEXT 10ml/min MAX
・LC-9130 II NEXT 30ml/min MAX



LC-9110 II NEXT / LC-9130 II NEXT

JAI 日本分析工業株式会社

URL <http://www.jai.co.jp/> ISO9001/14001 取得

■本社・工場：〒190-1213 東京都西多摩郡瑞穂町武蔵 208 TEL 042-557-2331 FAX 042-557-1892
■大阪営業所：〒532-0002 大阪市淀川区東三国 5-13-8-303 TEL 06-6393-8511 FAX 06-6393-8525
■名古屋営業所：〒465-0025 愛知県名古屋市名東区上社 3-609-3D TEL 052-709-5400 FAX 052-709-5403

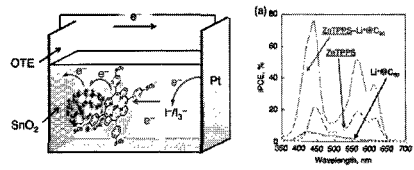
JAI Japan Analytical Industry Co., Ltd.



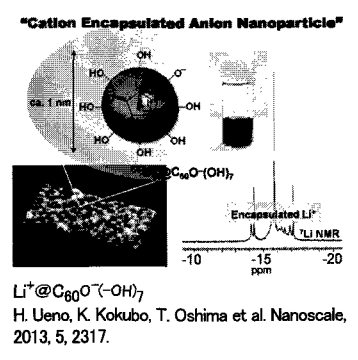
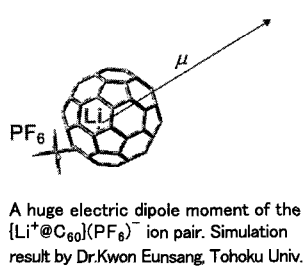
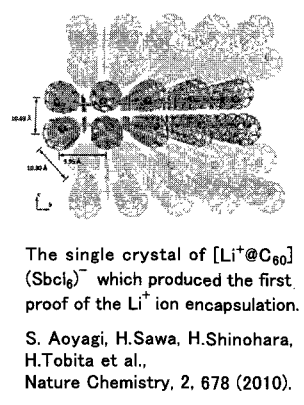
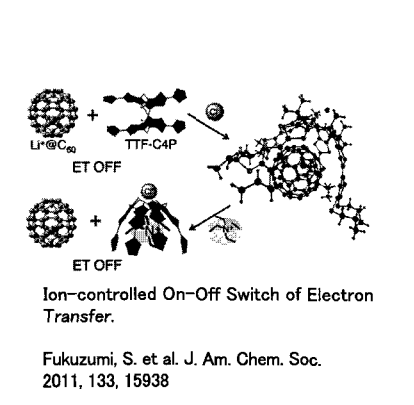
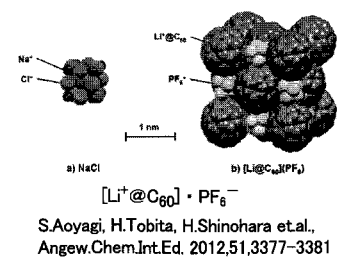
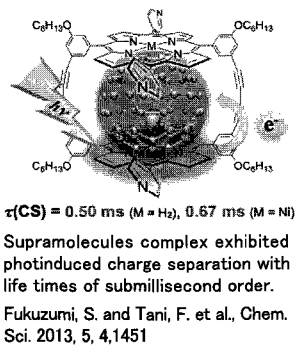
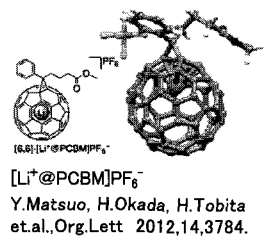
Li endohedral C₆₀ fullerene is C₆₀ fullerene Li⁺ ion encapsulation

This off-centered Li⁺ ion encapsulated in C₆₀ has opened up a new vista for interesting molecules and applications.

NEW!



「Li⁺@C₆₀ paves the way for high performance solar cells. K.Ohkubo et al., Chem. Commun., 2013, 49, 4474-4476」



001B01 Li ⁺ @C ₆₀ / C ₆₀ (Cluster)		
Chemical Formula: [Li ⁺ @C ₆₀] · n C ₆₀	1,000 mg	¥ 500,000
	500 mg	¥ 250,000
Powder, composed of Li ⁺ @C ₆₀ molecules each surrounded by (10 to 20) C ₆₀ molecules.		
001D04 Li ⁺ @C ₆₀ (PF ₆) ⁻ salt		
Chemical Formula: [Li ⁺ @C ₆₀](PF ₆) ⁻ salt	10 mg	¥ 210,000
	20 mg	¥ 390,000
	30 mg	¥ 570,000
	40 mg	¥ 747,000
	50 mg	¥ 930,000
[Li ⁺ @C ₆₀](PF ₆) ⁻ salt content > 95% (measured value)	over 50mg Price per mg	¥ 18,600
TS001 Li ⁺ @C ₆₀ /C ₆₀ /Li Cluster		
Powder, composed of Li ⁺ @C ₆₀ , Li and C ₆₀ packed in Ar atmosphere.	1,000 mg	¥ 400,000
	500 mg	¥ 200,000

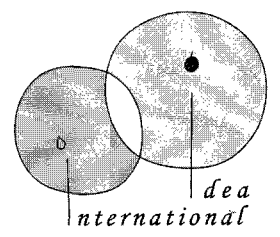
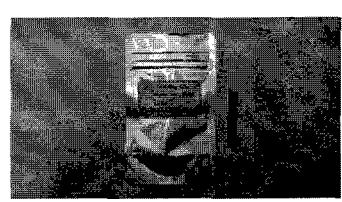
R&D, Production and Sales of Li⁺@C₆₀

Idea International Co., Ltd.

Head Office and Sendai R&D center
1-15-35 Sagigamori, Aobaku, Sendai, Miyagi, 981-0922 Japan
+81-22-342-8410

Joint Research Center
Takahashi-Lab. Hatchery Square, Tohoku-University, 6-6-04
Aramaki Aza Aoba, Aoba-ku, Sendai, Miyagi 980-8579 Japan
+81-22-795-3164

East Asian R&D Center
Rise Kokura Bldg. 2-1-1 Sakai-cho, Kukurakita-ku, Kitakyushu,
Fukuoka, 802-0005 Japan
+81-93-383-6577 Fax: +81-93-383-6271



e-mail : info@idea-i.jp
http://www.lic60.jp

溶液中の粒子のナノレベル微細化 分散に

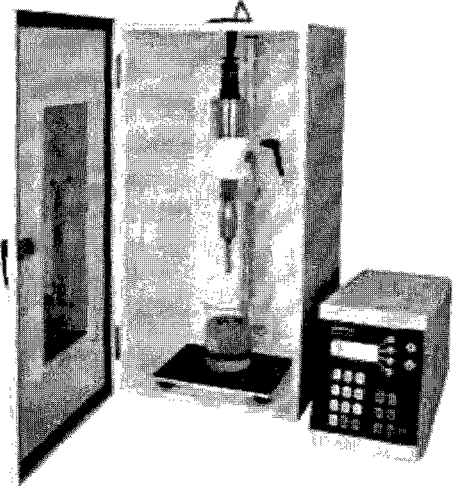
BRANSON 超音波ホモジナイザー

ホーン先端部の振幅の安定性を、より高めたAdvanceタイプになりました。

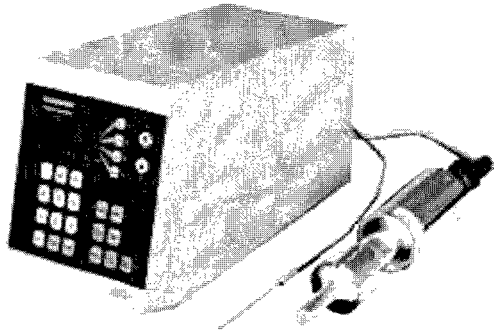
近年のナノテクノロジーの発展及び粉体関連技術の向上により、より微細な粒子に対する乳化分散処理の要望が増えてまいりました。

超音波ホモジナイザーを使用し、均質な乳化分散処理を行い、安定させることにより製品の機能は向上します。

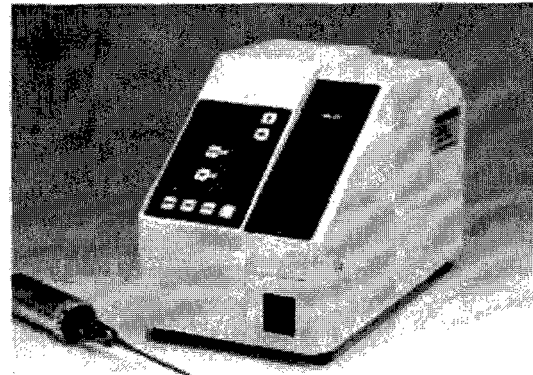
ブラソン社では20kHz機と40kHz機の2タイプを用意しております。1次粒子の凝集力にも拠りますが、20kHz機では100nm程度までの分散力があります。40kHz機は、さらに細かいレベルで分散ができる可能性があります。



20KHz 超音波ホモジナイザー
BRANSON SONIFIER シリーズ



高周波 40KHz 超音波ホモジナイザー
BRANSON SLPe シリーズ



ブラソン社の製品は、ホーン先端部の振幅の安定性が高く、強力なキャビテーションが得られ、効率良く再現性の高い分散処理が行えます。

主なアプリケーション

分散

カーボンナノチューブ 有機顔料 無機顔料 セラミック セメント 感光体 記録材料
磁性粉 粉末冶金 酸化鉄 金属酸化物 シリカ アルミナ カーボンブラック
ポリマー ラテックス 製紙 ファンデーション
研磨剤 電池 フィラー 光触媒 触媒 ワクチン 体外診断薬 歯磨き粉 シャンプー
半導体 電子基盤 液晶 貴金属 金属 宝石 タイヤ 発酵菌類 その他

乳化

エマルジョン製剤 農業 トナー ラテックス 界面活性剤 クリーム 乳液 クリーム 等

 **セントラル** 科学貿易

本社：111-0052 東京都台東区柳橋 1-8-1
Tel 03-5820-1500 Fax 03-5820-1515
URL <http://www.cscjp.co.jp/>

大阪支店：Tel 06-6325-3171 Fax 06-6325-5180
福岡営業所：Tel 092-482-4000 Fax 092-482-3797
札幌出張所：Tel 011-764-3611 Fax 011-764-3612

— フロンティア出版のナノテクノロジー・ナノマテリアルシリーズ —

有機・無機・金属ナノチューブ

—非カーボンナノチューブ系の最新技術と応用展開—

編集：清水敏美(産業技術総合研究所)
木島 剛(宮崎大学)
■体裁/B5判・330頁 ■価格/57,750円(税込)

ナノ材料のリスク評価と安全性対策

—生体・環境への影響,安全性対策・国内外動向—

監修：亘理文夫(北海道大学)
■体裁/B5判・317頁 ■価格/57,750円(税込)

ナノ空間材料の創製と応用

編集：有賀克彦(物質・材料研究機構)
■体裁/B5判・314頁 ■価格/57,750円(税込)

自己組織化ナノマテリアル

—フロントランナー85人が語るナノテクノロジーの新潮流—

企画：理化学研究所 フロンティア研究システム
時空間機能材料研究グループ
監修：国武豊喜(北九州市立大学/理化学研究所)
編集幹事：下村政嗣(北海道大学/理化学研究所)
山口智彦(産業技術総合研究所)
■体裁/B5判・392頁 ■価格/57,750円(税込)

グラフェンの最先端技術と拡がる応用

—グラフェンの材料科学,成長・合成技術,各種デバイス応用—

監修：尾辻泰一(東北大学)
■体裁/B5判・242頁 ■価格/57,750円(税込)

レアメタル・希少金属リサイクル技術の最先端

—ナノ・有機・メタラジーが広げるリサイクル技術—

監修：原田幸明(物質・材料研究機構)
■体裁/B5判・313頁 ■価格/57,750円(税込)

ナノインプリントの最新技術と装置・材料・応用

—ナノインプリント技術の最先端と拡がる用途—

編集：平井義彦(大阪府立大学)
■体裁/B5判・330頁 ■価格/57,750円(税込)

ナノオプティクス・ナノフォトニクスのすべて

—ナノ光技術の基礎から実用まで—

監修：河田 聡(大阪大学/理化学研究所)
編集：梅田倫弘(東京農工大学)
川田善正(静岡大学)
羽根一博(東北大学)
■体裁/B5判・352頁 ■価格/57,750円(税込)



フロンティア出版

〒110-0012 東京都台東区竜泉1-21-18 TEL:03-6802-1640 FAX:03-6802-1641 E-mail: info@frontier-books.com

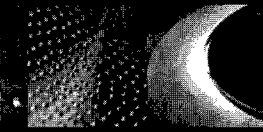
<http://www.frontier-books.com>

AIXTRON

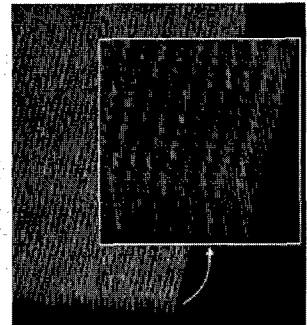
アイクストロン社の

カーボンナノチューブ&グラフェン成長用CVD装置

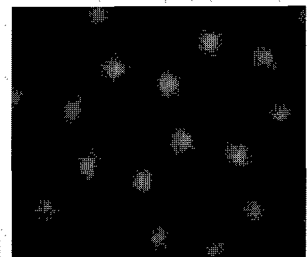
BM Series



Dense CNT



Horizontal SWCNT



Graphene

- 多様な基板サイズに対応
BM II System(2インチ基板用)、BM Pro System(4、6インチ基板用)、BM 300(300mm基板用)
- 1台の装置で、再現性の高いCNT及びグラフェン成長可能(最大8種類のガス系を搭載)
熱CVD、プラズマCVD、トップヒータによる熱輻射CVD等、多様な成長モード
- オリジナルの成長レシピ付
(シングルCNT用、ダブルCNT用、マルチCNT用、横方向CNT用、低圧プロセスCNT用、高速成長CNT用、
モノレイヤーグラフェン用、マルチレイヤーグラフェン用etc.)
- プラズマエッチングによる簡単クリーニング

アイクストロン株式会社

<http://www.aixtron.com>

E-mail: JAPANINFO@aixtron.com

〒140-0001 東京都品川区北品川 1-8-11 Daiwa 品川 North ビル 9F TEL: 03-5781-0931 FAX: 03-5781-0940

HORIBA

Scientific



更に進化したLabRAMシリーズ

顕微レーザーラマン分光測定装置

Raman Spectroscopy System

LabRAM HR

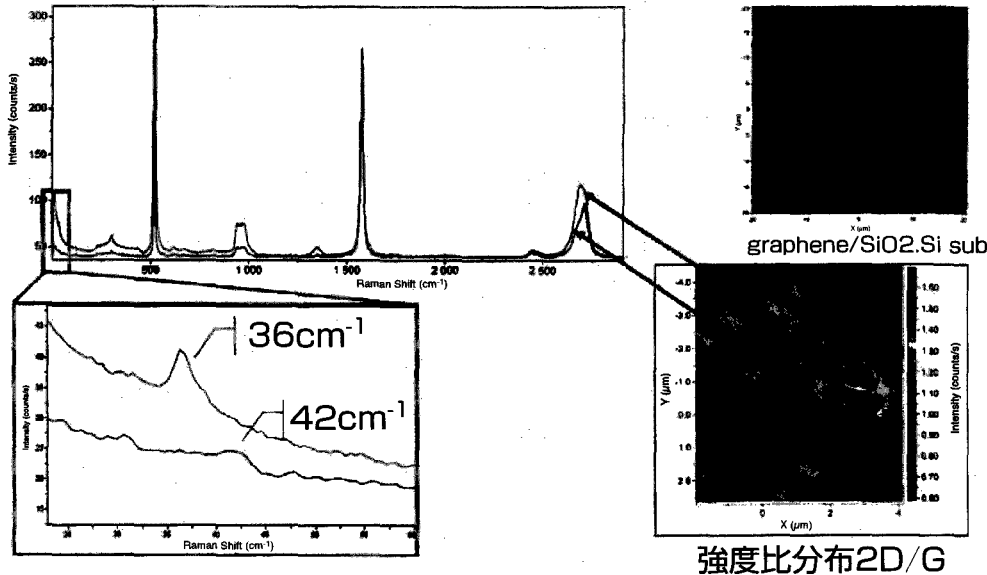
Evolution



- 空間分解能0.5 μm 実現
- オートアライメント対応
- Ultra Low Frequencyフィルタ対応
- ...



アプリケーション例: グラファイトE_{2g}ピークの測定



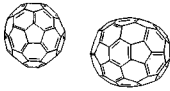
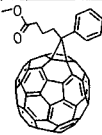
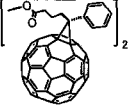
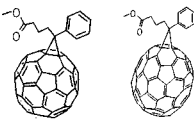
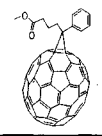
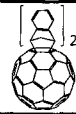
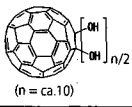
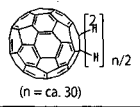
株式会社 堀場製作所 本社 〒601-8510京都市南区吉祥院宮の東町2番地 TEL: (075)313-8121 <http://www.horiba.com/jp/scientific/>
 ●つくば(0298)56-0521 ●東京(03)6206-4717 ●名古屋(052)936-5781 ●大阪(06)-6390-8011 ●福岡(092)292-3593
 ●製品の技術的なご相談をお受けします。カスタマーサポートセンター フリーダイヤル 0120-37-8045

Explore the future

Automotive Test Systems | Process & Environmental | Medical | Semiconductor | Scientific

HORIBA

nanom フロンティアカーボンのフラーレン製品

銘柄	分子構造	純度(HPLC面積%、代表値) 内容他	最低数量 (g)
nanom purple フラーレンC60		99	10
		99.5	2
		99.5/昇華精製品	2
		99.9/昇華精製品	1
		99.9/昇華精製/単結晶品	1
nanom orange フラーレンC70		97	1
		98/昇華精製品	0.5
nanom mix 混合フラーレン		C60, C70, その他高次 フラーレンの混合物 ※微粒化品(ST-F)もあります	50
nanom spectra [60]PCBM (phenyl C61-butrylic acid methyl ester)		99	1
		99.5	1
		99.9	0.5
nanom spectra E400 bis[60]PCBM (bis-phenyl C61-butrylic acid methyl ester)		98/異性体トータル ※位置異性体の混合物	1
nanom spectra E123 [60,70]PCBM		[60]PCBM、[70]PCBMの混合物	1
nanom spectra [70]PCBM (phenyl C71-butrylic acid methyl ester)	 主成分	99/異性体トータル ※位置異性体の混合物	0.5
		99.5/異性体トータル ※位置異性体の混合物	0.5
nanom spectra Q100 [60]インデン付加体		99	0.5
nanom spectra Q400 [60]インデン2付加体		99/異性体トータル ※位置異性体の混合物	1
nanom spectra D100 水酸化フラーレン		C ₆₀ OH _n n=10を主成分とする混合物	1
nanom spectra A100 水素化フラーレン		C ₆₀ H _n n=30を主成分とする混合物	1

銘柄、取扱数量等は予告無く変更する場合がございます。予めご了承下さい。

2013年1月8日現在

当社製品は、下記2社から購入いただけます。直接お問い合わせください。

・関東化学株式会社 試薬事業本部

〒103-0022 東京都中央区日本橋室町2-2-1 TEL:03-6214-1090 FAX:03-3241-1047

<http://www.kanto.co.jp> E-mail:reag-info@gms.kanto.co.jp

・第一実業株式会社 新事業推進室【担当: 鎰広(カギヒロ)】 E-mail:masaru.kagihiro@djk.co.jp

〒102-0084 東京都千代田区二番町11-19 TEL:03-5214-8579 FAX:03-5214-8503

<本資料に関するお問い合わせ先>

フロンティアカーボン株式会社【担当: 梶原】

〒100-8086 東京都千代田区丸の内2-6-1丸の内パークビルディング24階

TEL:03-3210-2620 FAX:03-3210-4606 <http://www.f-carbon.com>

※弊社へのお問い合わせはHPよりお願いいたします。